VYSOKÉ UČENÍ TECHNICKÉ V BRNĚ

BRNO UNIVERSITY OF TECHNOLOGY

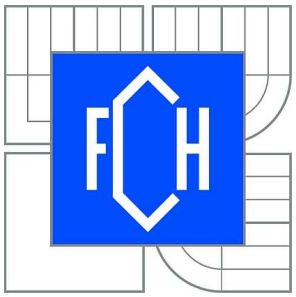

FAKULTA CHEMICKÁ
CENTRUM MATERIÁLOVÉHO VÝZKUMU

FACULTY OF CHEMISTRY
MATERIALS RESEARCH CENTRE

RHEOLOGY OF INORGANIC MATERIALS IN TECHNOLOGY

REOLOGIE V TECHNOLOGII ANORGANICKÝCH MATERIÁLŮ

DIZERTAČNÍ PRÁCE
DOCTORAL THESIS

AUTOR PRÁCE — Ing. MICHAELA WIRTHOVÁ
AUTHOR

VEDOUCÍ PRÁCE — prof. Ing. JAROMÍR HAVLICA, DrSc.
SUPERVISOR

BRNO 2012

Brno University of Technology
Faculty of Chemistry
Purkyňova 464/118, 61200 Brno 12

Doctoral thesis Assignment

Number of doctoral thesis:	**FCH-DIZ0065/2011**	Academic year: **2011/2012**
Institute:	Materials Research Centre	
Student:	**Ing. Michaela Wirthová**	
Study programme:	Chemistry, Technology and Properties of Materials (P2820)	
Study field:	Chemistry, Technology and Properties of Materials (2808V016)	
Head of thesis:	**prof. Ing. Jaromír Havlica, DrSc.**	
Supervisors:		

Title of doctoral thesis:

Rheology of Inorganic Materials in Technology

Doctoral thesis assignment:

• literature research about rheological properties of cement based materials
• observation of the effects of water to cement ratio and superplasticizer dosage on the rheological properties of fresh cement materials
• investigation of the static yield stress via several methods
• study of properties of cement paste during first hours of hydration

Deadline for doctoral thesis delivery: 31.8.2012

Doctoral thesis is necessary to deliver to a secreatry of institute in three copies and in an electronic way to a head of doctoral thesis. This assignment is enclosure of doctoral thesis.

Ing. Michaela Wirthová Student	prof. Ing. Jaromír Havlica, DrSc. Head of thesis	prof. Ing. Miloslav Pekař, CSc. Head of institute

In Brno, 3.7.2009

prof. Ing. Jaromír Havlica, DrSc.
Dean

ABSTRACT

The doctoral thesis deals with the study of the rheological behavior of the cement based systems. The introductory part includes theoretical knowledge about rheology and materials of interest (cement, self-compacting concrete, superplasticizers). A detailed description of the rheological behavior of the fresh cement based materials follows. In addition the hydration of the cement, calorimetry, Vicat test, X-ray powder diffractometry and scanning electron microscope are described. The experimental part is divided into two parts. First part is concerning the self-compacting concrete and their matrixes and includes basic characterization, rheological measurements and investigation of the static yield stress. Second part is regarding the cement pastes, which were tested via several methods with using the parallel plate rheometer, Vicat apparatus, isoperibolic and modular calorimeter, X-ray diffractometer and scanning electron microscope.

ABSTRAKT

Disertační práce se zabývá studiem reologického chování materiálů na bázi cementu. Úvodní část obsahuje teoretické poznatky týkající se reologie a zkoumaných materiálů (cement, samozhutnitelný beton, superplastifikátory). Poté následuje detailní popis reologických vlastností čerstvých cementových materiálů. Kromě toho je dále uvedena hydratace cementu, kalorimetrie, Vicatův test, rentgenová difrakční analýza a elektronová mikroskopie. Experimentální část práce je rozdělena do dvou částí. První část se zabývá základní charakterizací, reologickým měřením a studiem statické meze toku směsí samozhutnitelných betonů a jejich matric. Druhá část se týká cementových past, které byly podrobeny testování pomocí reometru, Vicatova přístroje, isoperibolického a modulárního kalorimetru, rentgenového difraktometru a elektronového mikroskopu.

KEYWORDS

rheology, cement, self-compacting concrete, thixotropy, flow curve, Vicat test

KLÍČOVÁ SLOVA

reologie, cement, samozhutnitelný beton, tixotropie, toková křivka, Vicatův test

WIRTHOVÁ, M. Rheology of Inorganic Materials in Technology. Brno: Brno University of Technology, Faculty of Chemistry, 2012. 165 s. Supervised by prof. Ing. Jaromír Havlica, DrSc.

DECLARATION

I declare that the doctoral thesis has been worked out by myself and all the quotations from the used literary sources are accurate and complete. The content of the doctoral thesis is the property of the Faculty of Chemistry of Brno University of Technology and all commercial uses are allowed only if approved by both the supervisor and the dean of the Faculty of Chemistry, BUT.

.....
Student's signature

Acknowledgements

I would like to express my gratitude to my supervisor Professor Jaromír Havlice DrSc. for his help and support during whole PhD study.

Special thanks to Professor Stefan Jacobsen for giving me the opportunity to come to Norway to Norwegian University of Science and Technology (NTNU), for spending many hours of his spare time discussing the rheology, concrete, teamwork and life in Norway too.

I want to thank to Klaartje De Weerdt for her valuable advices concerning the parallel plate rheometer and giving me the opportunity to participate on her research.

Thanks to laboratory engineers at NTNU Department of Structural Engineering Trond Auestad, Ove Loraas and Steinar Seehus for valuable assistance with the Viscometer programming in Natinal Instruments LabView and plate test set up adapting the Balance link software.

Thanks to my colleagues for the execution of the experimental part, namely: Martin Chytil, Jiří Másilko, Jitka Krouská and Jaromír Wasserbauer.

I am also grateful to family for support during last years. My final thanks go to Radek for his love, support, encouragement and patience.

CONTENT

1 OBJECTIVES OF THIS THESIS

This thesis is concerning the rheological properties of cement based systems, where the self-compacting concretes, their matrixes and the cement pastes are involved. The aims of this thesis are following:

- literature research about rheological properties of the cement based materials
- investigation of the static yield stress via several methods
- observation of effects of water to cement ratio and superplasticizer dosage on rheological properties of fresh cement materials
- study of properties of cement pastes during first hours of hydration

2 INTRODUCTION

Since civilization first start to build, the human race has sought materials that bind stones into solid formed mass. After the discovery of Portland cement in 1824, concrete has become the most commonly used structural material in modern civilization. The quality of the concrete structure is of course dependence on the quality of each constituent used in the concrete mixture. However, this is not the only controlling factor. The quality also depends very much on the rheological properties of the fresh concrete during placement into the formwork.

The rheology of concrete is often characterized by its workability. The workability of concrete is a performance index representing how easily it is constructed when used in actual structures and is a collective term of general performance that includes easiness of being mixed, transportability, void-filling ability, compactibility, finishability and resistance against segregation.

The rheological properties of fresh concrete are related to cement hydration and chemical interactions in the cement paste system. In addition, the rheological propoerties of concrete are also dependent on the aggregates contained in the mixture. But the evolution of the rheological properties at early ages depends almost entirely on the cement paste.

During the course of time, empirical test method of different types and quality have been developed and used to give some kind of rheological description of the fresh concrete. From basic tests like slump flow up to using the viscometers and advanced rheometers, which are very sensitive and give fundamental physical quantities. A standart method to estimate the setting time of the cement paste is the Vicat test. Although this test is widely used, there is only scarce literature dealing with the correlation of the test results with any physical or mechanical properties of tested material.

This thesis is focused on the rheological properties of cement based systems. First part is concerning the self-compacting concrete and their matrixes and second part is regarding the cement pastes. In addition the cement pastes were studied during first hours of hydration via calorimetry, X-ray powder diffractometry and scanning electron microscope.

3 THEORETICAL PART

3.1 Rheology

The rheology is the study of deformation and flow of matter. Rheology, as an independent branch of natural sciences, emerged more than 70 years ago. It is branch of physics (and physical chemistry) since the most important variables come from the field of mechanics. The term „rheology" originates from the Greek „rheos" meaning the river, flowing, streaming. Thus, rheology is literally „flow science". However, rheological experiments do not merely reveal information about the flow behavior of liquids, but also the deformation behavior of solids. The connection here is that a large deformation produced by shear forces cause many materials to flow [1, 2, 3].

3.1.1 Newtonian and non-Newtonian fluids

The two-plates model is used to define some fundamental rheological parameters (Fig. 1). The upper plate with the shear area A [m^2] is set in motion by the force F [N] and the resulting velocity v [m/s] is measured. The lower plate is stationary (v = 0). The distance h [m] is the distance between the plates and the liquid sample is sheared in the shear gap. It is assumed that the following shear conditions are existing [3]:

- The sample adheres to both plates and does not slide or slip along them.
- There are laminar flow conditions (i.e. flow in the form of layers), therefore no turbulent flow is occurring.

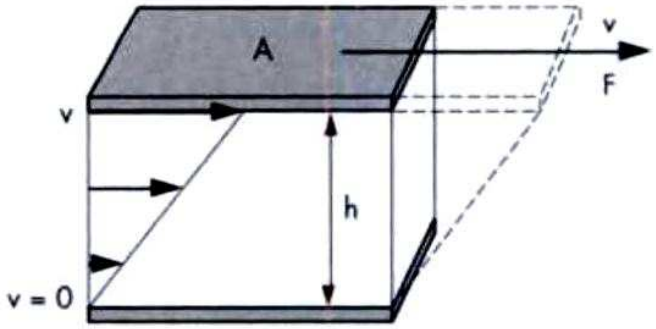

Fig. 1: Flow velocity of a fluid using the two-plates model for shear tests [3]

Each individual arrow symbolizes an individual flowing layer. The layers are moving along each other. Of course, this process happens without showing turbulent behavior. The real geometric conditions in the measuring system of a rheometer are not as simple as in the two-plates model. However, if the shear gap is narrow enough, the necessary requirements are fulfil and the determination for the following rheological parameters can be used.

The shear stress τ and shear rate $\dot{\gamma}$ are defined as (Fig. 1):

$$\tau = \frac{F}{A} \tag{1}$$

$$\dot{\gamma} = \frac{v}{h} \tag{2}$$

Sometimes the following terms are used as synonyms to shear rate: shear gradient, velocity gradient, strain rate, rate of deformation.

The definition of shear rate using differential variables has following form:

$$\dot{\gamma} = \frac{\mathrm{dv}}{\mathrm{dh}} \tag{3}$$

with the infinitely (differentially) small velocity difference dv between two neighbouring flowing layers and the infinitely (differentially) small thickness dh of one individual flowing layer.

For laminar and ideal viscous flow, the difference in velocity between neighbouring layers shows the same value (dv = const) since the velocity v(h) decreases linearly in the shear gap between the plates. All the layers are assumed to have the same thickness (dh = const). Therefore, the shear rate is showing a constant value everywhere between the plates [3].

The resistance which arises from the lack of slipperiness of the parts of the liquid, other things being equal is proportional to the velocity with which the parts of the liquid are separated from one another. This lack of slipperiness is what we call viscosity. It is synonymous with internal friction and is a measure of resistance flow [1].

Ideal viscous (or Newtonian) flow behavior is described formally using Newton's law [2, 3, 4]:

$$\tau = \eta \cdot \dot{\gamma} \tag{4}$$

where η is called the dynamic viscosity [Pa.s], which is qualitavely the property of a material to resist deformation increasingly with increasing rate of deformation. The dynamic viscosity divided by the density of the material is called kinematic viscosity. The shear stress divided by rate of shear when this quotient is dependent on the rate of shear is called as apparent viscosity [3].

According to the acceptance of the Newton´s law, the Newtonian and non-Newtonian fluids are distinguished. The Newtonian behaviour in experiment conducted at constant temperature and pressure has the following characteristic:

- The only stress generated in simple shear flow is the shear stress.
- The shear viscosity does not vary with shear rate.
- The viscosity is constant with respect to the time of shearing and the stress in the liquid falls to zero immediately the shearing is stopped. In any subsequent shearing, however long the period of resting between measurements, the viscosity is as previously measured.
- The viscosities measured in different types of deformation are always in simple proportion to one another, so, for example, the viscosity measured in a uniaxial extensional flow is always three times the value measured in simple shear flow.

A liquid showing any deviation from the above behavior is non-Newtonian [1].

3.1.2 Behavior of non-Newtonian liquid

The relationship between shear stress and shear strain is called the flow curve, and can take a variety of forms, as shown in Fig. 2. The simplest form is a straight line passing through the origin. This is called Newtonian behaviour, and is a characteristic of most simple liquids, such as water, white spirit, petrol, lubricating oil, etc., and of many true solutions, e.g. sugar in water. The other forms of flow curves in Fig. 2 all intercept the shear stress axis at some positive, non-zero value, i.e. flow will only commence when the shear stress exceeds this threshold value, which is often called the yield stress. A wide range of equations have been proposed to model the various shapes of flow curves found in practice [5].

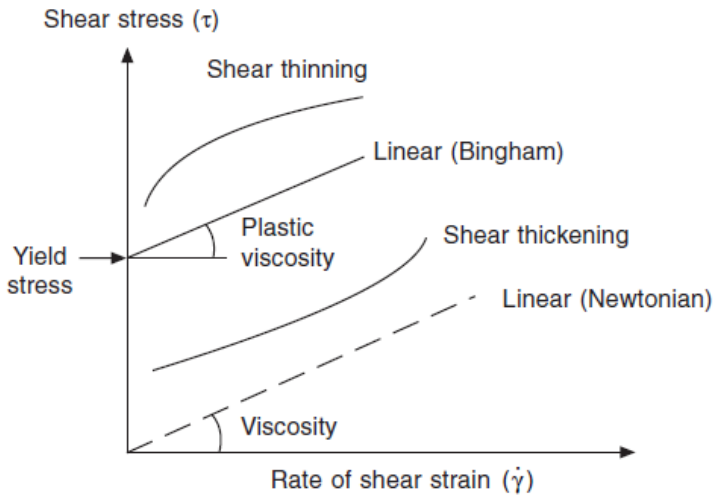

Fig. 2: Types of flow curves [5]

3.1.2.1 Shear-thinning liquid

In the vast majority of cases, the viscosity was found to decrease with increase in shear rate, giving rise to what is now generally called shear-thinning behavior although the terms temporary viscosity loss and pseudoplasticity have also been employed. For shear-thinning materials, the general shape of the curve representing the variation of viscosity with shear stress is shown in Fig. 3. The corresponding graphs of shear stress against shear rate and viscosity against shear rate are also given [1,3].

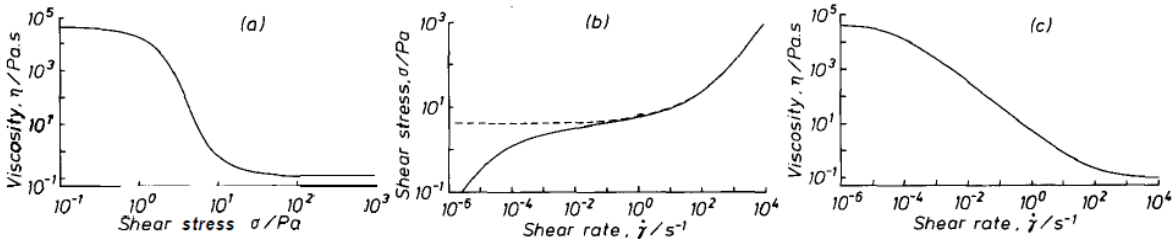

Fig. 3: Typical behavior of shear-thinning fluids. (a) Viscosity versus shear stress. Notice how fast the viscosity changes with shear stress in the middle of the graph; (b) Shear stress versus shear rate. Notice that, in the middle of the graph, the stress changes very slowly with increasing shear rate. The dotted line represents ideal yield-stress (or Bingham plastic) behaviour; (c) Viscosity versus shear rate. Notice the wide range of shear rates needed to traverse the entire flow curve. [1]

Examples of shear-thinning materials are polymer solutions and melts, suspensions of unsymmetrical particles, pastes, paints and other [6].

3.1.2.2 Shear-thickening liquid

We shall see that there are cases (albeit few in number) where the viscosity increases with shear rate. Such behavior is generally called shear-thickening although the term dilatancy has also been used. Typical examples of the shear-thickening phenomenon are given in Fig. 4. It will be observed that shear-thickening region extends over only about a decade of shear rate. In almost all known cases of shear-thickening, there is a region of shear-thinning at lower shear rates [1].

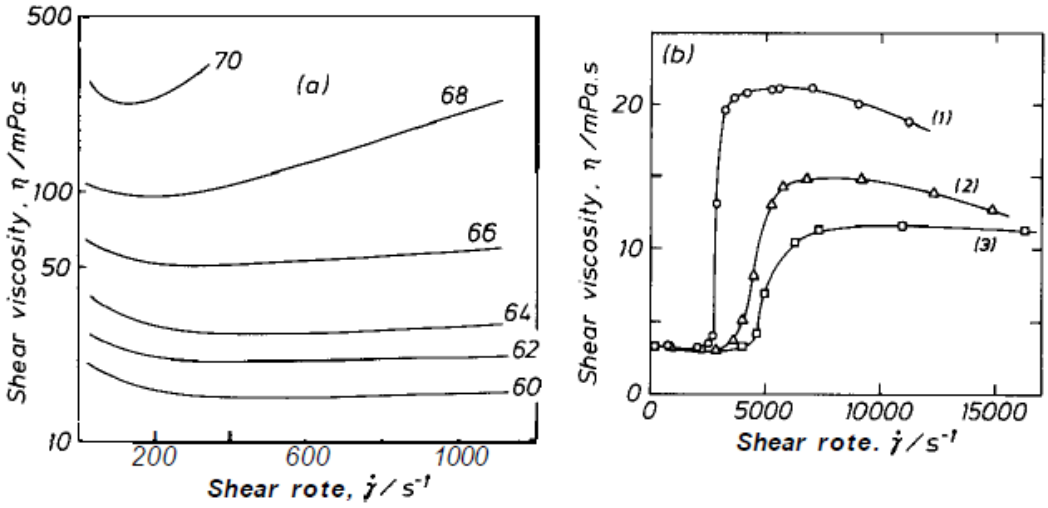

Fig. 4: Examples of shear-thickening behavior: a) polymer solution, b) aqueous suspensions of solid particles [1]

For dispersions, shear-thickening flow behavior should be taken into account at high particle concentrations and at high shear rates. Shear-thickening materials are much less common in industrial practice compared to shear-thinning materials. Nevertheless, shear-thickening behavior is desirable for special applications and is therefore encouraged in these cases. Usually, however, this behavior is undesiderable and it should never be ignored since this may lead to enormous technical problems and in some cases to the destruction of equipment, e.g. pumps or stirrers [3].

Examples of shear-thickening materials are dispersions with high concentration of solid matter or gel-like particle, ceramic suspensions, printing inks, honey and other [6].

3.1.2.3 Bingham liquid

By definition, Bingham liquids will not flow until a critical yield stress is exceeded. The Bingham equation describes the shear stress/shear rate behavior of many shear-thinning materials at low shear rates, but only over a one-decade range of shear rate [1]. As a Bingham fluid is represented some suspensions, slurries, oil paints etc. [6].

3.1.3 Thixotropic behavior and structural breakdown

Some materials have reversible time dependence, where the flow characteristics are influenced by the shear history of a material. At rest the material regains its original state. These types of materials are usually defined as thixotropic [7].

The accepted definition of thixotropy is according to Barnes [1] a gradual decrease of the viscosity under shear stress followed by a gradual recovery of structure when the stress is removed. Additional definitions of thixotropy are given in [8].

The phenomenon of thixotropy rises from the microstructure of the matrix system, due to aggregation and flocculation of suspended particles and the time taking to change this microstructure. In such a system, interaction occurs between the particles as a result of the attraction due to van der Waals forces and repulsion due to electrostatic and steric effects. The stability of the structure depends upon the existence of a potential energy barrier which prevents the particles from approaching close to one another. In this way, the weak physical bonds between particles give rise to aggregation. As the suspension is sheared, the weak

physical bonds among particles are ruptured, and the network among them breaks down into separate aggregates, which can disintegrate further into smaller fragments, whereas if the suspension is at rest the particle aggregation can re-flocculate and form again. These shear induced changes in microstructure take time and, if fully reversible, are referred to as thixotropy [7].

The term structural breakdown was made by Tattersal in 1954. Because no recovery in torque was measured in the corresponding experiment, structural breakdown was considered to be a different phenomenon than thixotropic behavior. The mechanism of structural breakdown is attributed to the process of breaking certain linkages between the cement particles, which are assumed to be formed by the hydration process. The breaking of linkages was considered to be an irreversible process and thus non-thixotropic. The time for structural breakdown is normally shorter than the time for structural build-up [9].

3.1.4 Rheological models

Fluids that have a viscosity dependent on shear rate exhibit non-Newtonian behavior. This behavior is difficult to describe with simple model. Equations that predicted the shape of the general flow curve need at least four parameters. One such is the Cross equation given by [1,3]:

$$\frac{\eta-\eta_\infty}{\eta_0-\eta_\infty}=\frac{1}{1+(\mathrm{K}\dot{\gamma})^{\mathrm{m}}} \tag{5}$$

where η_0 and η_∞ refer to the asymptotic values of viscosity at very low and very high shear rates respectively, K is a constant parameter with the dimension of time and m is a dimensionless constant. A popular alternative to the Cross model is the model due to Carreau:

$$\frac{\eta-\eta_\infty}{\eta_0-\eta_\infty}=\frac{1}{(1+(\mathrm{K}\dot{\gamma})^2)^{\mathrm{m}/2}} \tag{6}$$

where K and m have similar significance to the K and m of the Cross model. It is informative to make certain approximations to the Cross model, because if so doing, we can introduce a number of other popular and widely used models. For example for $\eta << \eta_0$ and $\eta >> \eta_\infty$ the Cross model reduces to form which with simple redefinition of parameters can be written:

$$\eta=\mathrm{K}_2\cdot\gamma^{\mathrm{n}-1} \tag{7}$$

This is the well known power-law model and n is called the power-law index, K_2 is called the consistency. Further if $\eta << \eta_0$ we obtain the Sisko model:

$$\eta=\eta_\infty+\mathrm{K}_2\dot{\gamma}^{\mathrm{n}-1} \tag{8}$$

If n is set equal to zero in the Sisko model, we get form which with simple redefinition of parameters can be written:

$$\tau=\tau_0+\eta_{\mathrm{p}}\dot{\gamma} \tag{9}$$

where τ_0 is yield stress and η_{p} is plastic viscosity. This is the Bingham model equation [1].

We can find other models in literature, for example [10]:

Herschel-Bulkley: $\tau=\tau_0+\mathrm{K}_2\dot{\gamma}^{\mathrm{n}}$ (10)

Robertson Stiff: $\tau=\mathrm{X}\cdot(\dot{\gamma}+\mathrm{Y})^{\mathrm{n}}$ (11)

Casson: $\tau^{1/2}=\tau_0^{\,1/2}+(\eta_{\mathrm{p}}\cdot\dot{\gamma})^{1/2}$ (12)

Eyring: $\tau=\mathrm{X}\cdot\sinh^{-1}\cdot(\mathrm{Y}\cdot\dot{\gamma})$ (13)

DeKee: $\tau = \tau_0 + \eta_p \cdot \dot{\gamma} \cdot e^{-\alpha\gamma}$ (14)

VomBerg: $\tau = \tau_0 + Y \cdot \sinh^{-1} \cdot \left(\frac{\dot{\gamma}}{Z} \right)$ (15)

where X, Y a Z are constants, α is a time dependent parameter.

Turian et al. [11] investigated the rheology of concentrated aqueous slurries of titanium dioxide, laterite, gypsum and silica flour. The power law, Bingham, Casson, Herschley-Bulkey and Sisko models were tested. The Sisko model which combines low- and intermediate shear power law with high shear Newtonian limiting behavior, was found to provide the best overall description of the flow curves for all slurries, at all solid loadings and over the entire range of shear rates.

3.1.5 Rheology of suspension

The rheology of suspensions has been subject of serious research for many years, mainly because of its obvious importance in a wide range of industrial applications. Two key factors affect this behavior, the volume fraction of solid particles in the suspension and the extent to which the particles are agglomerated or flocculated. Increasing the volume fraction of solid ϕ causes a considerable increase in viscosity. The effect of solids volume fraction on viscosity was recognized by Einstein, who proposed the relationship [12]:

$$\eta_s = \eta_c (1 - 2{,}5\phi) \quad (16)$$

where η_s is the viscosity of the suspension and η_c is the viscosity of the fluid phase. Because of non-Newtonian character of suspension, it should be used apparent viscosity in the previous equation. However, it was later realized that this equation only applies at quite low volume fractions. As the volume fraction is increased above a few percent, viscosity increases progressively from that predicted by eq. 16. Several equations have been proposed to better describe the full relationship between volume fraction and viscosity and one used extensively in colloidal suspensions was proposed by Kriger and Dougherty [1]:

$$\eta_s = \eta_c \left(1 - \frac{\phi}{\phi_m} \right)^{-[\eta]\phi_m} \quad (17)$$

where ϕ_m is the maximum possible volume fraction for the particular assemblage of particles, which has a value of 65 % for randomly close-packed spheres. The other parameter $[\eta]$ is intrinsic viscosity, defined as:

$$[\eta] = \lim_{\phi \to 0} \frac{\eta/\eta_c - 1}{\phi} \quad (18)$$

The intrinsic viscosity is 2.5 for spherical particles. Eq 17 correctly predicts the substantial increase in viscosity observed during increasing the volume fraction of solid to ϕ_m. The other factor affecting flow behavior is the extent to which particles are flocculated or dispersed. Flocculation is especially important for colloidal particles (particles smaller than 1 μm) which may flocculate spontaneously. Flocculated particles either form discrete aggregates or a gel. The forces are often fairly weak and easily broken by shear, so enough stress can be applied to cause disruption of the flocculated network such that the suspension begins to flow. The stress at which such a breakdown occurs is called the yield stress. Thus, the flocculation produces plastic behavior with the yield stress reflecting the forces holding particles together [12].

3.2 Cement

Cement is a hydraulic binder, i.e. a finely ground inorganic material which, when mixed with water, forms a paste which sets and hardens by means of hydration reactions and processes and which, after hardening, retains its strength and stability even under the water [13].

Portland cement is made by heating a mixture of limestone and clay, or other materials of similar bulk composition and sufficient reactivity, ultimately to a temperature about 1450 °C. Partial fusion occurs and nodules of clinker are produced. The clinker is mixer with a few percent of gypsum and finely ground to make the cement. The clinker typically has a composition in the region of 67 % CaO, 22 % SiO_2, 5 % Al_2O_3, 3 % Fe_2O_3 and 3 % of other components [14,15].

The abbreviations most widely used are as follows:

C = CaO	S = SiO_2	A = Al_2O_3
F = Fe_2O_3	$\overline{S}$ = SO_3	H = H_2O
N = Na_2O		

The major phases of Portland cement are tricalcium silicate (C_3S), dicalcium silicate (C_2S), tricalcium aluminate (C_3A) and ferrite phase of average composition C_4AF. In a commercial clinker they do not exist in a pure form. The C_3S phase is a solid solution containing Mg and Al and is called alite. In the clinker, it consists of monoclinic or trigonal forms whereas synthesized C_3S is triclinic. The C_2S phase occurs in the β form, termed belite, and contains in addition to Al and Mg, some K_2O. Four forms α, ά, β, and γ of C_2S are known although in clinker only the β form with a monoclinic unit cell exists. The ferrite phase, designed C_4AF, is a solid solution of variable composition from C_2F to C_6A_2F. In some clinkers small amounts of calcium aluminate of formula NC_8A_3 may also form [12].

3.3 Self-compacting concrete (SCC)

Awareness of self-compacting concrete (SCC) within the construction industry has grown year on year since it was developed in Japan in the late 1980s [16], and the quest for further understanding as to its capabilities and limitations has generated considerable interest in research worldwide.

SCC also known as self-consolidating concrete is a highly flowable concrete that can spread into place under its own weight and achieve good consolidation in the absence of vibration without exhibiting defects due to segregation and bleeding [17].

Feature/benefit analysis on the use of SCC would suggest that the following benefits should result [18]:

- increased productivity levels leading to shortened concrete construction time
- lower concrete construction costs
- improved working environment
- improvement in environmental loadings
- improved in-situ concrete quality in difficult casting conditions
- improved surface quality

Self-compacting concrete was developed to achieve durable concrete structures. The method for achieving self-compactibility involves not only high deformability of paste or mortar, but also resistance to segregation between coarse aggregate and mortar when the concrete flows through the confined zone of reinforcing bars [19].

According to The European Guidelines for Self-Compacting Concrete the SCC [20] is classified (via properties of fresh SCC- slump flow (SF), T_{500},...) into the following groups (Table 1 and 2). Slump-flow value describes the flowability of a fresh mix in unconfined conditions. It is a sensitive test (Fig. 5) that will normally be specified for all SCC, as the primary check that the fresh concrete consistence meets the specification. The test consists in filling a slump cone with the mixture without compaction, then the cone is lifted and the slump flow is final diameter of spread. The time to reach a spread of 500 mm is also measured.

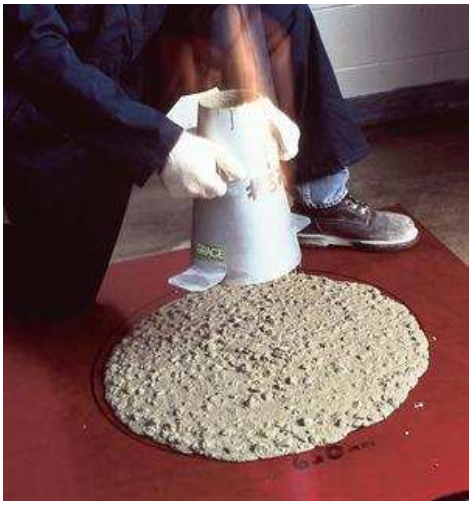

Fig. 5: The slump flow test [21]

The value of slump flow is related to the yield stress of fresh cement based materials [22,23], where the mini-cone was used for testing of fresh paste mixtures derived from SCC and evaluation of workability was done according to the formula:

$$\tau_0 = \frac{225 g \rho V_c^2}{4\pi^2 D_f^5} \tag{19}$$

where ρ, g, V_c and D_f are the density, the gravity, the conical volume and the final spread diameter respectively. Roussel et al. [23] showed that the model does not allow predicting low yield stresses because of surface effects. This means that small yield stress may be relevantly measured in this way by improving the wetting between the sample and the solid surface. Ideally, with a perfect wetting, infinitely small yield stress might be measured [24].

Table 1: Classification of SCC according to slump flow values SF [20]

	Properties and applications
SF1 (550 - 650 mm)	Unreinforced or slightly reinforced concrete structures that are cast from the top with free displacement from the delivery point (e.g. housing slabs). Casting by a pump injection system (e.g. tunnel linings). Sections that are small enough to prevent long horizontal flow (e.g. piles and some deep foundations).
SF2 (660 - 750 mm)	Suitable for many normal applications (e.g. walls, columns).
SF3 (760 – 850 mm)	Typically produced with a small maximum size of aggregates (less than 16 mm) and is used for vertical applications in very congested structures, structures with complex shapes, or for filling under formwork.

Target values higher than 850 mm may be specified in some special cases but great care should be taken regarding segregation and the maximum size of aggregate should then normally be lower than 12 mm.

Viscosity can be assessed by the T_{500} time during the slump-flow test or assessed by the V-funnel flow time. The time value obtained does not measure the viscosity of SCC but is related to it by describing the rate of flow. Concrete with a low viscosity will have a very quick initial flow and then stop. Concrete with a high viscosity may continue to creep forward over an extended time.

Viscosity (low or high) should be specified only in special cases such as those given below. It can be useful during mix development and it may be helpful to measure and record the T_{500} time while doing the slump-flow test as a way of confirming uniformity of the SCC from batch to batch.

Table 2: Classification of SCC according to T_{500} values [20]

	Properties and applications
VS1/VF1 ($T_{500} \leq 2$ s)	Good filling ability even with congested reinforcement. Capable of self-levelling. Generally the best surface finish. More likely to suffer from bleeding and segregation.
VS2/VF2 ($T_{500} > 2$ s)	No upper class limit but with increasing flow time it is more likely to exhibit thixotropic effects, which may be helpful in limiting the formwork pressure or improving segregation resistance. Negative effects may be experienced regarding surface finish (blow holes) and sensitivity to stoppages or delays between successive lifts.

3.4 Superplasticizer

Superplasticizers (SP), also known as high range water reducers, are chemicals used as admixtures where well-dispersed particle suspensions are required. These polymers are used as dispersants to avoid particle aggregation and to improve the flow characteristics of suspensions such as in concrete applications [25].

The basic advantages derived from the use of SP are follows [26]:

- Production of concrete having high workability for easy placement without a reduction in cement content or strength.
- Production of high strength concrete with normal workability, but with lower water content expressed by water to cement ratio w/c (w/c is the ratio of weight of water to the weight of cement used in concrete mixture).
- The possibility of making a mix having a combination of better than normal workability and lower than normal amount of water.
- Designing a concrete mix with less cement, but having the normal strength and workability.

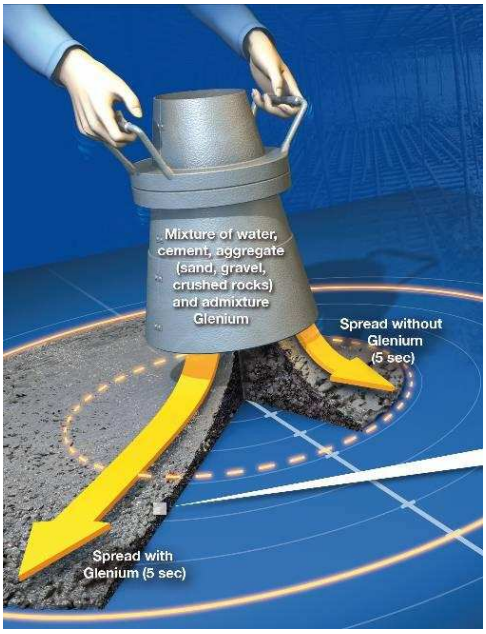

Fig. 6: Effect of SP on slump flow of cement system [27]

SP are linear polymers containing sulfonic acid groups attached to the polymer backbone at regular intervals. Most of the commercial formulations belong to one of four essential families [28, 29]:

- Sulfonated melamine-formaldehyde condensates (SMF)
- Sulfonated naphthalene-formaldehyde condensates (SNF)
- Modified lignosulfonates (MLS)
- Polycarboxylate derivates

The mode of action of SP involves surface adsorption, dispersion of the particles in the aqueous phase assisted by electrostatic repulsion and steric repulsion [26]. Effect of SP is shown on Fig. 6 and Fig. 7 where SP is used to increase the slump at a given w/c.

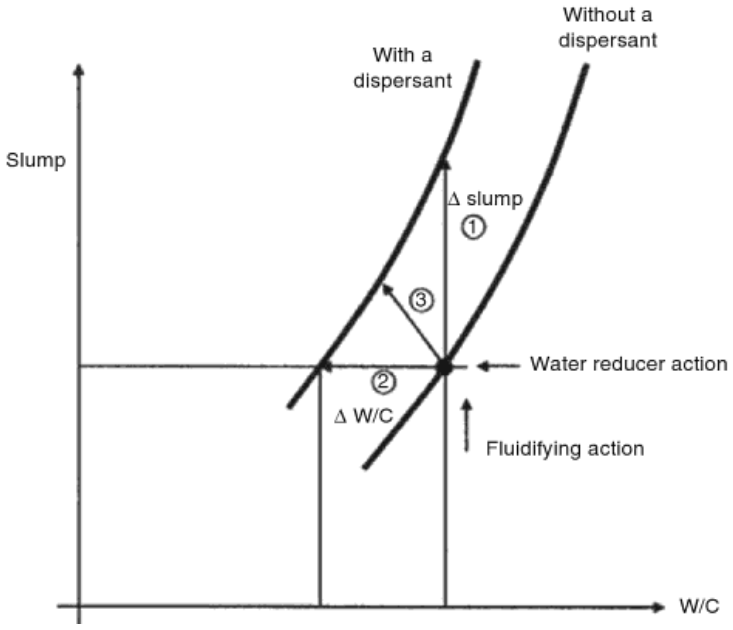

Fig. 7: Different uses of SP (1 to increase the slump at a given w/c, 2 to lower w/c for a given slump and 3 to increase the slump and decrease w/c at the same time)

The rate of hydration of cement is influenced by SP. The reported data on the effect of SP on the hydration are contradictonary because of the variations in the materials and conditions. There is a general consensus that SNF and SMF retard the hydration of C_3A. Hydration of C_3S is known to be retarded by the SP. There is also evidence that the C/S ratio of the C-S-H phase changed. In cements, the hydration of the C_3S phase is retarded, but to a lesser extent than when hydrated in the pure form because part of the admixture is adsorbed by the C_3A phase. Formation of ettringite may be accelerated or retarded by SP, depending on the amount of alkali sulfates present in cement [26].

3.5 Rheology of cement based systems

Rheology is the logical tool to characterize and describe the flow behavior, thickening, workability loss, stability and even compactability of fresh cement based particle suspension such as cement paste, mortar and concrete. To apply this tool, one has to be able to evaluate and choose material parameters of importance and to be able to obtain information about them, for example through testing. A great deal of effort has been spent on obtaining accurate and repeatable data on the rheological material parameters. Although the same trend and behavior is generally attained by different types of devices, the absolute value can however differ somewhat [30].

Rheological studies on cement pastes and concrete have been reviewed in books and several articles. The results in the literature show wide variations, many of which reflect the large effects of seemingly minor differences in experimental technique. Since the cement pastes do not show Newtonian behaviour, methods giving only a single parameter are inadequate [15].

For example Yaiha and Khayat [31] evaluated the effectiveness of various rheological models to estimate yield stress of high-performance cement grouts containing supplementary cementitious materials and rheology-modifying admixtures. The rheological models considered in the investigation included Bingham, Casson, Herschel-Bulkey and De Kee as well as a model propsed by the authors. Different estimates of yield stress were obtained when using the different models. The Bingham model resulted in higher yield stress estimates than the other models, while the Herschel-Bulkey model resulted in the lowest values for all tested mixtures.

Numerous researchers have successfully used the Bingham equation for characterization of rheological behavior of cement paste [32, 33, 34]. This model is applicable for most of mortars and concrete [35]. The validity of the Bingham equation has been verified [36] using different types of rheometers (BML, BTRHEOM, CEMAGREF-IMG, IBB, two-point) and different concrete compositions in international test at French laboratories. In another work the Bingham model and the Herschel-Bulkley model have received wide acceptance for characterization of fresh concrete [37].

This means, that values of two constants, yield stress and plastic viscosity, are necessary to define the behaviour of cement based systems. The first property providing a measure of shear stress required to initiate flow and second one a measure of the material resistance to flow after the material begins to flow [38].

In case of self compacting concrete, due to the addition of plasticizer or superplasticizer, it is known that the yield stress is much lower, compared to traditional concrete (Fig. 8) [5]. In order to maintain the stability of the concrete – to avoid segregation – the plastic viscosity must be higher, which can be achieved in several ways. It has been shown [39] that stability

against particle sinking in concrete at rest is much more sensitive to changes in static yield stress than to changes in plastic viscosity.

Due to the low yield stress, deviations from the Bingham model can occur, causing an apparent negative yield stress when using traditional rotational viscometry and resulting in a non-linear relationship between shear stress and shear rate. In Belgium and some surrounding countries, the shear thickening effect has been discussed and as a result the Bingham model is mostly not applicable in these cases [40]. In some cases such observations could be due to the insufficient evaluation of the equilibrium torque conditions during viscometer measurement, something that is not always reported [41]. Shear thickening is described in the literature as an increase in apparent viscosity with increasing shear rate. Two possible theories are considered to be applicable on SCC and their shear thickening behavior. One is based on the formation of clusters and the other is based on grain inertia [42].

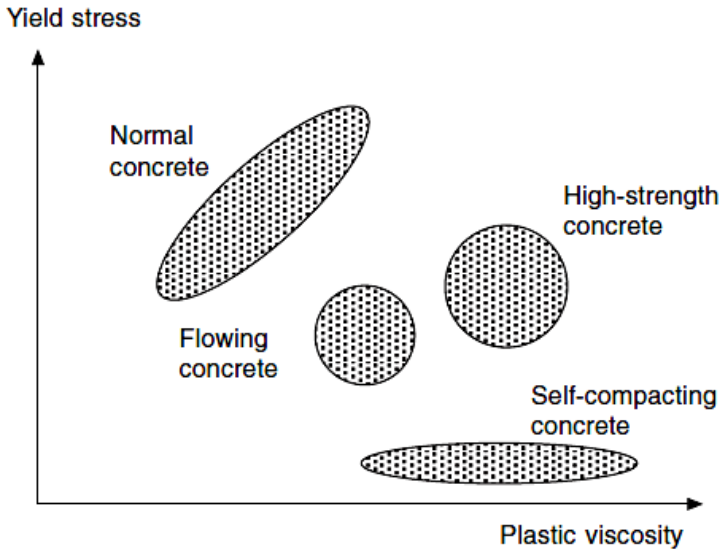

Fig. 8: Rheology of several types of concrete [5]

3.5.1 Factors affecting the rheology of cement based system

Some important factors affecting rheology of cement based system are summarized as follows [43, 44, 45, 46]:

- water-cement ratio
- chemical composition of cement
- chemical reactivity of filler
- particle size distribution, specific gravity, surface texture and geometrical shape of particles
- properties of chemical admixtures
- hydration time
- temperature and humidity of place where the paste is prepared and placed
- initial mixing conditions, such as mixing procedure, mixer type, speed, duration and capacity
- testing procedure such as test duration, measuring elements, geometry of the test accessory...

It has been shown that the most important of the factors listed above are the w/c ratio and specific surface. Studies performed on cement pastes of different chemical composition

indicated this factor bears a less effect on the rheology than w/c or fineness of cement [44, 47]. Type of superplasticizer will, however, also influence the flow properties of cementitious pastes due to their dependencies in cement chemistry, different dispersing mechanisms and retarding effects on the cement paste [48, 49, 50].

We should also recognize that irrespective of the absolute Bingham's parameters, it is equally important to know, how these parameters vary with the concrete's component materials, mix proportions etc. There is a considerable amount of published information on this, Fig. 9 is a schematic summary of typical effects of varying a number of factors individually, complied from several sources [5].

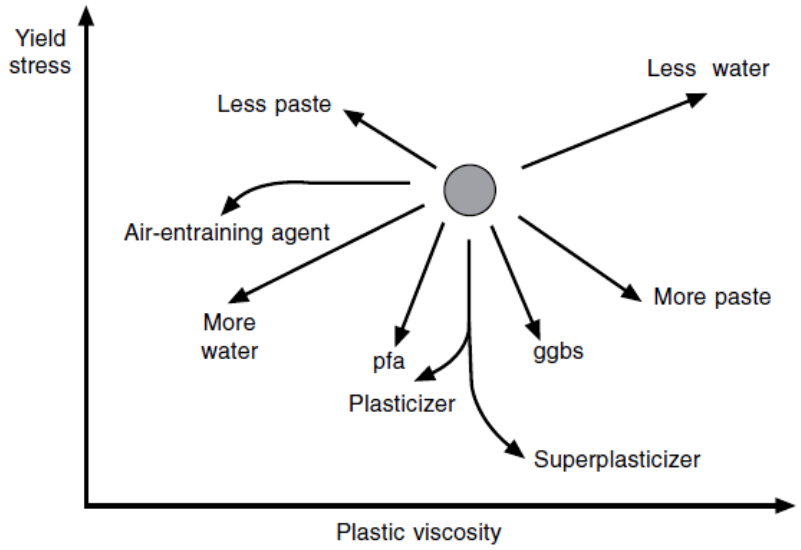

Fig. 9: Summary of the effect of varying the proportions of concrete constituents on the Bigham constants [5]

Typical values of yield stress and plastic viscosity for some cementitious materials, defined by the Bingham model, are shown in Table 3.

Table 3: Typical range of yield stress and plastic viscosity for cement paste, *mortar, "normal"* concrete (NC and flowing NC), and SCC, defined by the Bingham model [7]

	Cement paste	Mortar	NC	Flowing NC	SCC
τ_0 [Pa]	10-50	10-100	400-2000	100-400	10-100
η_p [Pa.s]	0.01-1	1-5	50-100	20-100	20-150

3.5.2 Thixotropy of cement based system

Thixotropy of cementitious materials is quantified by measuring of thixotropic loop (Fig. 10). This method is based on the fact, that because of the transient nature of thixotropy and the dependency of specific rheological properties on the flow history, the stress/shear rate curves measured successively in a viscometer during increasing and decreasing sequences of applied shear rates will not superimpose. During the increasing shear rate ramp, de-flocculation occurs but not quickly enough to reach the steady state shear stress. The measured stress is thus always higher than what would be obtained if steady state was reached. On the other hand, during the decreasing shear rate ramp, flocculation occurs but here again not quickly enough for steady state to be reached and the measured stress stays

lower than steady state. The area between the two curves is measured and is considered as representative of the work done per unit time and unit volume of the cement material to break some of the initially present linkages. It has to be noted that, in the case of a succession of shear rate steps, the loop appears only if the duration of the applied shear rate step is of course not sufficient for steady state to be reached [51].

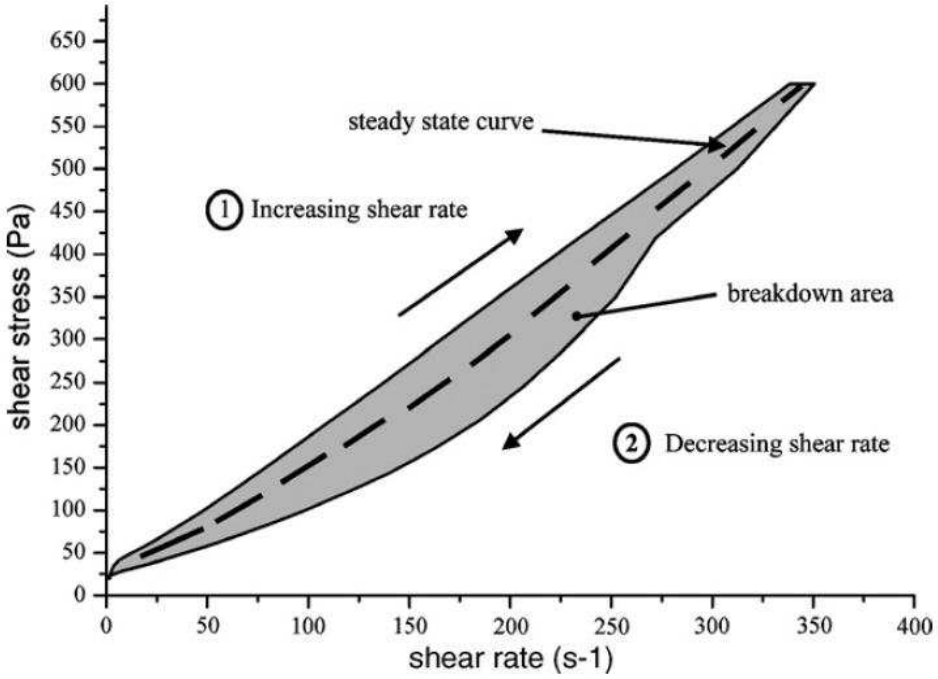

Fig. 10: Example of thixotropic loop obtained with a cement paste submitted successively to increasing and decreasing shear rate ramps [51]

3.5.3 Dynamic and static yield stress

Yield stress is dictated by the structure and strength of the network of cement particles interaction [52, 53]. Accumulated experimental and numerical evidence show that network rupture in particle suspension occurs when its initial structure has been sufficiently modified, namely for a critical strain γ_c [54]. This critical strain and the yield stress should then be releated by:

$$\tau_0 = G \cdot \gamma_c \tag{20}$$

where G is the shear elastic modulus as long as we assume a linear elastic behavior in the solid regime below the yield stress [55].

One common method of obtaining yield stress value is to extrapolate the shear stress versus shear rate curve back to the shear stress intercept at zero shear rate. Values obtained using this method will be strongly influenced by the rheological model (Bingham, Herschel-Bulkeley, etc. – see chapter 3.3) and shear range selected to represent the data [56].

The yield stress, measured in an undisturbed sample, is the static yield stress (Fig. 11). The yield stress of a completely broken down sample, often determined from extrapolation of the equilibrium flow curve, is the dynamic yield stress (Fig. 11). A static yield stress may be significantly higher than the dynamic yield stress. The idea of a static and dynamic yield stresses can be explained by assuming there are two types of structure in a thixotropic materials. One structure is insensitive to shear rate and serves to define the dynamic yield stress associated with equilibrium curve. A second structure, the weak structure, forms over a

certain period of time when the sample is at rest. Combined, the two structures cause a resistance to flow which determines the static yield stress [56].

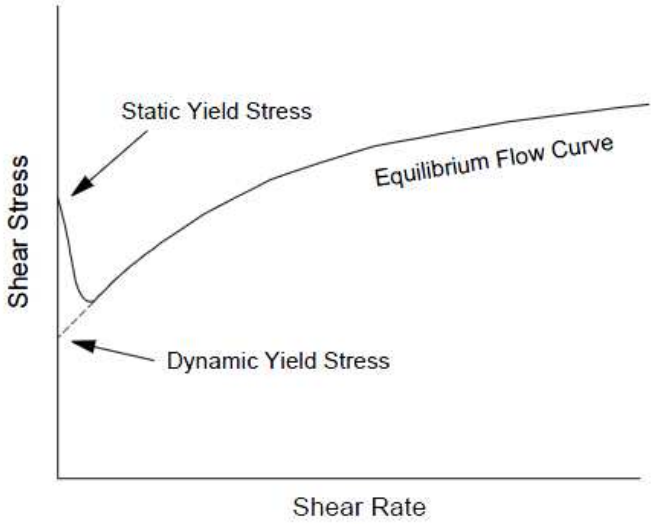

Fig. 11: Static and dynamic yield stress [56]

3.5.4 Yield value and cement based systems

When discussing the rheology of concrete in its fresh state, the dynamic yield stress τ_0 (Pa), is normally referred to as the stress needed to make the concrete flow or, in other words, describing the concrete resistance to flow. However, since the dynamic yield stress is the equilibrium value for a concrete in motion it is probably even better to use this value as the limit of concrete flowability, i.e., the stress needed to stop the flow rather than the concrete resistance to flow. That is why the dynamic yield stress of a SCC in general correlates well to its slump-flow value [57].

Instead, a more correct value of the stress needed to make a concrete flow from a state of rest is static yield value. This is the stress level necessary to exceed in order to break the structure within a concrete at rest and go from elastic via visco-elastic, visco-plastic to plastic behaviour.

So, the dynamic yield stress is of interest when considering flow properties and planning of formwork filling, pumping etc. The static yield stress and how this develops in the concrete at rest, is instead important for issues such as form pressure, time between casting of concrete layers, the time a SCC can be left at rest in a skip before emptying it etc. [57]. As already briefly mentioned, static yield stress is also important for the stability at rest with respect to sinking of aggregate particles.

3.6 Hydration of cement based systems

In cement chemistry, the term „hydration“ denotes the totality of changes that occur when an anhydrous cement, or one of its constituent phases, is mixed with water. The chemical reactions taking place are generally more complex than simple conversions of anhydrous compounds into the corresponding hydrates [15].

Chemically, the hydration of Portland cement consists of series of reactions between individual clinker materials, calcium sulfate and water, which proceed both simultaneously and successively at different rates and influence each other. The progress of the process depends on [13]:

- The rate of dissolution of the involved phases
- The rate of nucleation and crystal growth of the hydrates to be formed
- The rate of diffusion of water and dissolved ions through the hydrated material already formed

Knowledge of the hydration behavior of individual cement compounds and their mixtures forms a basis for interpreting the complex reactions that occur when Portland cement is hydrated under various conditions.

Tricalcium silicate and dicalcium silicate together make up 75 – 80 % of Portland cement. In the presence of a limited amount of water, the reaction of C_3S with water is represented as follows [12]:

$$3\ CaO{\cdot}SiO_2 + x\ H_2O \rightarrow yCaO{\cdot}SiO_2{\cdot}(x+y-3)H_2O + (3-y)Ca(OH)_2 \quad (21)$$

or typically

$$2[3CaO{\cdot}SiO_2] + 7\ H_2O \rightarrow 3\ CaO{\cdot}2SiO_2{\cdot}4H_2O + 3\ Ca(OH)_2 \quad (22)$$

The above chemical equation is somewhat approximate because it is not easy to estimate the composition of C-S-H and there are also problems associated with the determination of $Ca(OH)_2$. In a fully hydrated cement or C_3S paste, about 60-70 % of solid comprises C-S-H [12].

The mechanism of hydration of individual cement components and that of cement itself has been a subject of much discussion and disagreement. In the earliest theory, Le Chatelier explained the cementing action by dissolution of anhydrous compounds followed by the precipitation of interlocking crystalline hydrated compounds. Michaelis considered that cohesion resulted from the formation and subsequent desiccation of the gel [14].

Just as in the hydration process of C_3S, there are uncertainties involved in determining the stoichoiometry of the C-S-H phase found in the hydration of C_2S. The hydration of dicalcium silicate phase can be represented by the equation:

$$2[2CaO{\cdot}SiO_2] + 5\ H_2O \rightarrow 3\ CaO{\cdot}2SiO_2{\cdot}4H_2O + 3\ Ca(OH)_2 \quad (23)$$

The amount of $Ca(OH)_2$ formed in this reaction is less than that produced in the hydration of C_3S. The dicalcium silicate phase hydrates much more slowly than the tricalcium silicate phase [12].

Although the average C_3A content in Portland cement is about 4-11 %, it significantly influences the early reactions. The phenomenon of flash set, the formation of various calcium aluminate hydrates and calcium carbo- and sulfo-aluminates, involves the reactions of C_3A. Higher amounts of C_3A in Portland cement may pose durability problems [25].

Tricalcium aluminate reacts with water to form C_2AH_8 and C_4AH_{13} (hegagonal phases). These products are thermodynamically unstable so without stabilizers or admixtures they convert to the C_3AH_6 phase (cubic phase). The relevant equations for these reactions are [58]:

$$2\ C_3A + 21\ H \rightarrow C_4AH_{13} + C_2AH_8 \quad (24)$$

$$C_4AH_{13} + C_2AH_8 \rightarrow 2\ C_3AH_6 + 9\ H \quad (25)$$

In saturated $Ca(OH)_2$ solutions, C_2AH_8 reacts with $Ca(OH)_2$ to form C_4AH_{13} or C_3AH_6, depending on the condition of formation. The cubic form (C_3AH_6) can also form directly by hydrating C_3A at temperatures of 80 °C or above [59]:

$$C_3A + 6\ H \rightarrow C_3AH_6 \quad (26)$$

In Portland cement, the hydration of the C_3A phase is controlled by the addition of gypsum. The flash set is thus avoided. The C_3A phase reacts with gypsum in a few minutes to form ettringite as follows:

$$C_3A + 3CSH_2 + 26\ H \rightarrow C_3A{\cdot}3CSH_{32} \quad (27)$$

After all gypsum is converted to ettringite, the excess C_3A will react with ettringite to form the low sulfo-aluminate hydrate [12].

$$C_3A{\cdot}3CSH_{32} + 2\ C_3A + 4\ H \rightarrow 3[C_3A{\cdot}CSH_{12}] \quad (28)$$

The ferrite phase constitutes about 8-13 % of an average Portland cement. In Portland cement the ferrite phase may have a variable composition that can be expressed as $C_2(A_nF_{1-n})$ where $0 < n < 0.7$. On cement minerals, the ferrite phase has received much less attention than others with regard to its hydration and physico-mechanical characteristics. This may partly be ascribed to the assumption that the ferrite phase and the C_3A phase behave in a similar manner [12, 15].

The C_4AF phase is known to yield the same sequence of products as C_3A, however, the reactions are slower. In the presence of water, C_4AF reacts as follows:

$$C_4AF + 16\ H \rightarrow 2C_2(A,F)H_8 \quad (29)$$

$$C_4AF + 16\ H \rightarrow C_4(A,F)_{13} + (A,F)H_3 \quad (30)$$

Amorphous hydroxides of Fe and Al form in the reaction of C_4AF. The thermodynamically stable product is $C_3(A,F)H_6$ and this is the conversion product of the hexagonal hydrates. Seldom does the formation of these hydrates cause flash set in cement [12].

In cements, C_4AF reacts much slower than C_3A in the presence of gypsum. In other words, gypsum retards the hydration of C_4AF more efficiently than it does C_3A. The rate of hydration depends on the composition of the ferrite phase; that containing higher amounts of Fe exhibits lower rates of hydration. The reaction of C_4AF with gypsum proceeds as follows:

$$3\ C_4AF + 12\ CSH_2 + 110\ H \rightarrow 4\ [C_6(A,F)SH_{32}] + 2(A,F)H_3 \quad (31)$$

The low sulfo-aluminate phase can form by the reaction of excess C_4AF with the high sulfo-aluminate phase [12].

Although hydration studies of pure cement compounds are very useful in following the hydration processes of Portland cement itself, they cannot be directly applied to cements, because of complex interaction.

As a general rule, the rate of hydration in the first few days of cement compounds in cements proceeds in the order $C_3A > C_3S > C_4AF > C_2S$. The rate of hydration of the compounds depends on the crystal size, imperfections, particle size, particle size distribution, the rate of cooling, surface area, the presence of admixtures, the temperature, etc. [12, 14, 60] In a mature hydrated Portland cement, the products formed are C-S-H gel, $Ca(OH)_2$, ettringite (Aft phases), monosulfate (AFm phases), hydrogarnet phases and possibly amorphous phases high Al^{3+} and SO_4^{2-} ions.

3.7 Calorimetry

Calorimetry is the science of measuring the heat of chemical reactions or physical changes. The measurement is performed with a calorimeter [61].

The calorimeter is an instrument that allows heat effects in it to be determined by directly measurement of temperature. Accordingly, to determine a heat effect, it is necessary to establish the relationship between the heat effect generated and the quantity measured in the calorimeter [62].

The amount of heat dQ produced in a system during period of time dt can be calculated from Tian equation [63]:

$$\frac{dQ}{dt} = C_s\left(\frac{dT_{sample}}{dt}\right) + K\left(T_{sample} - T_S\right) \tag{32}$$

where T_{sample} and T_s are sample and surrounding temperature, C_s is heat capacity of the sample and K is heat exchange coefficient between the sample and the surroundings.

The first term in this equation (temperature differentiation with respect to time multiplied by heat capacity coefficient) presents the amount of heat stored in matter of calorimeter. The second term (heat flow coefficient multiplied by difference of temperature of the cell and surroundings) presents the amount of outlet heat [64].

3.7.1 Calorimetry of cement

Calorimetry of cement shows five steps during the hydration process (Fig. 12). In the first stage, as soon as cement comes into contact with water Ca^{2+} and OH^- ions are released into the solution phase. This is followed by a rapid release of heat that ceases within 10 – 12 minutes. This is called a preinduction period. In the second stage, the reaction rate is slow and it is known as the dormant or induction period. This may be extended by a few hours. At this stage the cement remains plastic and is workable. In the third stage, the reaction proceeds rapidly and accelerates with time, releasing a maximum amount of heat at the end of the acceleratory period. At this stage, a rapid crystallization of CH and C-S-H occurs. Initial set occurs at about the time when the rate of reaction becomes vigorous. The final set occurs before the end of the third stage. In the fourth stage, there is a slow deceleration. At the final stage there is only limited formation of products and at this stage, the reaction is diffusion controlled [12].

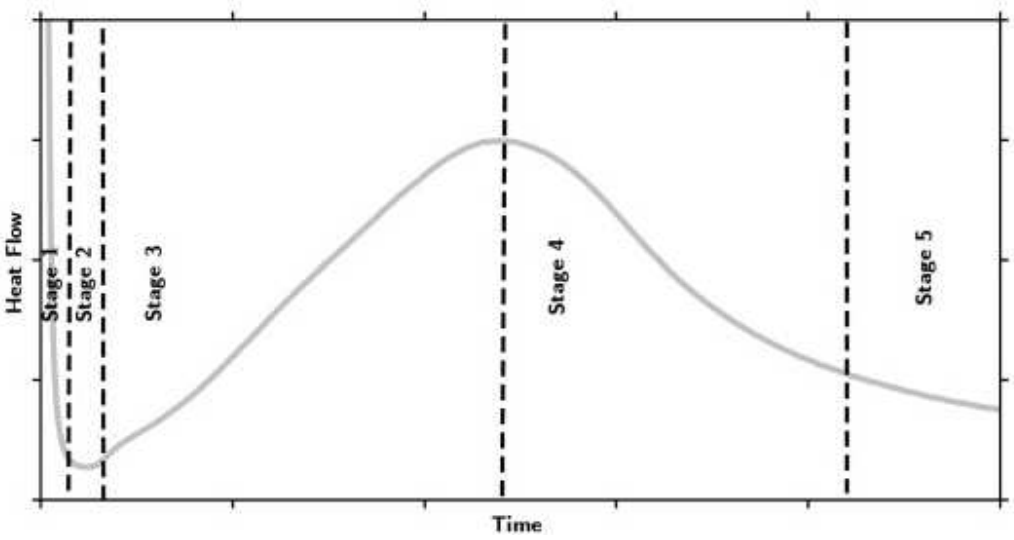

Fig. 12: Rate of heat evolution during hydration of portland cement [65]

The process of hydration of Portland cement with descriptions of main characteristic is shown on Fig. 13 [66].

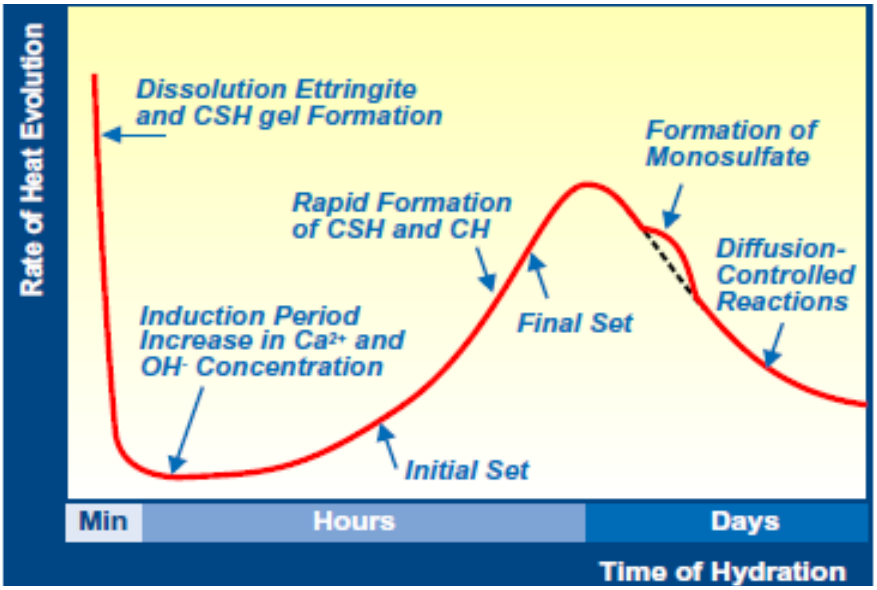

Fig. 13: Principal sketch of Portland cement hydration development and setting. [66]

3.8 Vicat test

A standard method to estimate the setting time of a cement paste is the Vicat test described in ČSN EN 196-3. The test consists in the measurement of the penetration depth of the steel cylinder needle which falls down under gravity (Fig. 14). A needle weighing 300 ± 1 g and diameter of 10.00 ± 0.05 mm is lowered on the surface of a specimen of fresh cement paste and the penetration depth is recorded. The cement paste is kept in a standard frustum 40 mm in height. In the standard method, the cement paste is required conform with normal consistency, which correspond to the penetration depth 34 ± 2 mm (the distance between the needle and the base plate is 6 ± 2 mm) [67].

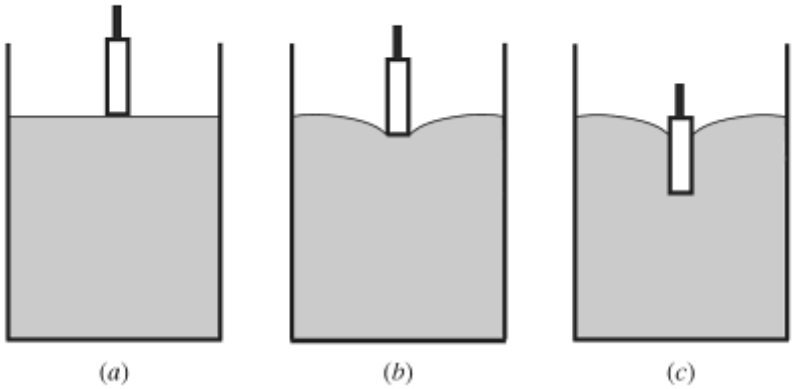

Fig. 14: Principle of the penetrometer: a) before test, b) before effective penetration, c) stoppage after some penetration [68]

The physical background of the test is based on the resistance of paste to dynamic penetration by a rod. The information obtained is very useful to compare cement settings properties [69].

Although the Vicat test is widely used technique, there is only scarce literature dealing with the correlation of the test results with any physical or mechanical properties of the material. The main reason for this probably lies in the fact that, up to recently, it was not possible to follow the evolution of a quantifiable physical or mechanical property of cement paste during setting. Consequently, this penetration test (as well as penetrometers of various shapes) has remained empirical, delivering strictly comparative values. The recent development of ultrasound spectroscopy allows for the measurement of the evolutions of both shear and bulk modulus during setting of cement paste. Based on this new technique, Lootens et al demonstrated the existence of a relation between shear yield stress and the force measured by penetrometers [70].

From a rheological point of view, yield stress is the only feature of the material, which can stop a needle penetration. Indeed, as the needle is penetrating the sample, the surface supporting the applied load increases. As a consequence, the stress applied on the tested material decreases. As long as the weight of the needle or the applied force creates in the sample a stress higher than yield stress, the needle keeps on penetrating the sample until the generated stress becomes lower than the yield stress and flow stops [68].

It is interesting to note that this test involve very low velocities and can thus be considered as quasi static flows. Therefore in first approximation the stress should be of the order of the yield stress. Indeed, there is a flow so the deformations are too high to consider that the material stays in the elastic regime. The stress is therefore higher than the yield stress. However, because the flow is so low, the contribution of plastic viscosity is very low, meaning that the stress should stay very close to the yield stress [70].

Let us consider the ideal case of a long cylinder of radius r already immersed to a depth h in the fluid initially at rest. Then the cylinder is moved through the paste along its axis (as shown in Fig. 15) under the action of a force F. We assume that the container is a cylinder of radius P, much larger that r_0, so edge effects is neglected [68].

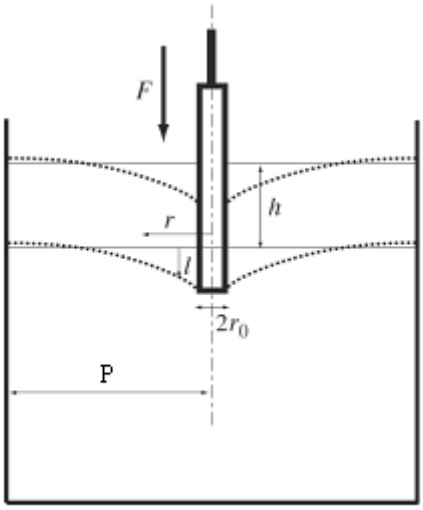

Fig. 15: Deformation of fluid as a result of applied force: initial (continuous horizontal line) and final (dotted line) position of the free surface of the sample [68]

The data analysis is based on the force balance equation of a static needle. Three phenomena act upon the needle: gravity, buoyancy and shearing at the needle interface [69].

The gravity is given by mass of object m and the acceleration of gravity g as shown in following equation:

$$F_g = m \cdot g \tag{33}$$

The buoyancy is the resistance force resulting from the immersion of a fraction of solid tool (needle):

$$F_b = \pi \cdot R^2 \cdot h \cdot \rho \cdot g \tag{34}$$

where R is the needle radius, h is the length of the immersed portion of the needle and ρ is the density of material.

The sheering at the needle is resistance force too and can be written as:

$$F_s = 2 \cdot \pi \cdot R \cdot h \cdot \tau \tag{35}$$

where τ is the local shear stress acting at the needle interface.

We first consider a cylinder and assume that the length of penetration is much greater than the cylinder radius ($h >> r_0$) so that edge effects remain negligible. In that case the flow in the fluid around the cylinder is basically a simple shear and the shear stress along the immersed part of the cylinder surface is equal to yield stress at stoppage [68].

The material yield stress at the surface of needle was deduced from previous equations resulting in following relationship:

$$\tau_0 = \frac{mg - \pi R^2 h \rho g}{2\pi Rh} \tag{36}$$

It could of course be noticed that the assumption of a quasi static flow does not seem to hold a priori for a falling load needle. However, it seems, according to experimental results, that what matters is the conditions under which the Vicat needle stops. As the needle is stopping, the flow may again be considered as slow and the contribution of the plastic viscosity neglected [70].

In Lootens work [70] is demonstrated, that there exists a systematic correlation between force measured by penetrometers and the yield stress of the tested materials. The case of penetrometer has been examined in detail with various needles, using experiments, finite

elements and fluid dynamics simulations. The extrapolated yield stresses are plotted in Fig. 16 and are very well correlated to the other type measurements.

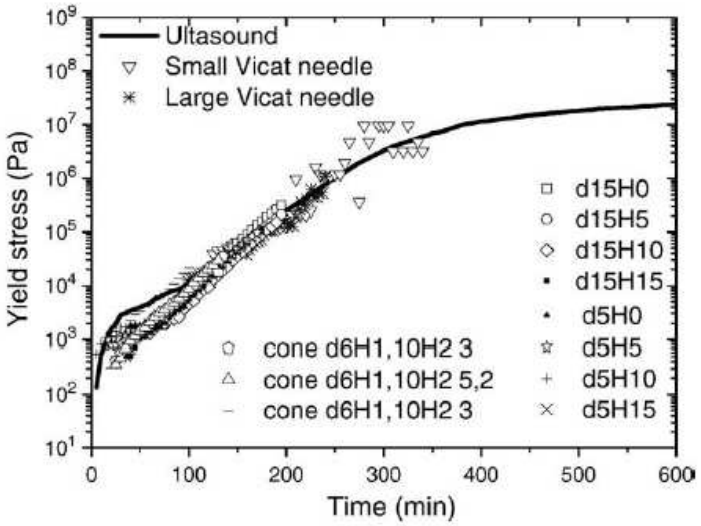

Fig. 16: Yield stress extrapolated from penetrometer force measurements with different tips, ultrasound measurement and Vicat needles. Small Vicat needle and large Vicat needle had a diameter 1 and 2 mm respectively. The first number in the legend is the diameter in mm of the hemispherical tip and second number is the height of the cylindrical section of same diameter placed above [70]

An analytical correlation, which allow for the calculation of the yield stress of the material from the experimental measurement has been derived. These relations are gathered in Table 4. They constitute a very useful library of correlations allowing for the comparisons of different test results and for the calculation of physical parameters from simple tests data [70].

Table 4: Relationships between test measurement and yield stress [70]

Test	Measurement type	Correlation with yield stress or compressive strength
Vicat with a needle of radius R	Measurement of penetration depth h in mm for an imposed load of 300 g.	$\tau_0 = \frac{3}{2\pi Rh}$
Hemispherical penetrometer of radius R	Measurement of a force F to maintain a given speed.	$\tau_0 = \frac{F}{3\pi R^2}$
Hemispherical penetrometer of radius R and connected cylinder of height h	Measurement of a force F to maintain a given speed.	$\tau_0 = \frac{F}{3\pi R^2 + 2\pi Rh}$
Conical penetrometer of radius R and cone height of $h2$ and connected cylinder of height h	Measurement of a force F to maintain a given speed.	$\tau_0 = \frac{F}{\pi R\sqrt{R^2 + h_2^2} + 2\pi Rh}$

According to Sant et al. [71] the Vicat needle apply an axial force of 2.94 N through a 300 g needle and two other forces are exerted by the paste on the needle and need to be accounted for to satisfy force equilibrium (Fig. 17). A skin resistance exerted on the penetrated surface of the needle which is dictated by the shear resistance of the material and compressive resistance exerted on the tip of needle.

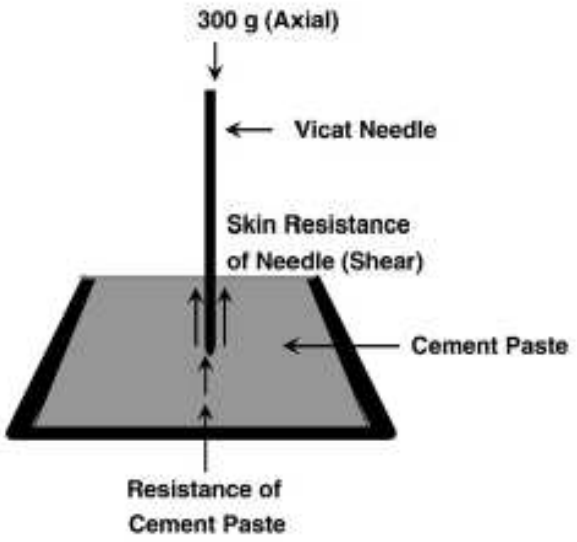

Fig. 17: A schematic illustration of the Vicat test [71]

The shear stress on the surface of the needle nearly equals the shear strength of the material. The compressive resistance can be approximated by assuming a plastic failure criterion in which case the compressive strength is equal to twice the shear strength. A force equilibrium analysis of this nature can be illustrated as shown in eq. 37:

$$\tau_0 = \frac{2.94}{2\pi Rh + 2\pi R^2} \tag{37}$$

Where 2.94 [MPa] is the axial stress exerted by the needle and r and h are the radius and depth of penetration of the needle respectively.

The representation of the obtained results from mentioned work [71] is shown in Fig. 18 which examines the shear stress evolution as a function of the time for rheological and Vicat techniques. This is additionally compared to rate of chemical shrinkage. The Vicat stress response is measurable at the end of the rheological measurement and is a continuation of the data obtained from rheological tests (the parallel plate rheometer was used).

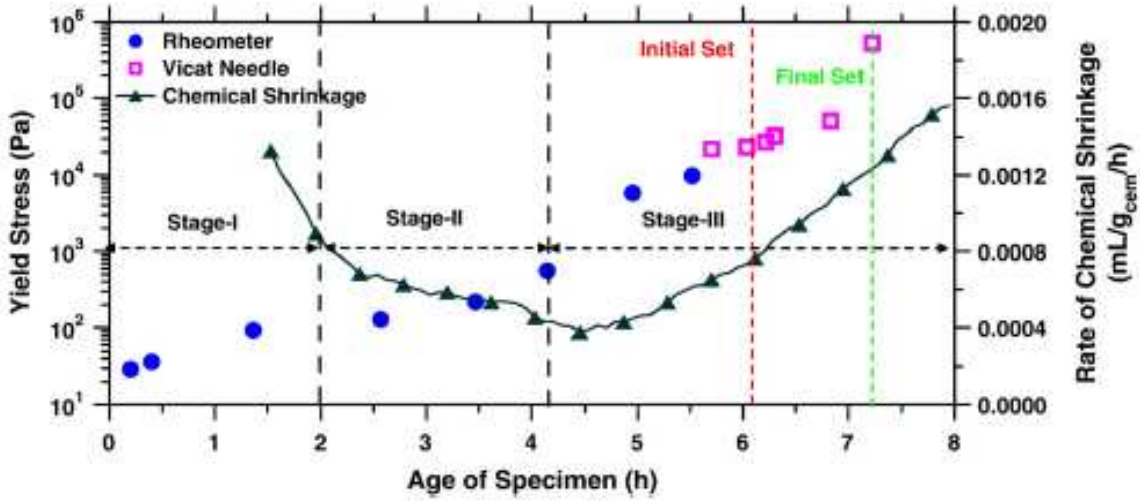

Fig. 18: The combined rheological and Vicat setting response for the plain cement paste mixture (w/c = 0.30)

The Vicat tests were used in the work of Struble and Lei to determine the normal consistency of cement pastes and setting time. A number of conclusions have been drawn from this study, where the hydration of paste and rheological properties were studied by means the isothermal calorimeter and rheometer. Concerning the Vicat test, it was pointed out, that Vicat needle penetration is not a well-defined rheological parameter but rather an empirical measurement produced by a complex and ill-defined stress state [72].

The initial setting time of the cement paste was determined with using Vicat needle test in work of Trtnik et al [73]. The evolution of certain ranges of ultrasonic pulse velocity values was compared with the evolution of the penetration of the Vicat test for each cement paste mixture separately. It was shown that the proposed wave transmission method can be used very effectively to monitor the hydration and formation of the structure of an arbitrary cement paste mixture. According to mentioned study, the estimation of the initial setting time of the cement paste with the ultrasonic wave transmission method is practical, reliable and has a prospect of application in construction practice.

The initial and final setting times of cement pastes have been assessed by means of the Vicat test in work [74] and [75]. In both works a broad experimental study has been performed, from the end of mixing up to 2 years, on a set of plain cement pastes prepared with the same type I ordinary Portland cement and various w/c ratio and cured at various constant temperatures. The temperature effects have been observed in first part [74], where was found out that an increase in the curing temperature within the range 10-50 °C produce a decrease in initial and final Vicat setting times in the respective setting period. The w/c effect was studied in second part [75] and between several results one can mention an example of w/c effect on the rate and the magnitude of chemical shrinkage. It was found out, that w/c does not influence the rate and the magnitude of chemical shrinkage in a significant manner within the w/c range 0.30 – 0.60 and for curing temperature ranging from 10 up to 50 °C. However, w/c has a kinetic effect within the range 0.25 – 0.30.

3.9 Rheometers

Instruments that measure the relationship between shear stress and strain rate are called rheometers. Rheometers, instruments for measuring flow behavior, usually operate in rotation and measure torque and rotational speed and the rheological parameters of stress and strain rate are computed from these measurements [12].

Often the rheometer employs coaxial cylinders, parallel plates or system cone-plate as shown in Fig. 19. Sample sits between and one of the cylinder, upper plate or cone rotates.

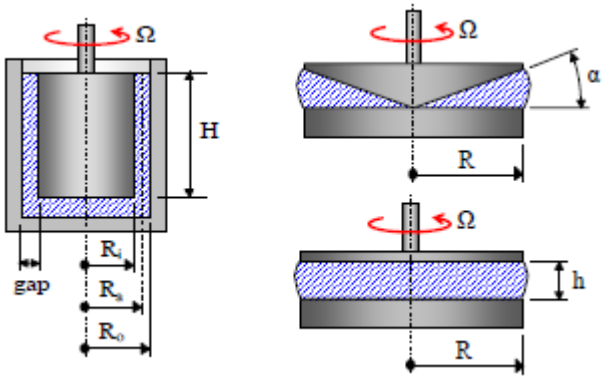

Fig. 19: Types of systems used in measurements with rheometers: on the left the concentric cylinders, on the right cone-plate and parallel plates

3.10 X-ray powder diffractometry (XRD)

X-ray powder diffraction (XRD) is a rapid analytical technique primarily used for phase identification of a crystalline material and can provide information on unit cell dimensions. The analyzed material is finely ground, homogenized, and average bulk composition is determined [76].

X-ray diffraction is the elastic scattering of x-ray photons by atoms in a periodic lattice. The scattered monochromatic x-rays that are in phase give constructive interference. Fig. 20 illustrates how diffraction of x-rays by crystal planes allows one to derive lattice spacings by using the Bragg's law [76]:

$$n_r \lambda = 2d \sin \Theta \qquad (38)$$

where n_r is an integer called the order of reflection, λ is the wavelength of x-rays, d is the characteristic spacing between the crystal planes of a given specimen and θ is the angle between the incident beam and the normal to the reflecting lattice plane.

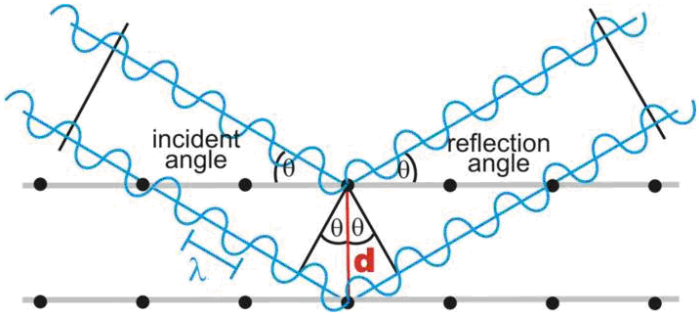

Fig. 20: Constructive Interference of reflected waves [77]

By measuring the angles θ, under which the constructively interfering x-rays leave the crystal, the interplanar spacings, d, of every single crystallographic phase can be determined.

3.11 Scanning electron microscope (SEM)

The scanning electron microscope (SEM) permits the observation and characterization of heterogeneous organic and inorganic materials on a nanometer to micrometer scale. The popularity of the SEM stems from its capability of obtaining three-dimensional-like images of the surfaces of a very wide range of materials. SEM images are used in a wide variety of media from scientific journals to popular magazines to the movies [78].

The backscatter SEM detectors use flat polished specimens and provide images based on variations in electron backscatter coefficients. Differences in them primarily reflect differences in chemical composition among the different featured present. Chemical components of high electron density have high backscatter coefficients and appear bright in the backscattered images. Conversely, components of lower electron density, such as most cement hydration products, have lower backscatter coefficients and appear less bright [79].

The imaging signal of greatest interest is beside backscatter electron the secondary electrons. These vary primarily as a result of differences in surface topography. The secondary electron emission, confined to a very small volume near the beam impact area for certain choices of the beam energy, permits images to be obtained at resolution approximating the size of the focused electron beam. The three-dimensional appearance of the images is due to the large depth of field of the scanning electron microscope as well as to the shadow relief effect of the secondary and backscattered electron contrast [78].

4 EXPERIMENTAL PART I

First part of the experimental part is concerning to the rheological properties of the self-compacting concretes and their matrixes. This part was done during 5 month´s Erasmus stay at the Norwegian University of Science and Technology, Department of Structural Engineering. Several tests were performed from the basic test to obtain the properties like slump flow, density, air content. Then the rheological parameters were measured with using the BML viscometer. For catching the static yield stress, the plate test was proposed and successfully done. The static yield stress and their change during aging were observed with using the ConTec viscometer 4 with very low applied rotational velocities. The inclined plane test, other test for finding the static yield stress was carried out during 3 weeks following intership. The matrixes of the tested mixture were studied with measurement with parallel plate rheometer.

At the end of the experimental part I the mixtures of SCC produced at a ready-mix concrete plant were tested. Three mixtures of SCC (filler stabilized, chemically stabilized and unstable) were subjected the rheological testing. The mixtures were sieving to obtaining mortar and mortars were characterized as well.

4.1 Testing of mortars I and II

4.1.1 Composition of mixtures I and II

Table 5 shows the composition of the mortar that was proportioned with a matrix volume fraction of 40 volume %.

The materials used are:

- Cement: Norcem Standard FA, which is Portland cement type CEM II/A-V 42.5 R contains up to 20 % fly ash with typical Blaine value 450 $m^2 \cdot kg^{-1}$
- Sand: Årdal 0/8 (low filler)
- Tau: NorStone Tau (rock type: quartz diorite)
- Superplasticizer (SP): ResconMapei SP-130 - Acrylic polymer with 30% dry solid, splitting type admixture, normal dosage = 0.3-1.2% of cement weight

Detailed information about the part materials (chemical composition, datasheets, sieve curves etc) are given in appendix. The sand used for mixture I had moisture 2.2 % and for mixture II 1.3 %, adsorbed water is accounted in w/c. The volume of the mixtures was 40 litres.

Table 5: Used materials and parameters

Material	Mixture I		Mixture II	
	Weight [kg]	kg/m^3	Weight [kg]	kg/m^3
Cement	17.285	432.1	17.285	432.1
Water	7.644	226.2	7.863	218.8
SP	0.110	2.8	0.110	2.8
Tau	2.273	56.8	2.273	56.8
Sand	63.771	1594.3	63.551	1588.8
	Moisture [%]	2.2	Moisture [%]	1.3
w/c	0.52		0.50	
SP [%]	0.6		0.6	

*in water content w/c is included water from sand

4.1.1.1 Mixing

Mix design was the same for the two mixtures. At first the solid materials were mixed 1 minute (dry mix). Then the water and SP were added and mixed for 2 min (wet mix). After 2 min of rest the mixture was re-mixed for 1 min. A 50 litre flat-bottomed, horizontal plane rotating counter-current Eirich paddle mixer was used.

4.1.2 Basic properties of mortar

The rheological properties of fresh mortar were characterized by measurements of slump flow and T500 according to EN 12350-8. Density and air content were determined too regarding EN 12350-6 and EN 12350-7. All tests were done immediately after mixing in time less than 10 min after water addition.

4.1.3 Measurement with BML viscometer

The ConTec BML 3 coaxial viscometer (Fig. 21) used in this work had rotating outer cylinder and stationary inner cylinder measuring the torque. The rheological measurements consisted of measuring torque T [Nm] as a function of rotational speed N [rps].

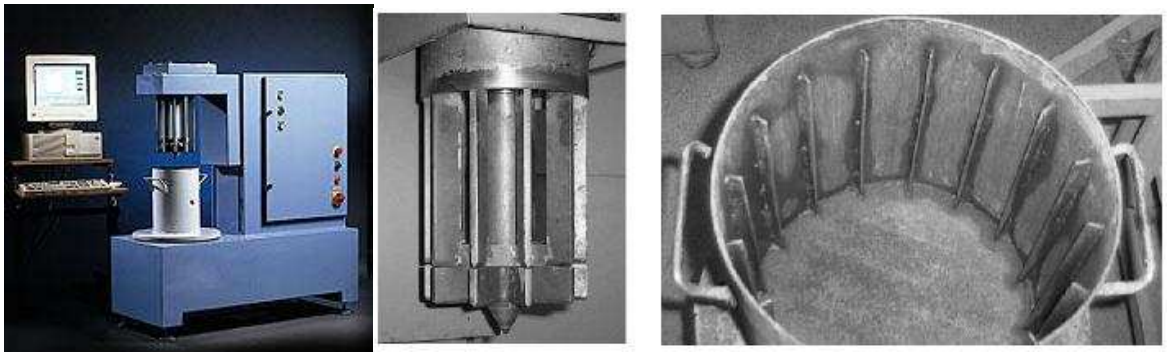

Fig. 21: ConTec BML viscometer with inner and outer cylinders [80]

By plotting measured torque T as a function of rotational speed N obtained during the shear history shown in Fig. 22 and Fig. 23 the equation: T = HN + G, was obtained from linear regression of the flow curve. The value H is slope of the line and G is the point of intersection with the ordinate. The equation used for converting H and G values into the dynamic yield stress τ_{dyn} and plastic viscosity η_p respectively is known as the Reiner-Rivlin equation (39). These two parameters were calculated using the following equations (41,41) [38,81]:

$$\Omega = \frac{T}{4\pi\eta_p h_i}\left(\frac{1}{R_i^2}-\frac{1}{R_o^2}\right)-\frac{\tau_{dyn}}{\eta_p}\ln\frac{R_o}{R_i} \tag{39}$$

$$\eta_p = \frac{H\left(\frac{1}{R_i^2}-\frac{1}{R_o^2}\right)}{4\pi h_i} \tag{40}$$

$$\tau_{dyn} = \frac{G\left(\frac{1}{R_i^2}-\frac{1}{R_o^2}\right)}{4\pi h_i \ln\frac{R_o}{R_i}} \tag{41}$$

where Ω is angular velocity of the outer cylinder [rad.s^{-1}] R_i is radius of inner cylinder [m], R_o is radius of outer cylinder [m] and h_i is height of inner cylinder [m]. The following values were used for the calculation of rheological parameters (Table 6):

Table 6: Dimensions of cylinders and height of immersed part of inner cylinder of BML viscometer

	Mixture I	Mixture II
R_i [m]	0.100	0.100
R_o [m]	0.145	0.145
h_i [m]	0.175	0.180

The shear histories shown in Fig. 22 and Fig. 23 show that equilibrium values were obtained at each rotational velocity. The Bingham regression is done on the equilibrium shear stresses at each deformation rate level on the down curve. From this technique dynamic, or Bingham, yield stress and plastic viscosity of the mixture at the given time were obtained.

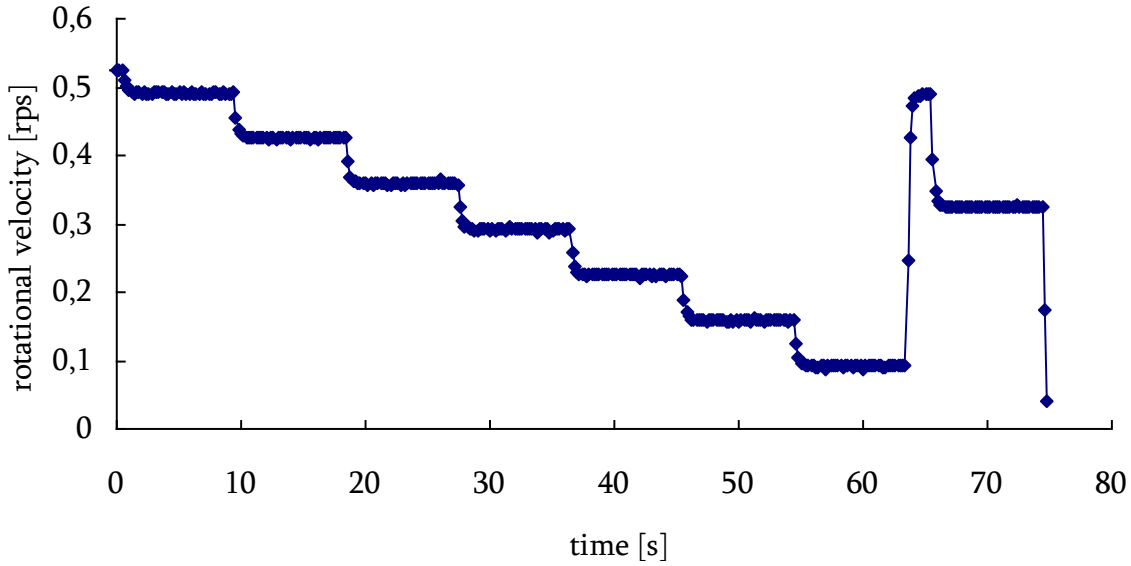

Fig. 22: Shear history of measurement with ConTec BML viscometer – mixture I

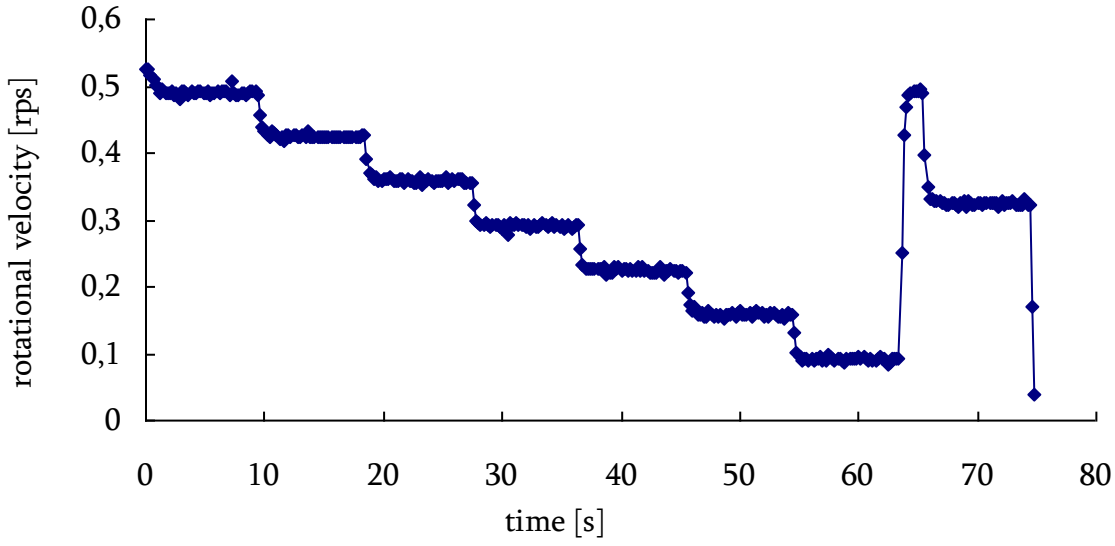

Fig. 23: Shear history of measurement with ConTec BML viscometer – mixture II

4.1.4 Static yield stress measurements with ConTec4 viscometer

Rheological measurements with the ConTec4 viscometer were performed in order to measure time development of torque T at very low, constant, rotational speed run in various test sequences. The obtained stress-rotation and then stress-strain curves were recalculated and the time-dependant development of yield stress value and structural build-up was found. Fig. 24 shows a photo of the ConTec 4 instrument with computer and the actual container with 4 mm half-cylinder surface roughness and the static core that were used. The gap between the container and the cylinder were 9 mm.

Fig. 24: ConTec4 with rotating container and static core

4.1.4.1 Testing of mixture I

The first and the last test were done 18 minutes and 83 minutes after water addition, respectively. After the first two tests the inner cylinder was pulled up and the mixture was stirred lightly by hand, without using mixer. Then, two other measurements were done and the inner cylinder was kept immersed in the mixture between these measurements. Before the last test this was done after moving the inner cylinder up and down, i.e. still no mixing.

4.1.4.2 Testing of mixture II

The first and the last tests were done 32 minutes and 94 minutes after water addition respectively. Before the last test only motion up and down were made with the inner cylinder (it means no mixing) and then the whole measurement was repeated.

4.1.4.3 Static yield test conditions

In these tests it was applied the rotational velocity N = 0.0015 rps (= 0.00942 rad/s), which is the slowest one with acceptable deviation. It was found that with used ConTec 4 viscometer the deviation of speed control grows almost exponentially with decreasing velocity and for our purpose to catch the static yield stress the lowest rotational speed we used was 0.0015 rps with maximum deviation of about 35 %. This low speed makes it possible to follow changes of torque in real time and allows reaching the static yield stress and structural breakdown, which comes after that.

First it was applied rotational speed 0.0015 rps for 200 seconds, then the rotation was stopped for 200 seconds (outer cylinder was static) and these two steps were repeated three times. After that the outer cylinder was „shaken" to relieve stress between the outer cylinder and the core to reach zero value of torque. The whole procedure was repeated two times again.

During the 200 seconds of measurement the cylinder turns 1.884 rad (0.00942·200 = 1.884 rad) which is 108° (alfa-deformation, see Fig. 25). So during one such measurement the cylinder turns less than a third of a whole revolution.

Before the second test only up- and down- movement with the inner cylinder was made (i.e. again no mixing) and then the whole measurement was repeated. This technique was applied in testing of mixture II.

In case of mixture I the duration of the applied rotation was changed. The last test with this mixture was carried out in a similar way, but after several stops of rotation the outer cylinder was „shook" to relieve residual stress between container and core to reach zero value of torque.

4.1.4.4 Analysis of measurement

The ConTec4 is, as described, a concentric cylinders viscometer. The outer cylinder is rotated a given velocity (N, ω) and the inner is stationary and includes a load-cell measuring the torque acting due to the drag from the fresh concrete. After some time of motion of the outer cylinder the point A goes to the point C as shown in Fig. 25.

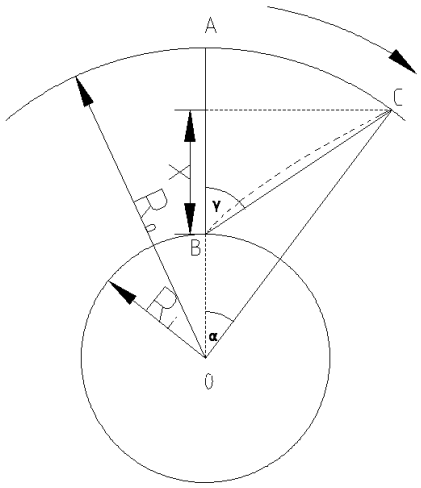

Fig. 25: Analysis of the angle γ

For calculation of the angle γ the following equation was deduced from Fig. 25 and some algebra:

$$\cos\gamma = \frac{R_0 \cos\alpha - R_i}{\sqrt{R_i^2 + R_0^2 - 2R_0 R_i \cos\alpha}} \tag{42}$$

where R_0 is 0.105 m and R_i is 0.085 m for the ConTec4 viscometer. This assumes a straight line BC which is probably not the case as pointed out by Billberg [85]. However, no effort was made to investigate to what extent the shear deformation between the inner and outer cylinder followed some other path, perhaps like indicated by the dotted curved line between B and C indicated in Fig. 25. This could perhaps have been done with some kind of color indicator sprinkled on the top surface. Still this would only reflect the surface shear and not

what is going on inside the mortar where some other kind of shear detection would have to be used. Clearly Fig. 25 could be a simplification.

4.1.4.5 Conversion of measured torque to shear stress

For conversion of torque to shear stress it was used the following relationship (43), where r is the radius where the shear stress acts and h_i is the height of the immersed part of the inner cylinder [2]:

$$\tau = \frac{T}{2\pi r^2 h_i} \tag{43}$$

The torque T is the same at all radii in a given time if we assume elastic constant shear modulus, G, (in addition to constant plastic viscosity) and the kind of linear shear-stress deformation angle ABC described in Fig. 25. Shear stress is inversely proportional to the square of the radius r – distance from the centre of symmetry. According to equation 43 the maximum shear stress is reached for maximum torque at the surface of the inner cylinder and minimum on the outer cylinder.

The yield stress is the minimum stress below which no flow occurs. According to eq. 43 the yield stress is first reached at the surface of the inner cylinder (and where later flow begins if high rotational speeds are applied). Then as the angular velocity is increased, the yield stress is reached at greater and greater radii from the inner cylinder until eventually it is reached at the surface of the outer cylinder. At sufficiently high rotational speed and assuming Bingham fluid behaviour plug flow is then assumed to be completely eliminated.

There was no visible motion in the whole mixture during measurement; only an area close to the outer cylinder could be seen moving. This motion was transferred via particle interactions and elastic and/or plastic and/or viscous type shear stress transfer through the whole mixture to the inner cylinder, which detected the value of the torque. That was the reason for using the radius of the inner cylinder R_i in eq. 43 instead of r for calculation of the yield stress. For calculation of shear stress the following dimensions of R_i, R_o and h_i were used (Table 7):

Table 7: Dimensions of cylinders and height of immersed part of inner cylinder of ConTec4 viscometer

	Mixture I	Mixture II
R_i [m]	0.085	0.085
R_o [m]	0.103	0.103
h_i [m]	0.138	0.139

The geometry and surfaces of the inner- and outer cylinders shown in Fig. 24 were designed to minimize end effects while giving maximum bond by Ø 4mm half-cylindrical roughness on the outer cylinder and vanes (or knifes) ensuring contact at the inner cylinder.

By alternating the applied rotational speed (0.0015 rps and 0 rps) during measurement with the ConTec4 viscometer the torque-time dependency was obtained. The maximum values of torque captured (see initial peaks after each start of rotation in Fig. 30, 36, 39, 43, 48, 49, 50, 52 and 54) were used for calculation of yield stress τ_0. When the rotation of the outer cylinder was stopped the torque surprisingly never reached zero value. The torque is maintained at a constant value when the rotation of the outer cylinder is stopped and these values of torques were used for calculation of stresses τ_{res} (according to the eq. 43), which we called the

residual stresses. The explanation for the existence of residual stress seems to be some tension between particles which still persists in the mixture after stopping rotation and confining the mix between the inner and outer cylinder in some kind of state of permanent shear stress. The dynamic yield value τ_{dyn} was called the stress which was reached after overcoming the maximal yield stress.

The difference between τ_0 and τ_{res} was called the mobilized stress τ_{mob} and was calculated according eq. 44:

$$\tau_{mob} = \tau_0 - \tau_{res} \tag{44}$$

To reach zero values of torque a light rotational ,,shaking" by hand was applied on the outer cylinder of the viscometer. This is seen as the largest peaks in Fig. 39, 43 and 52. The yield stress reached immediately after ,,shaking" is marked by * in Table 21, 25, 28, 29 and 32. If the yield value is reached directly after shaking (marked *), the stress is called fully mobilized τ_{fully} in tables Table 23, 27 and 31.

4.2 Plate test

The plate test is based on the fact that the slight deformation of material under its own weight, evaporation and other causes of volumetric change that occur, allow to transfer a part of this load to the plate by the mobilization of a shear stress on the plate. This shear stress is equal to the maximum value physically acceptable, which is the yield stress [82]. It is important to note here that, as opposed to a penetrometer test (Vicat needle), the plate is perfectly static [83]. The test set up is shown in Fig. 26 with both plate with rough surface, container for paste and balance.

Fig. 26: Test set up for plate test

The shear stress acting on the surface of the plate was calculated from the measured apparent mass evolution using the following equation [84]:

$$\tau(t) = \frac{g\Delta M(t)}{2S_p} \tag{45}$$

where ΔM is the measured variation in the apparent mass of the plate and S_p is the immersed surface of the plate.

The structuration rate of the tested material is A_{thix} [$Pa \cdot s^{-1}$] [51]. It is the rate of increase in the static yield stress of material in $Pa \cdot s^{-1}$ and also called structural build-up rate.

The structural build-up of micro mortar phase and SCC mixtures was intensively studied in Billberg's thesis [85]. Matrix is regarded as the continuous phase of concrete and thus incorporates all fine particles, water, air and chemical additives. In other words; matrix is what is left if all aggregate having particle size greater than 0.125 mm is removed from the concrete. The results show that the time-dependent static yield stress ranges from 7.8 $Pa \cdot min^{-1}$ for the densest paste (i.e. the lowest w/c = 0.34) down to 2.5 $Pa \cdot min^{-1}$ for the leanest paste (highest w/c = 0.42) [85, 86].

The SCC mixtures prepared and tested in Billberg`s work showed linear growth of static yield stress with time. The structural build-up ranged from 30 to 95 $Pa \cdot min^{-1}$. Common for all mixtures was the cement content equal to 320 $kg \cdot m^{-3}$, w/c ratio 0.58 and coarse aggregate (8-16 mm) equal to 30 % of total aggregate amount. From the results it is obvious, that an increased particle concentration increases the rate of structural build-up [85].

Roussel proposed the classification given in Table 8 according the author's own experience and other published results [51].

Table 8: Classification of SCC according to their flocculation rate [51]

Flocculation rate A_{thix} (Pa/s)	SCC type
Less than 0.1	Non-thixotropic SCC
Between 0.1 and 0.5	Thixotropic SCC
Higher than 0.5	Highly thixotropic SCC

4.2.1.1 Description of technique

The design of the plate test experimental device presented here was inspired from the device proposed by A. Perrot et al. [82]. The vessel (cylindrical, with a diameter 190 mm and 220 mm in height) was filled with the mortar to a height of 200 mm. The plate was 3 mm thick, 75 mm wide and 102 mm long. It was covered with sand paper with average roughness of 200 μm. The sand paper was used to avoid any slippage between the mortar and the plate. The plate was rigidly attached to the vessel during filling. To ensure reproducibility vibration was applied for 10 s (vibrating table). The plate was then attached below a balance with accuracy of ± 0.01 g. The height H of the immersed portion of the plate was measured at the beginning and it was 69 mm and 67 mm for the first and second mixtures respectively. The whole testing was carried out under constant conditions in a climate room at 50 % RH and temperature 20 ˚C. The testing was started at time 14 min and 24 min after water addition for the mixture I and mixture II respectively.

4.3 Parallel plate rheometer

Following the mortar studies a series of matrixes with the same binder composition and filler content were made and investigated with a MRC 300 rheometer produced by Paar Physica with parallel plate measuring system. The upper plate had a serrated surface to avoid slippage and the geometry of upper plate given by radius was 3 cm. The gap between the plates was set to 1.0 mm. The bottom plate was temperature controlled.

Proportioning of matrixes was varied so as to cover the composition of the matrixes in the previously investigated mortar according to the particle-matrix model [86]. The matrix phase consists of water, chemical admixtures (SP) and all fines, including cement, pozzolanes and

aggregate fines, i.e. particles < 0.125 mm. The mix composition is shown in Table 9, where matrix 1 corresponds to mortar tested previously (mixture II), matrix 2 had lower w/c ratio and matrix 3 had lower SP dosage. The total matrix volume was approximately 200 ml.

Table 9: Proportioning of matrixes

Matrix	w/c ratio	SP [%]	Cement [g]	Filler* [g]	Tau [g]
M1	0.5	0.60	216.89	21.24	28.51
M2	0.4	0.60	243.27	23.82	31.98
M3	0.5	0.50	216.89	21.24	28.51

* particle size 0-0.125mm with the same material as used in the sand

All matrixes were blended in a high shear mixer Braun (MR5550CA). The blending was performed by adding solid materials to the water with SP. All mixtures were mixing for 30 seconds then resting for 5 minutes and blending again for 1 minute.

The following tests were performed on prepared matrixes (test I – III). All tests were started at time 10 min after water addition (age 10 min). Test I was done to obtain basic rheological properties like gel strength, yield stress and plastic viscosity. Tests II and III were performed for a detailed study of static yield stress and only done for matrix M1, which corresponded to the composition of the matrix phase of the mortar (mixture II).

4.3.1 Test I (Basic characterization)

It was used following test sequence:

1) 30 sec mixing with constant shear rate 60 s^{-1}
2) 1 min rest
3) shear rate – stress curve with logarithmic sweep of stress from 0.1 up to 100 Pa in 60 points lasting 5 second each to measure gel strength
4) 30 sec mixing with constant shear rate 60 s^{-1}
5) 1 min rest
6) 1 min with constant shear rate 0.01 s^{-1} to measure stress-strain curve in 60 measuring points lasting 1 second each
7) 30 sec mixing with constant shear rate 60 s^{-1}
8) 1 min rest
9) 3 min with constant shear rate 0.001 s^{-1} to measure stress-strain curve in 180 measuring points lasting 1 second each
10) 30 sec mixing with constant shear rate 60 s^{-1}
11) 1 min rest
12) 1 min with constant shear rate 0.01 s^{-1} to measure stress-strain curve in 30 measuring points lasting 2 seconds each
13) 30 sec mixing with constant shear rate 60 s^{-1}
14) 1 min rest
15) Shear rate – stress curve with logarithmic sweep of shear rate from 0.01 to 60 s^{-1} in 20 measuring points lasting 6 seconds each to measure flow curve
16) Shear rate – stress curve with logarithmic sweep of shear rate from 60 to 0.01 s^{-1} in 20 measuring points lasting 6 seconds each to measure flow curve

Total time was 31.5 min.

4.3.2 Test II (Static yield stress)

Test parameters:

1) 1 min mixing with constant shear rate 60 s^{-1}
2) 1 min rest
3) 1 min with constant shear rate 0.001 s^{-1} to measure stress-strain curve in 60 measuring points lasting 1 second each
4) 4 min rest
5) 1 min with constant shear rate 0.001 s^{-1} to measure stress-strain curve in 60 measuring points lasting 1 second each
6) 4 min rest
7) back to point 3.

Total: 21 steps and 10 resulting curves (total time 48 min)

4.3.3 Test III (Static yield stress)

Test parameters:

1) 1 min mixing with constant shear rate 60 s^{-1}
2) 1 min rest
3) 1 min with constant shear rate 0.01 s^{-1} to measure stress-strain curve in 60 measuring points lasting 1 second each
4) 4 min rest
5) 1 min with constant shear rate 0.01 s^{-1} to measure stress-strain curve in 60 measuring points lasting 1 second each
6) 4 min rest
7) back to point 3.

Total: 21 steps and 10 resulting curves (total time 48 min)

4.4 Inclined plane test

Inclined plane tests were carried out to determine static yield stress of SCC and their mortars. The inclined planes were arranged with sandpaper with an average roughness of 200 μm. A small layer of water was sprayed onto the surface of the sandpaper in accodance with the measurement procedure [87]. The measuring cylinder with diameter 62 mm and height 120 mm was filled to 100 mm height for mortar and 120 mm for SCC. The filling time corresponded with time of start of measurement. After filling the cylinder was slowly lifted and the resulting spread was covered with a wide cylindrical container to avoid any evaporation from the mixture during the rest time. After 10 minutes of rest the covering container was removed and the spread was determined. The height of the spread (thickness) was determined by averaging five measurements near the central area. The upper plane was slowly lifted until it started to flow (Fig. 27). The angle of inclination was measured with protractor.

Fig. 27: The inclined plane test with sieved out mortar

The static yield stress was then calculated according to the following formula [87]:

$$\tau_0 = \rho g h_s \sin\varphi \quad (46)$$

where ρ is the density of the sample, g is the gravitational acceleration, h_s is the thickness of the spread and φ is the angle of inclination of the inclined plane.

4.4.1 Preparing mixtures and proportioning – plane test

The mixtures were prepared according to Table 10 where the proportioning, w/c and SP dosage are shown. The composition of the mortars were proportioned with the same matrix volume as in case of mixture I and II, that means 40 volume %. The used materials were the same too (appendix). The mixture S1 correspond to the mixture II in first part and mixtures S2 and S3 have different SP dosage. The moisture in the sand was 0.7 %. The volume of prepared mixture was 6 litres.

Table 10: Materials and parameters of mixtures

Materials [kg.m^{-3}]	SI	S2	S3
Cement	432.2	431.7	431.9
Sand	1567.2	1567.2	1567.2
Tau	56.8	56.8	56.8
Water	216.1	215.9	216.0
ResconMapei SP-130	2.6	4.3	3.5
SP %	0.6	1.0	0.8
w/c	0.5	0.5	0.5

4.5 Testing SCC mixtures inform ready-mix concrete plant

After initial studies of the S- mixes that were similar to the first M-mixes, static yield stress was measured on 3 different SCCs produced at a ready-mix plant and tested in a work of Klaartje de Weerdt in the summer of 2011. There the effect of stabilization on the surface quality of concrete elements was investigated [88]. The proportioning of the mixtures is shown in Table 11 and 12.

Table 11: Parameters of the three different ready mix SCCs used

Initial parameters	Filler stabilized	Chemically stabilized	Unstable SCC
w/c	0.678(*)	0.65	0.65
w/p	0.42	0.49	0.49
f/c (limestone filler) [%]	22.5	0.0	0.0
Admixtures	% of C	% of C	% of C
Air entrainer	0.65	0.65	0.65
SP	0.71	0.84	0.75
retarder	0.10	0.10	0.10
Stabilizer	0.0	0.75	0.0
Matrix	l/m^3	l/m^3	l/m^3
Matrix volume	332	310	310
Volume cement glue	299	276	276

(*) due to an error in the moisture content of the sand the w/c ratio of the filler stabilized SCC is 0.678 instead of 0.65

Table 12: Weighed in quantities for the production of the different SCCs

Materials [kg/m^3]	Filler stabilized	Chemically stabilized	Unstable SCC
CEM II/A-V 42.5 R	278.2	278.3	278.3
Limestone powder	62.5	0.0	0.0
Free water	177.8	178.2	178.2
0/8 mm Søberg aggregate	1001.2	1035.7	1035.7
8/16 mm Ramlo aggregate	819.2	847.4	847.4
Air entrainer	1.81	1.81	1.81
SP	1.98	2.34	2.09
Retarder	0.28	0.28	0.28
Stabilizer	0.0	2.09	0.0

The fresh concrete was characterized via several tests and some properties like density, air content, slump flow, plastic viscosity and yield stress (dynamic and static) were determined. The concrete was sieved to obtaining mortar with all particles smaller than sieve size 6.3 mm. The sieved mortars were characterized by Bingham parameters from flow curves using ConTec4 viscometer and static yield stress and density were determined as well.

5 RESULTS AND DISCUSSION I

5.1 Basic properties of mortar I and II

All mixtures were stable, distribution of coarse particles seemed to be homogeneous and no bleeding was observed. All measured parameters with testing times are shown in the Table 13. The higher value of slump flow of mixture I compared to the mixture II pointed out, that yield stress of mixture I is lower. As well a lower value of T_{500} of mixture I predicts lower value of plastic viscosity. Air content of mixture I was a little bit lower than the value obtained for mixture II which corresponds with the density difference. Compared to Table 1 mixture I after 8 minutes corresponded to class SF2 and in age 145 minutes was no longer self-compacting, whereas mixture II after 9 minutes correspond to class SF1. According to the classification of SCC with regard to T_{500} values (

Table 2) mixture I belonged to VS1/VF1 and mixture II VS2/VF2.

Table 13: Basic properties of fresh mixtures

Number of mixture	Time [min]	Fresh density [kg·m^{-3}]	Air content [%]	T_{500} [sec]	Slump-flow [mm]	Predicted yield (eq. 19) [Pa]	R [Pa/s]
I	8	2303	2.6	2.0	700	0.9	0.002
	145	-	-	-	485	5.4	0.001
II	9	2282	3.0	2.7	565	2.5	0.005

The measured slump-flow values were used in eq. 19 for predicting the yield stress (dynamic) of the mixtures (Table 13). If that value is connected with age of mixture, the rate of increasing of dynamic yield stress R [Pa/s] can be evaluated. The predicted yield stress for mixture I at age 8 min is 0.9 Pa, which correspond to the rate 0.002 Pa·s^{-1}. It should be noticed, that for the prediction of the yield stress at time 145 min the same value of density was used as in previous case (age 8 min). Mixture II showed lower slump-flow value which gave the predicted yield stress 2.5 Pa and rate of increasing 0.005 Pa·s^{-1}.

5.2 Characterization of fresh mortars with BML viscometer

Fig. 28 and 29 show the flow curves of the two mortars based on the shear histories in figures Fig. 22 and 23, both indicating a shear thickening tendency often seen on self compacting concrete [40,42]. That is, the Bingham model is not fitting the material behaviour perfectly as is also indicated by the correlation coefficients $\neq 1$.

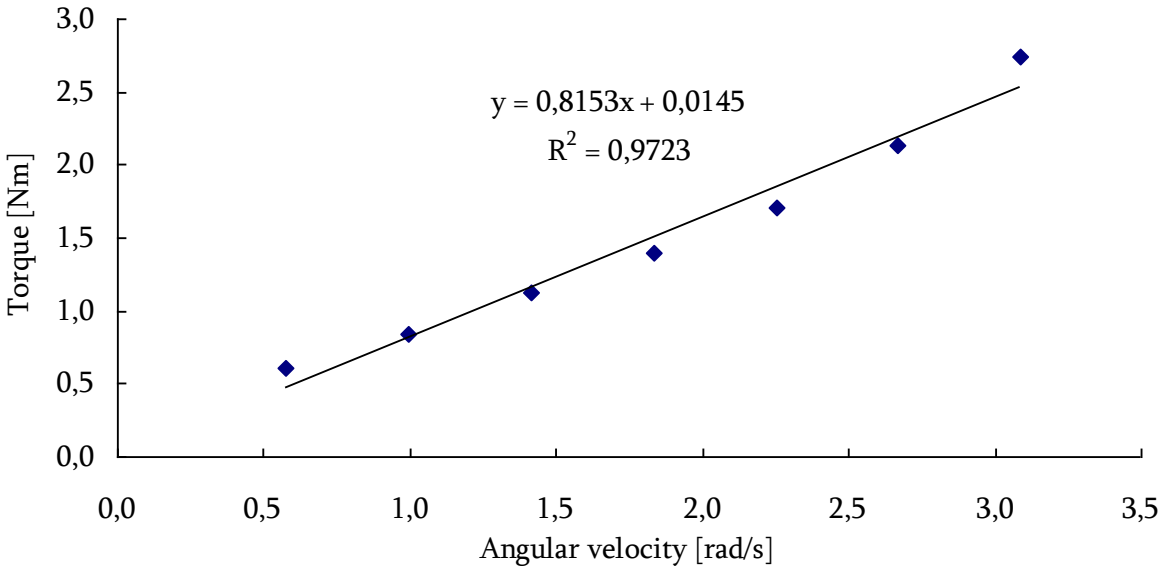

Fig. 28: Flow curve from measurement with BML viscometer of mixture I at time 11 min after water addition

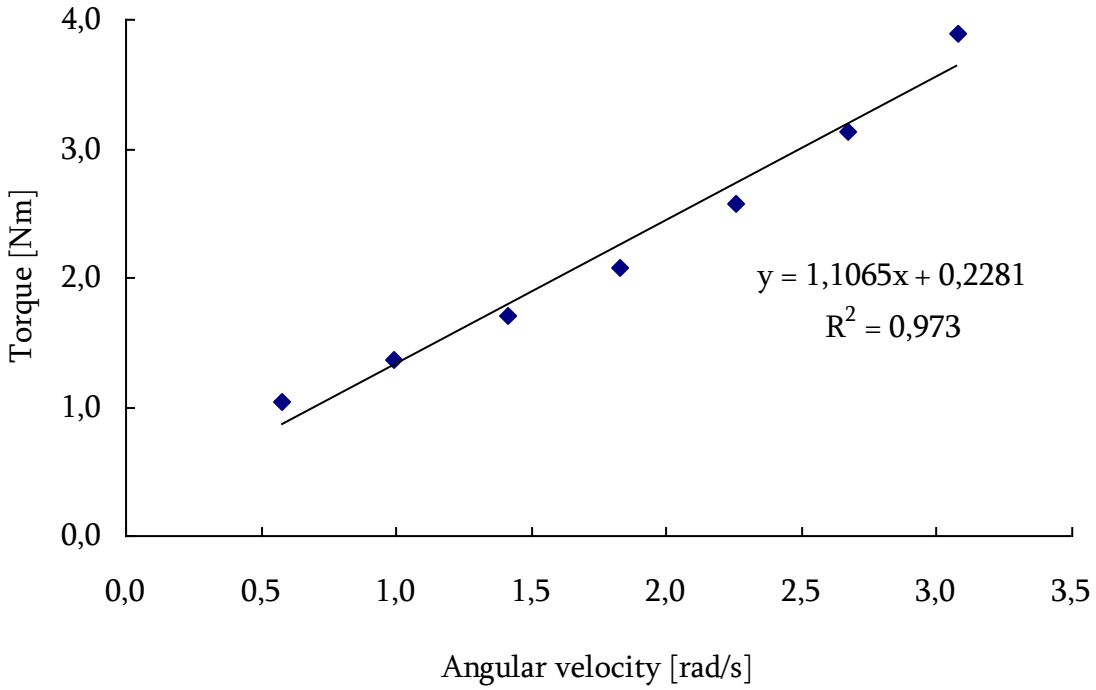

Fig. 29: Flow curve from measurement with BML viscometer of mixture II at time 20 min after water addition

Table 14: Results from measurement with BML viscometer

Number of mixture	Time [min]	τ_{dyn} [Pa]	η_p [Pa·s]	R [Pa·s^{-1}]
I	11	0.9	19.4	0.001
II	20	14.2	25.7	0.012

Dynamic yield stress and plastic viscosity were obtained based on the flow curves in figure Fig. 28 and 29. Dynamic yield stress reached the value 0.9 Pa and plastic viscosity 19.4 Pa·s for first mixture and 14.2 Pa and 25.7 Pa·s for second mixture. These differences correspond with results from the basic properties given in Table 13, where slump flow was 700 mm and 575 mm for first and second mixture, respectively. Plastic viscosity was a little bit different too also corresponding to that T_{500} was slightly higher for the second mixture.

The predicted yield stress of mixture I is in very good agreement with measured value, where the rate of increasing of yield stress is 0.002 Pa·s^{-1} and 0.001 Pa·s^{-1} for predicted and measured values respectively. A little bit worse agreement is obtained in case of mixture II, where the rate of increasing of yield value is 0.005 Pa·s^{-1} and 0.01 Pa·s^{-1} for predicted and measured values respectively.

5.3 Static yield stress measurements with the ConTec4 viscometer

5.3.1 Mixture I

Fig. 30, 32, 34, 36 and 39 show torque vs. time for the static tests of Mix I. Fig. 31, 33, 35, 37, and 40 show the variation in rotational speed during the experiment. Fig. 38, 41 and 42 show the calculated yield stress values at different ages. Table 15 - 23 show the parameters (static yield stress τ_0, structuration rate A_{thix} etc) determined from these results.

5.3.1.1 Age of mixture I 18 min

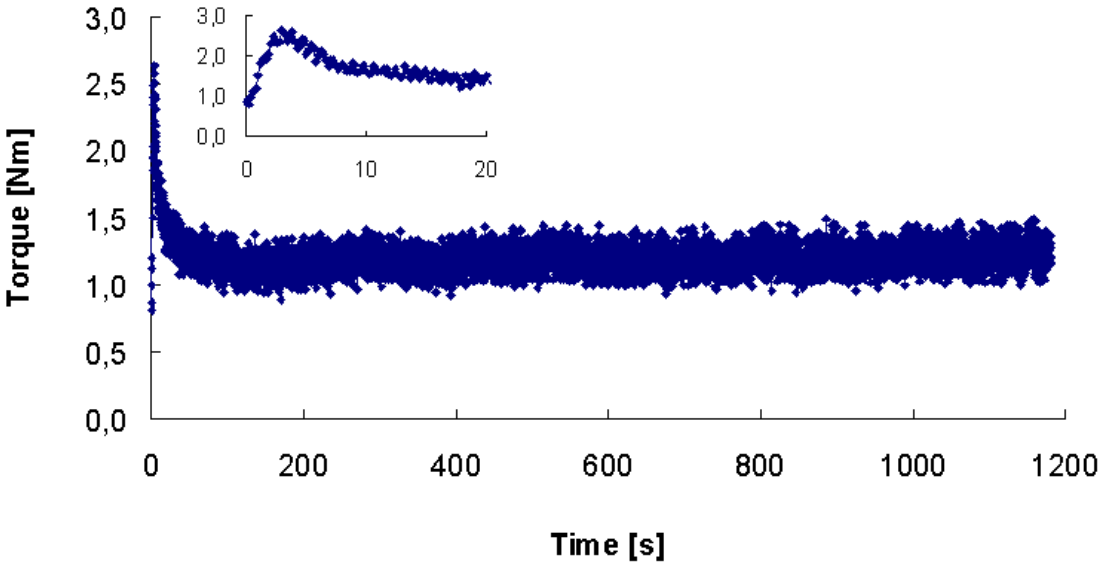

Fig. 30: Torque-time dependence of mixture I at age 18 min on start of measurement

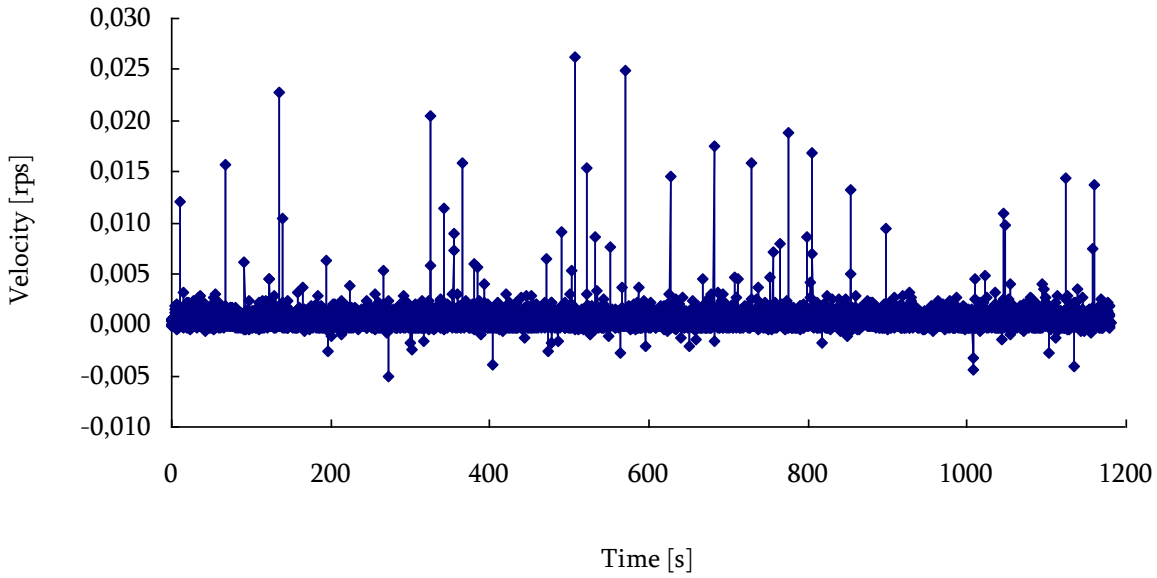

Fig. 31: Velocity profile of measurement - average value of velocity [rps] = *0,00057*

Table 15: Results for mixture I at age 18 min

Time [s]		T [Nm]	τ [Pa]		A_{thix} [Pa/s]
3		2.642	τ_0	421.8	0.389
100	200	1.137		181.4	-
200	300	1.183		188.8	-
300	400	1.162		185.6	-
400	500	1.184		188.9	-
500	600	1.200		191.5	-
600	700	1.167	τ_{dyn}	186.3	-
700	800	1.179		188.1	-
800	900	1.199		191.5	-
900	1000	1.205		192.4	-
1000	1100	1.216		194.1	-
1100	1180	1.232		196.7	-

In Fig. 30 the maximum value of torque is reached after 3 seconds, seen as a clear peak at the beginning of the experiment. Inserted in the figure is a higher resolution showing the linear nature of the deformation of the mortar before static yield is reached. The static yield stress takes the value 422 Pa and the succeeding average dynamic stress 181 Pa calculated from average torque reached in interval 100 – 200 seconds. Following dynamic stresses and average torque for given interval are shown in Table 15. The age of the concrete at the moment of reaching the yield stress was 18 min, so the structuration rate A_{thix} [Pa/s] is 0.389 Pa/s over these (18×60+3) seconds. Fig. 30 and Table 15 also show a tendency of slightly increasing dynamic stress during the experiment.

5.3.1.2 Age of mixture I 38 min

The next test was performed immediately after the previous one that means without remixing. Applied velocity was 0.002 rps instead of 0.0015 rps used in all tests. Fig. 32 shows measured dependence for mixture at the age 38 min and the velocity profile of the measurement is shown on Fig. 33.

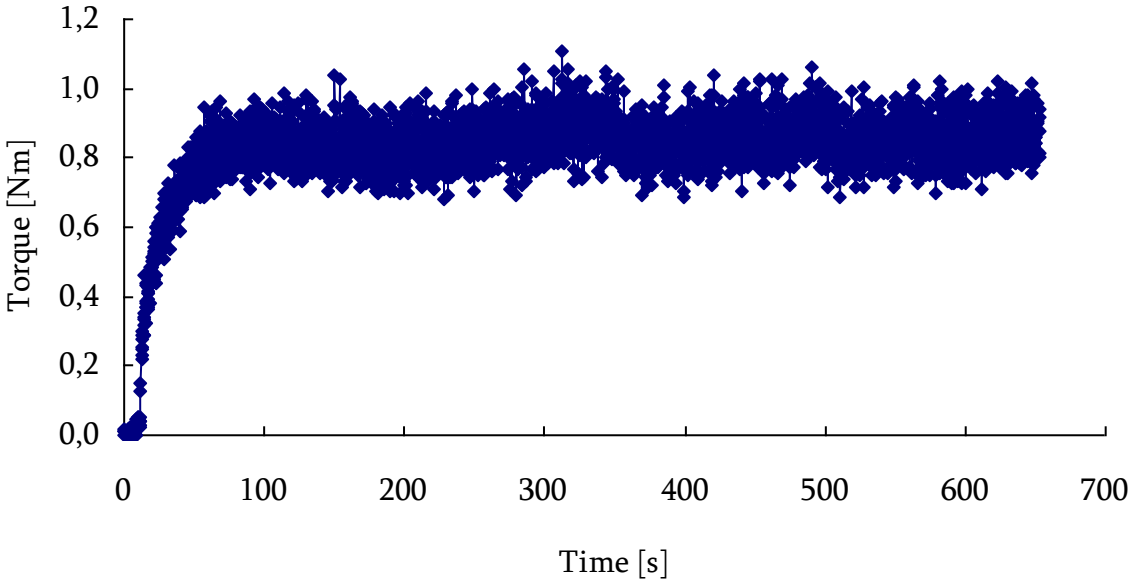

Fig. 32: Torque-time dependence of mixture I at age 38 min on start of measurement

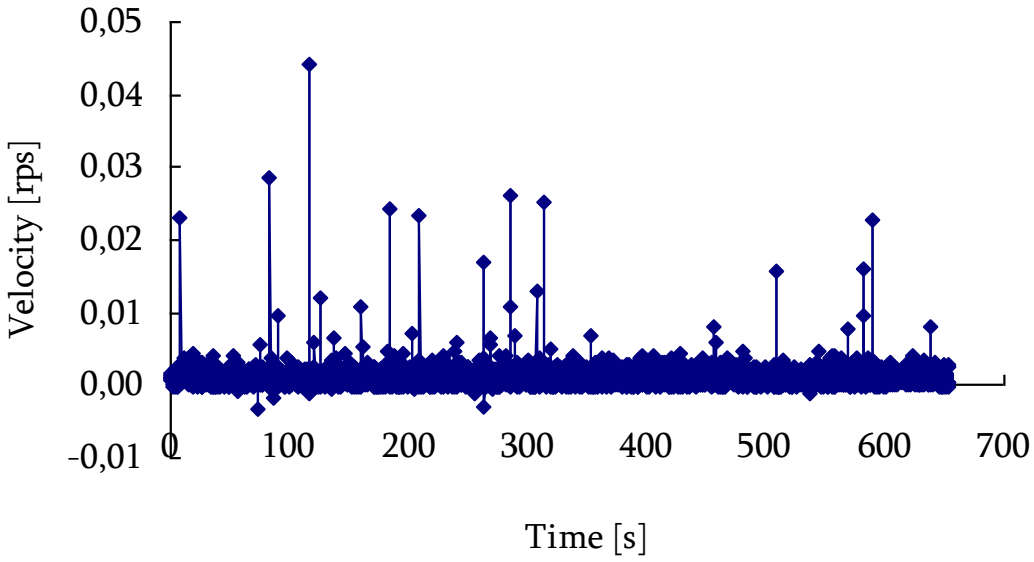

Fig. 33: Velocity profile of measurement - average value of velocity [rps] = *0,0012*

Table 16*:* Results for mixture I at age 38 min

Time [s]		T [Nm]	τ_{dyn} [Pa]
50		0.807	128.8
50	150	0.831	132.6
150	250	0.835	133.3
250	350	0.875	139.7
350	450	0.853	136.1
450	550	0.859	137.1
550	650	0.860	137.2

Fig. 32 shows torque-time dependence, where torque slowly increases during 50 seconds to value approximately 0.8 Nm which correspond to the stress 129 Pa. The absence of obvious yield stress is discussed in comments of measured curve in age 51.5 min (end of chapter 5.3.1.3.). The dynamic yield stresses were calculated for every 100 seconds interval as shown in Table 16 and oscillated around value 136 Pa. The lower values of stresses (compared with values reached at age 18 min, where maximum value of stress was 197 Pa) are caused by the sensitivity of the torque resistance in the sample on given velocity (0.002 rps), which was in this case higher (compare to the 0.0015 rps) and brought larger destruction of present crating structure.

5.3.1.3 Age of mixture I 51.5 min

Fig. 34 and Fig. 35 show the torque – time – and velocity variation, respectively for the next experiment run on the same material, but where the mortar was hand mixed after lifting the stationary inner cylinder before the start of the experiment as described already.

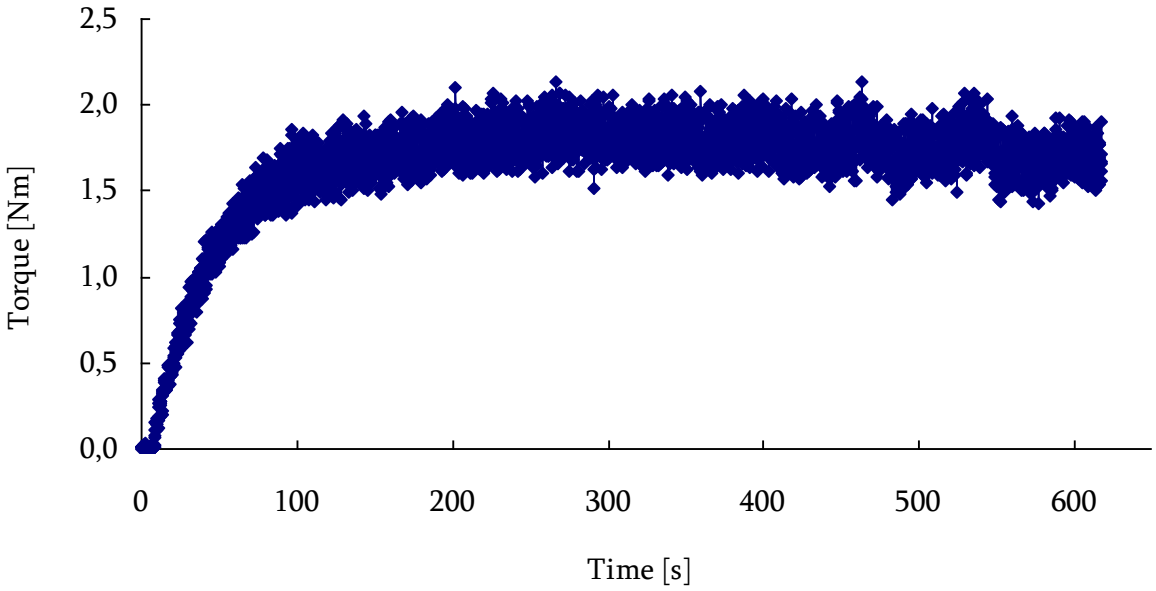

Fig. 34: Torque-time dependence of mixture I at age 51.5 min on start of measurement

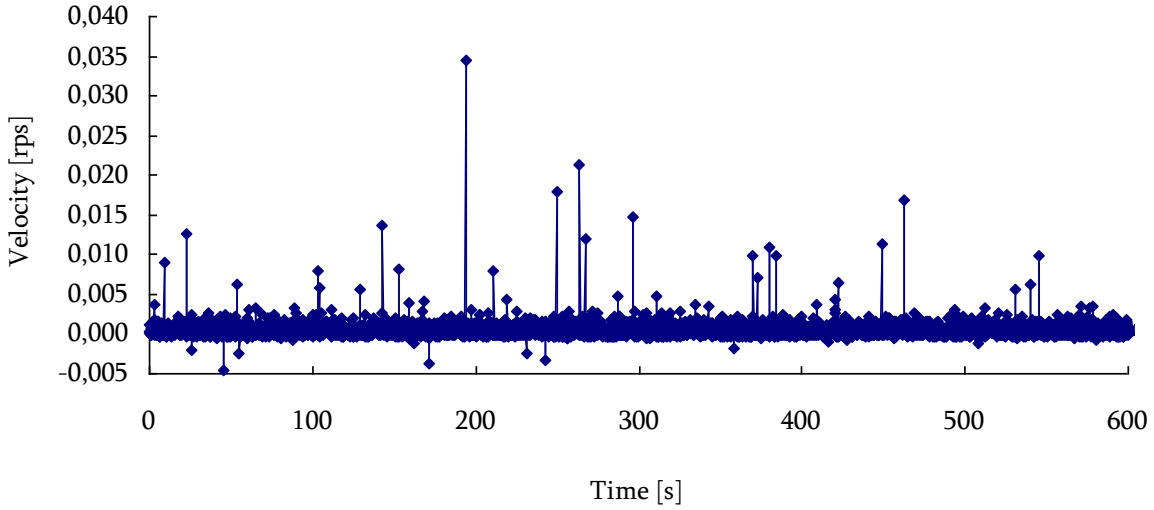

Fig. 35: Velocity profile of measurement - average value of velocity [rps] = *0.000599*

Table 17*:* Results for mixture I at age 51.5 min

Time [s]		T [Nm]	τ_{dyn} [Pa]
100		1.788	285.4
100	200	1.697	270.8
200	300	1.811	289.2
300	400	1.800	287.4
400	500	1.771	282.7
500	600	1.723	275.0

Fig. 34 shows that the torque value slowly increased and then oscillated around the value 1.8 Nm, which corresponds to the stress 285 Pa. The evaluation of dynamic yield stresses were done in the same way as in previous case by dividing measured dependence on 100 seconds intervals as shown in table 11. There is no obvious yield stress (as in previous case – Fig. 32) and the reason for this can be in this case the hand-mixing just before testing, which breaks new bonds in the growing structure. However, the reason for the different kind of peaks at the beginning of Fig. 30 (sharp) and Fig. 32 and 34 (gradual) is not known. Apparently the gradual type happens when the test starts from an unconfined state immediately after pouring (see also figures Fig. 39, 43 and 52), whereas the steep rise and clear break are seen after start from rest in a more confined state (see the same figures). It does not appear to be a condition that the concrete must be subjected to the residual stress since the abrupt rise to clear peaks are also seen after the "shaking" in figures (see also figures Fig. 39, 43 and 52). Apparently, time at rest in the container is the factor affecting the features of the stress increase "peak" like in Fig. 30 or "gradual" like in Fig. 34.

5.3.1.4 Age of mixture I 62 min

Fig. 36 shows the yield stress after repeated start/stop of mixture I. After the peaks (τ_0) a relatively steady value (τ_{dyn}) is maintained and as the viscometer rotation is stopped a residual stress (τ_{res}) remains as the viscometer is at rest. At new start a new, higher, peak is reached.

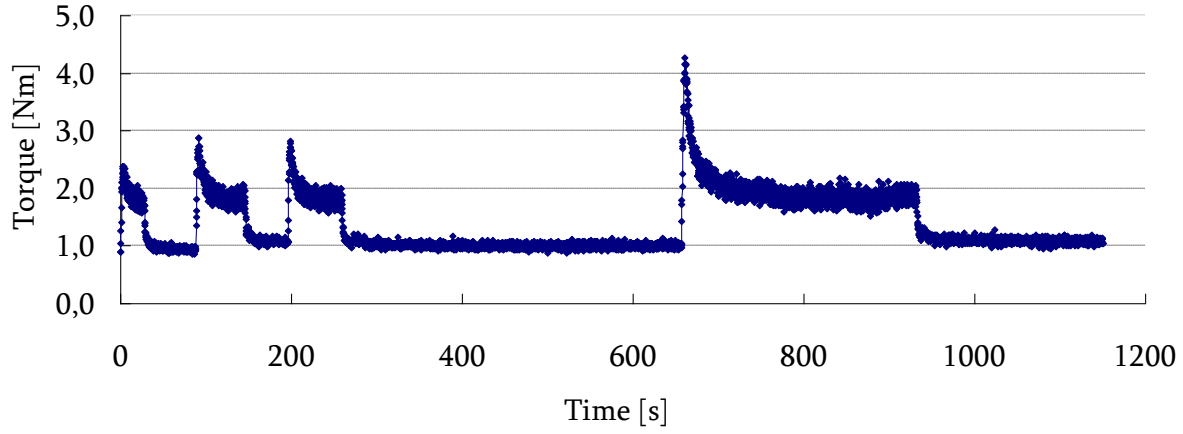

Fig. 36: Torque-time dependence of mixture I at age 62 min on start of measurement

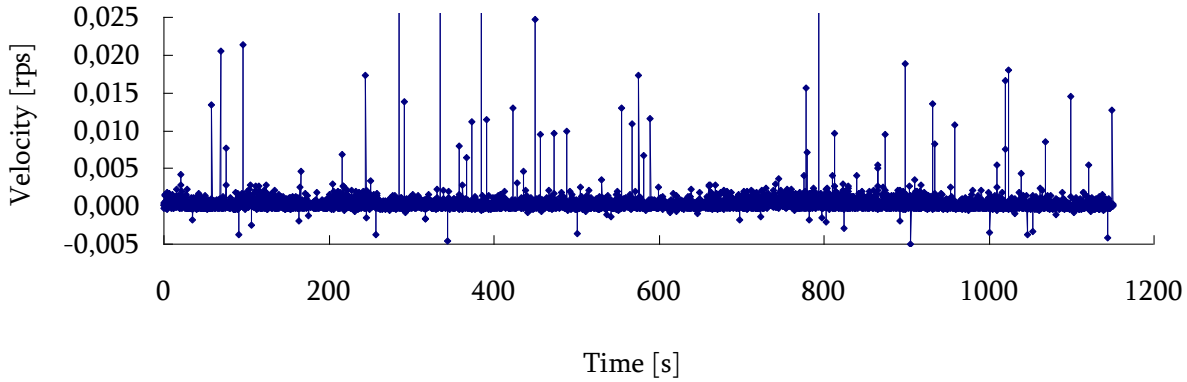

Fig. 37: Velocity profile of measurement

The evaluated stresses are shown in the following tables Table 18-20. There is a quite obvious increase of yield stress with time. The structuration rate calculated for these points grow from 0.10 Pa/s to 0.15 Pa/s (Table 18).

Table 18*: Development of yield stresses* τ_0 of mixture I

Age of SCC [s]	Age of SCC [min]	τ_0 [Pa]	A_{thix} [Pa/s]
3783	63	380.5	0.101
3872	65	458.7	0.118
3978	66	450.4	0.113
4440	74	664.9	0.150

Table 19: Development of residual stresses τ_{res} of mixture I

Age of SCC [s]	Age of SCC [min]	τ_{res} [Pa]
3868	64	146.3
3976	66	172.3
4436	74	159.6
4781	80	175.2

Table 20: Development of mobilized stresses τ_{mob} of mixture I

Age of SCC [s]	Age of SCC [min]	τ_{mob} [Pa]	A_{thix} [Pa/s]
3780	63	236.9	0.063
3868	64	312.4	0.081
3976	66	278.1	0.070
4436	74	505.3	0.114

All calculated stresses (τ_0, τ_{res} and τ_{mob}) and their time-development are shown in Fig. 38. The time development was calculated using linear regression, but the correlation coefficient is acceptable only for values of yield stress where R^2 = 0.9659. Interestingly, the linear regression in Fig. 38 shows a very different, higher, value of the structuration rate A_{thix} = 0.412 Pa·s^{-1}. This value is in the order of 2 – 6 times higher than the values of tables Table 15 - Table 19 where all A_{thix} values are calculated based on their individual ages from addition of water, i.e. from birth including part of the time in a less confined state. The highest value from regression is based on structural build up when confined in the viscometer and apparently is higher. However, both ranges of values are within the ranges indicated in Table 8, though within different flocculation rate classes. The reason for the much higher structuration rate in Fig. 38 thus is difficult to explain at present but possibly/probably the confinement plays an important role for A_{thix}. From Fig. 38 it seems that there is a constant difference between the confined (upper) and unconfined (middle) yield stress development regression lines. Of course remixing also plays a role, but the effect discussed above was obtained without remixing. The only factors were time and stress-state and the "shake" which rotated the container very little, less than 1/100th rotation, but enough to reduce the confinement.

Fig. 41 and 42 show that the yield stress is reduced by the stress release and that the time development of structural build-up probably is more complicated than the simple constant A_{thix} law indicates. This point was investigated in more detail on matrix based on the same cement, filler and SP in the Physica parallel plate viscometer presented later in this thesis.

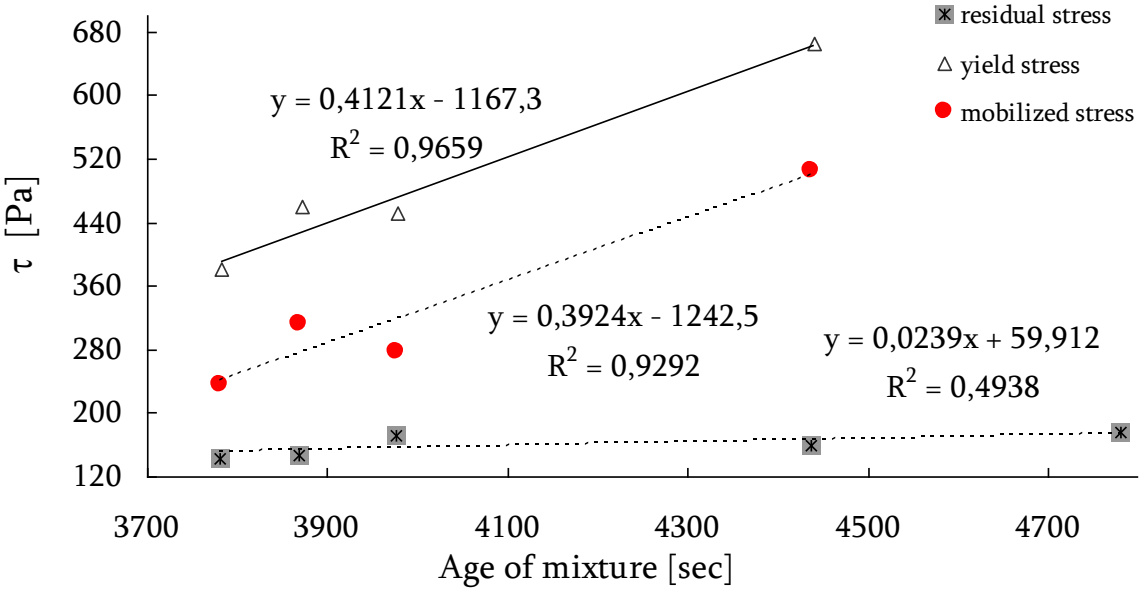

Fig. 38: Development *of stresses in mixture I, no release of stress ("shaking")*

5.3.1.5 Age of mixture I 83 min

Fig. 39 shows the torque-time dependence of mixture I at age 83 min after water addition with applying „shaking" to reach zero value of torque. The evaluated stresses and values of structuration rate are shown in the Table 21- 23.

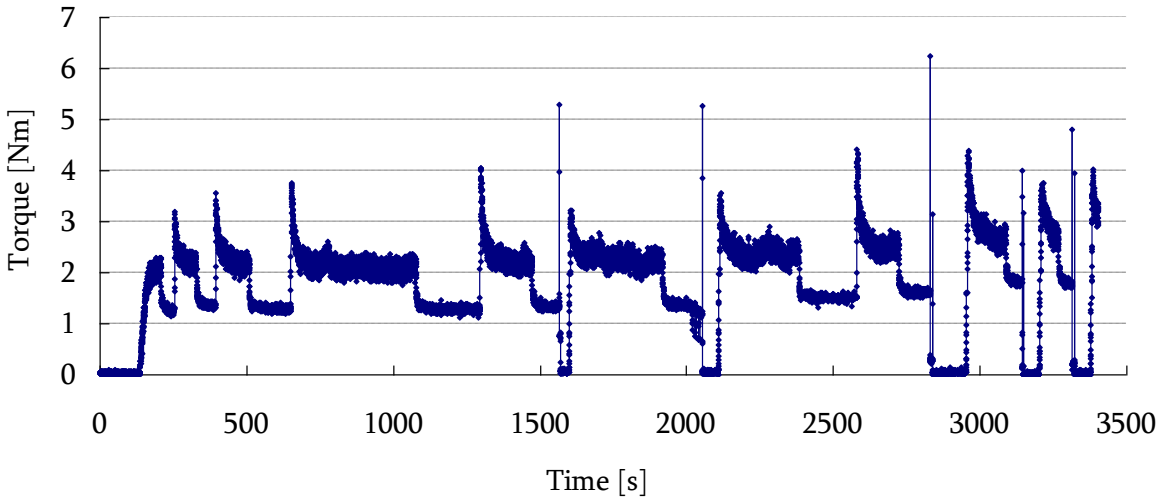

Fig. 39: Torque-time dependence of mixture I at age 83 min on start of measurement

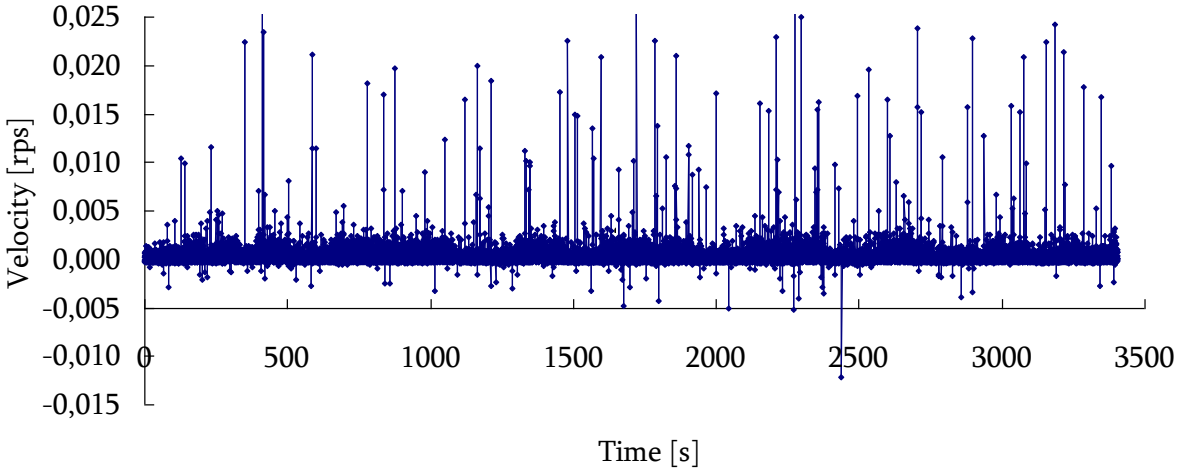

Fig. 40: Velocity profile of measurement

Table 21*: Development of yield stresses* τ_0 of mixture I

Age of SCC [s]	Age of SCC [min]	τ_0 [Pa]	A_{thix} [Pa/s]
5248	87	334.7	0.064
5295	88	510.1	0.096
5436	91	566.9	0.104
5694	95	601.0	0.106
6339	106	647.6	0.102
6646	111	512.2*	0.077
7155	119	567.8*	0.079
7621	127	703.2	0.092
8001	133	699.1*	0.087
8255	138	600.1*	0.073
8426	140	633.4*	0.075

The yield stress τ_0, which is reached after ,,shaking" is marked by *.

Table 22: Development of residual stresses τ_{res} of mixture I

Age of SCC [s]	Age of SCC [min]	τ_{res} [Pa]
5293	88	205.1
5432	91	218.3
5690	95	210.9
6335	106	207.1
6599	110	208.9
7040	117	220.4
7618	127	242.2
7865	131	259.3
8180	136	294.0
8353	139	282.3

Table 23: Development of mobilized τ_{mob} and fully mobilized τ_{fully} stresses of mixture I

Age of SCC [s]	Age of SCC [min]	τ_{mob} [Pa]	τ_{fully} [Pa]	A_{thix} [Pa/s]
5293	88	305.0	-	0.058
5432	91	348.6	-	0.064
5690	95	390.1	-	0.069
6335	106	440.5	-	0.070
6637	111	-	505.0	0.076
7146	119	-	560.2	0.078
7618	127	461.0	-	0.061
7990	133	-	689.6	0.086
8241	137	-	593.7	0.072
8415	140	-	627.3	0.075

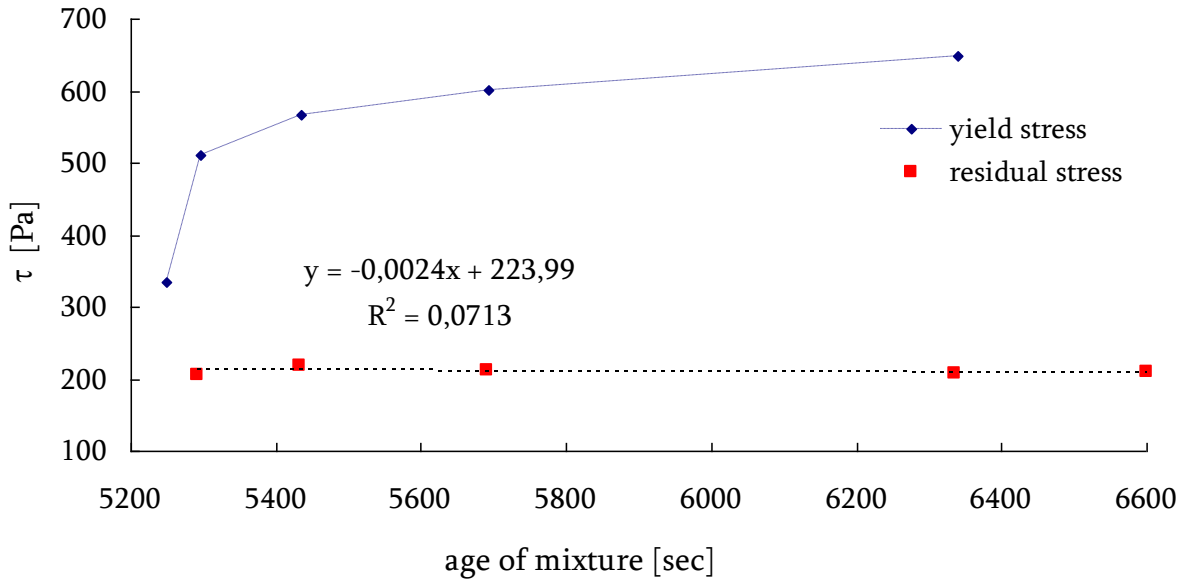

Fig. 41: Development of stresses evaluated from measured point before shaking though including points where stress has been released

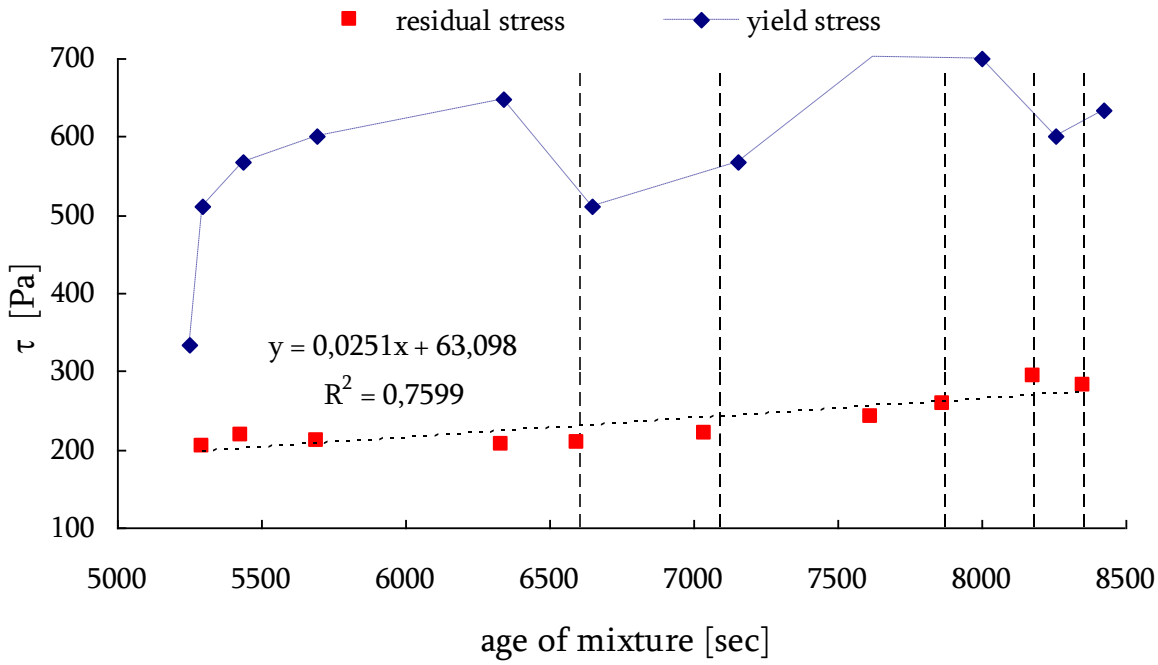

Fig. 42: Development of stresses in mixture I, dashed lines show shaking

The results in tables Table 15 - Table 23 from measurement with the ConTec4 viscometer show similar results of structuration rate (range from 0.06 to 0.15 Pa/s) for the whole torque-time dependency, except for the first testing with confinement, where the obtained structuration rate was almost ten times higher (A_{thix} = 0.389 Pa/s). These results can be comparable with result obtained in Billberg`s work, where structuration rate of micro mortar paste (w/c = 0.34) was equal to 0.13 Pa/s. Again, the result is affected by both age and confinement as well as the hand stirring after the results of Fig. 36 and before Fig. 39.

From Fig. 42 it is obvious that the yield stress, which was reached directly after shaking has a lower value than before. If the measuring is continuously going (without shaking), the yield stress increases. The reason is that the shaking affects the structure of the mixture in a way destructing some new bonds. This effect is typical for thixotropic materials as cement systems are.

5.3.2 Mixture II

5.3.2.1 First part of measurement – start at age of SCC 32 min

Figures 21 – 29 show the results of an effort to make a more systematical investigation of the yield stress build up with regular intervals of stress release by the "shaking" which presumably released the stress by a slight (less than 1/100th) manual rotation.

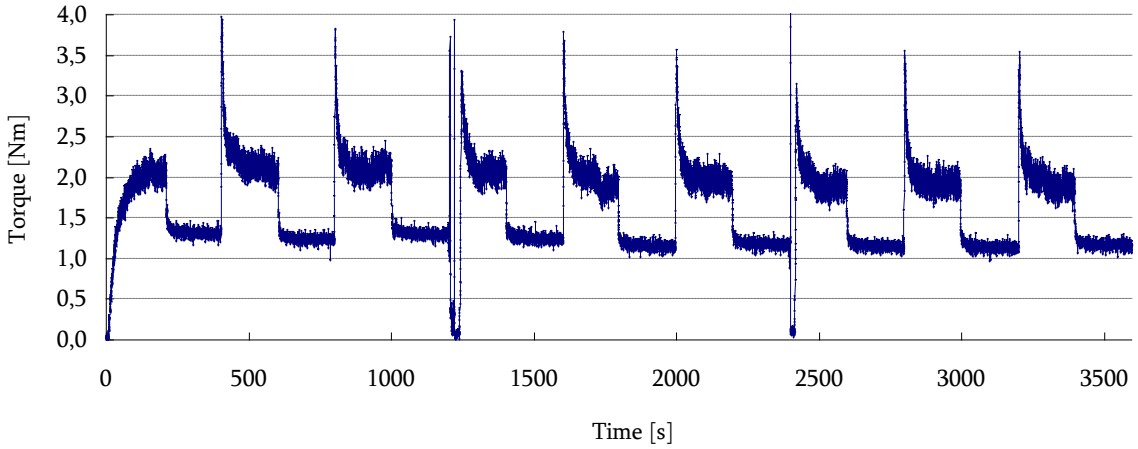

Fig. 43: Torque-time dependence of mixture II at age 32 min on start of measurement

Based on the experience with mixture I the evaluation of measured dependence was done more precisely on mixture II. The objective was to translate the torque-time dependence into stress – strain curves, thus evaluating the elastic behaviour at very low deformation. The measured torque-time dependency was divided into 34 steps and for every step the average velocity and corresponding stress was calculated (yield stress, residual stress, …). The first step is finished in T_{max1} = 2.004 Nm in time 209.999 sec. All values of velocity (software logged actual velocity 5 times per second during measurement) were used for calculation of the average value of velocity (arithmetical mean). The average value of the velocity for the first step is N_{a1} = 0.000538 rps. Then the angular velocity ω [rad·s^{-1}] was calculated, as well as the angle alpha. The following equations were used including a numerical example for the lowest speed:

$$\omega = N_a \cdot 2\pi \tag{47}$$
$$\omega = 0.00054 \cdot 2\pi = 0.00338 \text{ rad} \cdot \text{s}^{-1}$$

$$\Delta\alpha = \omega \cdot \Delta t \tag{48}$$
$$\Delta\alpha = 0.00338 \cdot 210{,}0 = 0.710 \text{ rad}$$

Then the angle γ was calculated using eq. 42, where the dimensions of the inner and outer cylinder of the ConTec4 viscometer and angle alpha were used. Delta γ was calculated for every step. At every step γ increases because of the contribution of the previous step. After the first step γ is 1.7 rad, after the third step gamma is 2.6 rad (=1.7 + 0.9) and so on. Thus the value γ belongs to the time at the end of each step (for example γ 6.8 rad is reached after 1001 sec). The calculated data for first 11 steps (part before first shaking) are shown in the following table:

Table 24: Results of values of velocity,α and γ for part of dependence before first shaking

Step	Time [s]			N_a [rps]	ω [rad/s]	Δ α [rad]	Δγ [rad]	γ [rad]	γ [°]
	from	to	Δ time						
1	0	210	210	0.00054	0.00338	0.710	1.7	1.7	96
2	210	215	5	0.00011	0.00067	0.003	0.0	1.7	97
3	215	403	187	0.00017	0.00109	0.203	0.9	2.6	150
4	403	405	3	0.00065	0.00411	0.011	0.1	2.7	153
5	405	604	199	0.00052	0.00330	0.654	1.6	4.3	246
6	604	607	3	0.00004	0.00023	0.001	0.0	4.3	246
7	607	801	194	0.00015	0.00097	0.188	0.9	5.2	296
8	801	804	3	0.00045	0.00284	0.010	0.1	5.2	300
9	804	1001	197	0.00048	0.00302	0.596	1.6	6.8	389
10	1001	1004	3	0.00010	0.00061	0.002	0.0	6.8	390
11	1004	1199	195	0.00010	0.00060	0.118	0.6	7.4	425

N_a – average velocity [rps]

According to the previous table and the above explanation the torque-time dependency was converted to a torque-gamma dependency.

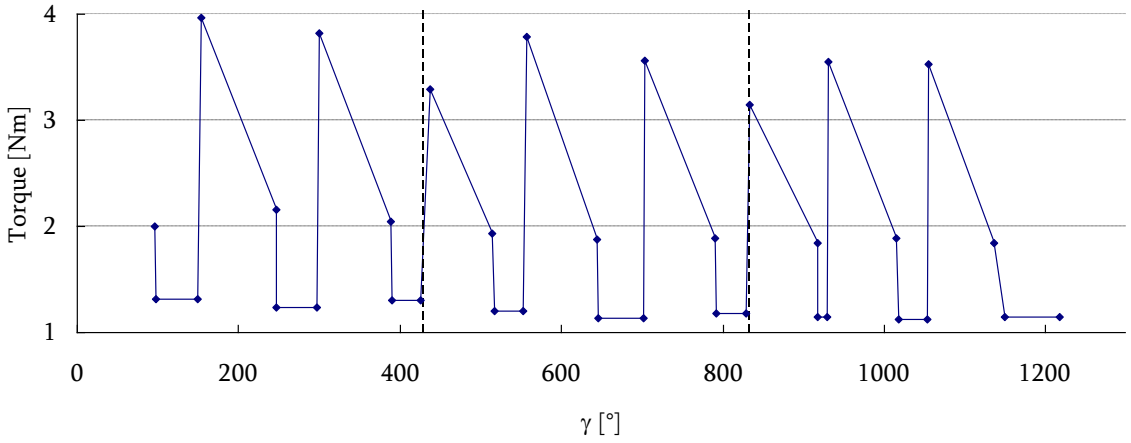

Fig. 44: Torque-gamma dependence evaluated from measured points of mixture II (dashed lines show shaking)

All points of torque-gamma dependence in Fig. 44 were used for calculation of stress according to equation 43 and the obtained dependency is shown in Fig. 45.

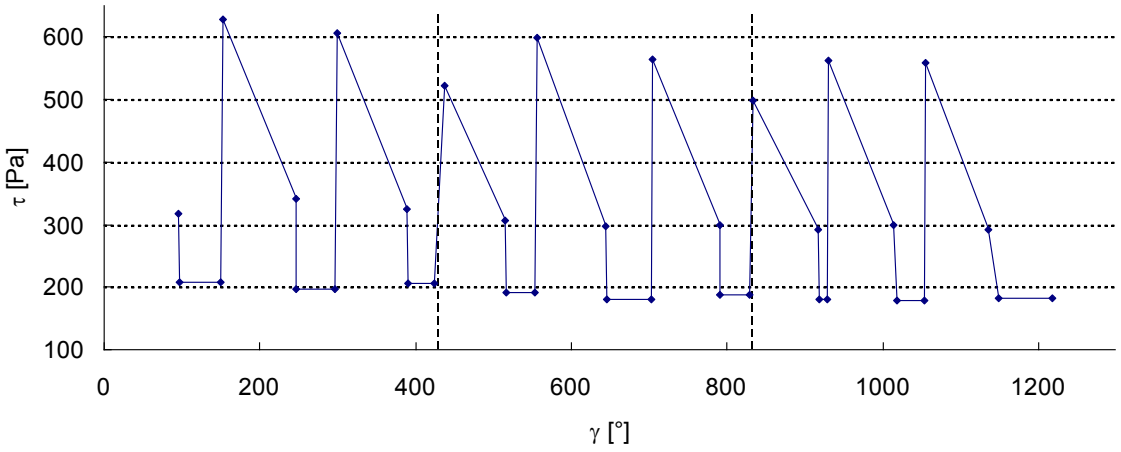

Fig. 45: Shear stress-gamma dependence evaluated from measured points of mixture II (dashed lines show shaking)

The mentioned dependency was analyzed by calculating static yield stress (τ_0), dynamic stress (τ_{dyn}), residual stress(τ_{res}) and mobilized stress (τ_{mob}). All results are shown in following tables (25-27) and Fig. 46 and Fig. 47.

Table 25: Development *of yield stresses* τ_0 of mixture II

Age of SCC [s]	Age of SCC [min]	τ_0 [Pa]	A_{thix} [Pa/s]	A_{thix} [Pa/s]
2130	35	317.0	0.149	
2325	39	627.9	0.270	
2724	45	605.5	0.222	
3167	53	522.1*	0.165	
3525	59	599.5	0.170	0.163
3919	65	564.4	0.144	
4340	72	498.1*	0.115	
4721	79	562.4	0.119	
5122	85	559.3	0.109	

The yield stress τ_0, which is reached after ,,shaking" is marked by *.

Table 26: Development of residual stresses τ_{res} of mixture II

Age of SCC [s]	Age of SCC [min]	τ_{res} [Pa]
2320	39	202.9
2720	45	198.9
3120	52	206.6
3520	59	190.9
3915	65	180.4
4310	72	187.7
4712	79	180.8
5113	85	178.8
5514	92	181.8

Table 27: Development of mobilized τ_{mob} and fully mobilized τ_{fully} stresses of mixture II

Age of SCC [s]	Age of SCC [min]	τ_{mob} [Pa]	τ_{fully} [Pa]	A_{thix} [Pa/s]	A_{thix} [Pa/s]
2325	39	425.0	-	0.183	0.122
2724	45	406.6	-	0.149	
3159	53	-	508.0	0.161	
3525	59	419.1	-	0.119	
3919	65	376.7	-	0.096	
4331	72	-	485.8	0.112	
4721	79	383.6	-	0.081	
5122	85	377.5	-	0.074	

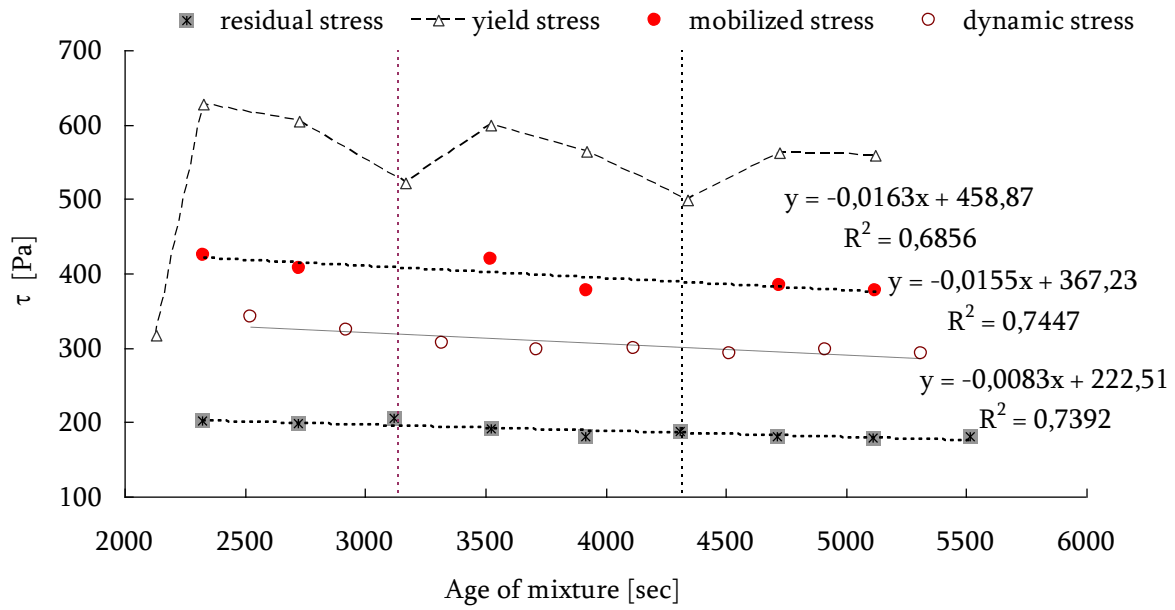

Fig. 46: Development of stresses in mixture II (dashed lines show shaking)

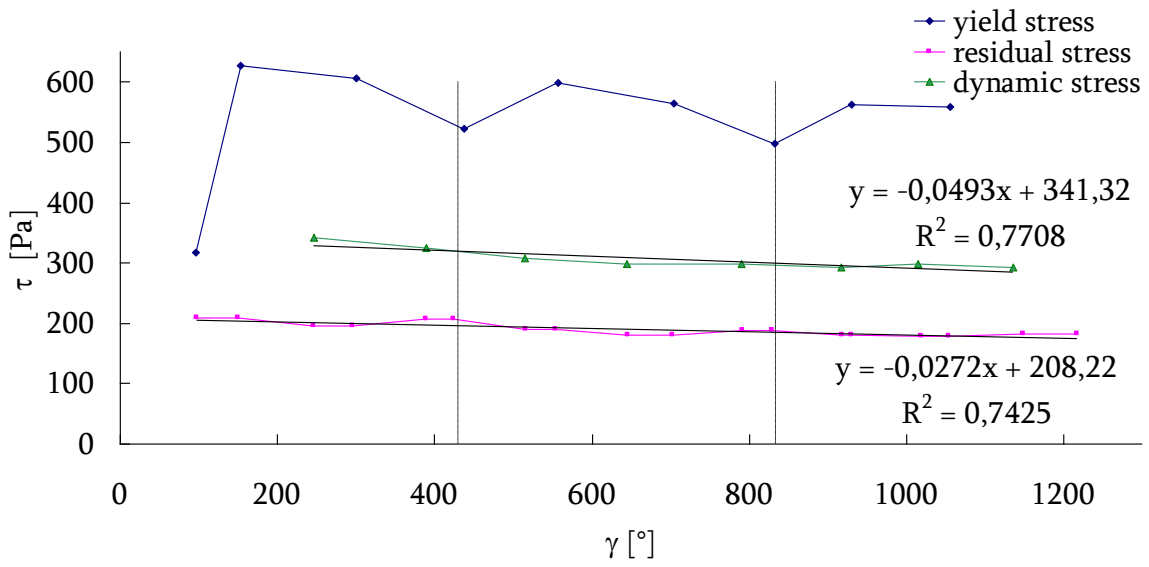

Fig. 47: Shear stress-gamma dependence of mixture II (dashed lines show shaking)

From Fig. 46 and 47 no clear increase of none of the stresses are seen except for from the first (gradual) to the second (sharp) maximum torque values reached in Fig. 47. However, between all values subsequent to the first value no clear increase was seen. Due to this the calculation procedure was reviewed resulting in a modified 2nd procedure of calculation and evaluation of the data.

5.3.2.2 Second procedure of calculation and evaluation

In this procedure the calculation of γ was done for every measured point. During measurement the software logged data every 0.2 seconds. Because of very slow rotation of the outer cylinder (0.0015 rps) and the low accuracy of the rotation control of the equipment, a lot of negative values of rotation velocities were logged as seen in figures 31, 33, 35, 37 and 40. Negative values of velocities means counter motion of the outer cylinder, which corresponds to a decrease of γ. These negative values thus contribute to the growth of γ due to the cosine function in equation 42, which is used for evaluating gamma. That means that negative value of velocity (for example -0.0015 rps) give negative value of angle alpha (-0.0019 rad in our case), but the value is positive after applying cosine function (cos (-0.0019 rad) = 0.999998) and is same as value obtained from positive value of velocity (0.0015 rps).

During the whole measurement 9 steps were made with the motion of the outer cylinder. Every step took 200 seconds that gives 9x200 = 1800 seconds of motion. When we assume the rotation velocity N = 0.0015 rps (0.0015 rps = 0.00942 rad/s), then 0.00942x1800 = 16.956 rad = 972° done during the whole measurement.

The angle γ was calculated for every measured point in the modified second procedure of evaluation and the final value of γ was 63 rad (3628°). It appears from this that the contributions of negative values of velocities on increasing the gamma are so large that this way is not applicable.

Anyway the evaluation of gamma was done in this way too and the results are shown in the following figures Fig. 48-50. The shear stress was calculated in the same way as previously that means using equation 43.

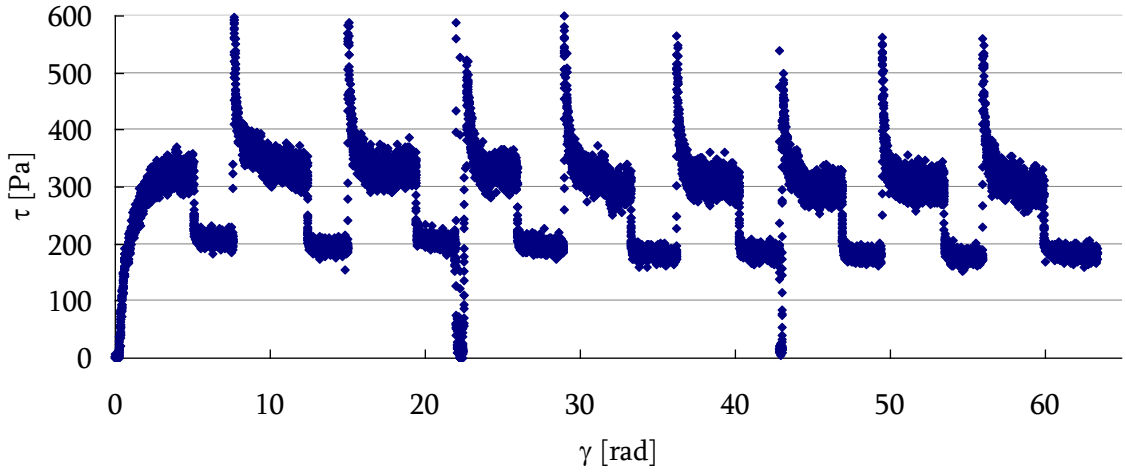

Fig. 48: Calculated dependency measured for mixture II evaluated with procedure 2 (which means calculation of gamma for every measured point) at starting age 32 min

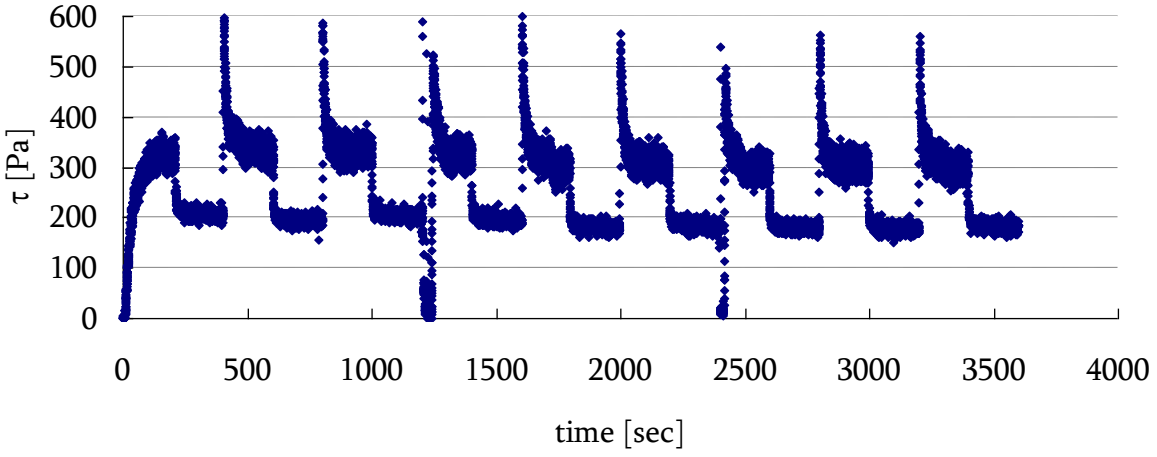

Fig. 49: Calculated dependency for mixture II, where measured torque was converted into stress according to eq. 43

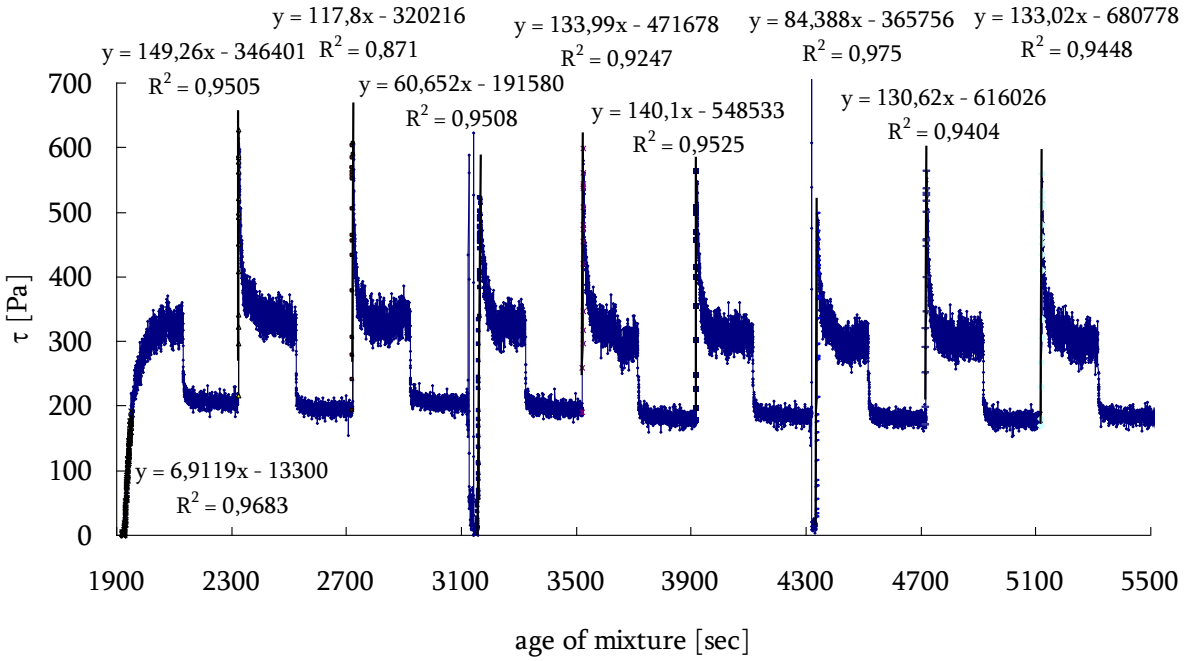

Fig. 50: Calculated dependency for mixture II

In the plot of stress versus age of mixture dependence (Fig. 50) a linear regression was applied on the linear parts of the curves. This means those parts of the curves when the rotation was applied and torque (stress) suddenly peaked reaching maximum values (the static yield stress). The slopes of these lines represent the rate of increase of stress at the moment of start of rotation (reaching the yield value). These values are proportional to the shear modulus G and are called B [Pa/s] in Table 28. G can be obtained by dividing B with the rate of shear (0.0015 s^{-1}). This development of G modulus is shown in Fig. 51 together with the clear increase of the G the modulus which was reached immediately after shaking. The increasing trend of G modulus can be found between values which were achieved between the shaking except for the first part of the measurement that means before first shaking.

Table 28: Obtained data for mixture II

age of mixture [min]	age of mixture [s]	τ_o [Pa]	A_{thix} [Pa/s]	B [Pa/s]	G [kPa]
35	2130	317.0	0.149	6.9	4.6
39	2325	627.9	0.270	149.3	99.5
45	2724	605.5	0.222	117.8	78.5
53	3167	522.1*	0.165	60.7	40.5
59	3525	599.5	0.170	134.0	89.3
65	3919	564.4	0.144	140.1	93.4
72	4340	498.1*	0.115	84.4	56.3
79	4721	562.4	0.119	130.6	87.1
85	5122	559.3	0.109	133.0	88.7

The yield stress τ_0, which is reached after „shaking" is marked by *.

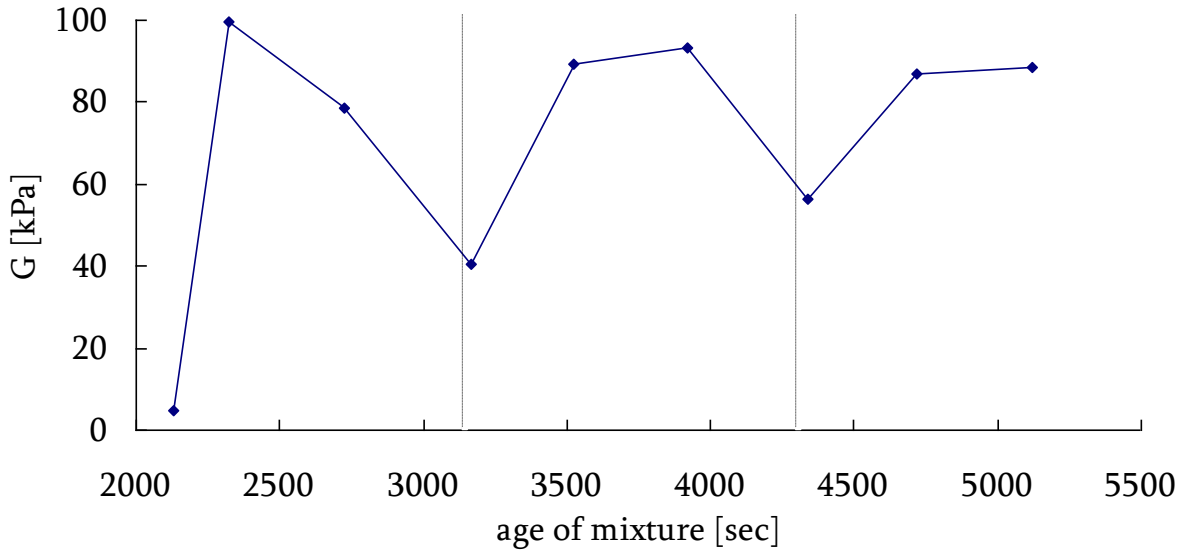

Fig. 51: Development of G modulus of mixture II (dashed lines show shaking)

5.3.2.3 Second part of measurement – start at age of SCC 94 min

Fig. 52 and 53 show the results of repeating the whole experiment at age 94 minutes with mixture II. Torque-time dependency (Fig. 52) was evaluated in the same way of calculation of stresses as shown in tables Table 29-31 and Fig. 53.

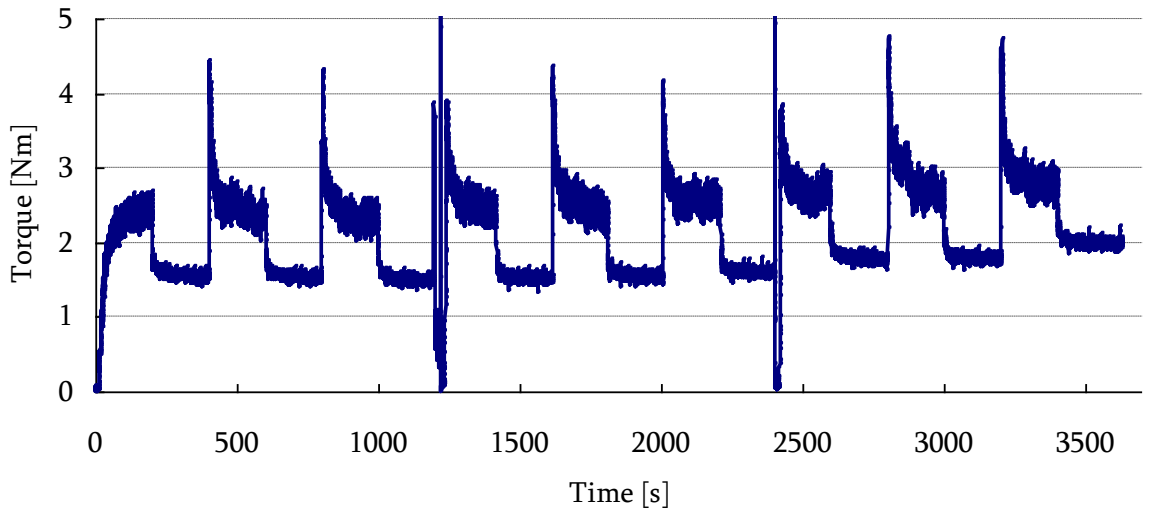

Fig. 52: Torque-time dependence of mixture II at age 94 minutes from water addition to start of measurement

Table 29: Development of yield stresses τ_0 of mixture II

Age of SCC [s]	Age of SCC [min]	τ_0 [Pa]	A_{thix} [Pa/s]	A_{thix} [Pa/s]
5840	97	381.8	0.065	
6045	101	702.6	0.116	
6444	107	685.0	0.106	
6883	115	611.2*	0.089	
7259	121	689.3	0.095	0.090
7647	127	659.1	0.086	
8065	134	603.8*	0.075	
8444	141	752.7	0.089	
8844	147	748.1	0.085	

The yield stress τ_0, which is reached after „shaking" is marked by *.

Table 30: Development of residual stresses τ_{res} of mixture

Age of SCC [s]	Age of SCC [min]	τ_{res} [Pa]
6040	101	237.9
6440	107	236.3
6729	112	238.1
7241	121	243.3
7640	127	245.2
8016	134	255.2
8440	141	279.7
8817	147	282.8
9268	154	314.8

Table 31: Development of mobilized τ_{mob} and fully mobilized τ_{fully} stresses of mixture

Age of SCC [s]	Age of SCC [min]	τ_{mob} [Pa]	τ_{fully} [Pa]	A_{thix} [Pa/s]
6040	101	464.7	-	0.077
6440	107	448.8	-	0.070
6866	114	-	591.3	0.086
7640	127	444.1	-	0.058
8016	134	403.9	-	0.050
8047	134	-	598.5	0.074
8817	147	469.9	-	0.053
9268	154	433.3	-	0.047

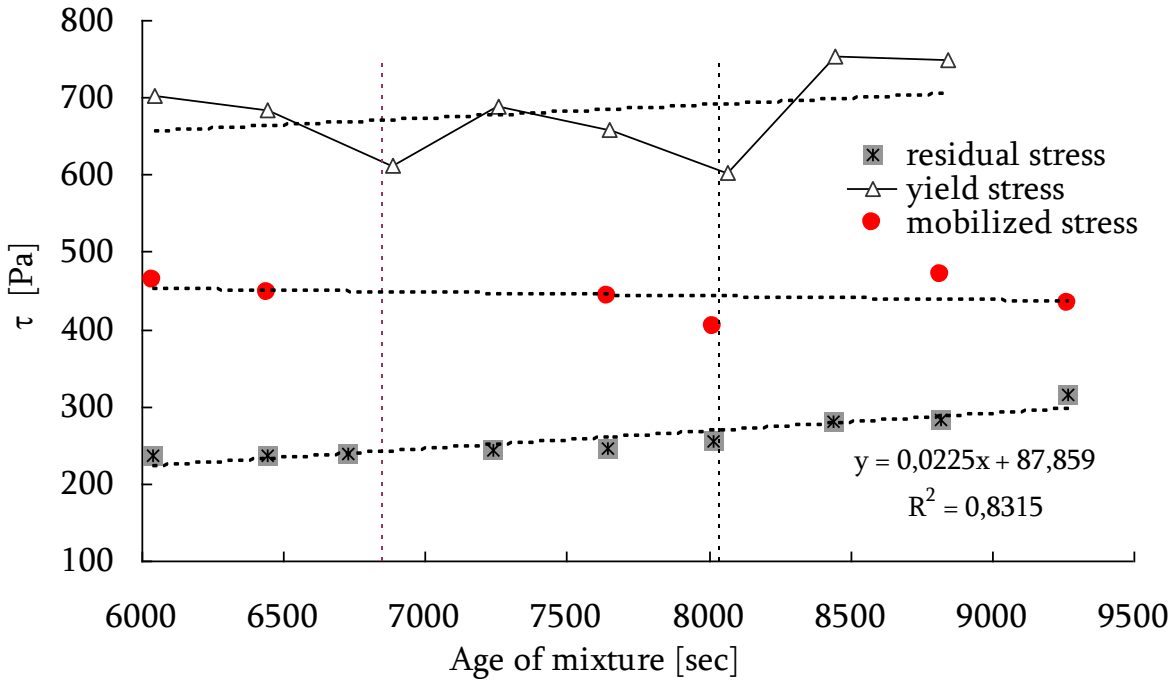

Fig. 53: Development of stresses evaluated for mixture II

Fig. 53 shows more tendency of structural build-up over the period of the experiment than does Fig. 46. However, compared to figures Fig. 38 and Fig. 41 the time dependency is less clear.

The structuration rate ranges from 0.16 Pa/s which is an average obtained in the first part of the measurement to 0.09 Pa/s which is an average of the second part. This indicates a slowing structural build-up of mixture. Again, the results are affected by age and confinement as well as motion up and down with inner cylinder before second testing. According to Roussel´s classification (Table 8) the mixture II belongs to thixotropic SCC.

According to procedure 2, where every measured point was used for calculation of the stress value, the following dependency was obtained (Fig. 54). The linear regression was applied on the linear part of curves and B as well as G modulus was obtained in same way as mentioned before (Table 32).

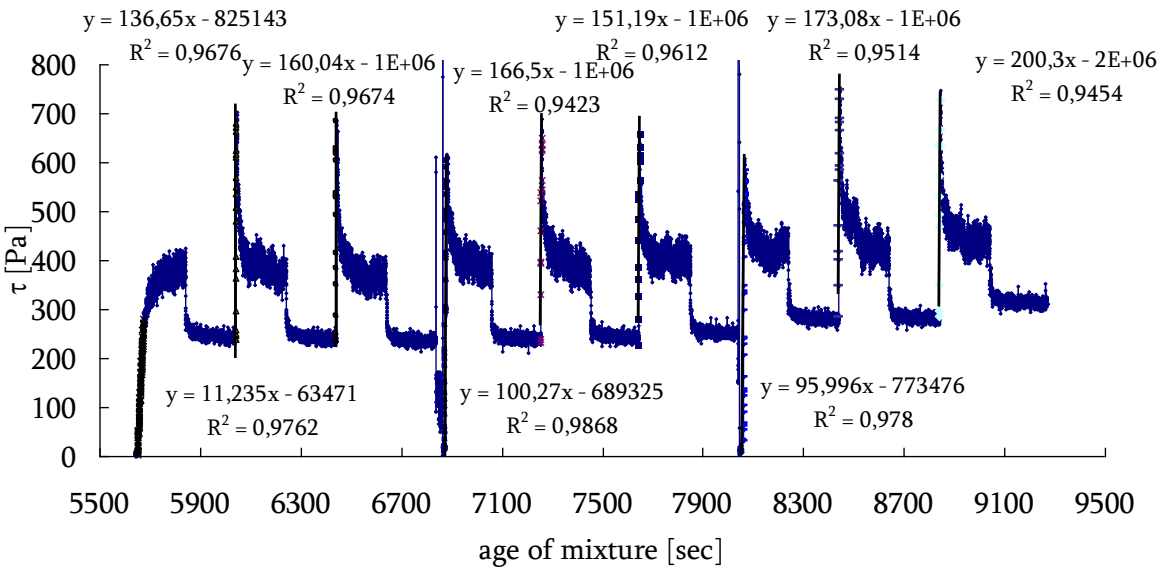

Fig. 54: Calculated time-dependency of stresses for mixture II at age 94 minutes from water addition to start of measurement

Table 32: Obtained data for mixture II

age of mixture		τ_o [Pa]	A_{thix} [Pa/s]	B [Pa/s]	G [kPa]
[min]	[s]				
97	5840	381.8	0.065	11.2	7,5
101	6045	702.6	0.116	136.7	91,1
107	6444	685.0	0.106	160.0	106,7
115	6883	611.2*	0.089	100.3	66,9
121	7259	689.3	0.095	166.5	111,0
127	7647	659.1	0.086	151.2	100,8
134	8065	603.8*	0.075	96.0	64,0
141	8444	752.7	0.089	173.1	115,4
147	8844	748.1	0.085	200.3	133,5

The yield stress τ_0, which is reached after ,,shaking" is marked by *.

Development of G modulus is shown in Fig. 55, where an obvious increase of the G modulus before first and after second shaking can be deduced. The G moduli obtained during the second part of the measurement (Fig. 55) are higher than G moduli from the first part of the measurement (Fig. 51) due to the aging of the mortar.

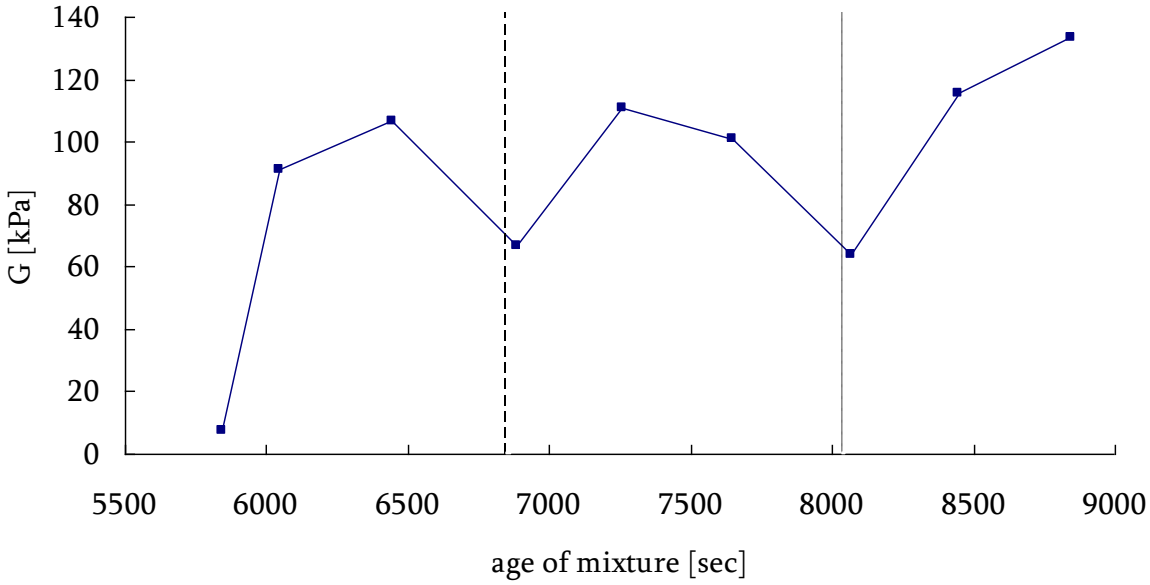

Fig. 55: Development of G modulus of mixture II (dashed lines show shaking)

5.4 Plate test

The result from the plate test gives the time-dependency of yield stress. The structuration rate A_{thix} was obtained from linear regression. These gave the values 0.021 Pa/s = 1.26 Pa/min for the mixture I and 0.014 Pa/s = 0.83 Pa/min for the mixture II (Fig. 56 and Fig. 57).

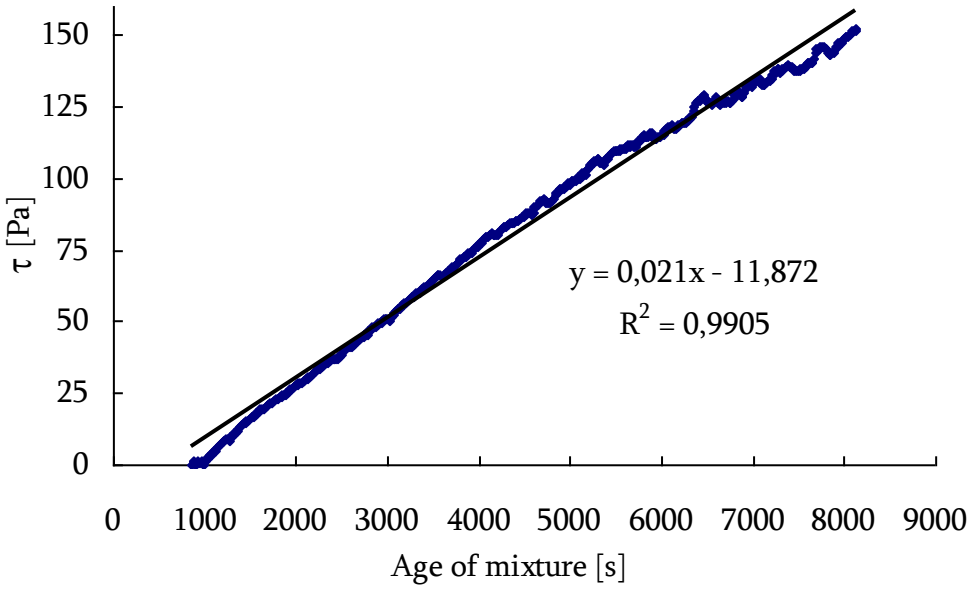

Fig. 56: Obtained curve from plate test for mixture I

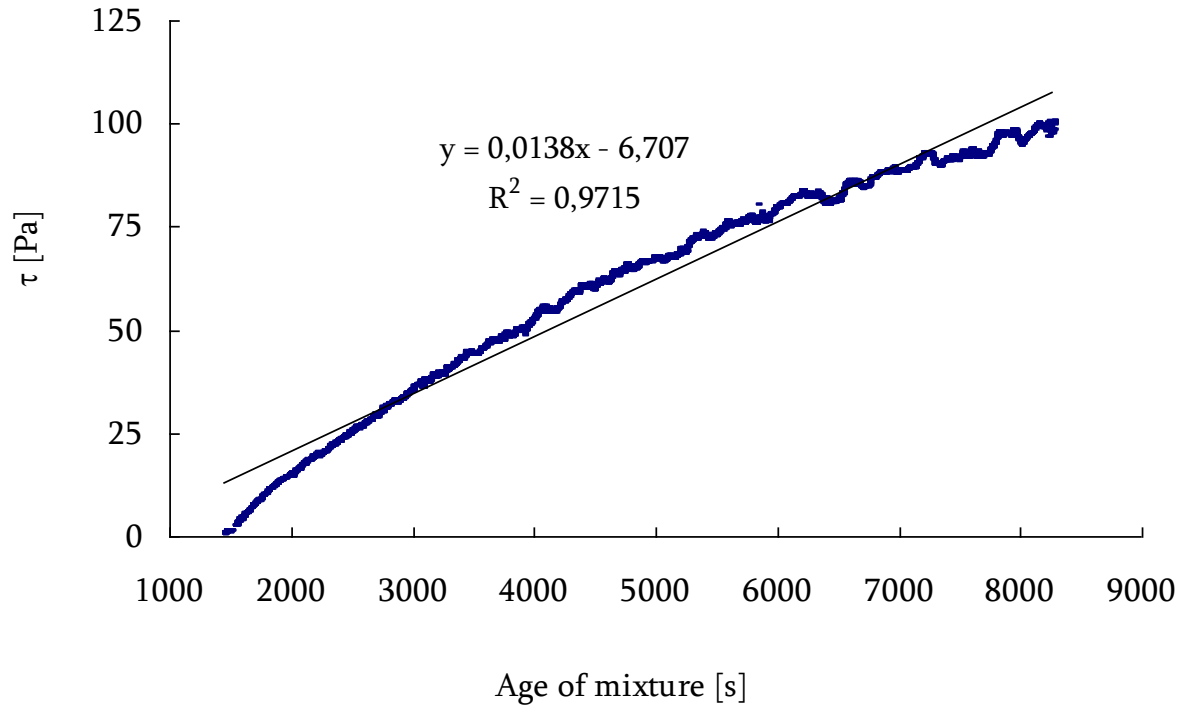

Fig. 57: Obtained curve from plate test for mixture II

Clearly this method gives very low increase of yield stress values compared to the viscometer values given in tables 15, 18, 20, 21, 25, 28, 29 and 32. It should be noted that the plate test we used was mainly developed for cement paste. Possibly the roughness of the sandpaper on the plate (Fig. 26), which was approximately 0.2 mm, did not reflect the same yield as the rougher surface of the core of the viscometer which has larger knifes (Fig. 24). According to the Roussel`s classification (Table 8) the tested mixtures belongs to non-thixotropic SCC.

5.5 Conclusions for static yield stress measurements

An investigation on the time-dependant development of yield stress in two similar self-compacting mortars using slowly rotating ConTec4 viscometer and a newly developed plate test was made. The results from the ConTech4 revealed that both the static yield stress and structuration rate depend on the confinement conditions. A much higher static yield stress was obtained with a residual stress in the confined mortar in the viscometer gap compared to yield stress developing in unconfined state at start or after a release of the residual stress by a shaking movement of the viscometer.

A more detailed analysis based on data filtration of negative rotation values showed structuration rate of similar magnitude and also allowed to evaluate the shear modulus G which also showed a very clear increase with time.

Finally, measurements with the plate test showed much lower absolute values of yield and lower structural build-up rate, possibly due to the low plate roughness designed for paste tests as opposed to the larger vanes of the viscometer core. Also the deformation conditions around the plate and the viscometer core vary.

5.6 Results of measurement with parallel plate rheometer

The gel strength was determined first from the resulting curves in test I. Then the shear moduli (modulus of rigidity G) were calculated from the linear part of shear stress – strain curves according to the equation [1]:

$$\tau = G \cdot \gamma \quad (49)$$

G moduli were found at various ages of the matrixes, so rate of change of G (dG/dt) was determined too. Flow curves were evaluated using the Bingham model and parts of down curves always in range of shear rate 3 – 60 s^{-1} were used for this. All rheological parameters are related to their age (age 0 min is the moment of first contact of water with solid materials) at the start of measurement.

5.6.1.1 Test I

Fig. 58 shows the measured curves obtained during sequence 3 and gel strengths are shown in Table 33, Fig. 59, 60 and 61 show measured curves obtained during testing with constant shear rate to reach the static yield stresses. The results from these figures are shown in Table 34, 35 and 36, where the static yield stress and G moduli are evaluated. Fig. 62 shows the obtained flow curves with evaluation of Bingham's parameters that are given in Table 37. Table 38 summarizes results from test I.

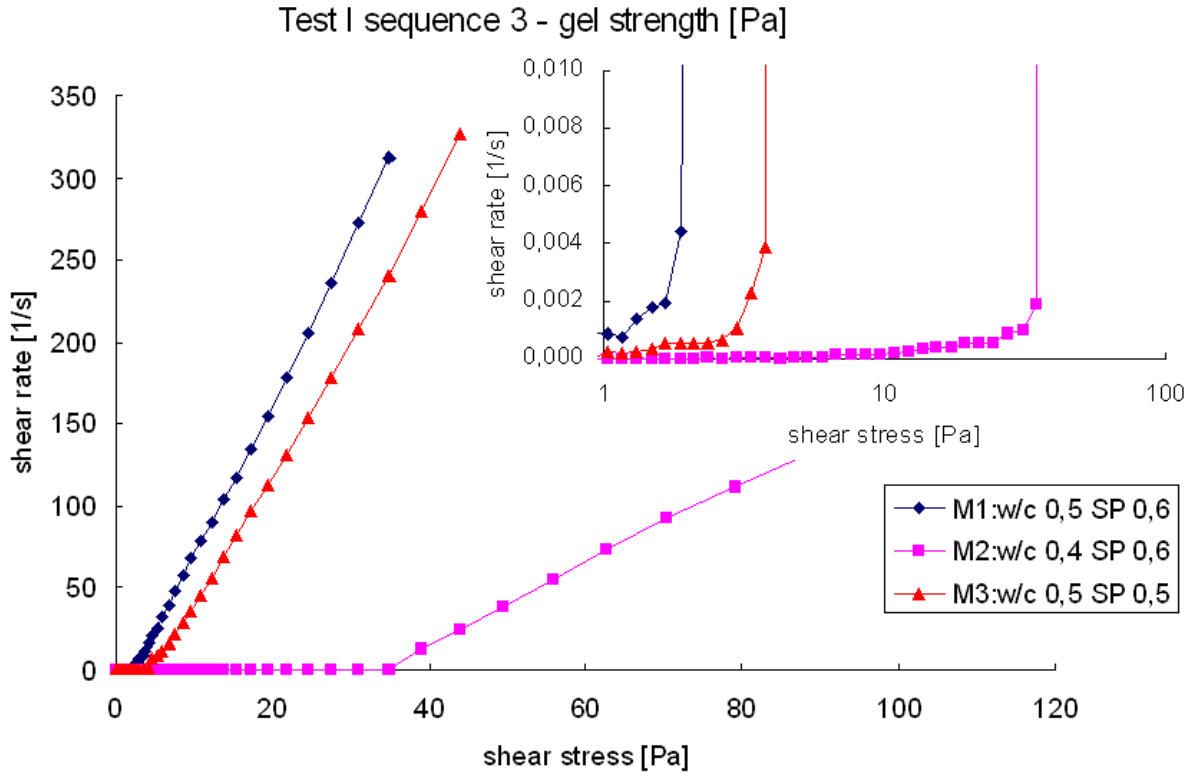

Fig. 58: Gel strength with logarithmic stress sweep of tested matrixes (age of matrixes on start of measurement 11.5 min)

Table 33: Resulting gel strength of matrixes

Matrix	Gel strength [Pa]	Age [min]
M1 w/c=0.5,SP=0.6	2.1	11.5
M2 w/c=0.4,SP=0.6	34.9	11.5
M3 w/c=0.5,SP=0.5	3.8	11.5

The gel strength of the first matrix M1 (corresponding with mortar tested in previous tests) was 2.1 Pa. A decrease of SP content led to a little bit higher value of gel strength: 3.8 Pa. There was a much larger effect on gel strength on decrease of w/c ratio for matrix M2 with gel strength 34.9 Pa. The obtained curves from the next sequences of test I are the following:

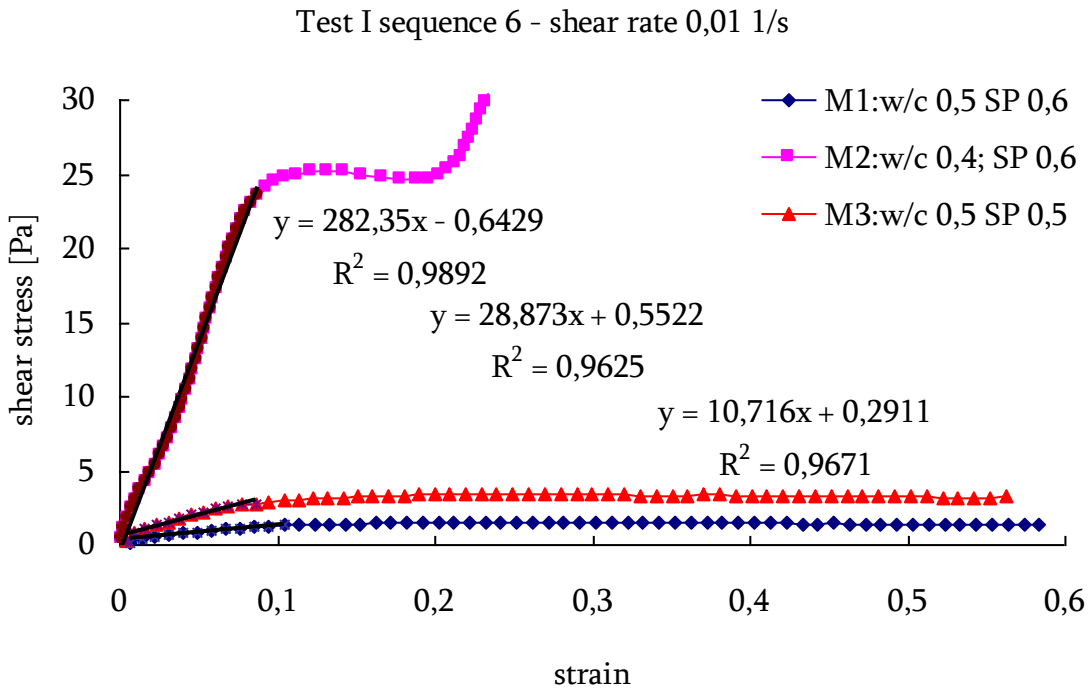

Fig. 59: Stress-strain curves obtained from test I sequence 6 for all matrixes (age of matrixes on start of measurement 18 min)

Table 34: Resulting G moduli and static yield stress of matrixes from sequence 6

Matrix	Age [min]	G modulus [Pa]	Static yield stress [Pa]
M1	18.0	10.7	1.5
M2	18.0	282.4	25.2
M3	18.0	28.9	3.4

The highest G modulus was observed for matrix M2 with the lowest w/c ratio: 282.4 Pa. The curve for matrix M2 showed clearest linearity in Fig. 59 and also the clearest point where the elastic deformation changed to plastic. The value was 25.2 Pa. The end of this curve shows a strange behaviour as shown by rapid increase of shear stress, possibly due to dilatancy at particle rearrangement and change of packing state at interaction at early shear-movement of this most densely packed matrix. Shear stress – strain curves of matrix M1 and M3 have short linear parts before coming to almost constant stress. The G moduli take the values 10.7 Pa and 28.9 Pa respectively. The static yield stress (evaluated as the maximum value reached during measurement) was 1.5 Pa and 3.4 Pa for M1 and M3 respectively.

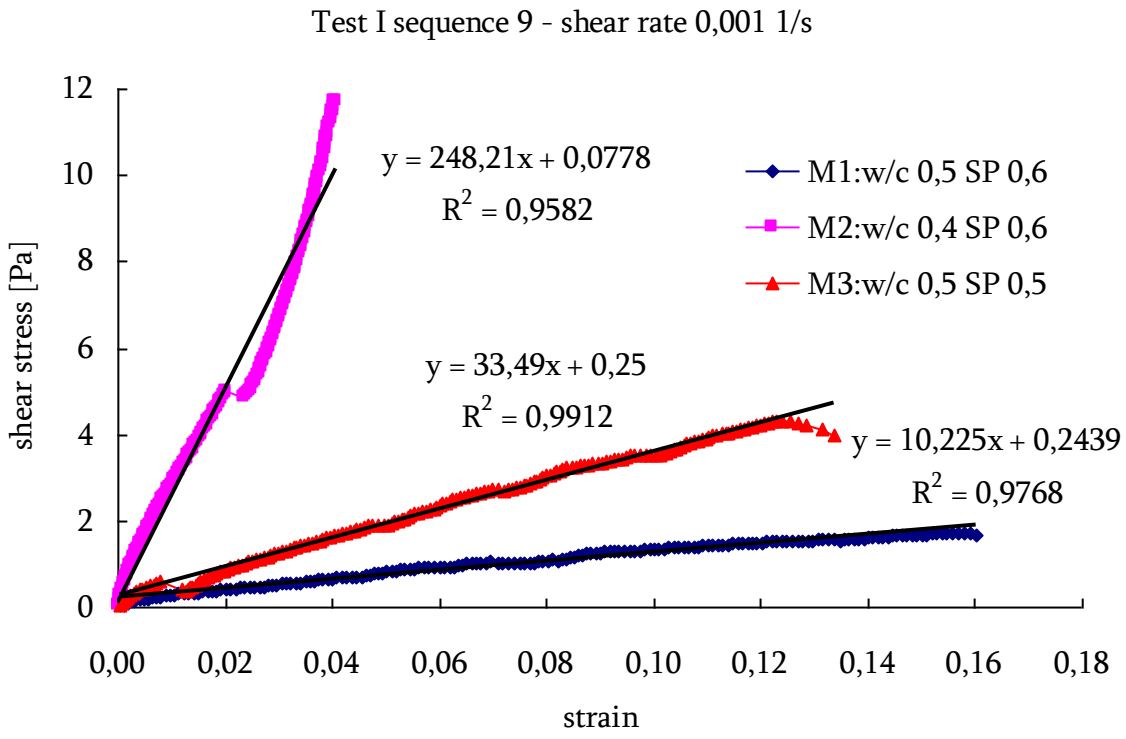

Fig. 60: Resulting curves obtained from test I sequence 9 for all matrixes (age of matrixes at start of measurement 20.5 min)

In sequence 9 (shown on fig. 38 and Table 35) the slowest shear rate (0.001 s^{-1}) was used. This very low value of shear rate should give high values of G moduli because of high sensitivity. However, this only seems to be the case for matrix M3 with value of G modulus 33.5 Pa. G modulus of matrix M1 is practically the same as the value obtained in sequence 6 and it is 10.2 Pa and the G modulus obtained for matrix M2 is a little bit lower compared with previous sequences and reaches the value 248.2 Pa. The static yield stress was caught only for matrix M3, whereas the other matrixes didn't reach the static yield stress because of very low shear rate and not long enough measurement time. The static yield stress of matrix M3 was 4.3 Pa which is a little bit higher value than the value obtained in the previous test sequence (3.4 Pa). This observation is in line with the findings of others [56] observing that applied shear rate strongly affects the static yield stress.

Table 35: Resulting G moduli and static yield stress of matrixes from sequence 9

Matrix	Age [min]	G modulus [Pa]	Static yield stress [Pa]
M1	20.5	10.2	-
M2		248.2	-
M3		33.5	4.3

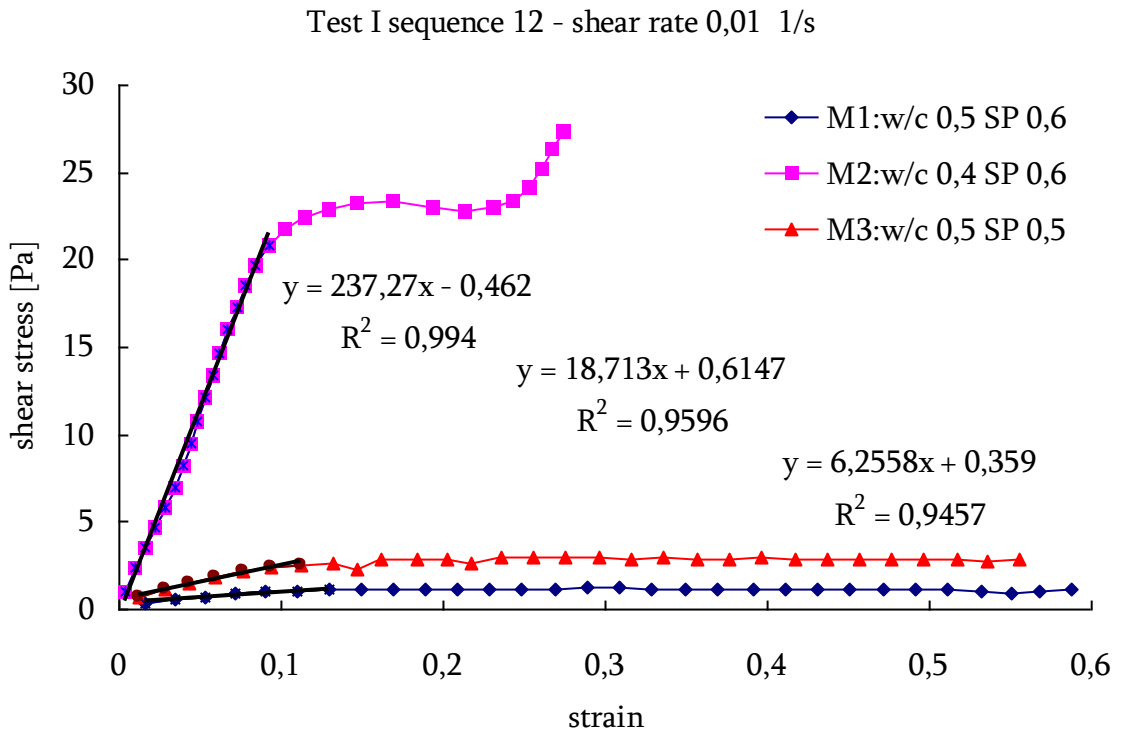

Fig. 61: Resulting curves obtained from test I sequence 12 for all matrixes (age of matrixes on start of measurement 25 min)

Fig. 61 shows sequence 12 which is similar to sequence 6. All obtained values of G moduli are lower compared to the results from sequence 6 and 9. This can be explained by the shear history of the samples (look at the test description) and some breaking of transient bonds in the matrixes during aging (setting). Again the same behaviour is seen for w/c 0.40. All values of G moduli and their change with time are shown in Table 36. The ratio dG/dt seems to be more suitable for comparison of results, because these values are almost the same for each sequence (0.01 and 0.01 Pas.s^{-1} for M1; 0.25 and 0.20 Pas.s^{-1} for M2; 0.03 and 0.03 Pas.s^{-1} for M3) except the last sequence (12) where these values are lower because of the shear history of the samples as mentioned. G moduli obtained during test I are summarized in Table 36.

Table 36: Results of G moduli of matrixes obtained by test I

sequence	Age of matrix [min]	Matrix	G modulus [Pa]	dG/dt [Pa/sec]
6	19.0	M1	10.7	0.01
		M2	282.4	0.25
		M3	28.9	0.03
9	20.5	M1	10.2	0.01
		M2	248.2	0.20
		M3	33.5	0.03
12	25.0	M1	6.3	0.00
		M2	237.3	0.16
		M3	18.7	0.01

The last sequence of test I consisted of measuring flow curves of matrixes in shear rate ranging from 0.01 to 60 s^{-1}. The obtained curves are shown in Fig. 62 and the rheological parameters plastic viscosity and yield stress are listed in Table 37. Again we see the possible consequence of dilatancy for M2 (w/c = 0.40) in the early part of the flow curve at early particle interaction and rearrangement.

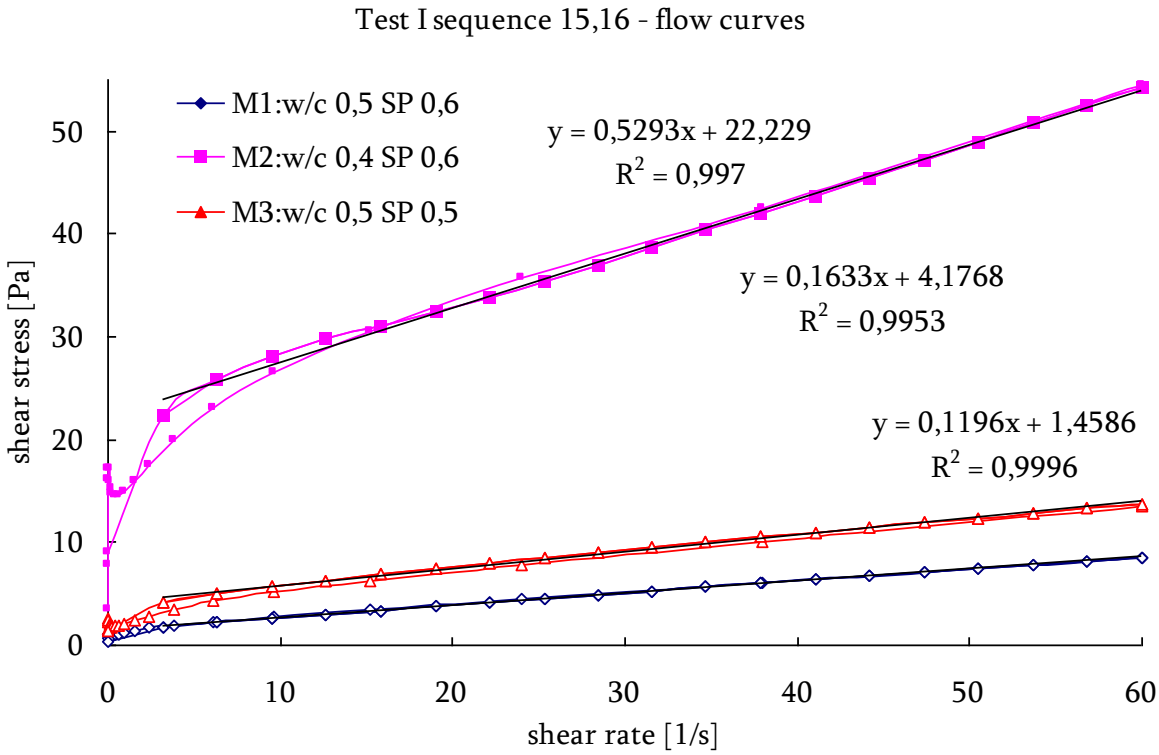

Fig. 62: Flow curves of matrixes (age of matrixes on start of measurement 27.5 min and 29.5 min for up-curve and down-curve respectively) with linear regression of down-curves

Table 37: Obtained results from evaluation of flow curve

Matrix	Plastic viscosity [Pa.s]		Dynamic yield stress [Pa]	
	Up-curve	Down-curve	Up-curve	Down-curve
M1	0.12	0.12	1.5	1.5
M2	0.61	0.53	19.1	22.2
M3	0.17	0.16	3.4	4.2
Age [min]	27.5	29.5	27.5	29.5

The Bingham's parameters were evaluated for up and down flow curves. In case of matrix M1 the flow curves were coincident, and therefore also the Bingham's parameters. The flow curves of matrix M2 had different behaviour during very low shear rates and beyond a shear rate of approximately 15 s^{-1} the flow curves became identical. That is the reason for a bit lower plastic viscosity and higher yield stress evaluated from the down-curves compare to the up-curves. The flow curves of matrix M3 show similar tendency. Therefore only yield stress is a little bit higher in case of evaluation from down curves.

The lowest values of plastic viscosity (0.12 Pa.s) and yield stress (1.5 Pa) were found for matrix M1 with the highest water and SP content. As in case of values of gel strength the effect of w/c is more important than SP dosage and led to increasing plastic viscosity to 0.53

Pa.s and yield stress 22.6 Pa (matrix M2). Decreasing SP dosage changed the parameters to 0.16 Pa.s and 4.2 Pa respectively (matrix M3).

Table 38: Obtained results from test I for all matrixes

sequence	Test description	Age [min]		M1	M2	M3
3	-	11.5	Gel strength	2.1	34.9	3.8
6	shear rate 0.01 s^{-1}	18.0	Static yield stress	1.5	25.2	3.4
			G modulus	10.7	282.4	28.9
9	shear rate 0.001 s^{-1}	20.5	Static yield stress	-	-	4.3
			G modulus	10.2	248.2	33.5
12	shear rate 0.01 s^{-1}	25.0	Static yield stress	1.2	23.4	2.8
			G modulus	6.3	237.3	18.7
15	flow curve-up	27.5	Plastic viscosity	0.12	0.61	0.17
			Yield stress	1.5	19.1	3.4
16	flow curve-down	29.5	Plastic viscosity	0.12	0.52	0.16
			Yield stress	1.5	22.6	4.2

All results obtained during the test I are summarized in Table 38. If the gel strength is compared with the static yield stress of matrixes, in all cases the gel strength achieved higher value. This is connected with quite rapid change of stress (logarithmic sweep) during sequence 3 and more sensitive measurement during sequences where the constant shear rate was used (sequence 6, 9 and 12).

The static yield stresses obtained during sequence 12 are a little bit lower than values obtained during sequence 6, were the same shear rate was applied. This fact should be connected with breaking new bonds during measurement despite of creating new structure during aging of samples. The static yield stress evaluated for matrix M3 in sequence 9 (the applied shear rate was 0.001 s^{-1}) is higher compared to the stresses obtained in sequence 6 and 12 (the applied shear rate was 0.01 s^{-1}), which is in compliance with theoretical knowledge.

The dynamic yield stress obtained from flow curves is same as static yield stress in case of matrix M1. The dynamic yield stress of matrix M2 is lower than the static, which is in compliance with theory [56]. On the other hand matrix M3 showed opposite behaviour.

5.6.1.2 Test II

In this test the behaviour of samples under the constant shear rate 0.001 s^{-1} was studied. The obtained curves (Fig. 63) were nearly linear. The lowest regression coefficient 0.92 was found for the last sequence in test II. Results of G moduli and their change with time are shown in the Table 39. G modulus increases with time (from 24 Pa to 32 kPa) due to aging (setting) of matrixes. The rate of increase of G (dG/dt) increases almost exponentially as shown on Fig. 64.

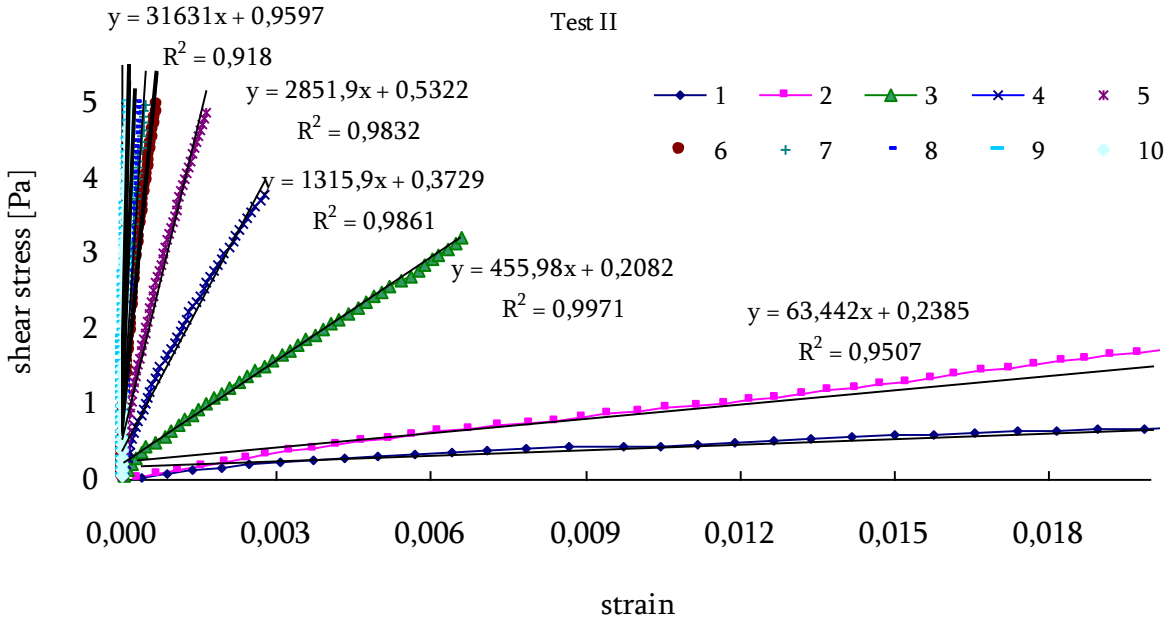

Fig. 63: Measured shear stress- strain curves with linear regressions for evaluation of G moduli (age of matrixes on start of measurement of first curve was 12.0 min and time between individual steps was 5 min)

Table 39: Results from test II

	G [Pa]	age [min]	dG [Pa]	dt [sec]	dG/dt [Pa/sec]
1	24.4	12	24.4	720	0.0
2	63.4	17	39.0	300	0.1
3	456.0	22	392.6	300	1.3
4	1315.9	27	859.9	300	2.9
5	2852.0	32	1536.1	300	5.1
6	6878.7	37	4026.7	300	13.4
7	10479.0	42	3600.3	300	12.0
8	15582.0	47	5103.0	300	17.0
9	27083.0	52	11501.0	300	38.3
10	31631.0	57	4548.0	300	15.2

*age of matrixes on start of measurement of curve

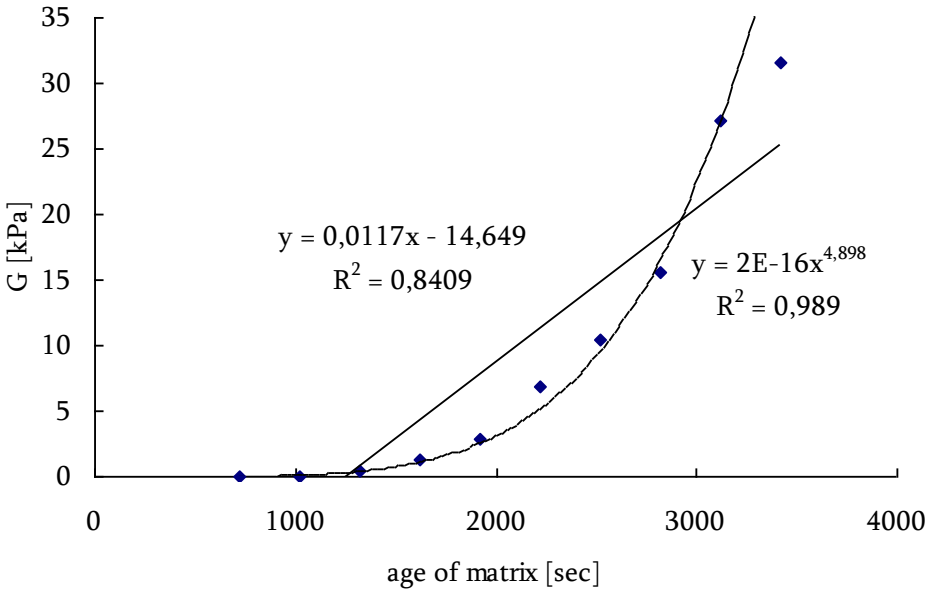

Fig. 64: Development of G modulus obtained from test II

5.6.1.3 Test III

The behaviour of the samples was studied in this test under the constant shear rate 0.01 s^{-1}. The lower shear rate compared to the previous test was chosen to reach yield stress in different steps. G moduli were evaluated via linear regression of the initial part before reaching the yield stress (maximum value of shear stress). The first measured curve has no clear yield stress, the stress only slowly increased and then was almost constant, so the static yield stress was evaluated as the highest shear stress reached during measurement. The results of yield stresses, A_{thix}, G moduli and their changes are shown in Table 40.

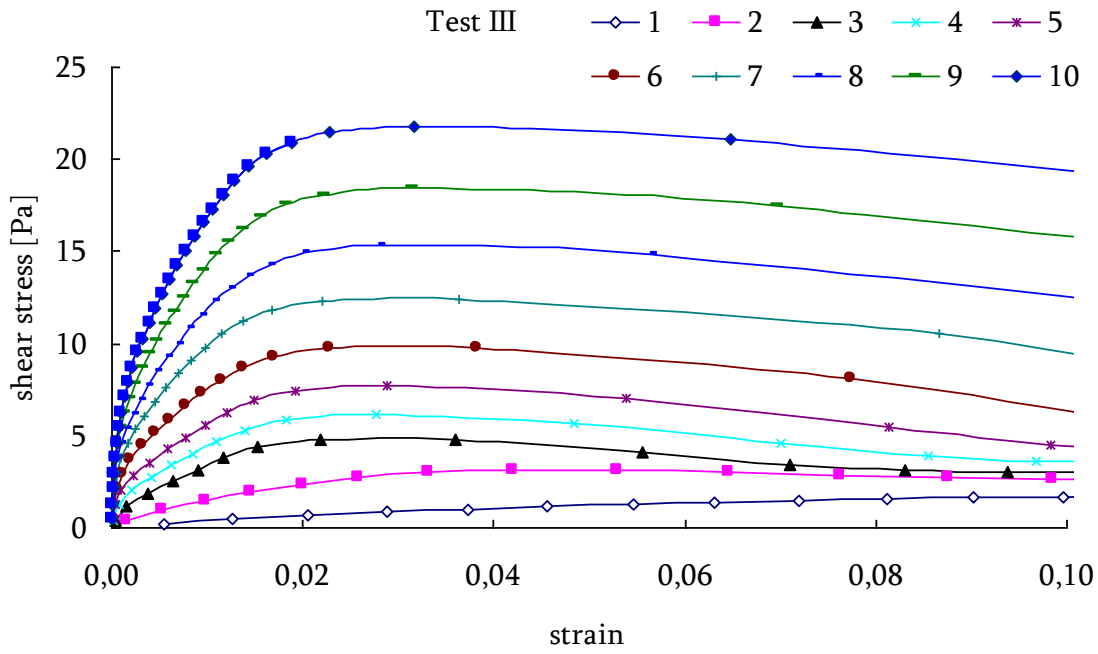

Fig. 65: Measured shear stress - strain curves during test III
(age of matrixes on start of measurement of first curve was 12 min and time between individual steps was 5 min)

Table 40: Results from test III

step	age [min]	yield stress [Pa]	A_{thix} [Pa/s]	G [Pa]	dG	dt [sec]	dG/dt
1	12	1.9	0.003	9.8	9.8	720	0.014
2	17	3.2	0.003	80.9	71.1	300	0.237
3	22	4.8	0.004	201.2	120.3	300	0.401
4	27	6.1	0.004	287.4	86.2	300	0.287
5	32	7.7	0.004	403.6	116.2	300	0.387
6	37	9.7	0.004	489.6	86.0	300	0.287
7	42	12.4	0.005	649.3	159.7	300	0.532
8	47	15.3	0.005	792.3	143.0	300	0.477
9	52	18.5	0.006	904.8	112.5	300	0.375
10	57	21.8	0.006	1076.3	171.5	300	0.572
		average	0.005			average	0.357

Graphic representation of time development of yield stresses and G moduli with linear regression are shown on Fig. 66 and Fig. 67. The rate of increase of yield stress and G moduli are 0.008 Pa/s and 0.394 Pa/s respectively.

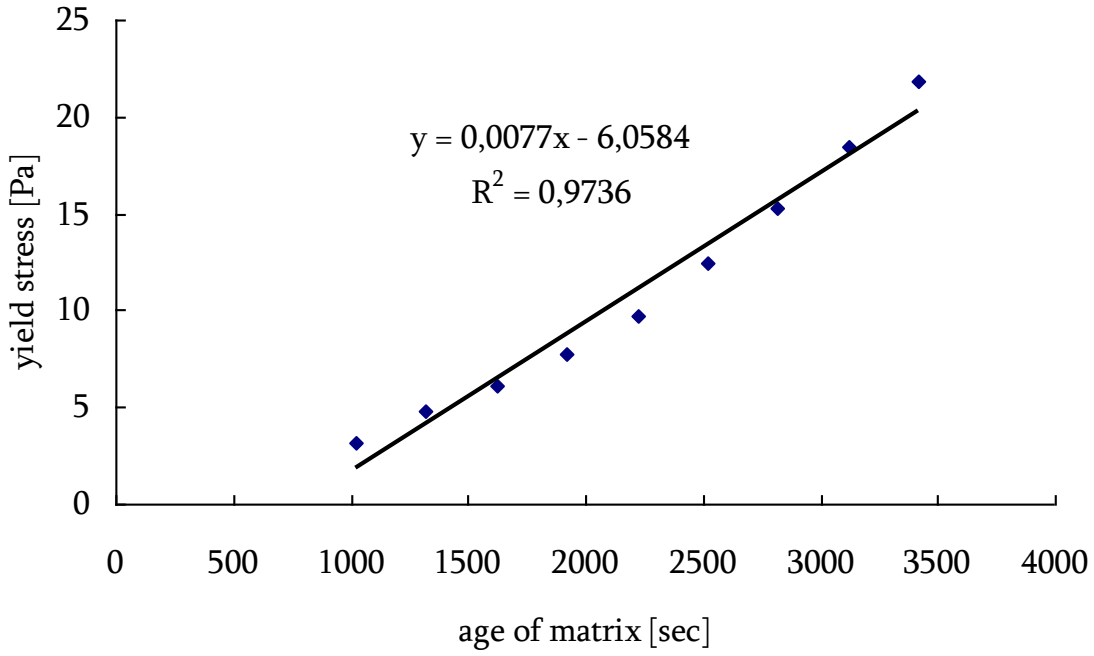

Fig. 66: Development of yield stress during aging of matrix

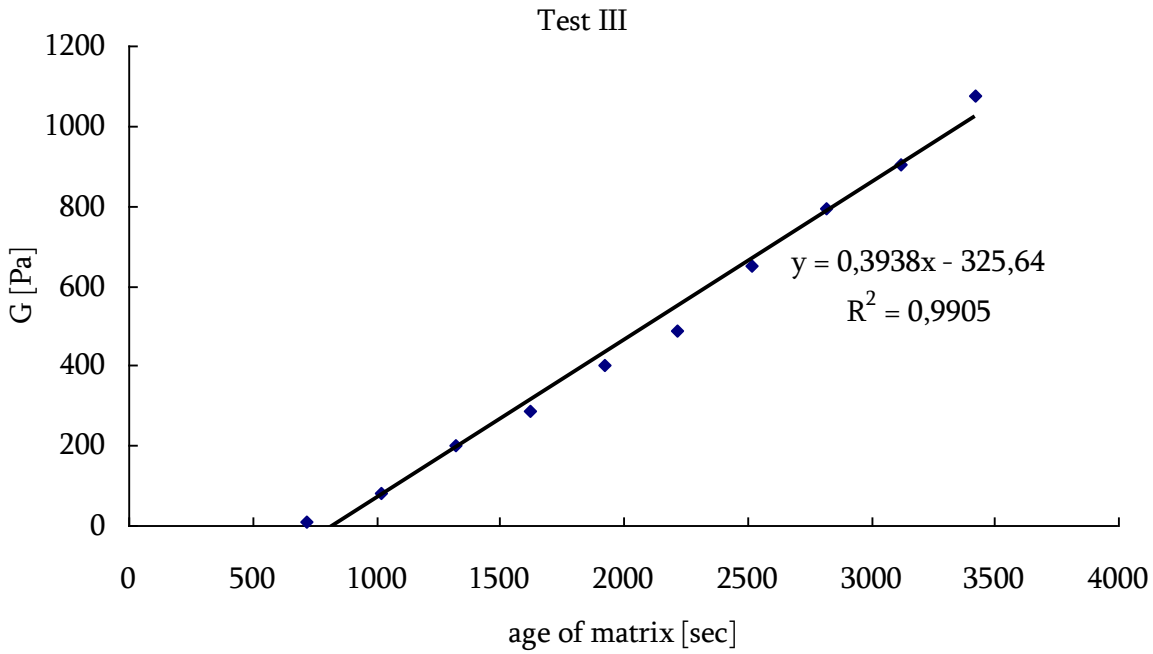

Fig. 67: Development of G modulus during aging of matrix

5.6.1.4 Conclusion parallel plate rheometer

Measurement with parallel plate rheometer was used for the study of rheological properties of matrixes. At first the gel strength was determined for all matrixes and took the value from 2.1 Pa to 34.9 Pa. Flow curves of tested matrixes were evaluated using Bingham model and plastic viscosity range from 0.12 to 0.52 Pa.s and yield stress from 1.5 to 22 Pa. One can say that all these rheological parameters are much more influenced by w/c ratio than SP dosage.

The static yield stress of the matrices was very shear history dependant and varied very little over time (Table 34, 35, 38) for test I and was very similar to dynamic yield stress (Table 37). One reason was the unclear maxima of the constant shear rate tests at 0.01 and 0.001 s^{-1} so that the gel strength test with increasing deformation at exponential stress increase seems better. Shear modulus G seems to give an even safer measure of the structural build-up with clear linear increase of G over time ($dG/dt \approx$ constant) with $R^2 = 0.97$ and 0.99 (Fig. 66 and Fig. 67). Then the behaviour of matrixes was studied under constant shear rate and from linear part of obtained curves G moduli were evaluated. G modulus is strongly influenced by magnitude of shear rate which is used for testing. In case of lower shear rate (0.001 s^{-1}) the resulting G moduli will have higher value (24 – 4548 Pa) than moduli obtained in test with higher shear rate (0.01 s^{-1}) (G increased from 10 to 1076 Pa). That is true for yield stress as well.

If the results from matrix's test are compared to the results from mortar tests, the plastic viscosity of mortar is 25.7 Pa.s and matrix more than hundred times lower 0.12 Pa.s. Yield stress of mortar was determined on 14.2 Pa and matrix ten times lower 1.5 Pa. The structuration rate A_{thix} for mortar was determined on 0.163 Pa.s for first part of measurement and 0.90 Pa.s for second part. Much lower value of the structuration rate was found for matrixes, only 0.005 Pa.s.

5.7 Inclined plane test

No angle of inclination was found during the testing of mixture S1, because the flow properties, especially the yield stress of the mixture was too high. Previous testing of this mixture II showed a dynamic yield stress value of 14 Pa (from testing with BML viscometer). For the other tests the mixtures with higher SP dosage were used. The results of mixtures S1-S3 are shown in Table 41.

Table 41: Results from plane test

mixture	Age of mixture [min]	ρ [kg.m^{-3}]	Spread [mm]	h_s [m]	φ [°]	Static yield stress [Pa]	A_{thix} [Pa/s]
S1	19	2247.6	120	0.053	-	-	-
S2	23	2328.1	203	0.014	34	178.8	0.130
S3	18	2265.4	163	0.021	43	318.3	0.295

The static yield stress of mixture S2 was 179 Pa and the structuration rate 0.13 Pa/s which corresponds to thixotropic SCC according Roussel´s classification. The lower dosage of SP in mixture S3 compared to the S2 that reduced SP dosage increases the yield stress.

As already mentioned mixture S1 had too high yield for the inclined plane test with spread 120 mm and height 5.3 cm. Properties measured previously for mixture II (for example slump-flow 565 mm, T500 2.7 sec, structuration rate around 0.1 Pa/s…) may be representative for S1 but were not measured for S1 so its SCC properties are not known.

5.8 Testing of mixtures S2 and S3 with using ConTec4 viscometer

5.8.1.1 Mixture S2

Mixture S2 was unstable with bleeding and aggregate separation. During measurement with viscometer segregation could be seen after testing when the sample was poured from the outer cylinder and bigger particles were left at the bottom. Torque-time dependency was not evaluated from Fig. 68 because of the unstability.

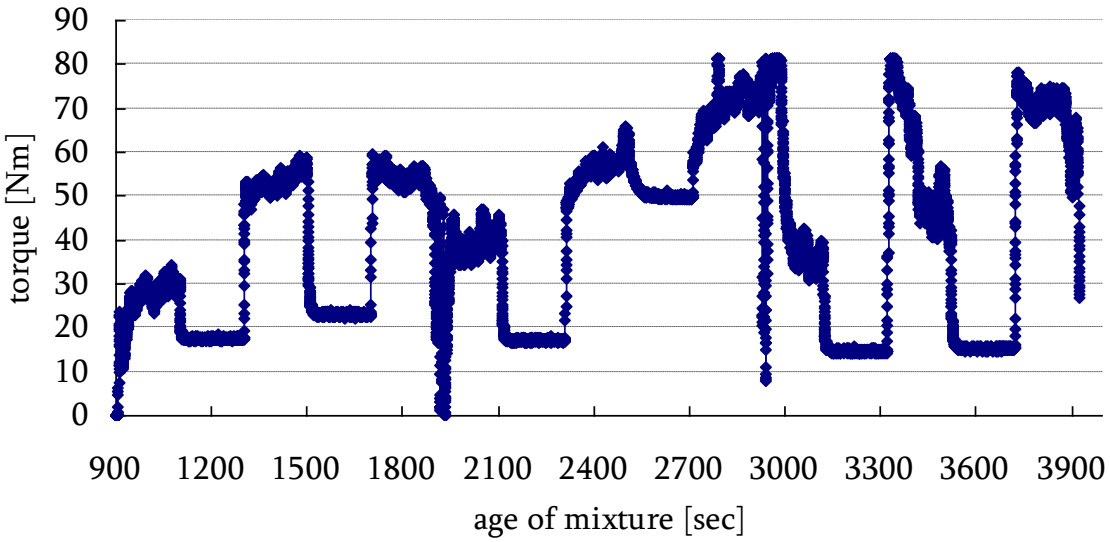

Fig. 68: Torque-time dependence ofunstable mixture S1 at age 15 min

5.8.1.2 Mixture S3

Mixture S3 was stable, the distribution of coarse particles seemed to be homogeneous and no bleeding was observed. The rheological measurements with the ConTec4 viscometer were carried out to determine plastic viscosity and yield stress by applying decreasing levels of shear rates as shown in Fig. 69. After that the static yield stress was determined as described before by measuring the torque-time dependency as very low rotation velocity was applied and stopped every 200 second. During this measurement the inclined plane tests were performed.

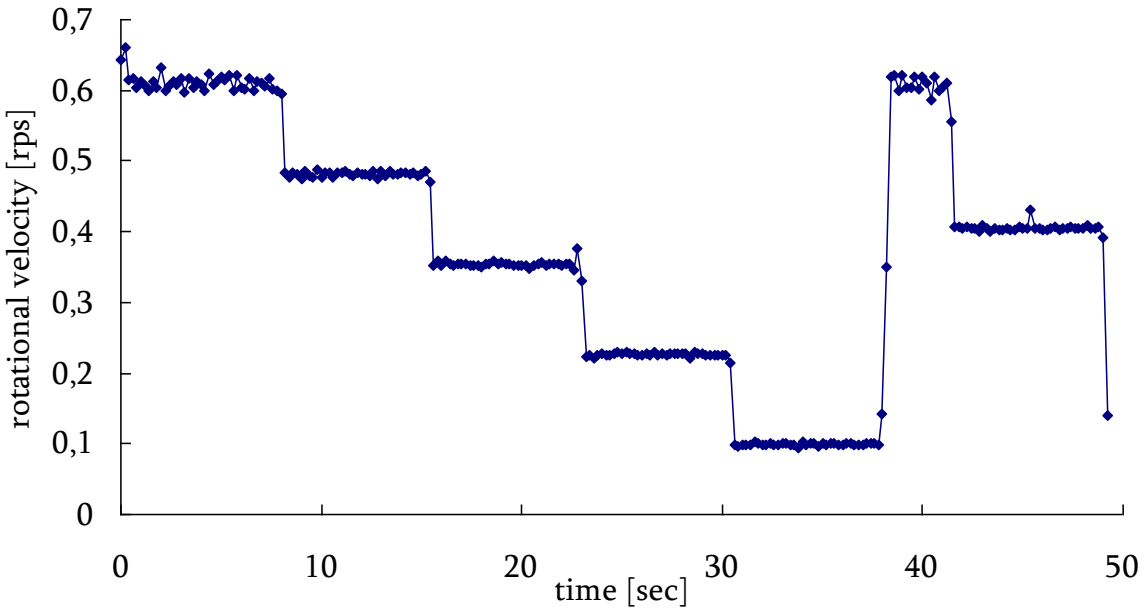

Fig. 69: Rotation history of measurement with ConTec4 viscometer – mixture S3

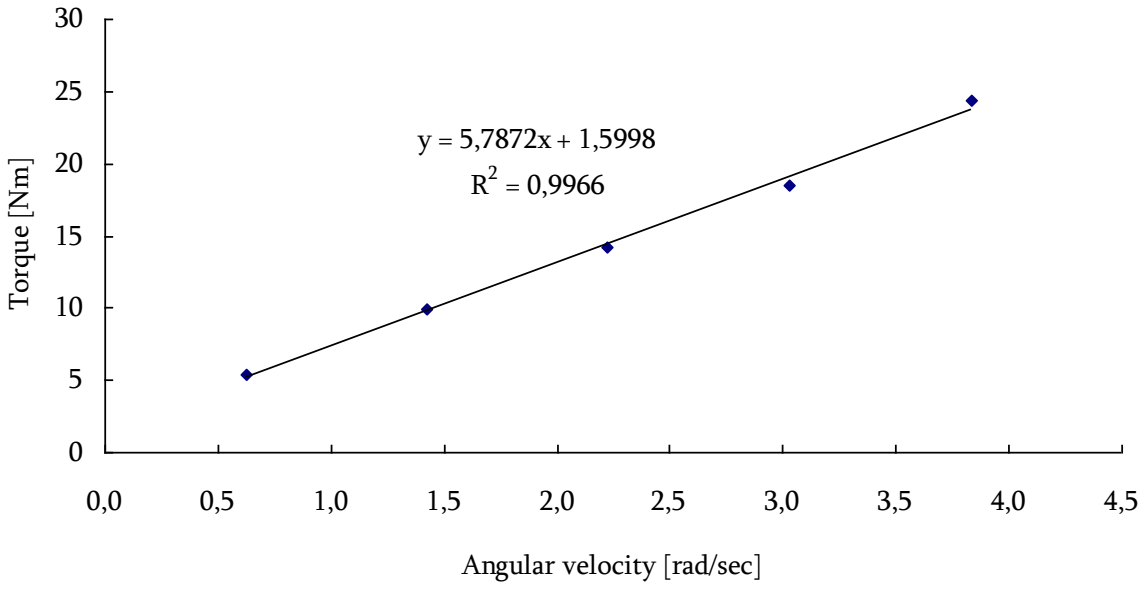

Fig. 70: Resulting curve from measurement with ConTec4 viscometer of mixture S3 at time 14 min after water addition

Table 42: Obtained rheological properties of mixture S3

Time [min]	Dynamic yield stress value [Pa]	Plastic viscosity [Pas]
14	209.0	145.2

The rheological properties of mixture S3 are shown in Table 42. Dynamic yield stress reached 209.0 Pa which seems to be consistent with the value of static yield stress 318.3 Pa. Compared to mixture II the yield stress and plastic viscosity are ten times higher (yield stress and plastic viscosity of mixture II determined using the BML viscometer were 14.2 Pa and 25.7 Pa.s respectively). Mixture S3 has similar proportioning to mixture II, only SP dosage is higher (0.8 % compared to 0.6 %). The viscometer size effect due to the very narrow gap between the torque sensing core and the outer container of the small ConTec4 viscometer is the reason for the much higher values of S3.

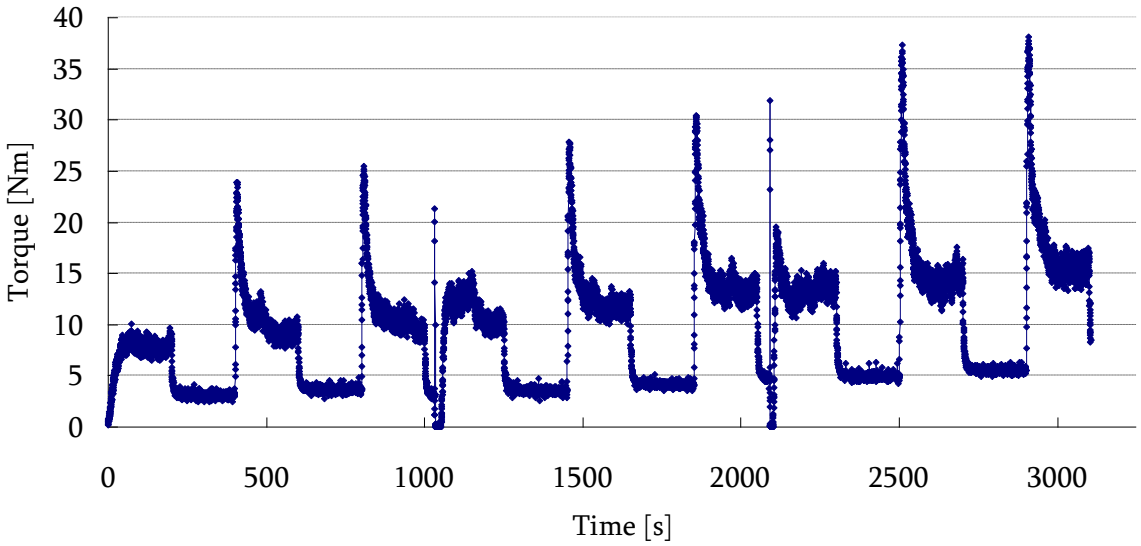

Fig. 71: Torque-time dependency of mixture S3 at age 24 min on start of measurement

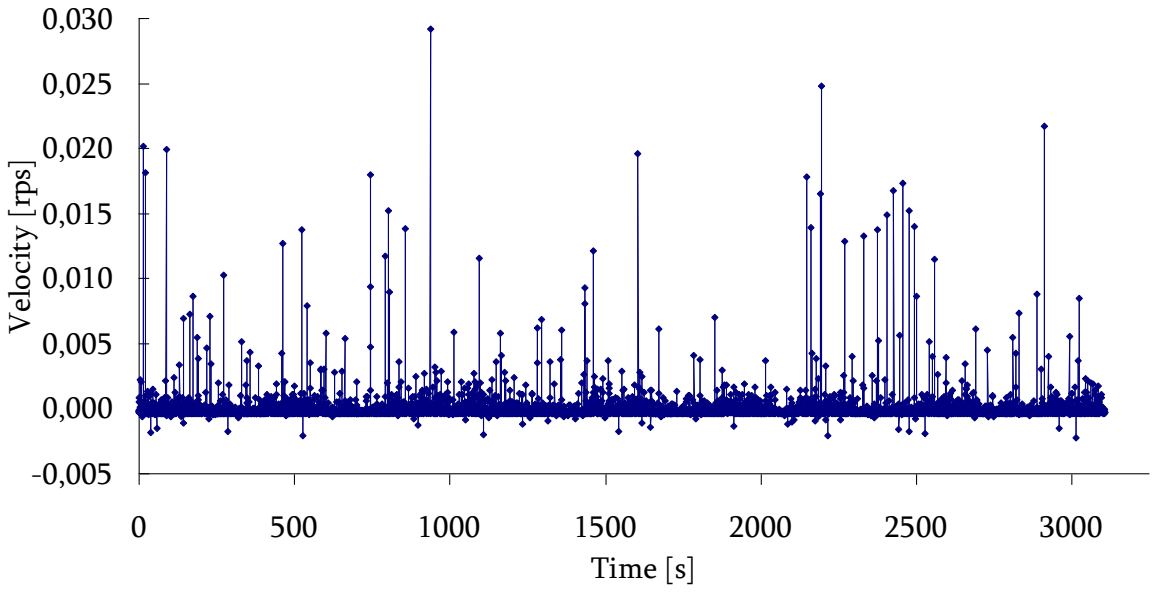

Fig. 72: Velocity profile of measurement

The measured torque-time dependency is shown on Fig. 71 and the velocity profile on Fig. 72. The dependence was evaluated according to procedure 2 with linear regression to evaluate the B and G modulus (Fig. 73). The static yield stresses were evaluated from maximum values of torques which were reached immediately after applying the rotation. The yield stress reached on start of testing and immediately after first shaking show the gradual type of peak, the other stresses show sharp types of peaks as seen earlier and this is most probably due to the effect of confinement by the residual stress on yield stress build-up. Apparently the moderate pressure affects the thixotropic structural build-up, as seen from Fig. 73 and partly for Fig. 39 and Fig. 43 where the peaks after "shaking" are lower compared to peaks starting from a confined stress state. The results for mixture S3 are summarized in Table 43.

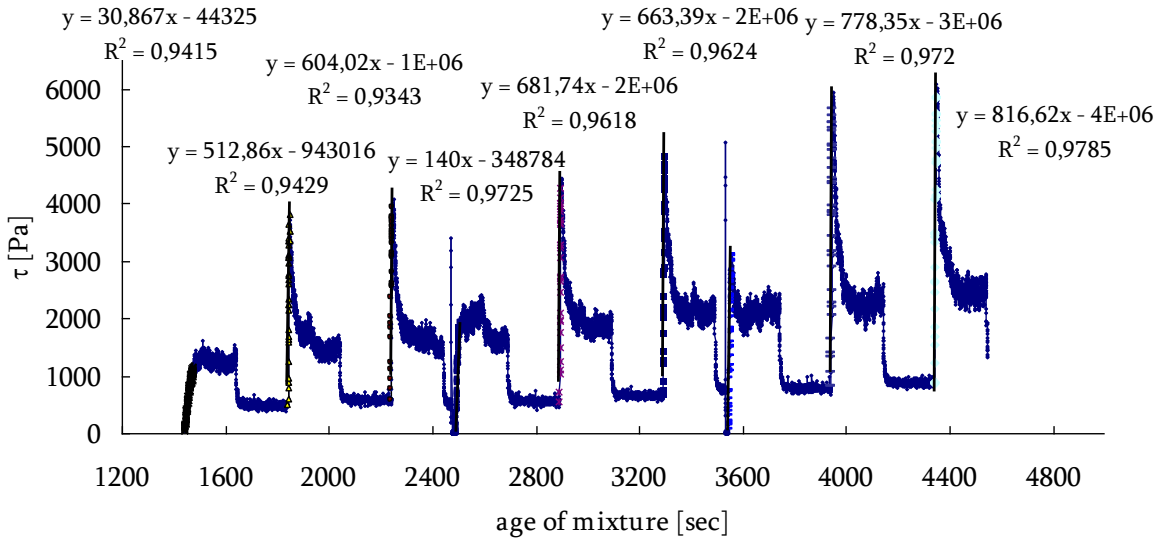

Fig. 73: Calculated time dependency of shear stress for mixture S3 with linear regressions to determine B

Table 43: Obtained data for mixture S3

age of mixture		τ_o [Pa]	A_{thix} [Pa/s]	B [Pa/s]	G [kPa]
[min]	[s]				
25	1475	1411.4	0.957	30.8	20,5
31	1847	3818.3	2.068	512.9	341,9
37	2249	4072.0	1.811	604.0	402,7
37	2240	2236.1	0.894	140.0	93,3
48	2897	4453.3	1.537	681.7	454,5
55	3299	4852.8	1.471	663.4	442,3
59	3551	3114.9*	0.877	322.2	214,8
66	3949	5954.4	1.508	778.4	518,9
72	4349	6082.5	1.399	816.6	544,4

The yield stress τ_0, which is reached after ,,shaking" is marked by *.

The values of the static yield stresses increase almost linearly (R^2 = 0.9588) as shown on Fig. 74, where the first stress and stresses reached immediately after shaking were showed as a crosses with linear increasing tendency.

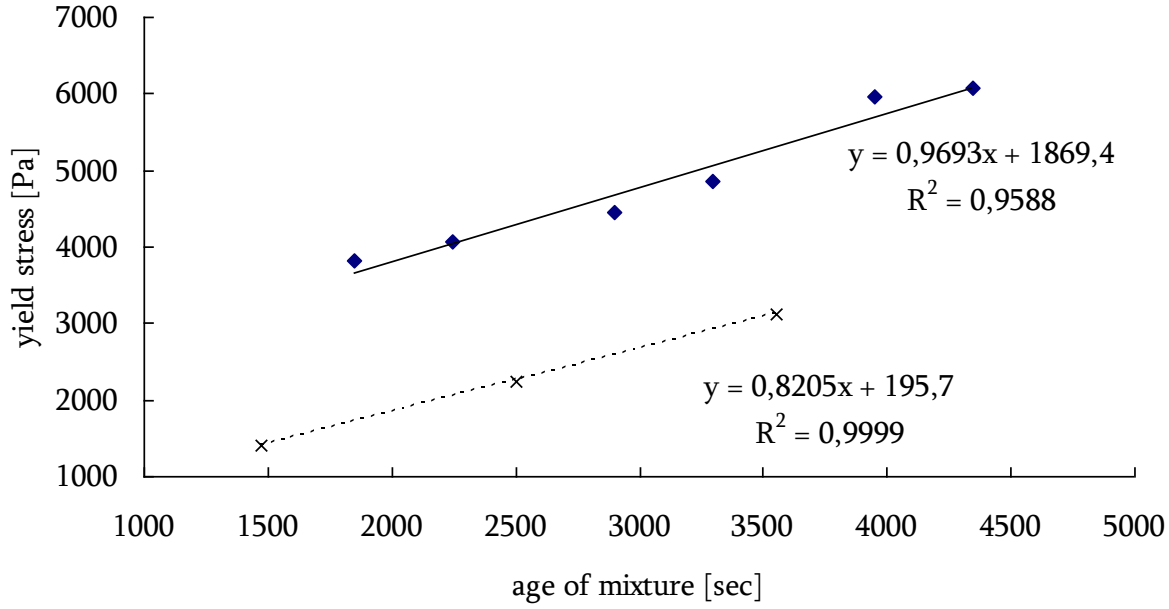

Fig. 74: Development of static yield stresses of mixture S3, lower line shows the unconfined first yield stress and stresses which were reached immediately after shaking and upper line shows confined yield stress reached during confinement by the residual stress

The obtained values of yield stress are more than ten times higher than dynamic yield stress evaluated from Bigham's curve (Table 42). This leads to high structuration rate, which was approximately 1.5 Pa/s. Comparing this value with results for mixture II (the difference between mixture II and S3 was in SP dosage, 0.6 % and 0.8 % for mixture II and S3 respectively) where A_{thix} was approximately 0.2 Pa/s as shown in Table 28 seems to be unexplainable, because according literature knowledge [5], the SP dosage should lead to a decrease of the yield values. The mixture S3 was quite stable, so the effect of segregation in outer cylinder couldn't be so significant. Possibly a slightly more well-dispersed mix and/or slight difference in cement- and/or SP composition over the time period (almost a year) could have contributed to the difference from mixture II.

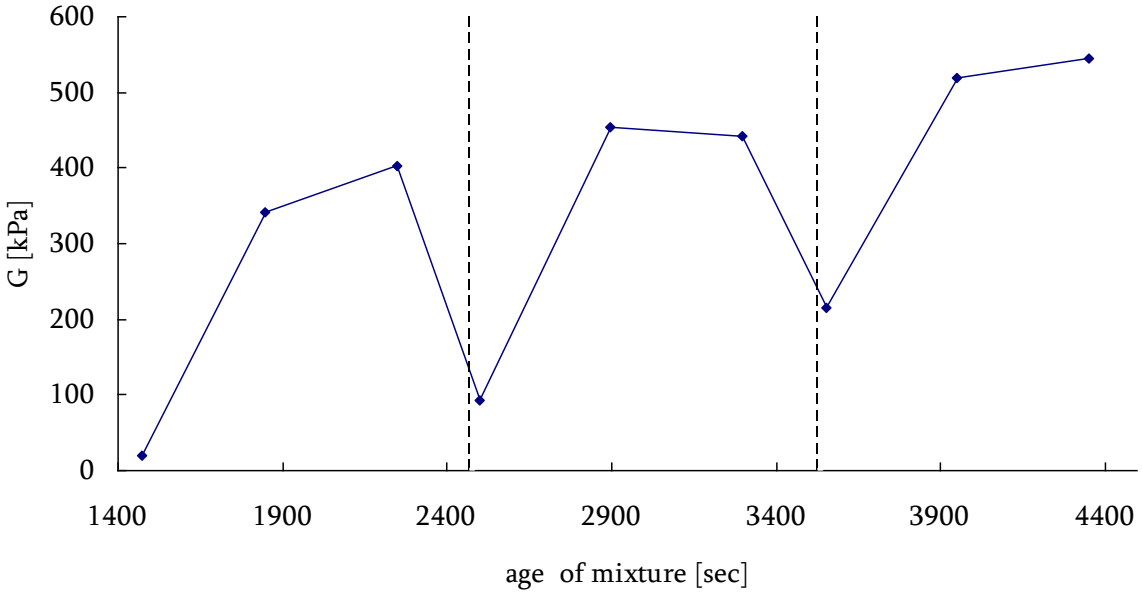

Fig. 75: Development of G modulus of mixture S3 (dashed lines show shaking)

Development of G modulus is shown on Fig. 75, where the increase of G modulus reached immediately after shaking is clearly seen. The G moduli obtained between shaking have increasing tendency. The maximal values of G modulus reached approximately 550 kPa after 72 min, which is ten times higher value compare to the G modulus obtained in case of mixture II (Table 28). Again, since the tests were done on similar materials more than half a year later than mix I and II this could be bart of the explanation for differences. Clearly the static yield stress is a sensitive parameter both in terms of test method, test set-up, test conditions (confinement, shear history, age…) and material composition.

5.9 Results for the mixtures from the concrete plant

The structural build up of sieved mortar was investigated in detail using the ConTec4 viscometer. Testing was performed in the same way as in previous measurement alternating the applied rotation speed. All achieved results concerning the three tested mixtures are published in the work by Klaartje de Weerdt et al. [88]. The measured torque-time dependencies were evaluated according to procedure 2 with linear regression to evaluate the B and G modulus and the static yield stress were evaluated too.

5.9.1.1 Sieved mortar from filler stabilized SCC mixture

Torque-time dependency of filler stabilized mixture is shown on Fig. 76, velocity profile of measurement is shown on Fig. 77 and the calculated yield stress – time dependency on Fig. 78. The yield stress reached at start of testing shows gradual types of peaks, other stresses show sharp type of peak. The results for filler stabilized mixture are summarized in Table 44 and on Fig. 79 and Fig. 80.

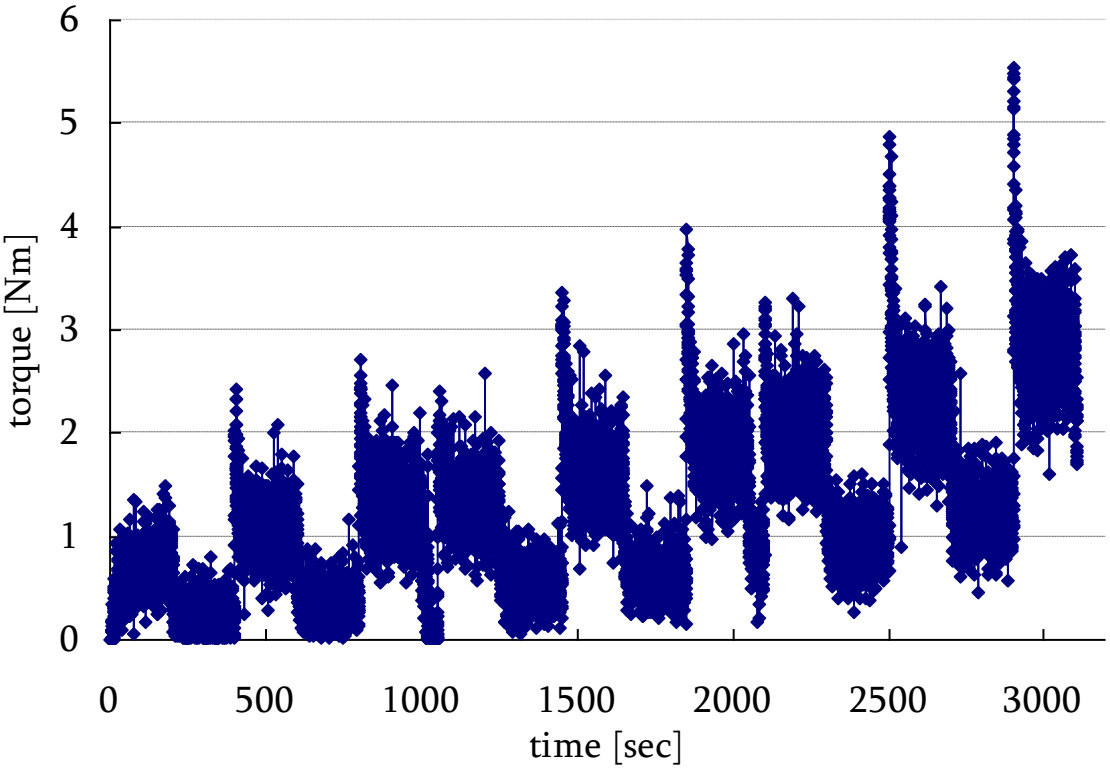

Fig. 76: Torque-time dependence of filler stabilized mixture

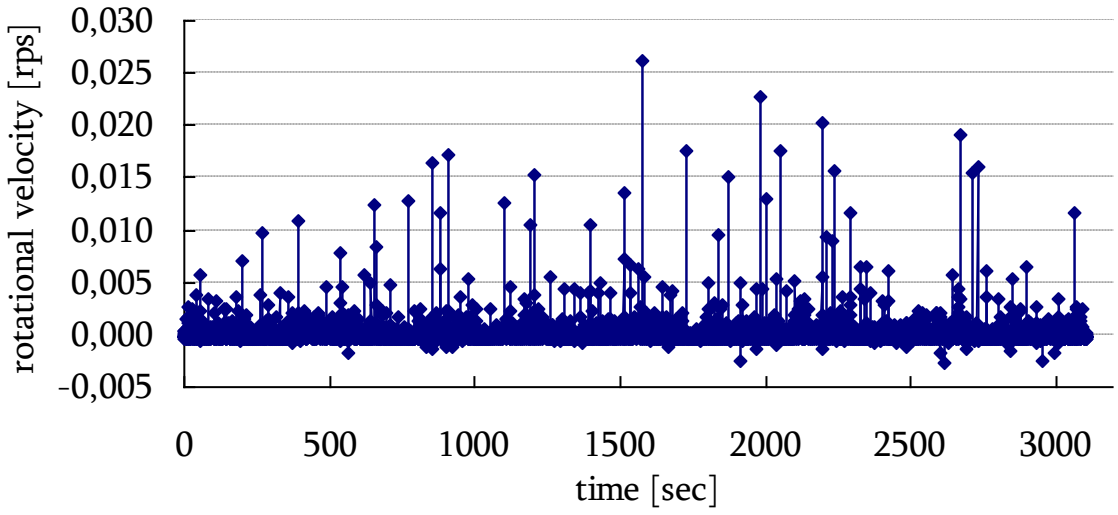

Fig. 77: Velocity profile of measurement

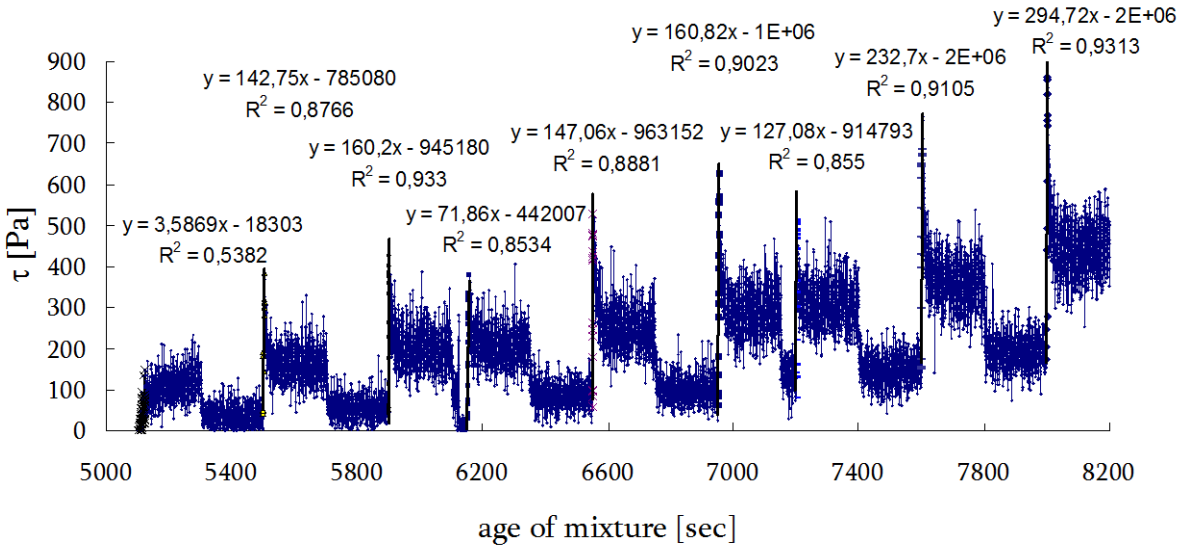

Fig. 78: Calculated time-dependency of stress (including yield stress) for filler stabilized mortar with linear regressions to determine B

Table 44: Obtained data for filler stabilized mortar

age of mixture		τ_o [Pa]	A_{thix} [Pa/s]	B [Pa/s]	G [kPa]
[min]	[s]				
88	5300	167.9	0.032	3.6	2.4
92	5503	383.3	0.070	142.8	95.2
98	5903	426.1	0.072	160.2	106.8
103	6156	377.8*	0.061	71.9	47.9
109	6553	527.8	0.081	147.1	98.1
116	6953	626.7	0.090	160.8	107.2
120	7203	513.7*	0.071	127.1	84.7
127	7605	765.7	0.101	232.7	155.1
133	8004	872.9	0.109	294.7	196.5

The yield stress τ_0, which is reached after ,,shaking" is marked by *.

As shown on Fig. 79 the yield stress has an increasing linear tendency with low decrease immediately after shaking. Nevertheless after that the increase of yield stress is continuing, so the stresses reached immediately after shaking (first one, i.e. yield stress build-up at un-confined conditions in the ConTec4 after shaking to release the residual stress) are showed as crosses and had linear tendency too. In the end the yield stress reached the value almost 900 Pa. The rate of increase of yield stress slowly increased and reached the value 0.11 Pa/s, which correspond to the thixotropic mixture according the Roussel´s classification in the Table 8. Similar tendency had development of G modulus as shown on Fig. 80.

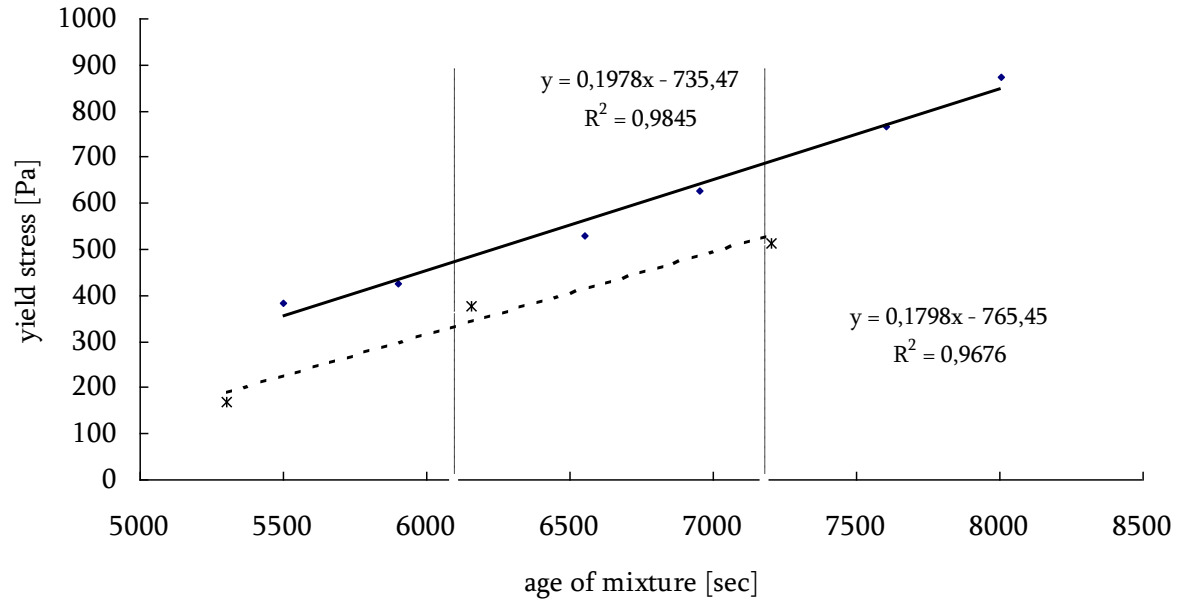

Fig. 79: Development of yield stresses of filler stabilized mortar (dashed lower line shows unconfined yield stress and top-curve shows time development of yield stress confined by residual stress in viscometer)

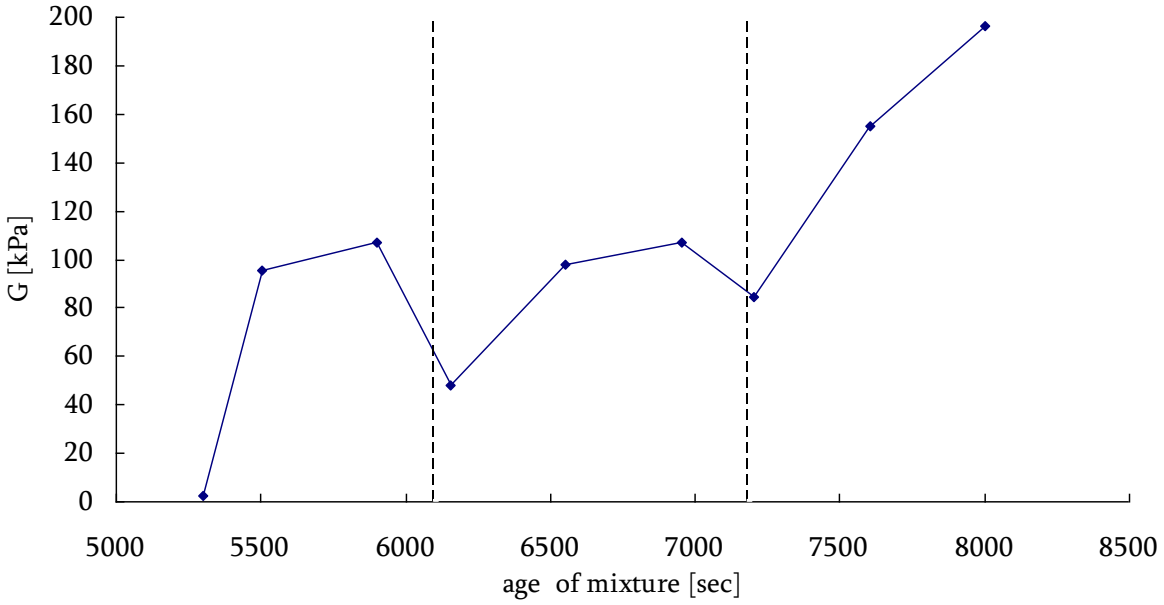

Fig. 80: Development of G modulus of filler stabilized mortar (dashed lines show shaking)

5.9.1.2 Sieved mortar from chemically stabilized SCC mixture

Torque-time dependency of the chemically stabilized mixture is shown on Fig. 81, velocity profile of measurement is shown on Fig. 82 and calculated dependence of stress on Fig. 83. The yield stresses reached in start of testing and immediately after shaking show gradual type of peak, others show sharp type of peak. The results for chemically stabilized mixture are summarized in Table 45 and in Fig. 84 and Fig. 85.

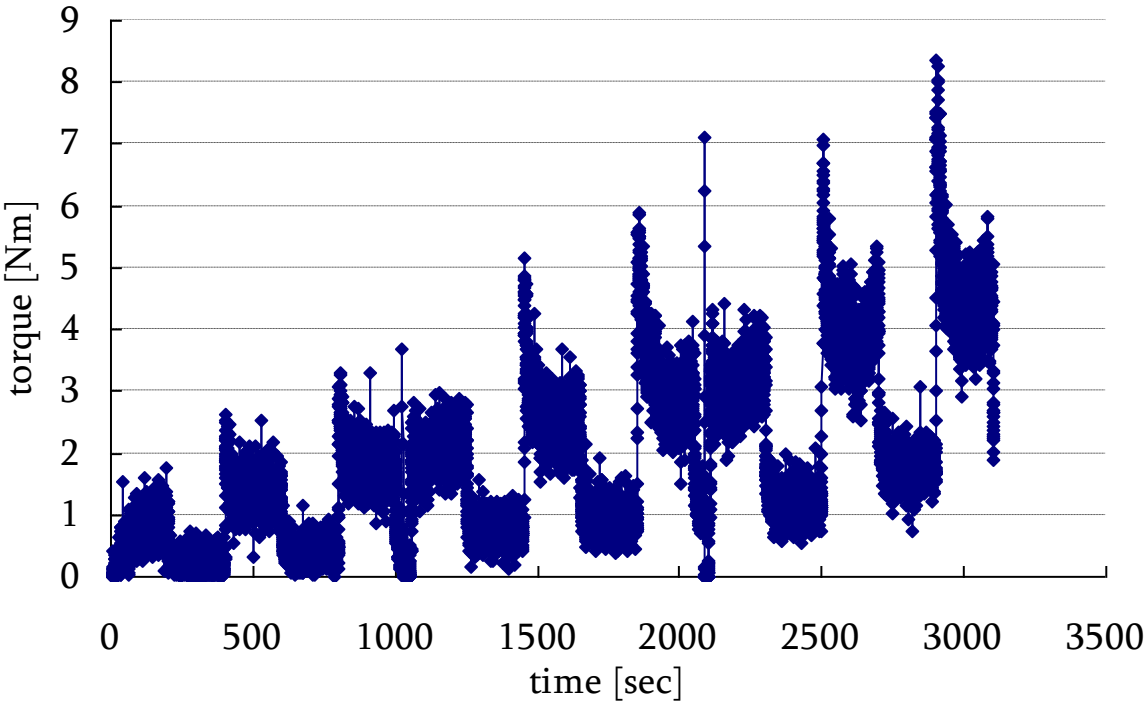

Fig. 81: Torque-time dependence of chemically stabilized mixture

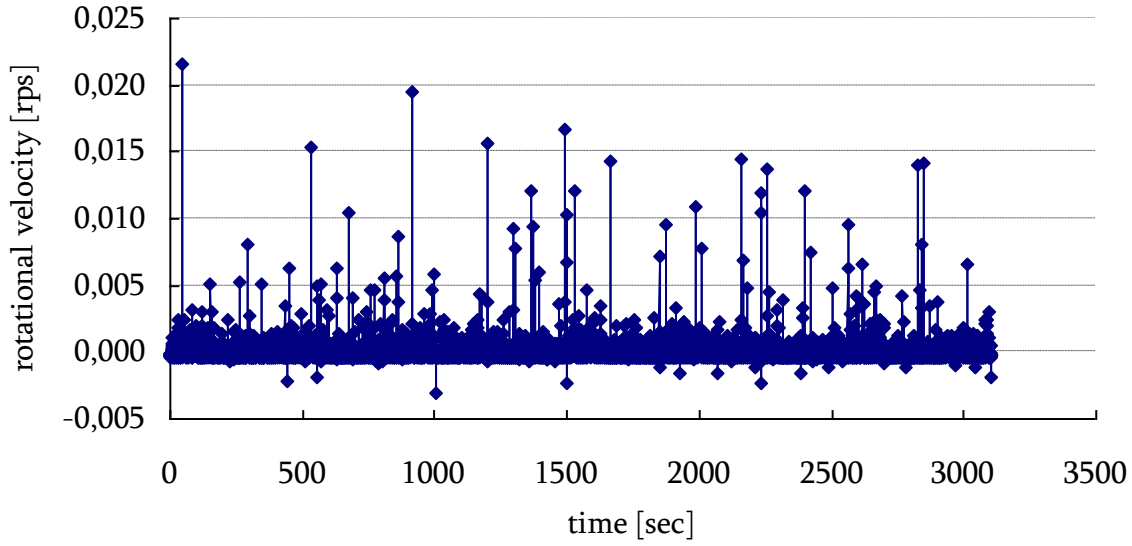

Fig. 82: Velocity profile of measurement

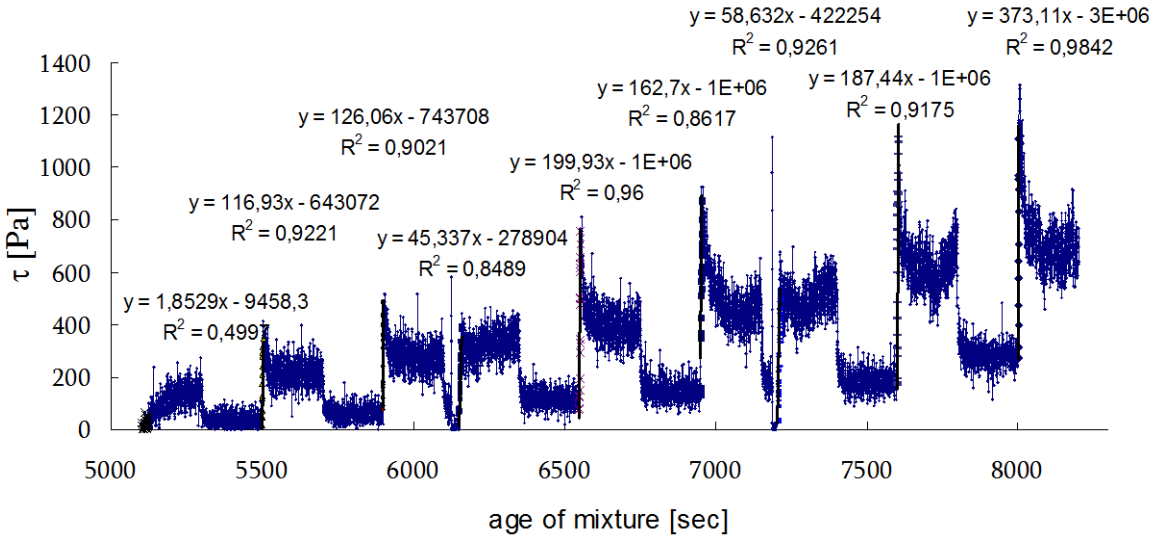

Fig. 83: Calculated time-dependency of stress for chemically stabilized mortar with linear regressions to determine B

Table 45: Obtained data for chemically stabilized mortar

age of mixture		τ_o [Pa]	A_{thix} [Pa/s]	B [Pa/s]	G [kPa]
[min]	[s]				
88	5298	208.4	0.039	1.9	1.3
92	5506	414.4	0.075	116.9	77.9
98	5906	520.4	0.088	126.1	84.1
103	6162	441.3*	0.072	45.3	30.2
109	6556	810.1	0.124	199.9	133.3
116	6957	927.4	0.133	162.7	108.5
120	7213	679.3*	0.094	58.6	39.1
127	7605	1113.6	0.146	187.4	124.9
133	8005	1315.3	0.164	373.11	248.7

The yield stress τ_0, which is reached after ,,shaking" is marked by *.

The yield stress has increasing linear tendency with low decrease immediately after shaking as shown on Fig. 84. After that the increasing of yield stress is continuing, so the stresses reached immediately after shaking (and first one) are showed as crosses and had linear tendency too. In the end the yield stress reached the value approximately 1315 Pa. The rate of increase of yield stress slowly increased and reached the value 0.16 Pa/s, which correspond to the thixotropic mixture according Roussel´s classification shown in Table 8, and is similar to the filler stabilized mixture. The tendency of development of G modulus was similar as shown on Fig. 85.

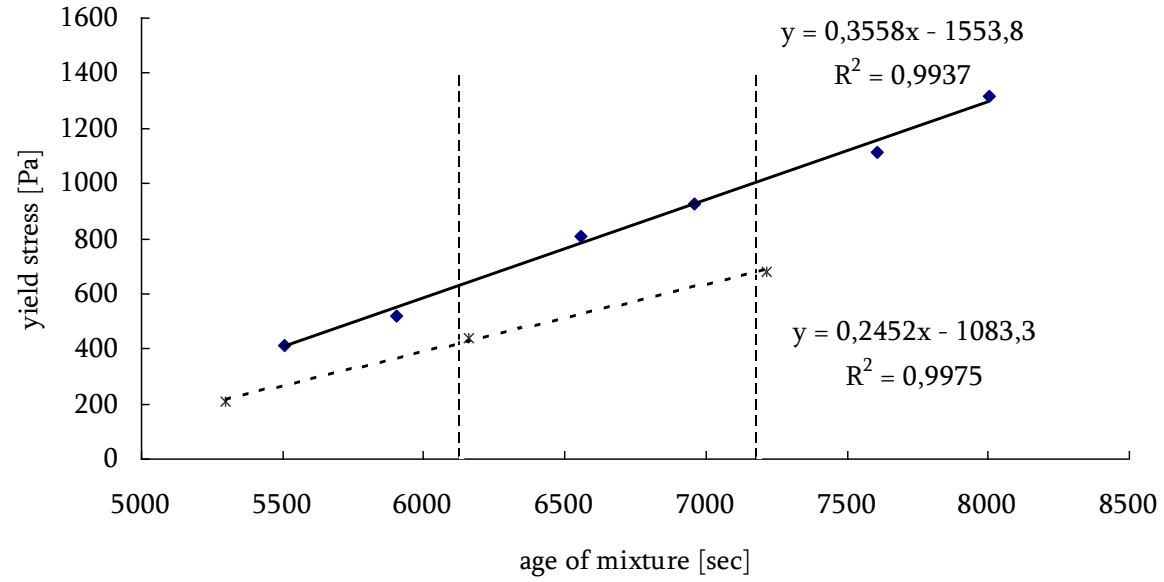

Fig. 84: Development of yield stresses of chemically stabilized mortar (dashed lines show shaking)

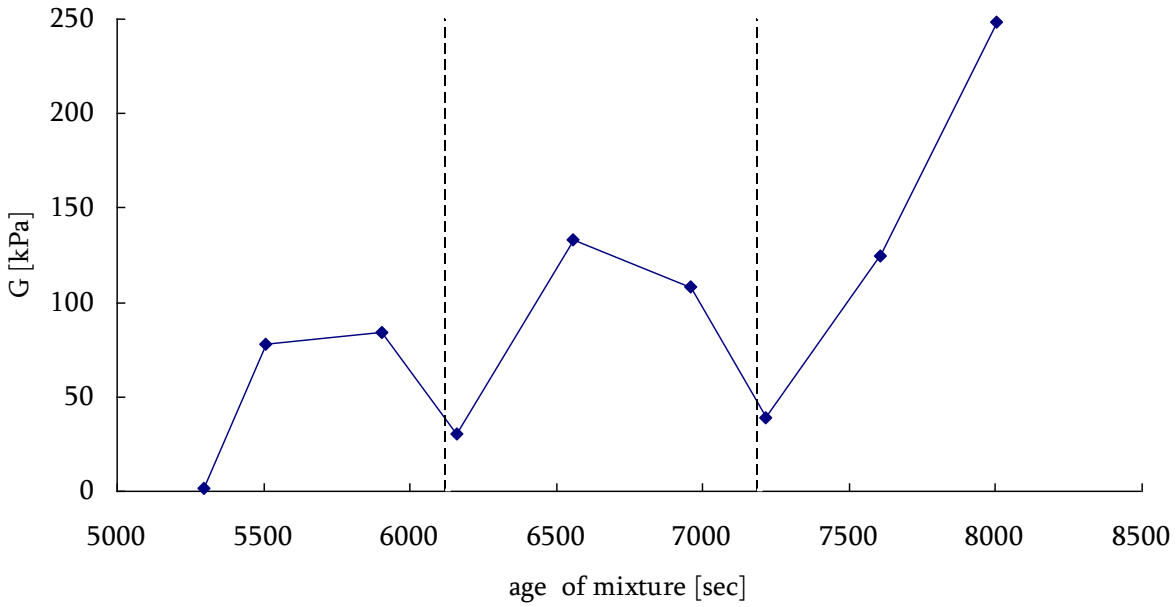

Fig. 85: Development of G modulus of chemically stabilized mortar (dashed lines show shaking)

5.9.1.3 Sieved mortar from unstable SCC mixture

The torque-time dependency of the unstable mixture is shown in Fig. 86 whereas the velocity profile of measurement is shown in Fig. 87 and the calculated time-dependency of stress in Fig. 88. The yield stress shows gradual types of peaks only at start of the measurement (first peak), then the sharp types followed. The results for the unstable mixture are summarized in Table 46 and Fig. 89 and Fig. 90.

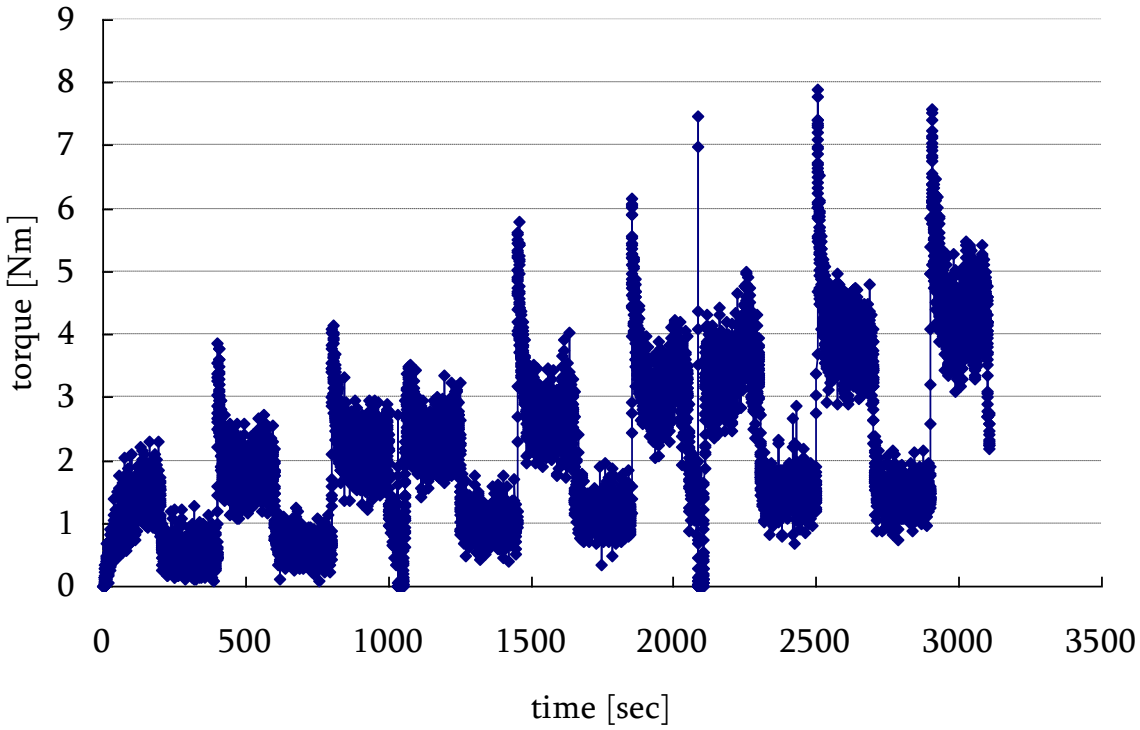

Fig. 86: Torque-time dependence of unstable mixture

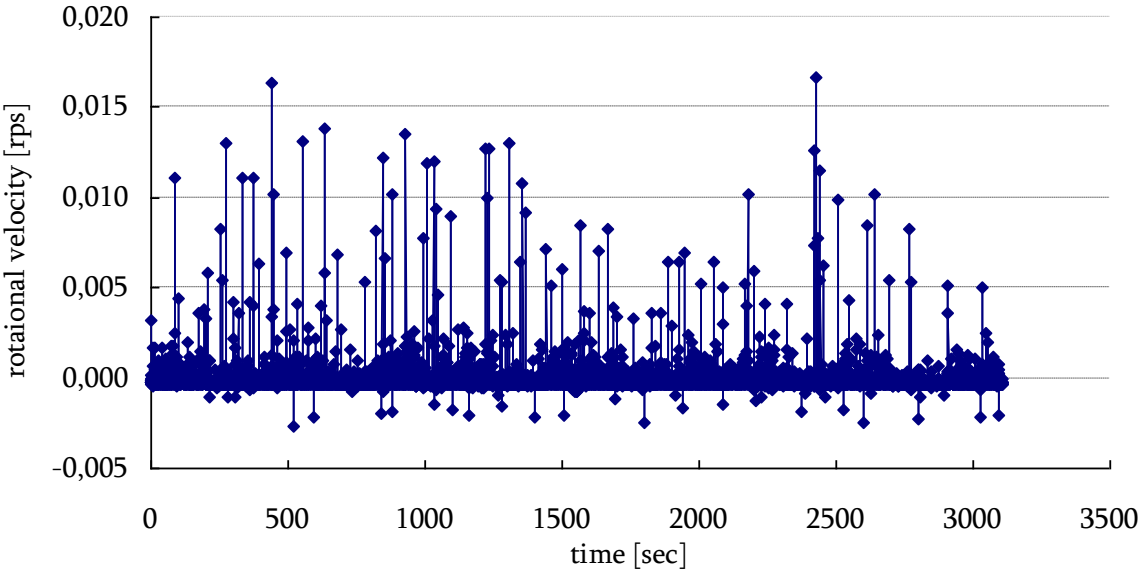

Fig. 87: Velocity profile of measurement

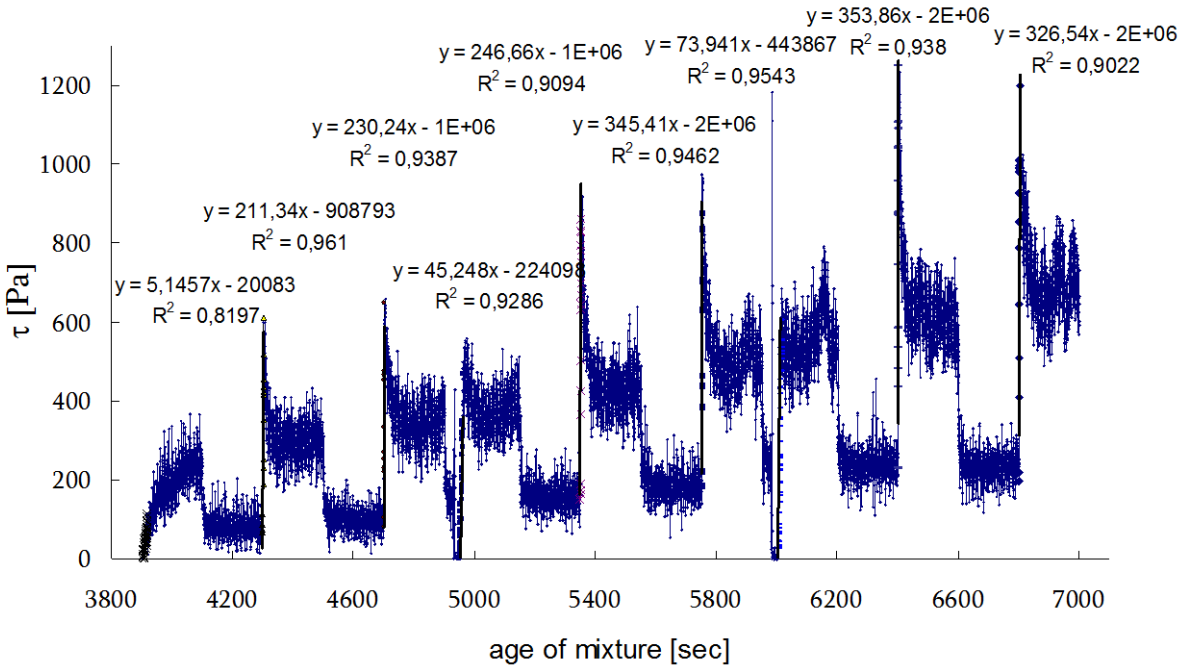

Fig. 88: Calculated time-dependency of stresses for unstable mortar with linear regressions to determine B

Table 46: Obtained data for unstable mortar

age of mixture		τ_o [Pa]	A_{thix} [Pa/s]	B [Pa/s]	G [kPa]
[min]	[s]				
68	4100	264.4	0.064	5.1	3.4
72	4303	612.8	0.142	211.3	140.9
78	4703	649.6	0.138	230.2	153.5
83	4974	558.2*	0.112	45.2	30.1
89	5356	918.4	0.171	246.7	164.5
96	5753	975.6	0.170	345.41	230.3
100	6028	654.0*	0.108	73.9	49.3
107	6403	1249.9	0.195	353.9	235.9
113	6803	1199.3	0.176	326.5	217.7

The yield stress τ_0, which is reached after ,,shaking" is marked by *.

As shown in Fig. 89 the development of yield stress was similar to previous mixtures (linear and increasing) and in the end reached the value approximately 1200 Pa. The rate of increase of yield stress slowly increases and reached the value 0.18 Pa/s. This corresponds to thixotropic mixture according Roussel´s classification in Table 8, as for filler and chemically stabilized mixtures. The tendency of development of G modulus was strongly affected by shaking as shown on Fig. 90, where G moduli reached immediately after shaking were several fold lower than others. In case of unstable mixture the increase of the yield stress during aging of the mixture should be affected by segregation. As mentioned above, measurements with viscometers are not suitable for unstable mixtures, so the presented dependency should be assessed with caution.

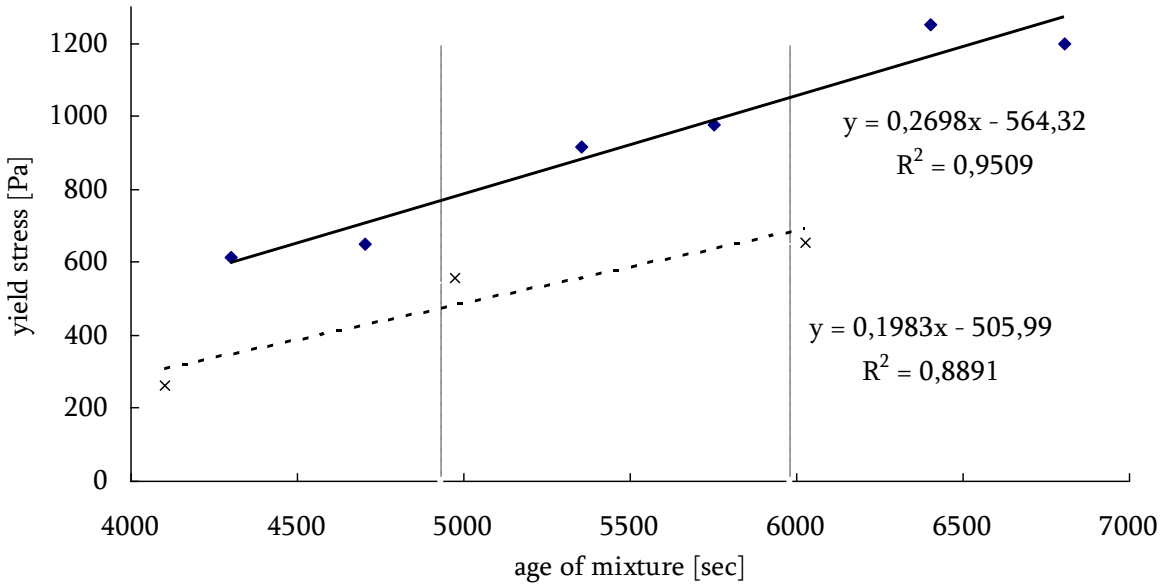

Fig. 89: Development of yield stresses of unstable mortar (dashed lines show shaking)

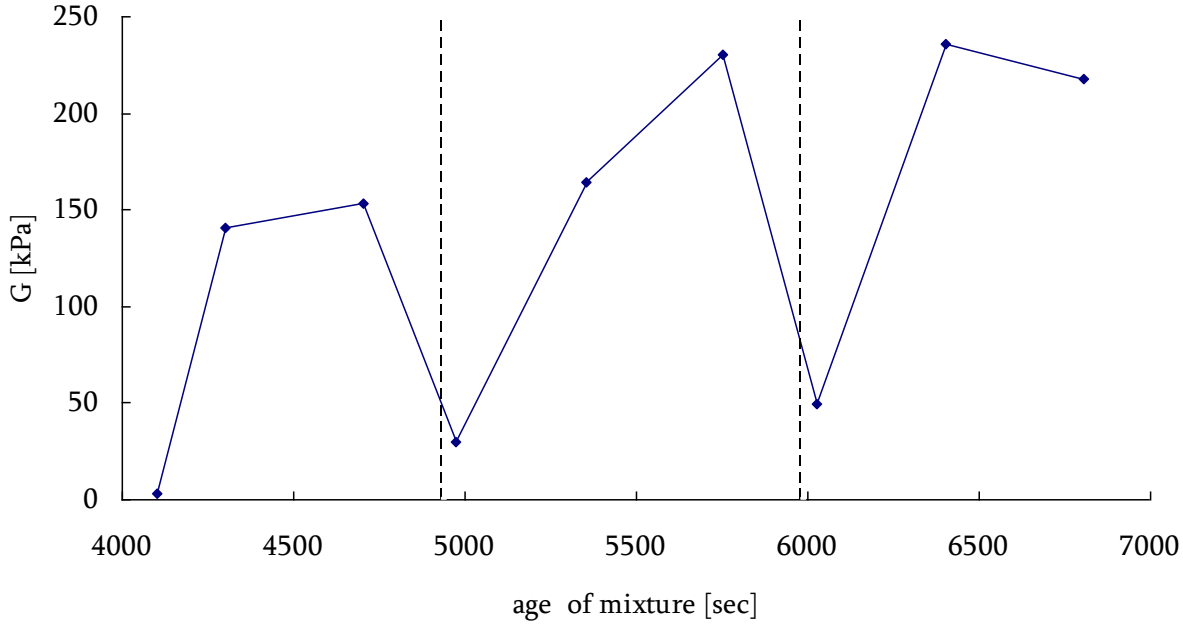

Fig. 90: Development of G modulus of unstable mortar (dashed lines show shaking)

5.9.2 Conclusion yield stress of ready mixed SCC

All results for concrete and their sieved mortar are shown in Table 47. Filler stabilized and chemically stabilized mixtures had similar plastic viscosity. Concerning static yield stress value, the filler stabilized mixture had higher yield stress. In the case of the unstable mixture, visible segregation was observed and therefore rheological properties of this mixture are less valid.

Static yield stresses of concrete determined by inclined plane test were always higher than dynamic yield stress and this measurement is more suitable for mortar than for concrete, because the determination of the angle of inclination is more difficult in case of concrete. For

concrete movement of coarse aggregate can occur at first (before the mixture starts to flow). So the inclined plane test is strongly dependent on the stability of the mixture. Thus visual observation when conducting the test rather than the yield stress value itself is possibly an indication of stability. Another factor is the volume of the sample. In this test it was used only small sample volumes (dimensions of cylinder is 62 mm in diameter and 120 mm in height which gives 362 ml) and sampling is tricky and difficult to make representative due to small volume in case of SCC (the worst sampling was in case of unstable SCC). So there is some limitation for samples which are suitable for using the plane test (stability, rheological properties….).

Testing of mortars gave surprising value of yield stresses and plastic viscosities, because these values were higher than in case of unstable and chemically stabilized concrete. The static yield stresses determined in the inclined plane test correspond to the increasing values of yield stresses evaluated from torque-time dependency in the ConTec4 viscometer.

According to the structuration rate all tested mortars were thixotropic mixtures. The structuration rate in all cases increased and the maximum values were found for unstable mixture, apparently because of unstability. The B and G modulus was highest in case of chemically stabilized mixture.

Yield stress was higher under confined conditions compared to under non-confined conditions (Fig. 46, 74, 79 and 84). The rate of increase of static yield stress over time, however, is quite similar as observed from two series of tests made with almost a half year in between.

Shear modulus seems to be a more sensitive parameter for structural build up than yield stress and this parameter was investigated in detail for matrix using the Physica Rheometre.

Table 47: Properties of concrete and their mortar

	Unstable SCC	Filler stabilized	Chemically stabilized
Density [kg/m^3]	2427	2368	2408
Air [%]	0.3	1.4	0.7
SF [mm]	685	660	670
T500 [s]	0.66	0.58	1.44
BML			
Yield stress [Pa]	91.7	94.0	54.9
Plastic viscosity [Pa.s]	0.6	6.2	9.0
Inclined plane			
Spread [mm]	148	205	312
Angle [°]	23	26	13
Static yield stress [Pa]	428	295	101
MORTAR			
ConTec4			
Yield stress [Pa]	109.7	63.4	95.9
Plastic viscosity [Pa.s]	24.6	9.8	63.8
A_{thix} [Pa/s]	0.18	0.11	0.16
B [Pa/s]	326.5	294.7	373.1
G kPa	217.7	196.5	248.7
Inclined plane			
Density [kg/m^3]	2360	2241	2356
Spread [mm]	200	228	261
Angle [°]	17	15	11
Static yield stress [Pa]	102	68	31

The A_{thix}, B and G are shown only for the closing part of measurement and correspond with the highest values, which were obtained

6 EXPERIMENTAL PART II

Second part of experimental measurement was concerning on the properties of the cement pastes from two types of the cement with different w/c and SP dosage. The rheological measurements were done with using the parallel plate rheometer. The cement pastes were tested via Vicat test too to observe the depth of penetration with connection to the w/c. The heat evolution was studied with using isotermal calorimeter and with modular microcalorimeter. The phase composition was studied with using in-situ XRD analysis. The partly hydrated samples of the cement were prepared and tested with using the scanning electron microscopy and XRD analysis.

6.1 Used materials and preparing of cement pastes

Ordinary Portland cements type I was used along with liquid superplasticizer Glenium Ace 40 (polycarboxylate ether polymers) and destilled water. Two cements were used, cement Mokrá 52.5 N and Ladce 42.5 N (see appendix).

The mixing of cement samples (based on ČSN EN 196-3) were still same that means the same mix method, same mixer and same amount of cement (500 g) were used. In all cases, the cement powder was added to the preweighed quantity of water and mixing was conducted at room ambient temperature. The reason for this is in influence of mix design on rheological properties of fresh cement paste as shown for example in work of researches from Northwestern University in USA [89].

Cement pastes were prepared by adding cement into a Kitchen Aid mixer already containing water and SP in some cases. The pastes were stirring for 1.5 minutes and after 30 second of rest the samples were re-mixed for another 1.5 minutes.

6.2 Rheological measurement

After mixing the pastes were placed in the rheometer and squeezed between the parallel plates. The gap between plates was set on 1 mm and excess paste was removed. The rheological properties were investigated using a TA Instruments parallel-plate rheometer AR G2 with 25 mm diameter steel plate. The temperature was kept constant at 25 °C by a Pelltier plate system.

The first rheological measurement was taken at 20 min after the first contact between cement and water. Subsequently, a new cement paste sample from the same mixture was tested every 20 minutes up to one hour. The tested samples are listed in Table 49 and 49.

Table 48: Composition of the tested cement pastes

Mokrá 52.5 N		Ladce 42.5 N	
w/c	SP [%]	w/c	SP [%]
0.288	0.3	0.252	0.3
	0.6		0.6
	0.9		0.9
0.320	0.3	0.32	0.3
	0.6		0.6
	0.9		0.9

% SP are referred to the weight of the cement

Table 49: w/c of the tested cement pastes

	w/c							
Mokrá 52.5 N	-	0.288	0.300	0.320	0.340	0.360	0.380	0.400
Ladce 42.5 N	0.260							

It was used following test sequence for testing the samples of cement pastes:

1) 30 sec mixing with constant shear rate 1 s^{-1}
2) 2 min rest
3) 3 min with constant shear rate 0.01 s^{-1} to measure stress-strain curve in 30 measuring points lasting 6 seconds each
4) 1 min rest
5) shear rate – stress curve with logarithmic sweep of stress from 2 up to 2000 Pa to measure gel strength during 2 min
6) 1 min rest
7) Shear rate – stress curve with logarithmic sweep of shear rate from 0.01 to 50 s^{-1} in 30 measuring points lasting 4 seconds each to measure flow curve (up curve)
8) 30 sec with constant shear rate of 50 s^{-1} in 6 measuring points lasting 5 seconds each
9) Shear rate – stress curve with logarithmic sweep of shear rate from 50 to 0.01 s^{-1} in 30 measuring points lasting 4 seconds each to measure flow curve (down curve)

For evaluating the error of measurement, the mixture prepared from the cement Ladce 42.5 N with w/c = 0.34 were tested 5 times. This sample was chosen because it lies in the middle of series with different w/c. No SP dosage was used in this case, because the samples with SP showed behaviour more similar to fluid and therefore more suitable for testing between parallel plate systems.

6.3 Vicat test

In this work, the procedure was modified by using the same Vicat device while the cement paste was prepared without attempting to achieve normal consistency. The reason being, the Vicat test is used here to measure the penetration depth of cement pastes and not to determine the standard setting time.

The paste was transferred into the measuring cell and the needle was driven on the surface of the sample. The test started at age of 6.5 minutes of sample, which means 6.5 minutes after first contact cement with water. The first obtained value of depth of penetration was recorded after 30 seconds of penetration and second after 3.5 minutes of penetration.

The tested pastes varied in w/c, in case of the cement Mokrá 52.5 N was interval of w/c 0.272 – 0.300 and for the cement Ladce 42.5 N was 0.236 – 0.254 (the w/c increased in 0.004 in comparison with previous one). Total 15 different compositions were used and every composition was measured 3 times, which gives in total 45 tested samples.

6.4 Calorimetry

The heat of hydration of early age cement pastes have been studied by means of isoperibolic calorimetry and modular microcalorimeter TAM III (TA Instruments).

At first the isoperibolic calorimetry was used for study of heat evolution during first 25 hours of cement paste age. The isoperibolic calorimeter is constructed using thermo-insulating box (made from styrofoam), proper vessel (200 ml styrofoam crucible) and thermal

sensor. Cement and water (eventually SP) were mixed in same way as in previous cases. Water to cement ratio was 0.252 and 0.288 for tested pastes which correspond to the normal consistency of cement Ladce 42.5 N and Mokrá 52.5 N respectively. The heat of hydration was measured in case of samples with SP dosage as well and 0.6 % SP was used (with respect to the mass of cement). The tests were performed at 25 °C (room temperature) and with using 350 g of the cement paste.

The more accurate instrument for studying of the heat evolution of hydration of cement samples is modular microcalorimeter which makes it possible to observe first stage (preinduction preiod) of hydration, because the samples were mixed inside the microcalorimeter at the constant temperature 25 °C. The testing cell is designed for limited volume of sample, so only 0.5 g of cement was used. The water (or water with SP) was added during the first minute of testing, which lasted one hour. The samples composition was chosen with respect of very low volume of samples and w/c was 0.5. It was tried a lower water content too, but after the testing (one hour) the sample was quite dry. The tested samples are listed in the Table 50:

Table 50: Composition of the tested cement pastes

Cement	w/c	% SP	Instrument
Ladce 42.5 N	0.252	-	Isotermal calorimeter
		0.6	
	0.288	-	
		0.6	
	0.500	-	Modular microcalorimeter
		0.6	
Mokrá 52.5 N	0.252	-	Isotermal calorimeter
		0.6	
	0.288	-	
		0.6	
	0.500	-	Modular microcalorimeter
		0.6	

6.5 Particle size distribution

The particle size distribution was measured via laser diffraction with using laser particle size analyze of difractometer Sympatec Helos KR with range of measurement 0.1– 1 750 μm. Both cement powders were measured via dry dispergation with using three different objectives for more accurate results.

6.6 Density of the pastes

The densities of pastes were determined via pycnometric method which consisted of measurement of mass of pastes in the vessel which were compared with mass of the vessel with water, which density is well known. The composition of the tested pastes were same as in case of the paste measured via Vicat test, because the value of density is necessary for the models predicting the yield stress from the depth of the penetration. Every sample was tested 3 times.

6.7 Preparation of the partly hydrated cement samples

The hydration of cement pastes were studied via testing of partly hydrated samples of cements. It was used two mentioned cements and water dosage was chosen for obtaining the normal consistency of samples (see Vicat test). The w/c ratio for cement Ladce 42.5 N and Mokrá 52.5 N was 0.252 and 0.288 respectively. The hydration was stopped with using the addition of acetone at time 20 min, 40 min and 60 minutes after first contact of cement with the water. In given time 20 g of cement paste was putted into the baker and 100 ml of acetone was added. Then the suspension was filtrated and washed twice with using 30 ml of ethanol. In the end the sample was dried in stove for one hour, where the constant temperature 40 °C was set up.

6.8 X-ray powder diffractometry (XRD) analysis

The XRD analysis is a useful tool for determine crystalline phase in inorganic materials. The method of in-situ XRD analysis is a workable tool for a standard investigation of the early hydration of ordinary Portland cement. The diffraction patterns were recorded by a diffractometer Empyrean (PANalytical).

6.8.1 Measurement of partly hydrated samples

All cement samples with the partly stopped hydration were tested via XRD analysis. As a reference sample was used the powder of given cement.
The measurement condition was following:

- Scan Axis: Gonio
- Start Position [°2Th.] 5.0012
- End Position [°2Th.] 89.9822
- Step Size [°2Th.] 0.0130
- Scan Step Time [s] 95.8800
- Anode Material: Cu
- K-Alpha1 [Å] 1.54060
- K-Alpha2 [Å] 1.54443
- Generator Settings 30 mA, 40 kV

6.8.2 In-situ XRD analysis

For the in-situ XRD analysis the cement pastes were prepared in same way like in previous cases and then the pastes were filled into the sample holder. The surface of the paste was smoothed and then covered by Kapton film. The first measurement of the sample was carried out at age 5 min.
The measurement condition was following:

- Scan Axis: Gonio
- Start Position [°2Th.] 5.0104
- End Position [°2Th.] 60.0000
- Step Size [°2Th.] 0.0130
- Scan Step Time [s] 15.045
- Anode Material Cu
- K-Alpha1 [Å] 1.54060
- K-Alpha2 [Å] 1.54443
- Generator Settings 30 mA, 40 kV

The measurement of one diffraction pattern last approximately 5 minutes. The in-situ XRD analysis was carried out with the samples of the cement paste with water content which correspond with normal consistency determined with using Vicat apparatus (w/c was 0.252 and 0.288 for tested pastes from cement Ladce 42.5 N and Mokrá 52.5 N respectively). The effect of SP dosage (0.6 % with respect to the mass of cement) was observed too.

6.9 Scanning electron microscope (SEM)

The analysis with scanning electron microscope was recorded by a JEOL JSM-7400F. The microstructure (via backscatter and secondary electrons) and atomic composition were obtained for partly hydrated samples. Same as in case of XRD analysis as the reference sample was used the powder of given cement. The powder of tested sample was placed on the carbon tape attached to the sample holder. Several regions were examined to make sure that the observed structures were representative of the sample.

The EDX analyses (Energy Dispersive X-ray analysis) of the samples were done too. It is a technique used for identifying the elemental composition of the specimen or an area of the interest.

The particles of Portland cement are readily identified because all clinker components are crystalline, with typical crystal sizes ranging from about 1 μm to as much as 60 mm. Clinkers are normally ground to size between about 2 μm to about 80 μm. The typical mean diameter is usually of the order to 10-12 μm. In general, the grinding does not separate individual crystals, but breaks up the clinker mass as a whole. Thus most individual grains in cement contain fragments of several different kinds of crystals which were adjacent to one another in the clinker. The largest grains may contain some unbroken crystals as well. Small intact crystals of the interstitial components are almost always present in the larger cement grains [79].

7 RESULTS AND DISCUSSION II

7.1 Rheological measurements of the cement pastes

Every 20 minutes the sample of the cement paste was tested via parallel plate rheometer. Series of test sequences were done and in following chapters the G modulus, gel strength, flow curves and Bingham's parameters as well as the thixotrpic area were evaluated.

7.1.1 G modulus

G modulus was evaluated from the shear stress-strain dependence, which was measured during sequence 3, when the constant shear rate 0.01 s^{-1} was applied. As an example of measured data with linear regressions for evaluating G modulus are presented measured data for the sample of the cement paste prepared from the cement Mokrá 52.5 N with w/c = 0.288 and 0.6 % SP shown in Fig. 91.

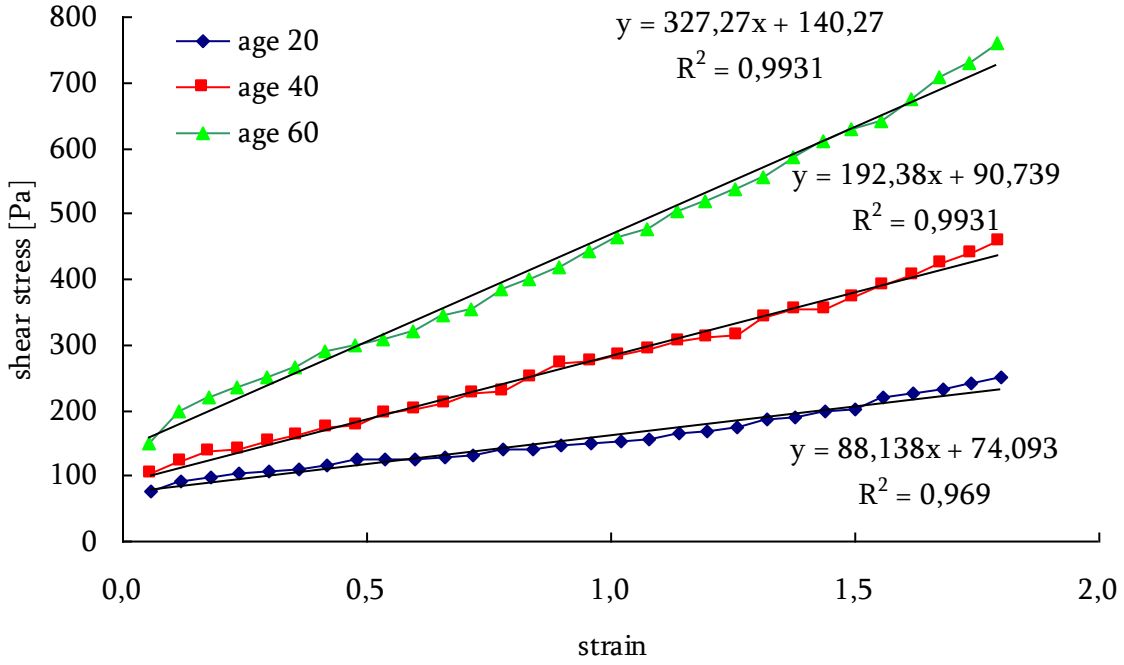

Fig. 91: M*easured data of sequence 3 for the cement paste prepared from the cement Mokrá 52.5 N* with w/c = 0.288 and 0.6 % SP at ages 20, 40 and 60 min

During aging of the cement paste, the increasing of G modulus was observed. In case of the sample prepared from the cement Mokrá 52.5 N with w/c = 0.288 and 0.6 % SP the G modulus increased during one hour from 88 Pa to 327 Pa.

If we compare the change of G modulus with the age of other samples, in some cases we can observe decreasing of G modulus during aging, which is caused by slippage of sample, because of aging and creating new structure in the system. This effect is significant in samples with very low w/c and after 40 or 60 minutes of hydration. In some cases it was observe the unstability of samples (sedimentation, bleeding), which led to less accurate taking of samples. As mentioned above, the rheological measurements are not suitable for unstable samples, so the results belonging to the unstable cement pastes should be assessed with caution.

The standard error of determination of G modulus was evaluated on 18 Pa with the confidence 95 % that means that obtained value of G modulus lie between confidence limits with probability 95 %. This error is significant in case of samples with low G modulus, which were detected only in samples with high SP dosage. The error was determined by evaluating 5 measurements of five samples, which were prepared in same way with same composition.

Comparing of the evaluated values of the G modulus of pastes without SP dosage, the effect of water content was observed. G modulus strongly decreases with w/c and rapidly in case of pastes from the cement Mokrá 52.5 N. In range of w/c from 0.288 to 0.320 the G modulus decreases from 45 kPa to 0.1 kPa and in range of w/c from 0.260 to 0.300 the G modulus decreases from 16 kPa to 0.7 kPa for the cement Mokrá 52.5 N and Ladce 42.5 N respectively.

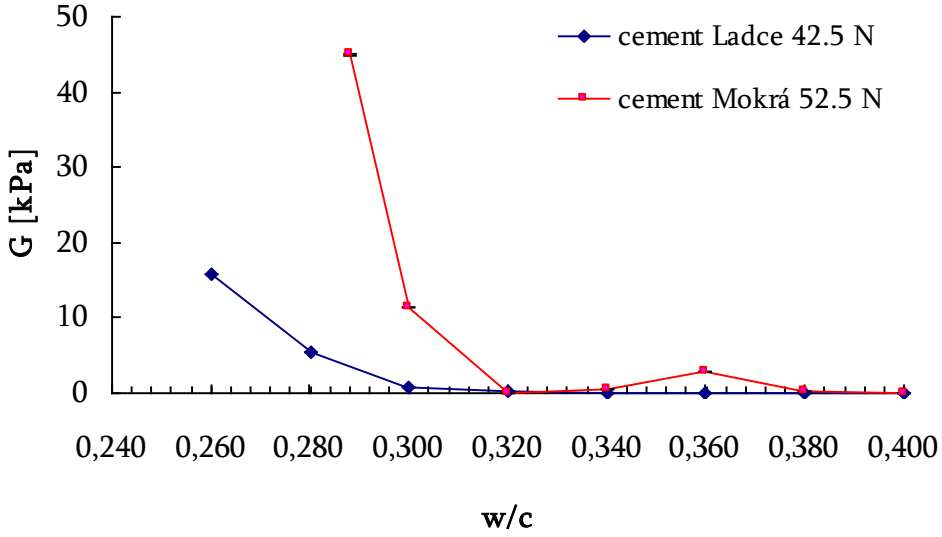

Fig. 92: Effect of w/c on the G modulus for the cement pastes prepared from the cement Ladce 42.5 N *and Mokrá 52.5 N*

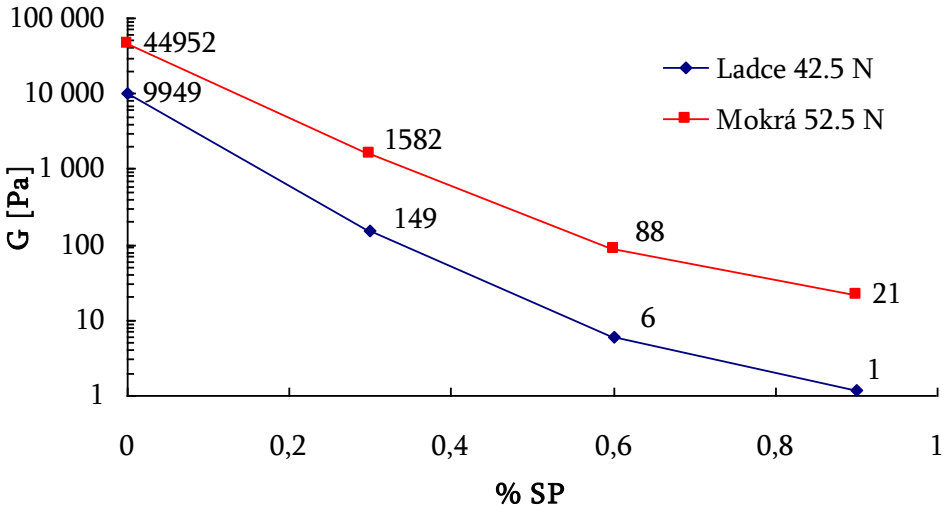

Fig. 93: Effect of SP dosage on G modulus for samples with w/c corresponding to the normal consistency (w/c = 0.288 and 0.*252 in case of the pastes from the cement Mokrá 52.5 N and* Ladce 42.5 N respectively)

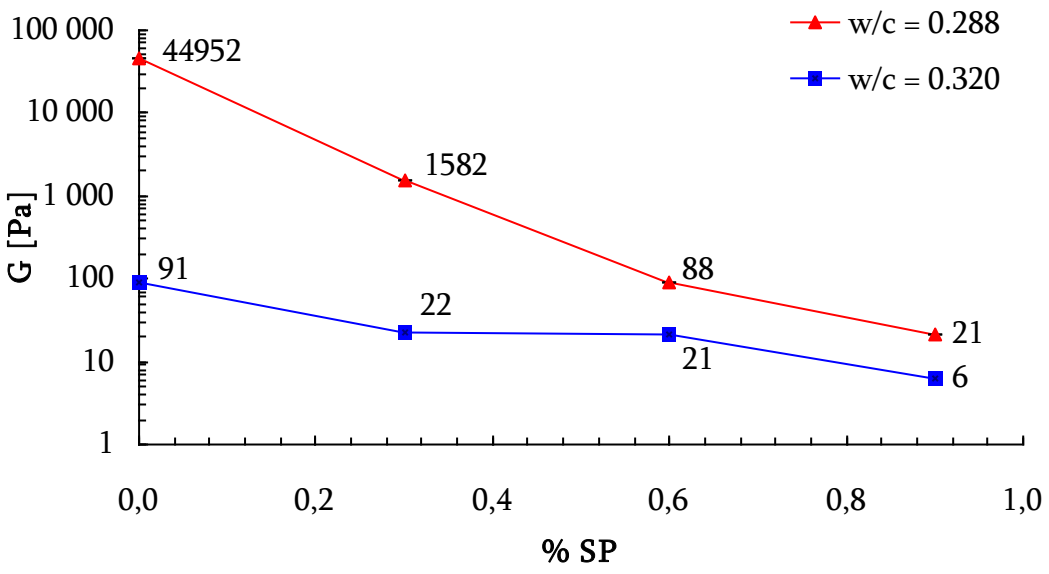

Fig. 94: Effect of SP dosage and w/c on G modulus of the pastes prepared from the cement *Mokrá* 52.5 N

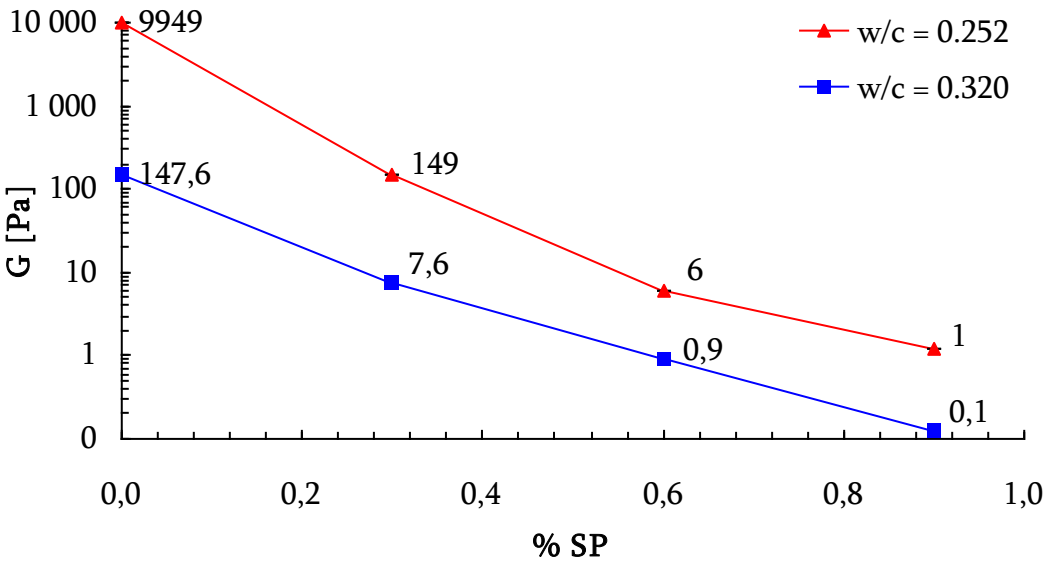

Fig. 95: Effect of SP dosage and w/c on G modulus of the pastes prepared from the cement Ladce 42.5 N

In case of cement pastes with SP dosage we can observe, that SP have important effect on G modulus and with increasing dosage of SP the G modulus significantly decrease. On Fig. 93 there are shown dependences of G modulus on SP dosage in case of the cement pastes with w/c, which correspond to the normal consistencies of pastes without SP. That means w/c = 0.288 and 0.252 for the cement pastes prepared from the cement Mokrá 52.5 N and Ladce 42.5 N respectively. The strongest effect of SP was observed in case of the cement pastes from the cement Mokrá 52.5 N, where G modulus decreases from 45 kPa to 1,6 kPa by using

0.3 % SP. Same dosage of SP reduce the G modulus from 10 kPa to 0.1 kPa in case of the cement pastes from Ladce 42.5 N.

For comparison the data of the samples with same SP dosage and different w/c the Fig. 94 and Fig. 95 are shown. In both cases the w/c had more important influence on G modulus than the SP dosage. One can say that in cases of higher content of SP (more than 0.3 %) the G modulus took the value around ones which is practically in range of the standard error.

7.1.2 Gel strength

The gel strength was evaluated as the last point of shear stress where the shear rate was about zero. As an example of measured data of sequence 5 of the rheological measurement is obtained data for the same sample as in previous case (the cement paste prepared from the cement Mokrá 52.5 N with w/c = 0.288 and 0.6 % SP).

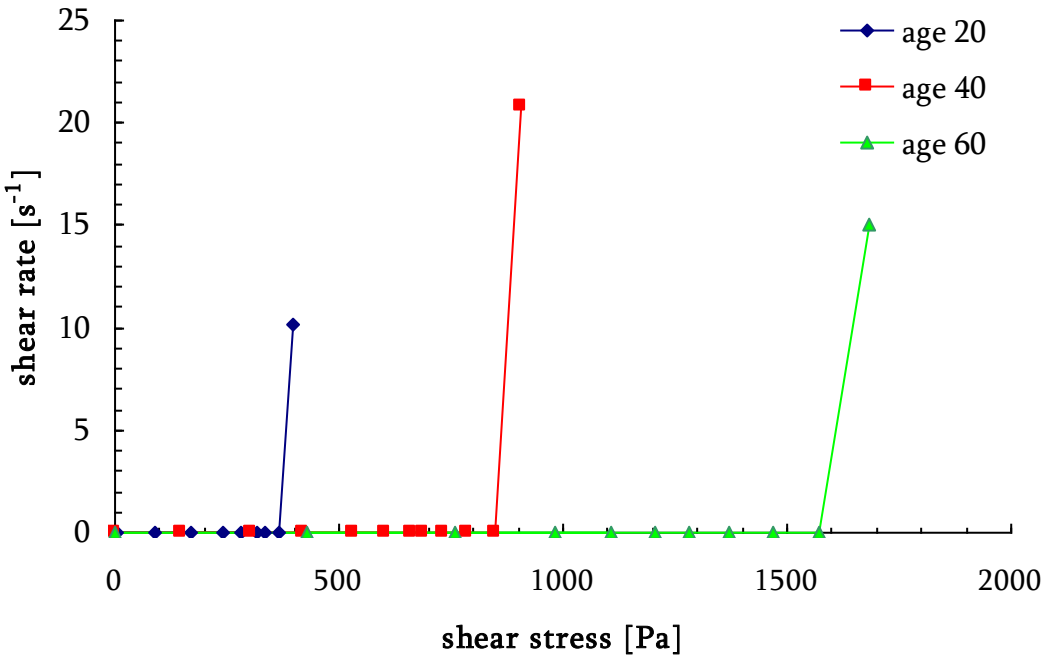

Fig. 96: Measured *data of sequence 5 for the cement paste prepared from the cement Mokrá 52.5 N* with w/c = 0.288 and 0.6 % SP at ages 20, 40 and 60 min

Same as in case of development of G modulus, the gel strength increased during aging of the cement paste. In mentioned sample the gel strength grew from 365 Pa at age 20 min through 846 Pa at age 40 min up to 1571 Pa at age 60 min.

The deviations from expected values of gel strength during aging were observed along with deviations found out in case of evaluating the G modulus. This fact is attributed to difficult sampling which was connected with stability of prepared cement pastes. The standard error of determination of gel strength was evaluated as 27 Pa with the confidence 95 %.

The effect of w/c on the value of the gel strength is shown in Fig. 97. The strong dependence of w/c on the gel strength was observed. The gel strength decreased from 7493 Pa through 3004 Pa to 1654 Pa while the w/c decreased from 0.288, through 0.300 to 0.320 in case of the pastes from the cement Mokrá 52.5 N. Similar effect was observed for the cement

paste prepared from the cement Ladce 42.5 N where the decrease from 6843 Pa, through 5871 up to 1026 Pa corresponded with the changes of w/c from 0.260 through 0.280 to 0.300.

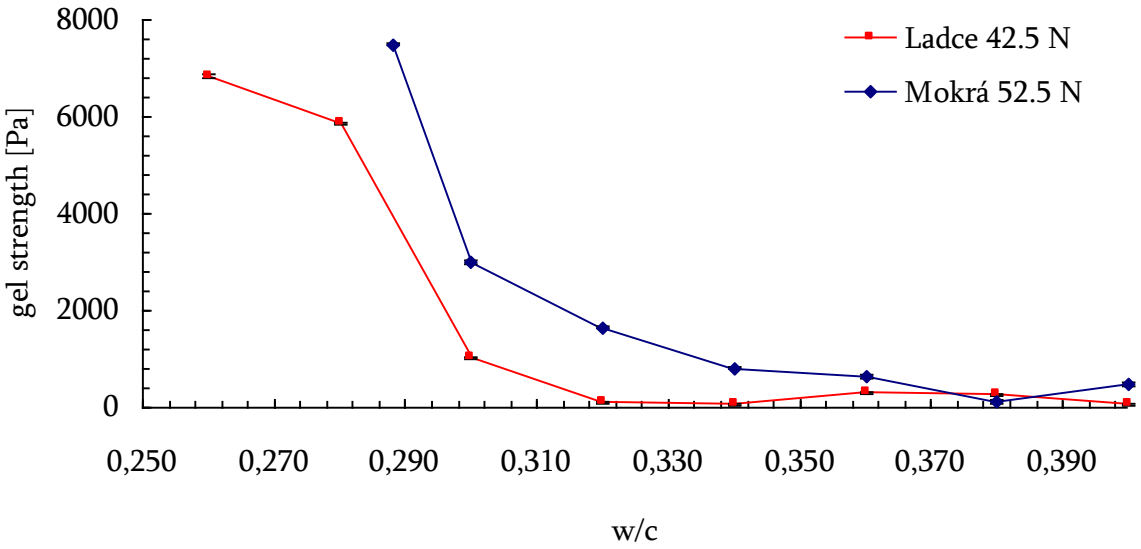

Fig. 97: Effect of w/c on the gel strength for the cement pastes prepared without SP

Gel strength is significantly affected by SP dosage as shown on Fig. 98 and Fig. 99. The effect is stronger in samples with lower w/c in both cases of used cements. If we compare the gel strength of samples with w/c corresponding to the normal consistency, the dosage of SP decreased the gel strength from 7493 Pa through 2300 Pa, 365 Pa to 93 Pa along with addition 0.3 % SP in case of the pastes from the cement Mokrá 52.5 N. As mentioned before, the weaker effect was observed in case of higher w/c (0.320), where the evaluated gel strength decreased from 559 Pa through 150 Pa, 130 Pa to 38 Pa along with addition 0.3 % SP.

The cement pastes prepared from the cement Ladce 42.5 N showed decrease of the gel strength from the value 3855 Pa through 846 Pa, 37 Pa up to 13 Pa along with addition 0.3 % SP. In case of higher w/c (0.320) the decrease of the gel strength came through the values 1371 Pa, 46 Pa, 6 Pa and 2 Pa. It should be noticed, that last three mentioned values should be used with the caution because of standard error of determination.

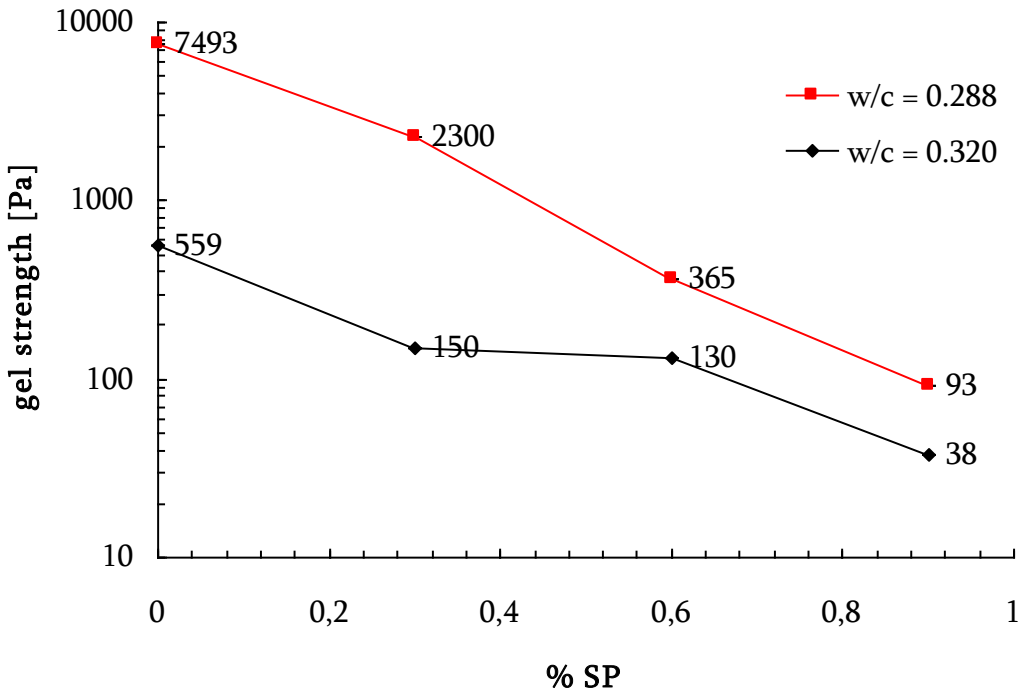

Fig. 98: Effect of SP dosage on gel strength of the pastes from the cement *Mokrá 52.5 N*

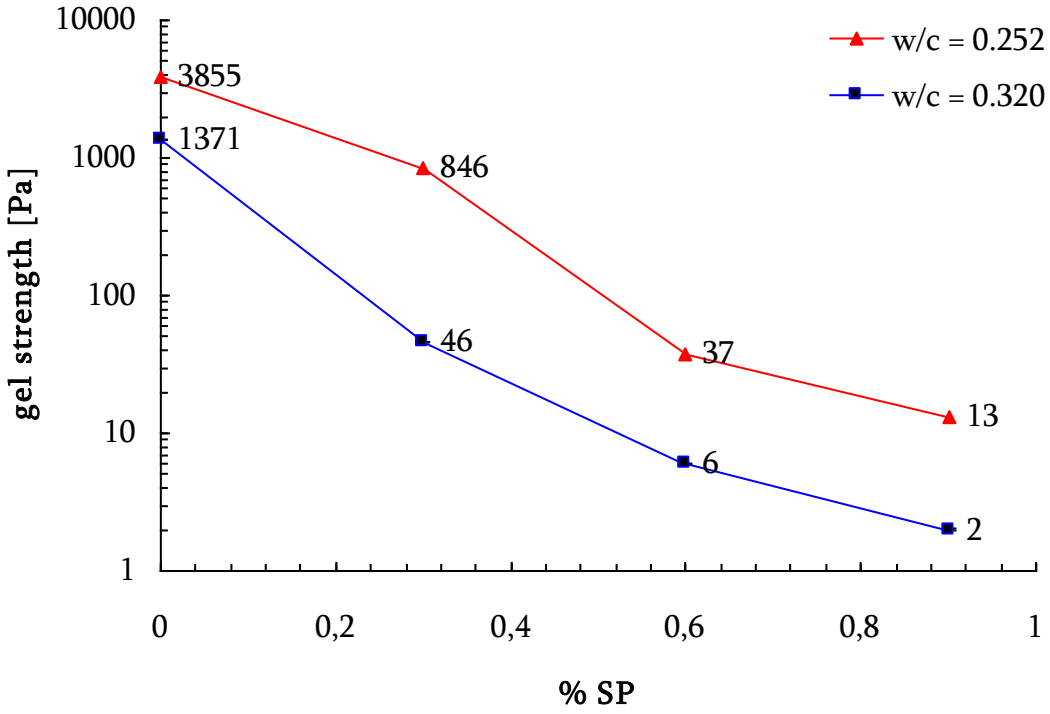

Fig. 99: Effect of SP dosage on gel strength of the pastes from the cement Ladce 42.5 N

7.1.3 Flow curves

The measured flow curves were evaluated with using Bingham model, which gives the value of yield stress (dynamic) and plastic viscosity. For evaluation the same range of shear rates of down curve was used: 1 s^{-1} – 50 s^{-1}.

In case of the samples with SP dosage, the yield stress obtained with using the Bingham model had negative value, which has not physical meaning. That was the reason for applying different model for evaluation of measured values. According the theoretical knowledge (chapter 3.8.) the Herschley-Bulkey model is sometimes applied to fit experimental data of the cement based systems. The results of fitting the data by the Herschley-Bulkey model are yield stress, consistency and power law index n. When the n is higher than 1, the equation signifies a shear thickening behavior and with n lower than 1, a shear thinning behavior (while a Bingham behavior for n = 1).

The Herschley-Bulkey model is concerning to the following samples: pastes from the cement Mokrá 52.5 N with w/c = 0.320 and 0.9 % SP and pastes from the cement Ladce 42.5 N with more than 0.6 % SP dosage. For comparison of the rheological parameters, whole series of samples with same w/c and different SP dosage were evaluated with using the Herchley-Bulkey model. The evaluation was done with using the software Rheology Advantage Data Analysis, version 5.5 from TA Instruments. The example of evaluation of measured data is shown in Fig. 100.

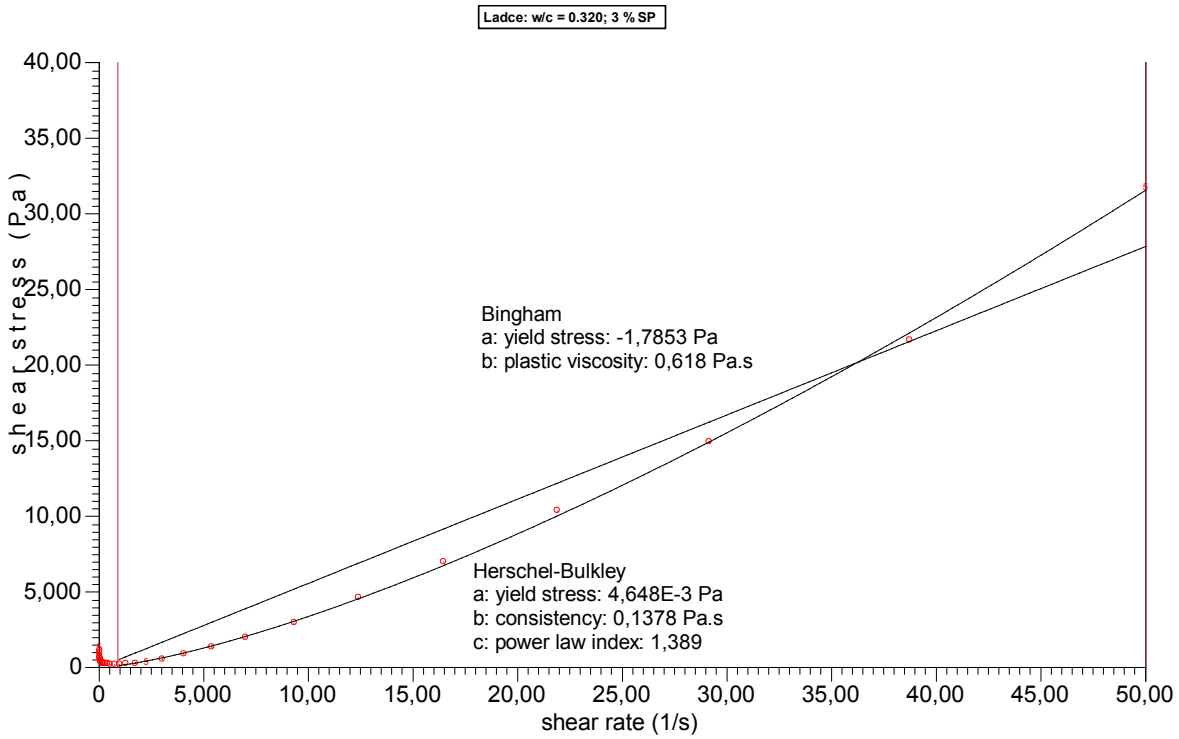

Fig. 100: Example of evaluation of rheological parameters for the sample from the cement Ladce 42.5 N with w/c 0.320 and 3 % SP

7.1.3.1 Plastic viscosity

Plastic viscosity of the samples is influenced by w/c and with increasing water content the plastic viscosity is slowly decreasing in case of the pastes from the cement Ladce 42.5 N. In case of the pastes from the cement Mokrá 52.5 N, one can say, that plastic viscosity oscillates

around approximate value 2.5 Pa.s, except of the first point, which belongs to the paste with the lowest w/c (Fig. 101). In this case, the big change of the plastic viscosity was observed along with increasing w/c from 0.288 to 0.300. The cement paste with lower w/c showed very stiff behavior and 0.288 was the lowest w/c, where the rheological measurement should be done. After 40 minutes the sample was so stiff, that it was difficult to test it. It was a good example of slippage during measurement, because the rheological parameter at time 40 and 60 minutes were lower that previous. The similar situation with the possibility of slippage was observed in sample from the cement Ladce 42.5 N with the lowest w/c (0.260) too. The error of the evaluated values of plastic viscosity was determine on 0.02 Pa.s obtained by evaluating 5 measurements of five samples, which were prepared in same way with the same composition.

Plastic viscosity of the samples from the cement Mokrá 52.5 N reached little bit higher values than pastes from the cement Ladce 42.5 N, except of samples with w/c = 0.300, where first mentioned took the value 2.1 Pa.s and second 2.7 Pa.s.

The plastic viscosity of the samples from the cement Ladce 42.5 N shows slowly decreasing from the value 3.8 Pa.s at w/c 0.280 to the value 1.0 Pa.s at w/c = 0.400. First obtained value at w/c 0.260 is lower than the following because of high possibility of slippage during measurement due to very low w/c as mentioned before.

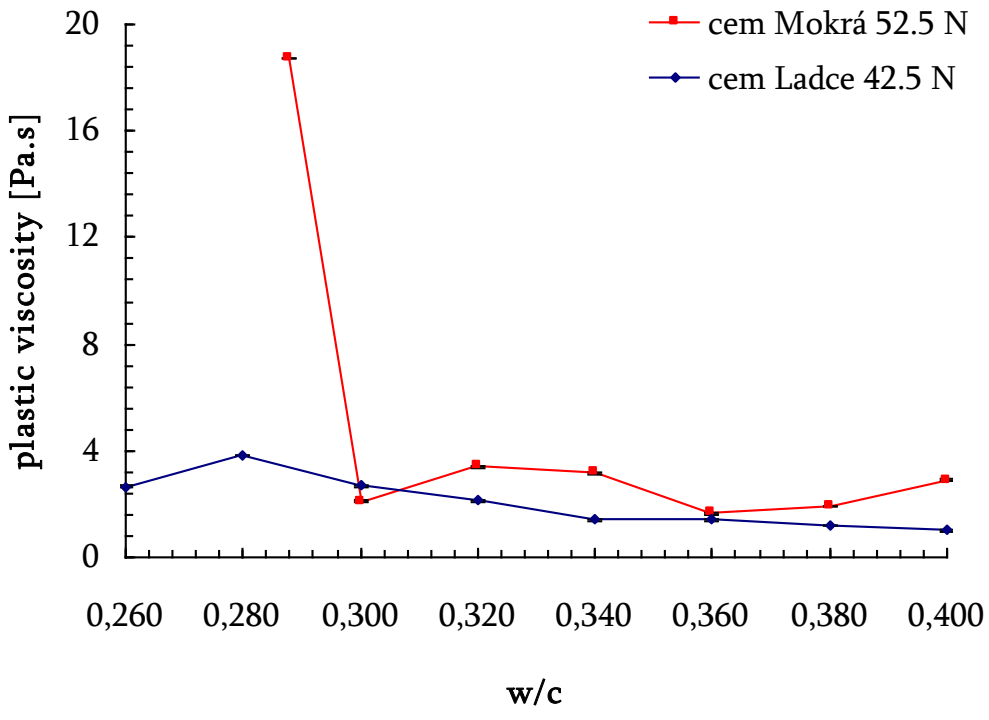

Fig. 101: Iinfluence of w/c on the plastic viscosity of the cement pastes

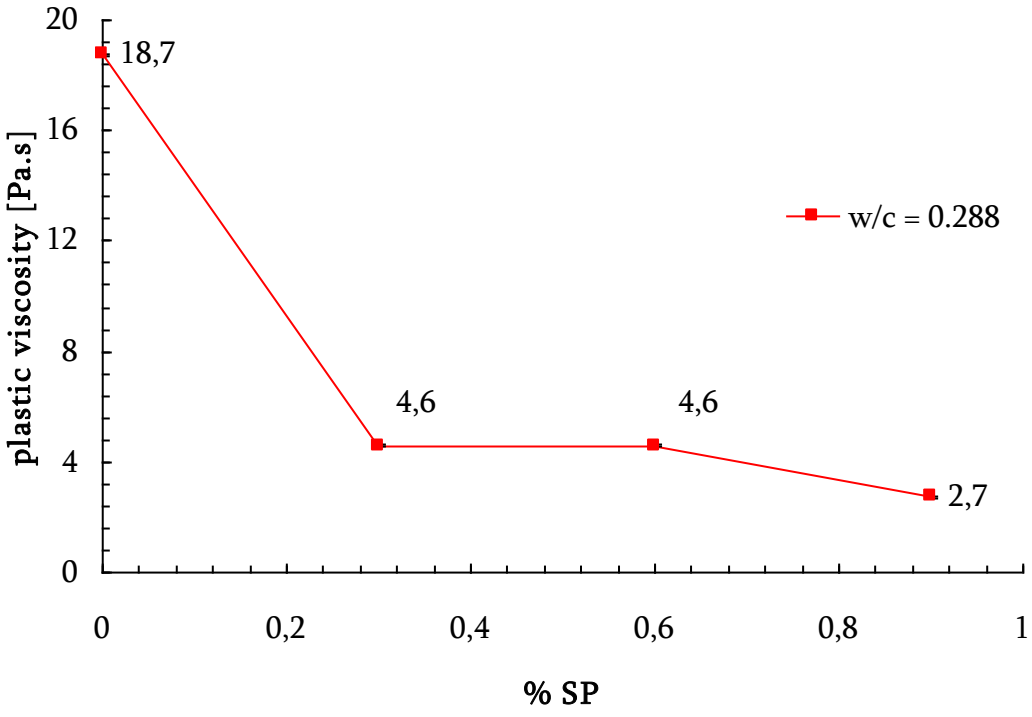

Fig. 102: Influence of SP dosage on the plastic viscosity on the pastes from the cement Mokr*á 52.5 N*

The effect of SP dosage on plastic viscosity can not be omitted. In Fig. 102 there is shown rapid decrease of plastic viscosity which was caused by using 0.3 % SP. Other addition of SP had not so strong effect.

As mentioned before, other samples were evaluated with using the Herschel-Bulkey model. So comparison of the samples where the SP was used continues in following chapter, where the yield value, consistency and power law index are calculated.

7.1.3.2 Yield stress

The yield stress of samples without SP dosage was calculated as the Bingham parameter and their dependence on w/c is shown in Fig. 103. As we expected, the yield stress decrease with increasing water content from 5633 Pa to 13 Pa and from 219 Pa to 5 Pa in case of maximal and minimal w/c in cement pates from the cement Mokrá 52.5 N and Ladce 42.5 respectively. The standard error of the determination of yield stress took the value 3 Pa. This error is significant in cases of samples with high w/c (especially for the pastes from the cement Ladce 42.5) and with maximal SP dosage.

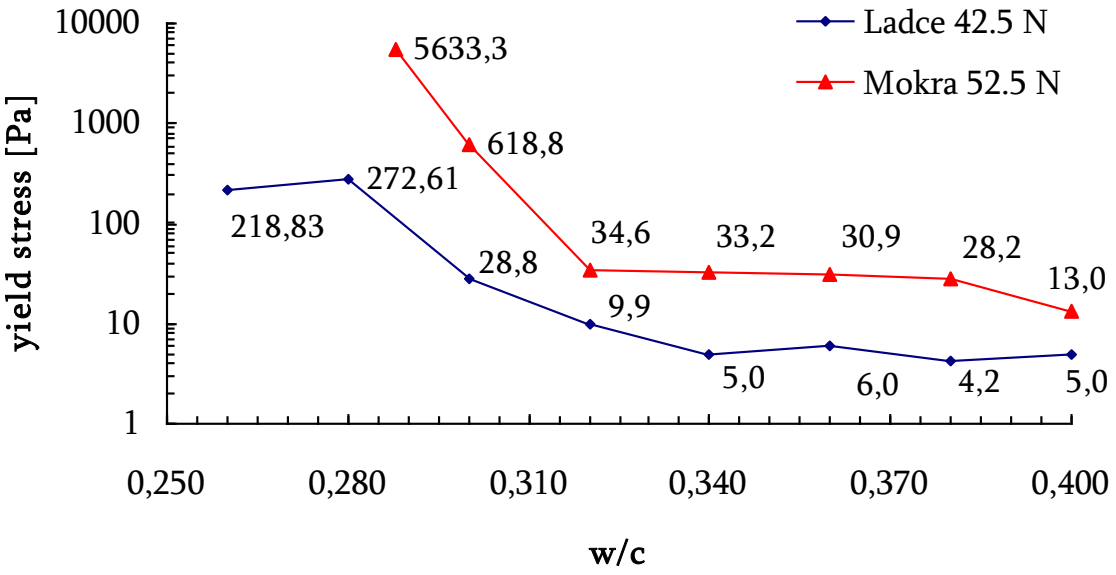

Fig. 103: Influnence of w/c on yield stress

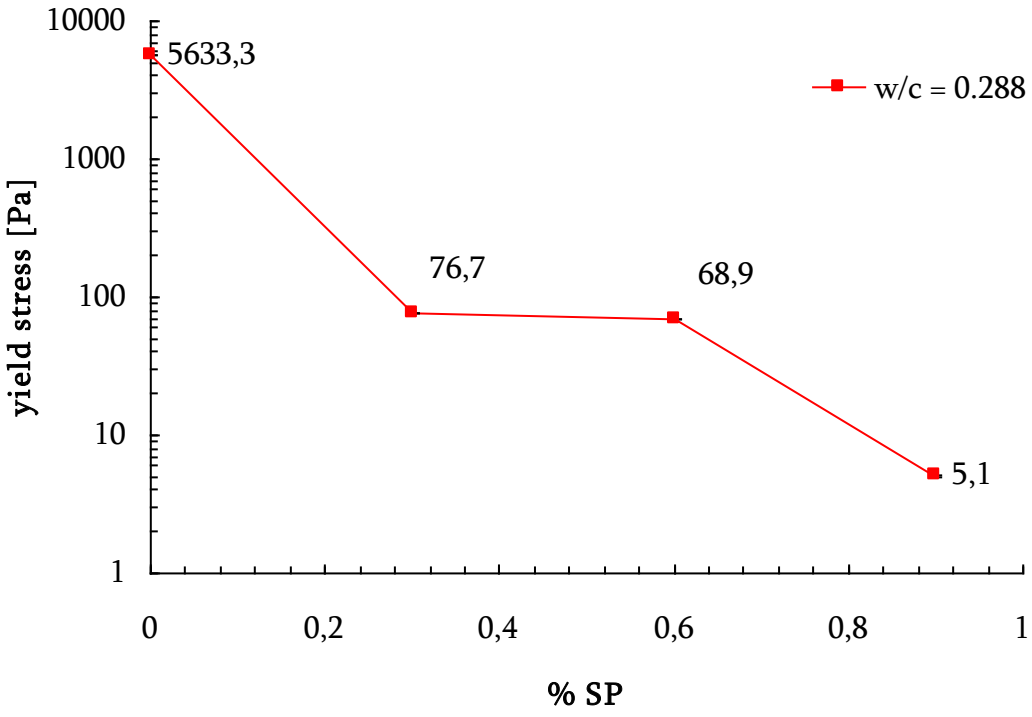

Fig. 104: Influence of SP dosage on yield stress for the cement pastes prepared from the cement *Mokrá 52.5 N with w/c = 0.288*

The significant effect of SP on the yield stress was observed whereas the addition of 0.3 % SP changed the value from 5633 Pa to 77 Pa (Fig. 104). Other addition of SP decreased the yield stress up to 5.1 Pa.

7.1.3.3 Evaluation with using the Herschel-Bulkley model

The samples of the cement paste, where the Herschel-Bulkey model were used are listed in Table 51 along with obtained rheological parameters. According to the power law index, one can say, that the SP dosage (0.6 % and more) caused shear-thickening behavior in case of the samples from the cement Ladce 42.5 N. Samples with lower SP dosage showed rather shear-thinning behavior (for example sample with w/c = 0.32 and 0.3 % SP n = 0.8) or almost Bingham behavior (for example sample with w/c = 0.252 and 0.3 % SP n = 0.9).

Concerning the samples prepared from the cement Mokrá 52.5 N, the shear-thickening behavior was determined only in case of sample with the highest SP dosage. Other samples showed Bingham behavior and shear-thinning tendency in case of the sample with 0.3 % SP.

Table 51: Obtained rheological parameters of the cement pastes from Herschel-Bulkey model

cement	w/c	% SP	Yield stress [Pa]	Konsistency [Pa.s^n]	n
Ladce 42.5 N	0.252	0	95.7	4.7	0.92
		0.3	46.6	4.2	0.90
		0.6	2.2	0.5	1.29
		0.9	0.1	0.4	1.30
	0.320	0	12.1	2.5	0.95
		0.3	3.6	2.6	0.80
		0.6	0.3	0.1	1.43
		0.9	0.0	0.0	1.70
Mokrá 52.5 N	0.320	0	35.0	3.3	1.01
		0.3	15.8	9.2	0.71
		0.6	11.1	1.4	1.08
		0.9	1.6	0.5	1.28

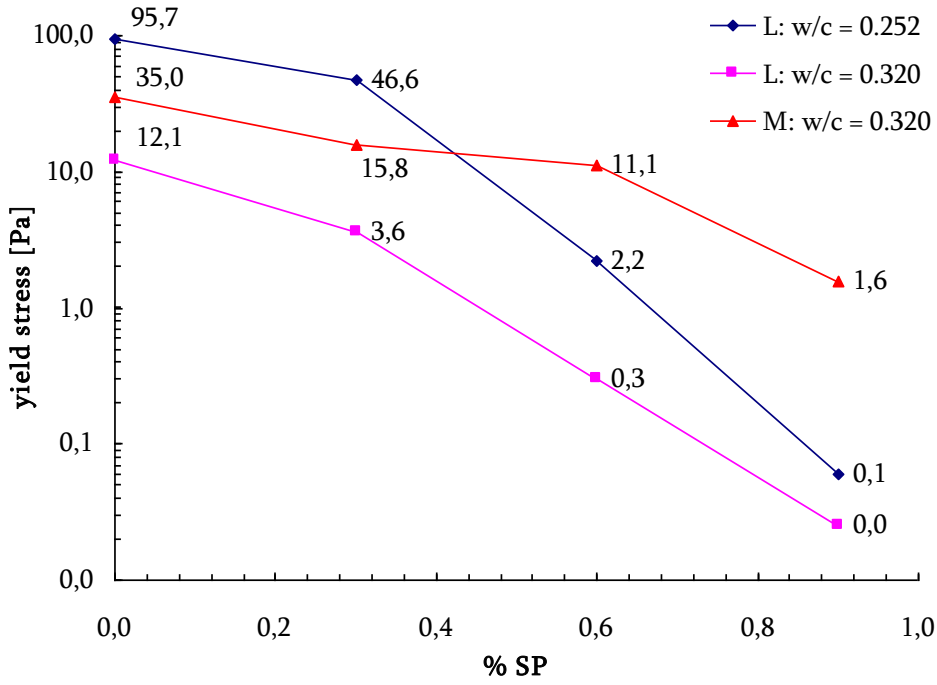

Fig. 105: Effect of SP dosage on yield stress of the cement pastes (L = cement Ladce 42.5 N and M = *cement Mokrá 52.5 N)*

The SP dosage showed again the important influence on the yield stress. In case of lower w/c (0.252) the effect of SP is more significant and led to decrease the yield stress from 96 Pa up to almost 0 Pa. The yield stress obtained for series with higher w/c (0.320) showed slower decrease from 12 Pa to 0 Pa. Similar results showed the samples from the pastes the cement Mokrá 52.5 N, where the yield stress decreased from 35 Pa to 2 Pa by addition of SP.

7.1.3.4 Static yield stress

In some cases the static yield stress was recognized during the measurement of flow curves (correspond with theoretical knowledge shown on Fig. 11). This fact had important effect on calculated area between flow curves. A good example of flow curve with distinct static yield stress is shown on Fig. 106.

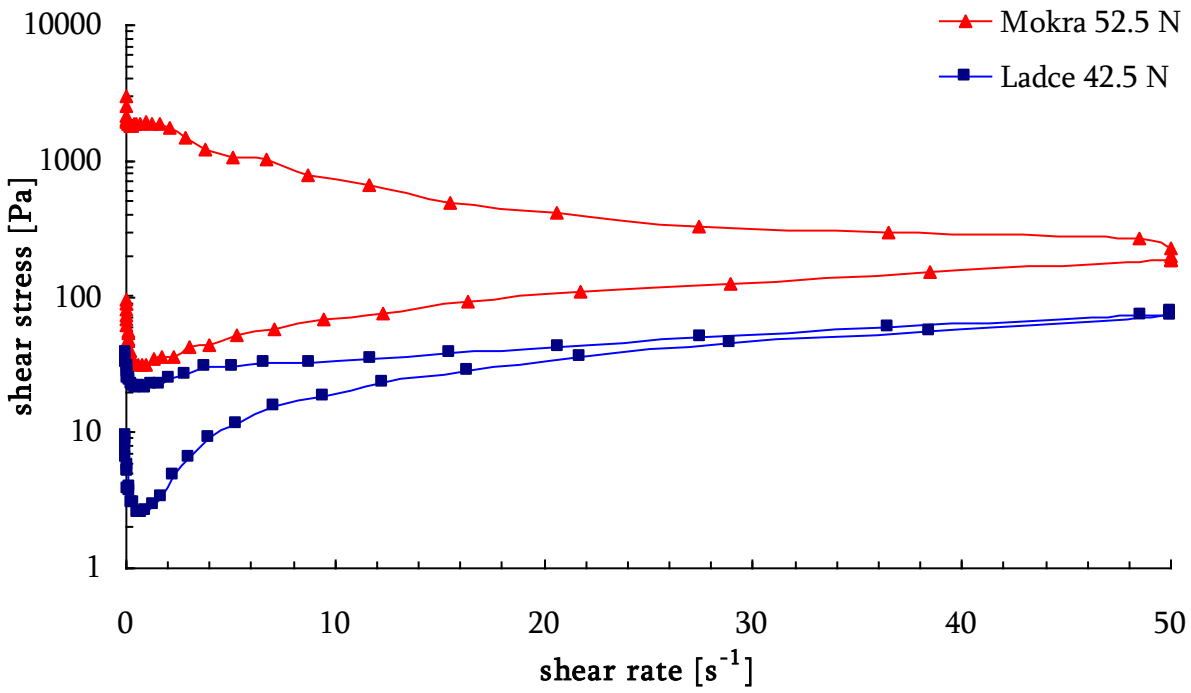

Fig. 106: Obtained flow curves of the paste with w/c = 0.34 from both used cement

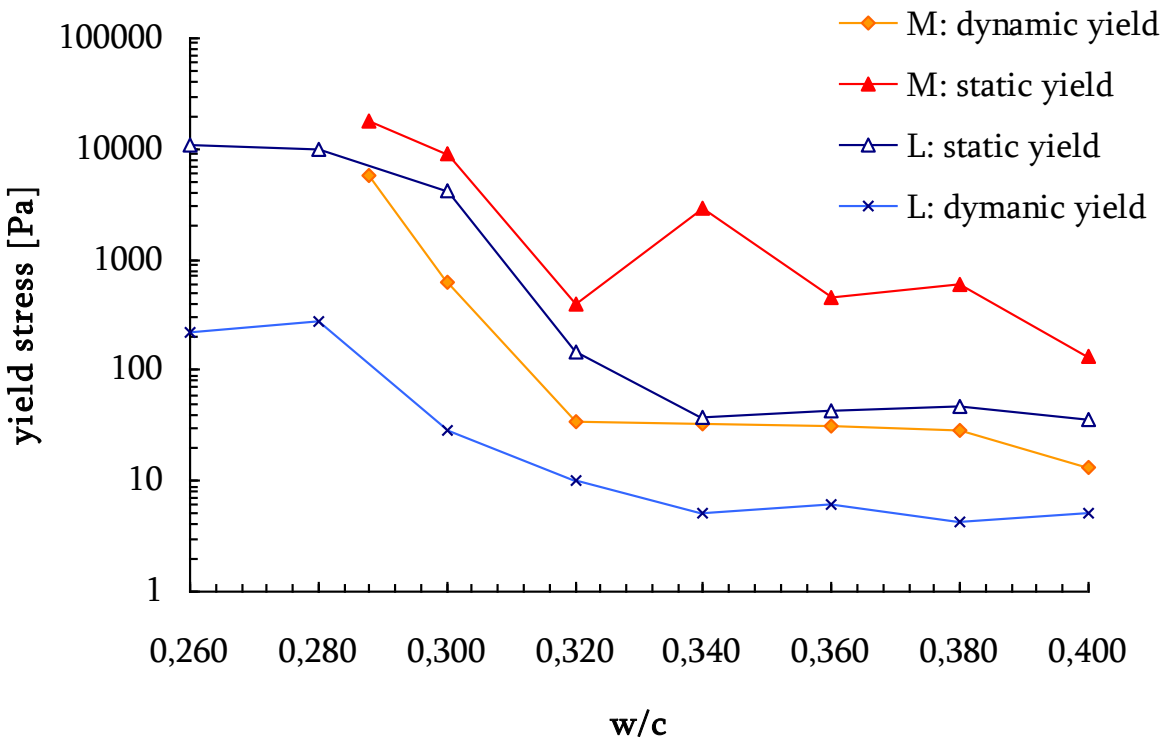

Fig. 107: Dymanic and static yield stresses of samples with connection to the w/c

For comparison the static and dynamic yield stress the dependencies on Fig. 107 were constructed. In all cases the obtained result of static yield stresses are higher than dynamic, which is in good agreement with theoretical knowledge. Similar decreasing dependence which was obtained during evaluation of the dynamic yield was observed for the static yield stress. In case of the samples from the cement Ladce 42.5 N the values of the static yield are consistent with the dynamic yield values and both decreased with increasing w/c. Samples from the cement Mokrá 52.5 N showed not so clear decrease of static yield as previous series.

In cases of the samples with SP (Fig. 108), the SP dosage reduced the static yield stress from 17 530 Pa up to 53 Pa in case of the pastes from the cement Mokrá 52.5 N with w/c 0.288. The pastes with higher w/c (0.320) showed slower decrease of static yield stress and in case of the highest SP dosage (0.9 %) the static yield stress wasn't obvious.

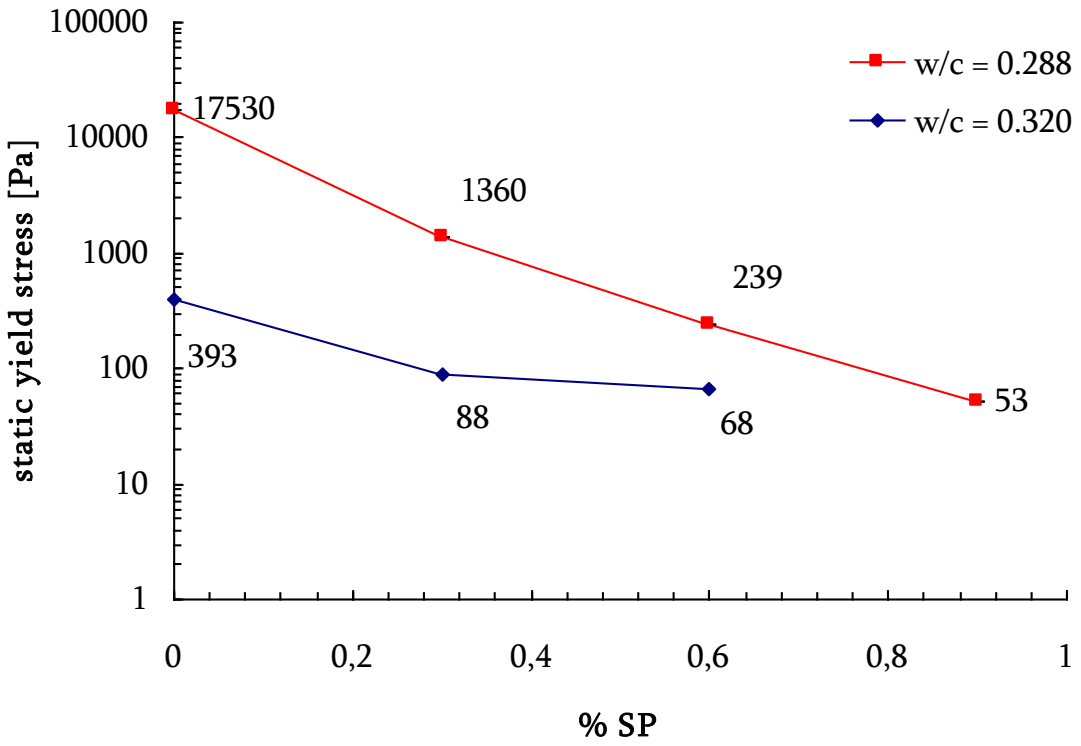

Fig. 108: Effect of SP dosage on the static yield stress of the ce*men pastes from the cement Mokrá* 52.5 N

The cement pastes from the cement Ladce 42.5 N with SP dosage showed the static yield stress only in case of the sample with w/c = 0.252 and 0.3 % SP and took the value 150 Pa. Other dosage of SP caused disappearance of the static yield stress.

In conclusion, the measurement of the static yield stress is very sensitive, because this stress is reached with using very low shear rates.

7.1.3.5 Apparent viscosity

Apparent viscosities were evaluated for every measured point of down curve. The obtained dependencies are shown in Fig. 109 and Fig. 110, where the whole range of w/c for the both used cements is presented.

As mentioned before, the w/c has strong effect on the rheological parameters of the cement pastes. The significant changes of apparent viscosities occurred when the w/c is lower than 0.320 in cases of the samples from the cement Mokrá 52.5 N. The samples from the cement Ladce 42.5 N show gradual increase of apparent viscosities with decreasing w/c and all values are lower compare to the samples with same composition from the cement Mokrá 52.5 N.

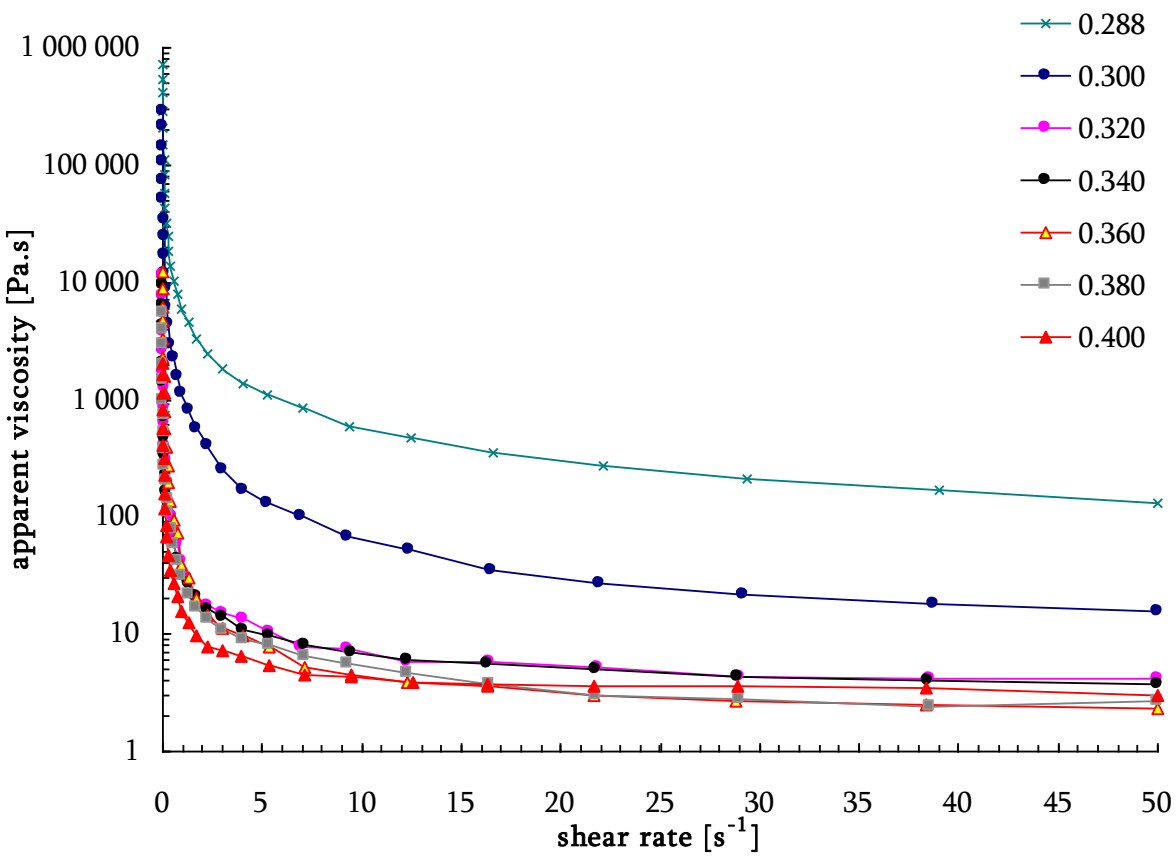

Fig. 109: Apparent viscosities of the samples from the cement *Mokrá*52.5 N with w/c range from 0.288 to 0.400

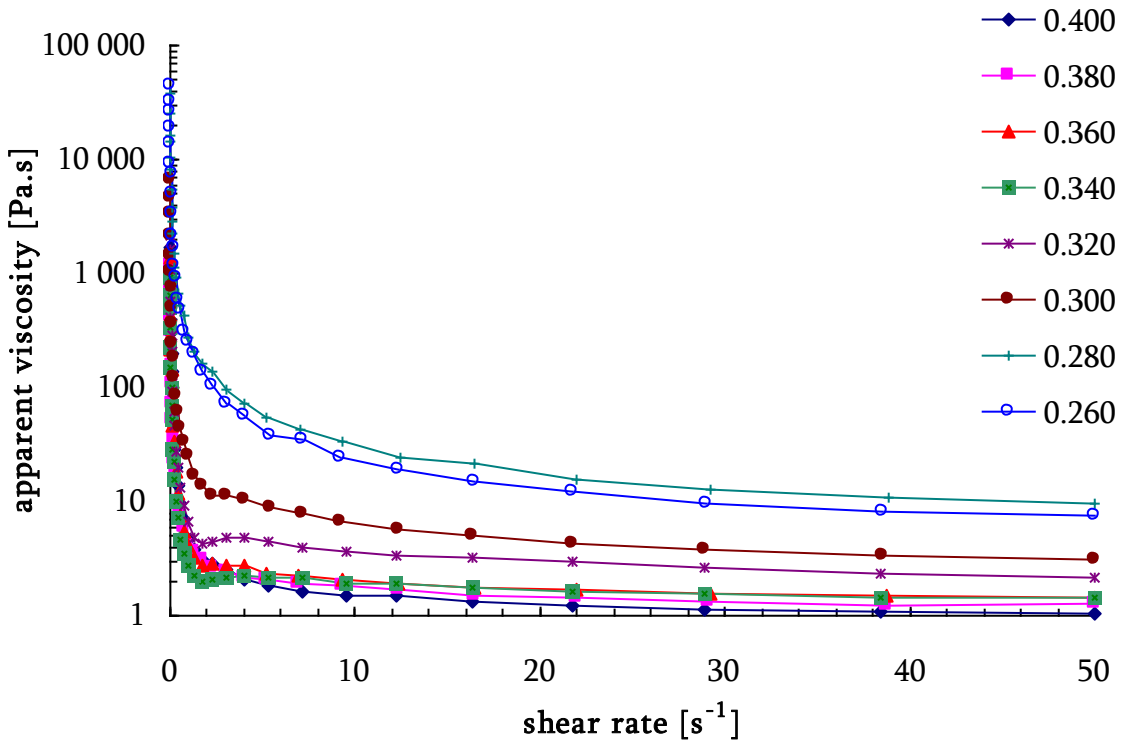

Fig. 110: Apparent viscosities of the samples from the cement Ladce 42.5 N with w/c range from 0.260 to 0.400

Influence of SP on apparent viscosity is shown on Fig. 111 and Fig. 114. Concerning the pastes from the cement Mokrá 52.5 N with lower w/c (0.288), the effect of SP became evident at 0.9 % SP. Samples with higher w/c demonstrate obvious influence of SP, which consist in decreasing apparent viscosity. Comparing w/c for samples with same SP dosage, it was proved, that increasing of water content decrease the apparent viscosity.

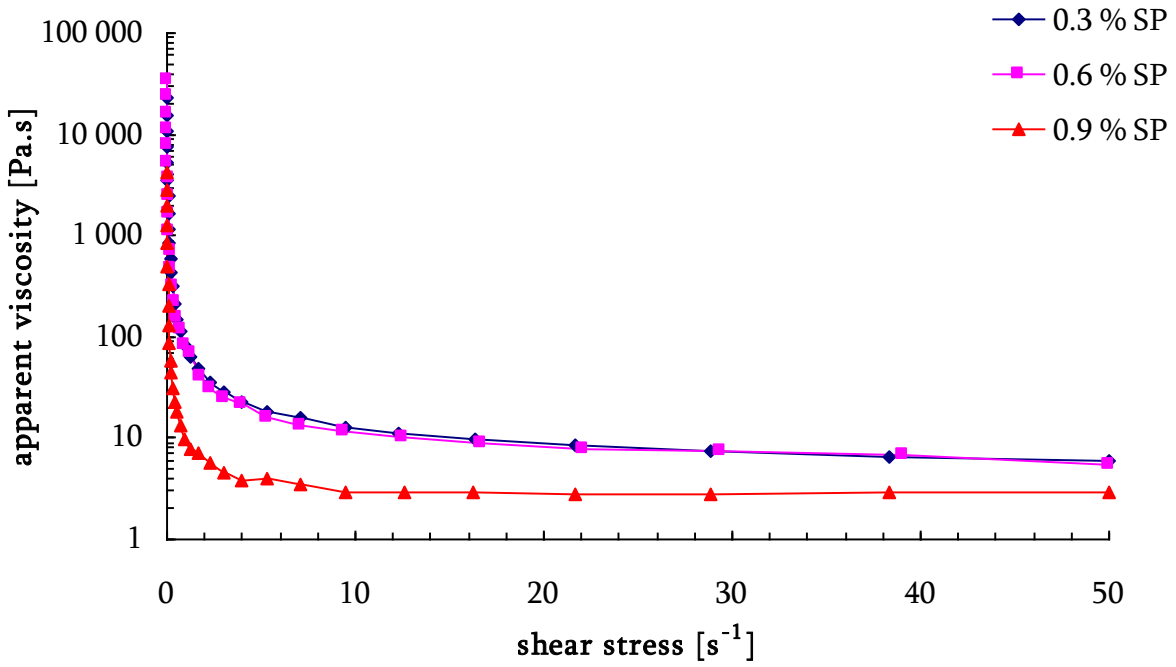

Fig. 111: *Effect of SP dosage on the apparent viscosity of the pastes from the cement Mokrá 52.5 N* with w/c = 0.288

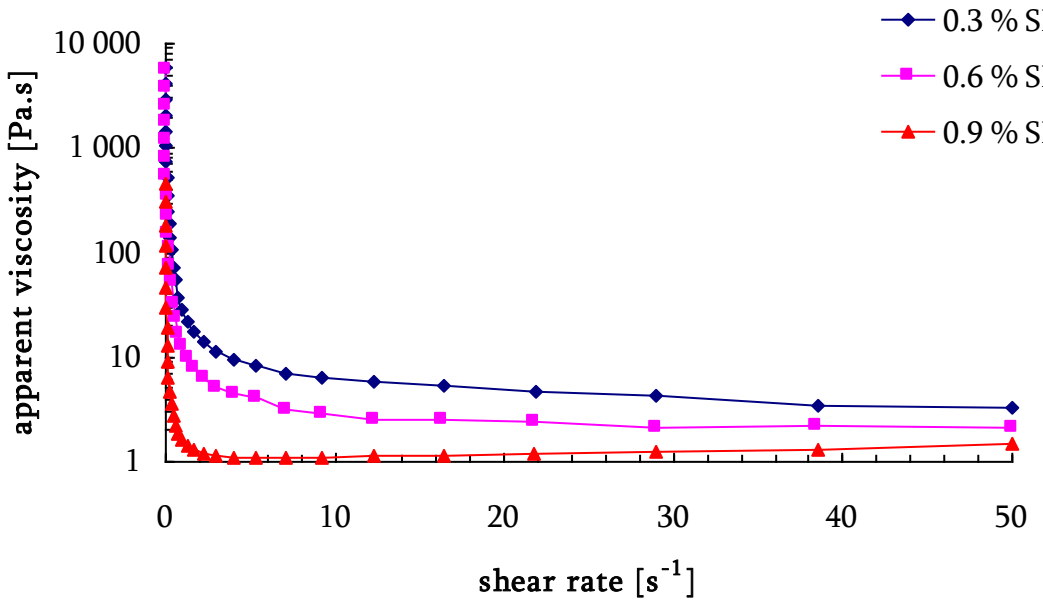

Fig. 112: *Effect of SP dosage on the apparent viscosity of the pastes from the cement Mokrá 52.5 N* with w/c = 0.320

Similar results as in case of pastes concerning the cement Mokrá 52.5 N were obtained in case of the pastes from the cement Ladce 42.5 N (Fig. 113 and Fig. 114). The effect of SP dosage is already obvious by addition 0.3 % SP. In case of lower w/c, the SP dosage significatly decreased the apparent viscosity (compare to the previous discussion). Same as previous results showed the influence of the w/c, the samples from the cement Ladce are not exception.

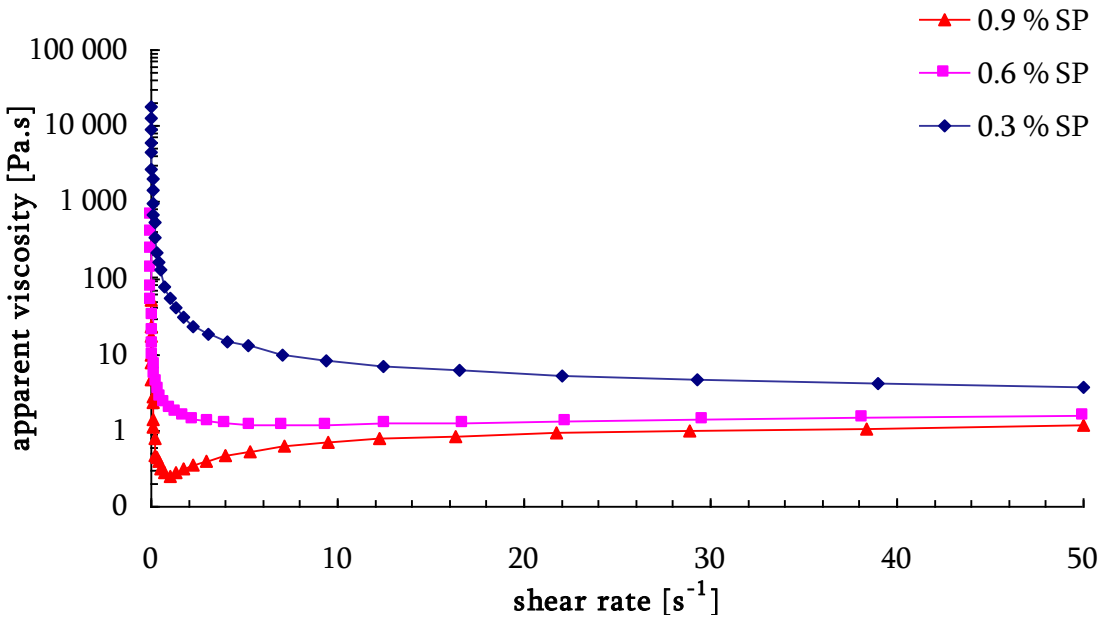

Fig. 113: Effect of SP dosage on the apparent viscosity of the pastes from the cement Ladce 42.5 N with w/c = 0.252

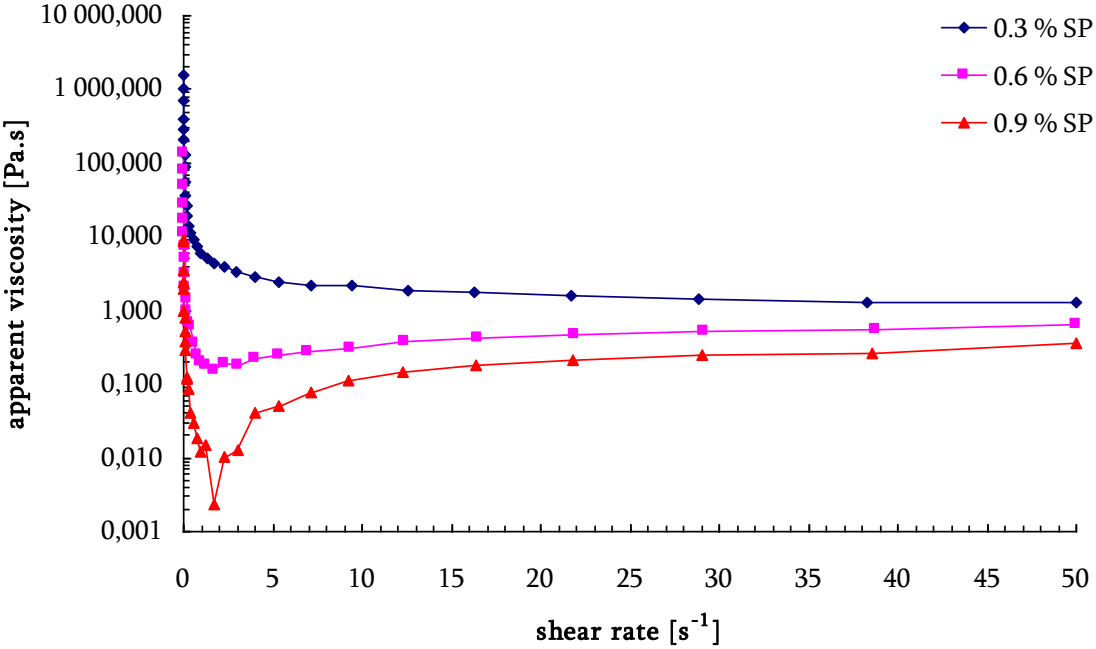

Fig. 114: Effect of SP dosage on the apparent viscosity of the pastes from the cement Ladce 42.5 N with w/c = 0.320

7.1.3.6 Thixotropic area

The thixotropic area was calculated as an area, which is defined by thixotropic loop (the area between up and down flow curve). The trapezoidal numerical integration method for evaluation of the value of the thixotropic area was used. The thixotropic area is influenced by w/c as well as SP dosage. With increasing w/c the thixotropic area is decreasing (Fig. 115). That means that the Bingham parameters from up and down curves became more similar than in cases with low w/c, where the parameters are significantly different. The strongest effect of water content on the thixotropic area was observed in samples from the cement Ladce 42.5 N.

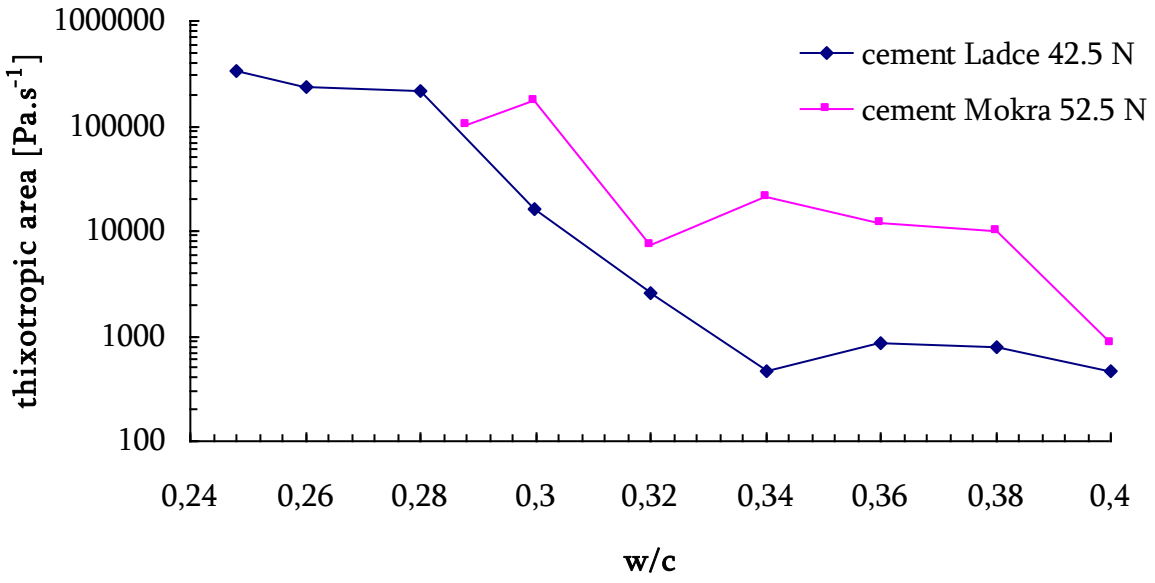

Fig. 115: Influence of w/c on the thixotropic area

It is very well see (Fig. 116), that effect of SP dosage has important influence on thixotropic area. In case of sample without SP and w/c 0.252 (the cement Ladce 42.5 N) the area is much more than hundred times higher than area obtained in case of the sample with SP. Significant effect on magnitude of the area have already low SP dosage. In case with the highest dosage of SP (0.9 % with respect to the mass of cement) and w/c = 0.252 the area had negative value, which corresponds with fact, that Bingham parameters are higher for the down curve than for the up curve. This refers to unstability of prepared sample which was really observed.

Effect of SP is not so significant in case of cement pastes with higher water content (w/c = 0.320), where thixotropic area of pates with SP is almost twenty times higher than the area of sample with 0.3 % SP. In case of sample with 0.6 % of SP, where the area is three times higher than in previous samples (0.3 % SP), the sedimentation was observed, which led to infelicitous sampling. The sample with 0.9 % SP showed very high flowability which causes very low value of the thixotropic area as well as other rheological parameters.

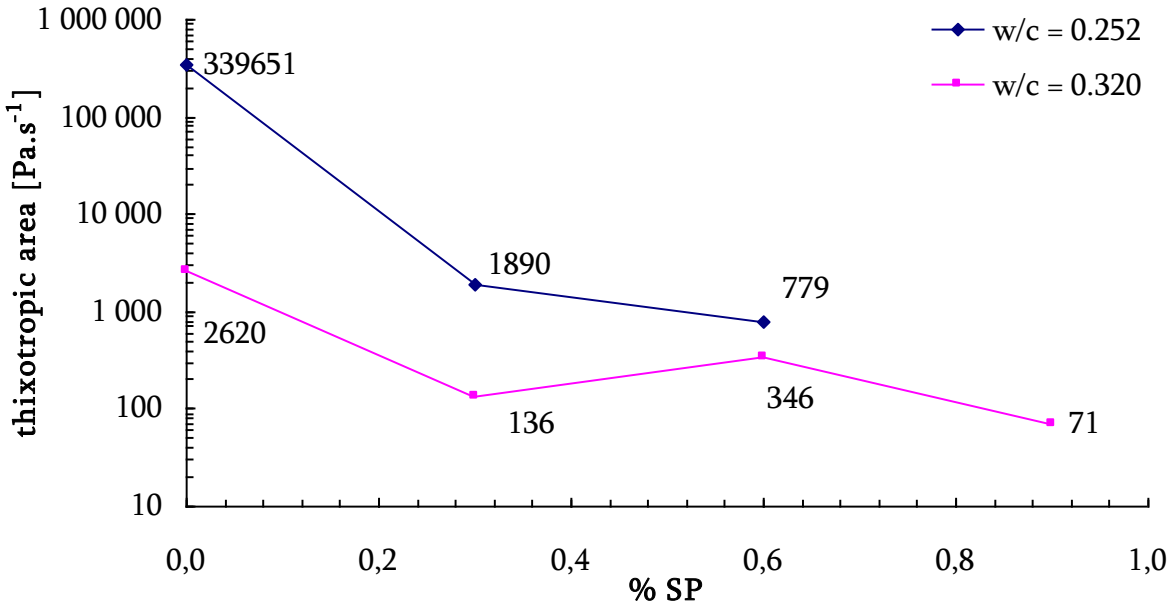

Fig. 116: Influence of SP dosage on the thixotropic area of the samples from the cement Ladce 42.5 N

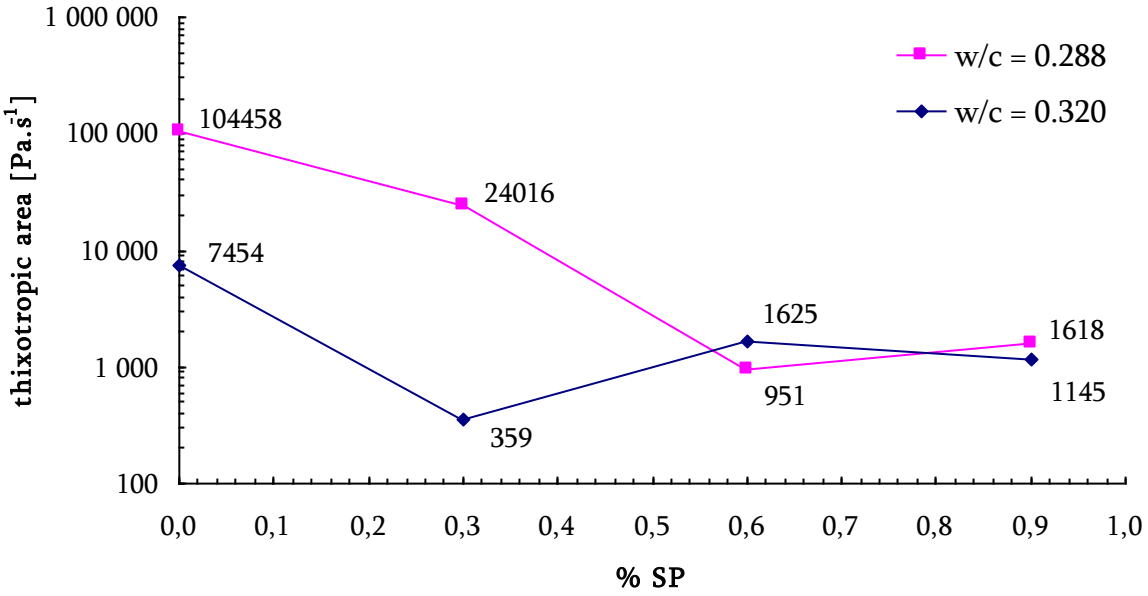

Fig. 117: Influence of SP dosage on the thixotropic area *of the samples from the cement Mokrá 52.5 N*

In case of the samples prepared from the cement Mokrá 52.5 N the effect of SP was little bit lower compare to the samples from other cement, but still significant. Same as in case of the paste from the cement Ladce 42.5 N the SP dosage had strong effect on thixotrpic area. The increasing SP dosage led to the decreasing the thixotropic area as seen in series with w/c 0.288. Strange behavior (again affected by unstability of samples) was observed in cases with high SP dosage and water content.

7.1.4 Aging

All samples of the cement pastes were tested at age 20, 40 and 60 minutes after first contact of the cement with water. With aging of samples the sampling became complicated, because the unstability was observed almost in every other sample. This obstacle occurred more often at age 60 min than at 40 min. The unstability consists in creation of the thin water layer, which is titled as a bleeding in concrete terminology. On the other hand quite stiff layer of solid particles create on the bottom of vessel with the sample. It was proved, that if the sample was took from bottom part the rheological parameters were higher than in case of sampling form upper layer. It was tried to remix the sample with the spoon before testing, but the mixing broke down the creating structure which caused the lower rheological parameters same as in case of testing the upper layer of sample.

7.1.5 Conclusion remarks from rheological measurement

It was observed and proved, that the rheology of cement pastes changes during the induction period, when reactivity of the system is low. According to the literary knowledge the rheological changes are due to the agglomeration of the particles [90]. Several rheological parameters were evaluated and their dependence on composition (w/c and SP dosage) and type of the cement as well.

7.2 Density of cement pastes

The obtained densities are shown in Table 52 and Fig. 118. For calculation the density of water 1 000 kg·m^{-3} was used. The maximal standard deviation was ±10 kg·m^{-3} and was obtain in case of the samples with the lowest water content. This result corresponds with the fact, that during measurement it was difficult to work with quite stiff cement paste.

Table 52: Obtained densities of the cement pastes

Mokrá 52.5 N		Ladce 42.5 N	
w/c	Density [kg·m^{-3}]	w/c	Density [kg·m^{-3}]
0.272	2129	0.232	2190
0.276	2128	0.236	2185
0.280	2114	0.240	2175
0.284	2107	0.244	2171
0.288	2101	0.248	2167
0.292	2099	0.252	2168
0.296	2090	0.256	2160
0.300	2093		

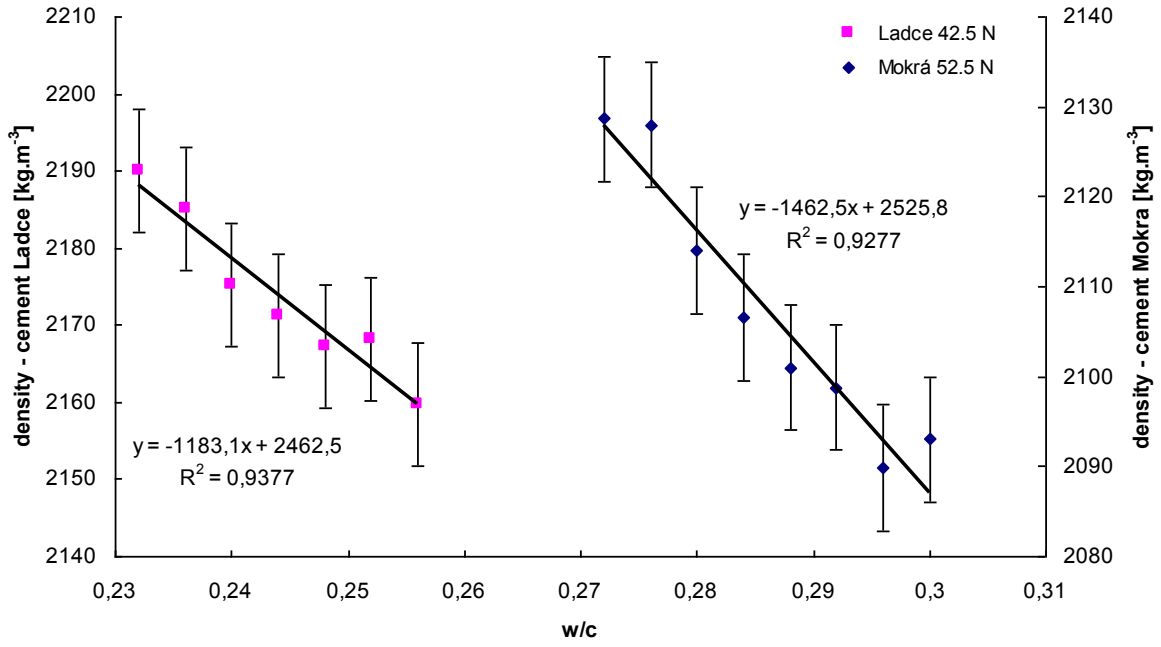

Fig. 118: Densities of prepared cement pastes

7.3 Vicat test

The measured distance between the needle and the base plate was recalculated on the depth of penetration h, which is shown on the Table 53 and Fig. 119 and Fig. 120. The linear regression was used for smoothing the measured data. The normal consistency was determined on w/c 0.252 and 0.288 in case of the cement Ladce 42.5 N and Mokrá 52.5 N respectively.

Table 53: Obtained values from measurement with Vicat apparatus

cement	w/c	First values (at age 7 min)				Second values (at age 10 min)			
		h1	h2	h3	average	h1	h2	h3	average
Ladce 42.5 N	0.232	2.0	4.0	5.0	3.7	15.0	13.0	16.0	14.7
	0.236	8.5	7.5	8.0	8.0	20.0	20.5	18.5	19.7
	0.240	14.0	12.0	11.0	12.3	25.0	24.0	24.0	24.3
	0.244	15.0	17.0	18.0	16.7	29.0	29.0	28.5	28.8
	0.248	25.0	24.0	25.0	24.7	29.5	29.5	30.0	29.7
	0.252	32.5	31.0	32.0	31.8	33.0	32.0	32.5	32.5
	0.256	39.0	39.5	38.5	39.0	39.0	39.5	38.5	39.0
Mokrá 52.5 N	0.272	15.0	13.0	11.0	13.0	25.0	22.5	21.5	23.0
	0.276	15.0	14.5	18.0	15.8	19.5	21.5	23.0	21.3
	0.280	23.0	22.0	22.5	22.5	28.0	25.0	28.5	27.2
	0.284	29.5	27.0	26.0	27.5	31.5	29.5	29.0	30.0
	0.288	31.0	33.5	31.5	32.0	31.5	34.5	32.0	32.7
	0.292	34.0	37.0	36.0	35.7	35.0	38.5	37.0	36.8
	0.296	36.0	38.5	39.0	37.8	37.0	39.0	39.0	38.3
	0.300	36.5	39.0	39.0	38.2	36.5	39.0	39.5	38.3

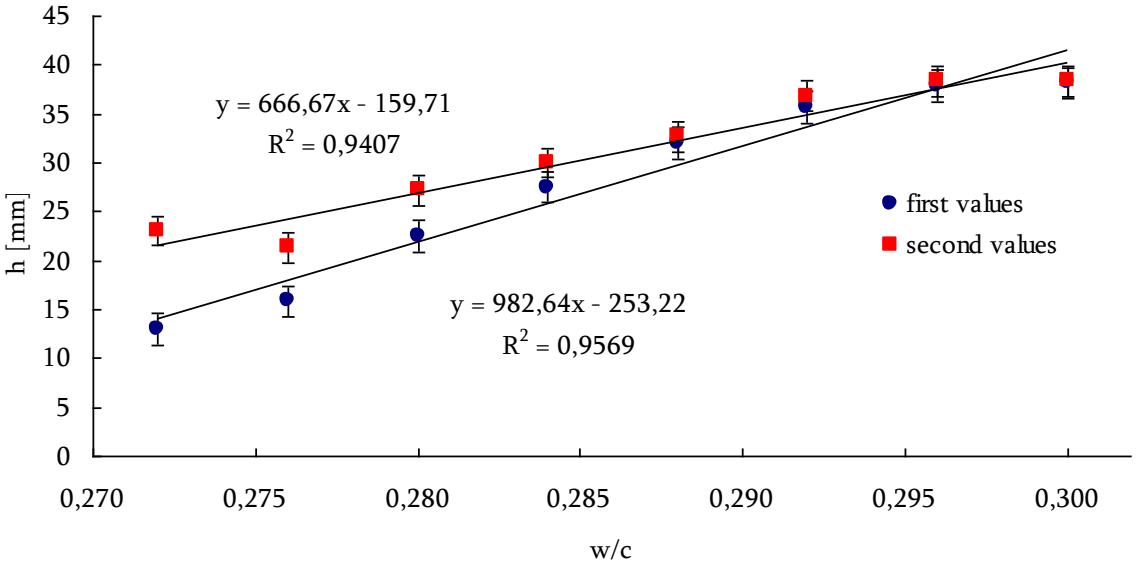

Fig. 119: Measured depths of the penetration for the cement paste prepared with using the cement *Mokrá* 52.5 N

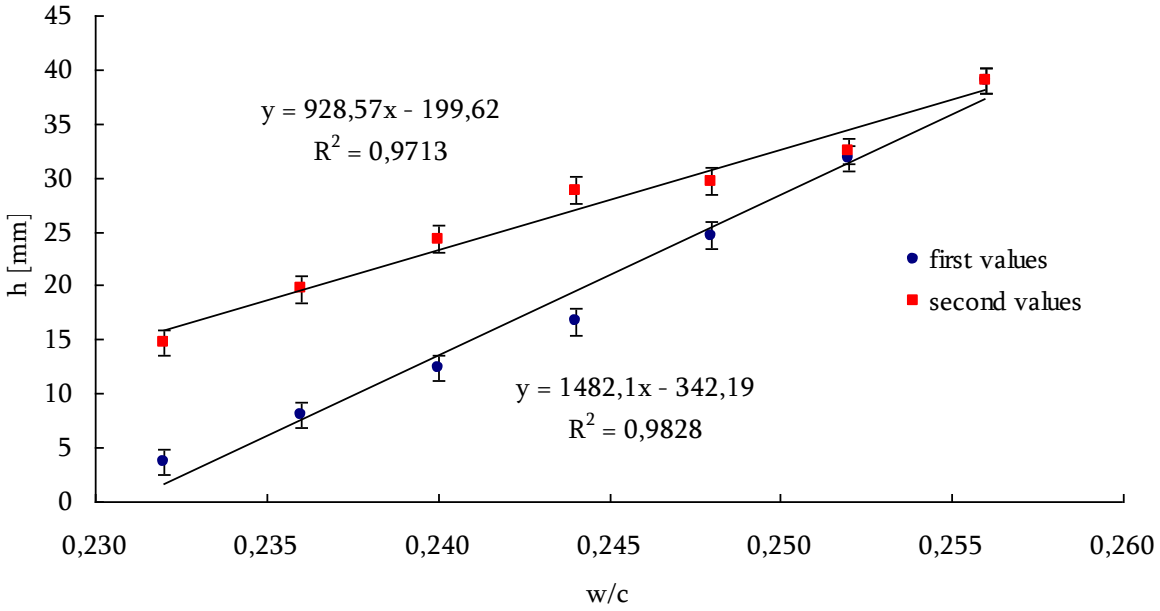

Fig. 120: Measured depths of the penetration for the cement paste prepared with using the cement Ladce 52.5 N

The Vicat test is very sensitive to water content in the samples, which gives some limitation and only narrow interval of w/c should be tested. With increasing w/c the depth of penetration grows almost linearly (the worst correlation coefficient $R^2 = 0.9407$ was obtained in case of cement pastes prepared with using the cement Mokrá 52.5 N and with the duration of penetration 3.5 min – second values). The cement pastes from the cement Ladce 42.5 N were more sensitive on water content and the depth of penetration increased in range of w/c more rapidly.

Obtained values of the depths of penetrations were used for calculations of yield stress. Three models for calculation of the yield stress (Table 54) were used according to the theoretical knowledge mentioned in chapter 3.8.

Table 54: Used models for the prediction of the yield stress

Model 1	Model 2	Model 3
$\tau_{01} = \frac{3}{2\pi Rh}$	$\tau_{02} = \frac{2.94}{2\pi Rh + 2\pi R^2}$	$\tau_{03} = \frac{mg - \pi R^2 h \rho g}{2\pi Rh}$

The obtained values of yield stresses calculated according to the mentioned models are shown in table Table 55 and 56 and Fig. 121 and 122. Both values (first and second measured values) were used for calculation results are shown in following tables.

Table 55: Predicted yield stresses from the first values obtained for the paste from the cement *Mokrá* 52.5 N

w/c	h [mm]	τ_{01} [Pa]	τ_{02} [Pa]	τ_{03} [Pa]
0.272	13.0	7346	5199	7182
0.276	15.8	6031	4492	5887
0.280	22.5	4244	3403	4128
0.284	27.5	3472	2879	3368
0.288	32.0	2984	2529	2887
0.292	35.7	2677	2301	2585
0.296	37.8	2524	2185	2434
0.300	38.2	2502	2168	2413

Table 56: Predicted yield stresses from the second values obtained for the paste from the cement *Mokrá* 52.5 N

w/c	h [mm]	τ_{01} [Pa]	τ_{02} [Pa]	τ_{03} [Pa]
0.272	23.0	4152	3342	4037
0.276	21.3	4476	3554	4356
0.280	27.2	3515	2909	3410
0.284	30.0	3183	2674	3083
0.288	32.7	2923	2485	2827
0.292	36.8	2593	2237	2502
0.296	38.3	2491	2160	2402
0.300	38.3	2491	2160	2402

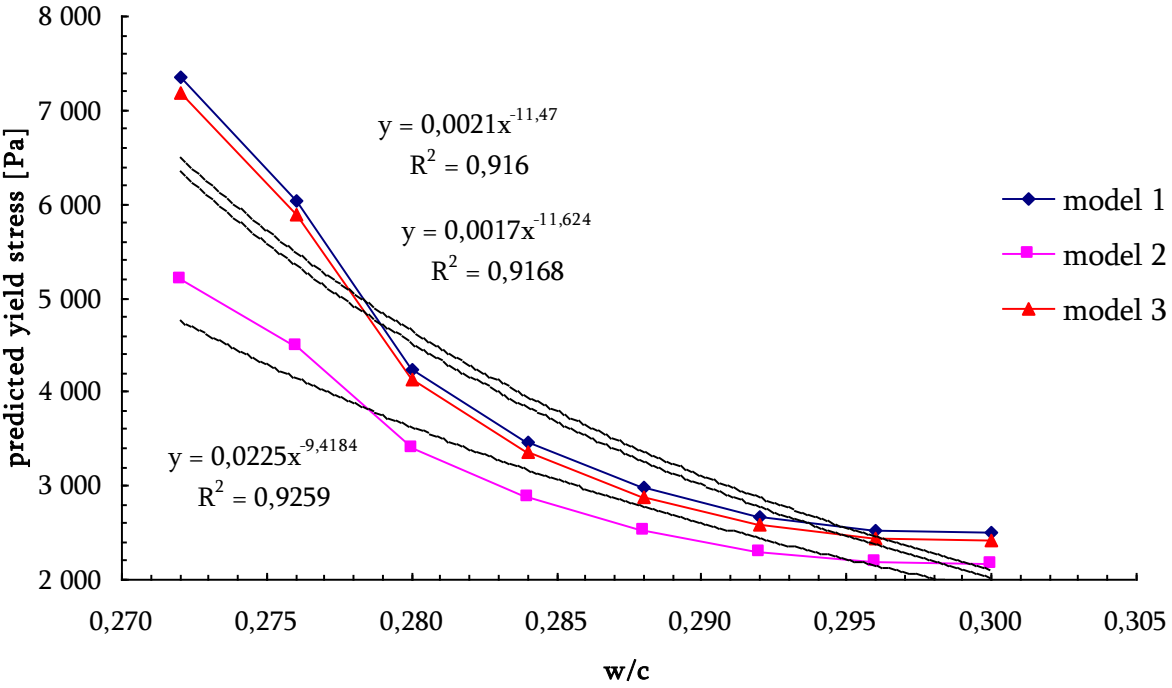

Fig. 121: Predicted yield stress according to the mentioned model, where the first values of measured depth of penetration*were used; the samples were prepared from the cement Mokrá 52.5 N*

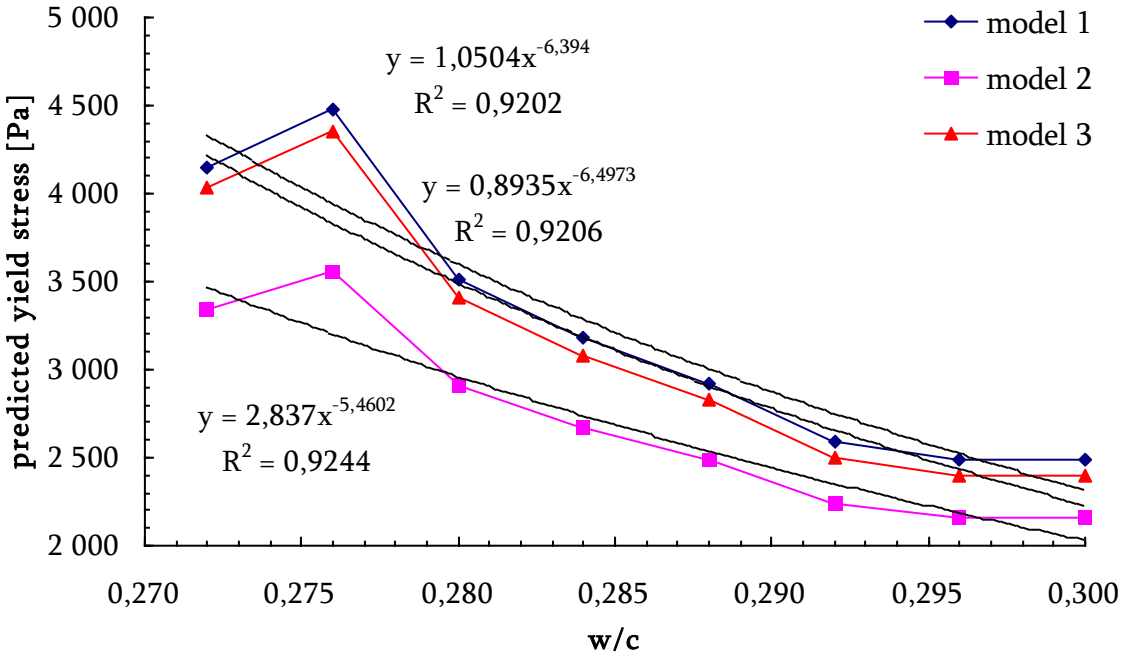

Fig. 122: Predicted yield stresses according to the mentioned models, where the second values of measured depth of penetration were used; the samples were prepared *from the cement Mokrá 52.5 N*

The predicted values of the yield stresses show same tendency and in case of the model 1 and 3 the values are much closed. The reason is in the origin of prediction. The model 3

considers the buoyancy (compared to the model 1), which is in this case very low. Model 2 give lower values of yield stresses than the previous.

The predicted yield stresses from the first measured values looks more consistent and gradual decrease was observed with increasing w/c. When the second values were used for evaluation of yield stresses, the predicted values were lower because the depths of penetrations were higher due to longer duration of the penetration. The duration of the penetration played important role in cases of samples with low w/c. The strange results are shown for the second values of paste with w/c = 0.272 and 0.276, because second mentioned had lower value of the depth of penetration than first one. This was maybe caused by inhomogenity and presence some air defects in the prepared samples.

For fitting the dependence of the predicted yield stresses on w/c was used power function, which had the best correlation coefficient. The obtained equations shows the change of the yield stress with connect to the w/c of the samples. With using parallel plate rheometer, the dependence of yield stress (dynamic and static) on w/c was observed too (Fig. 103 and Fig. 107). The obtained dependence of measured yield stresses (concerning the cement Mokrá 52.5 N) is shown in following figure with using the power function for fitting the data:

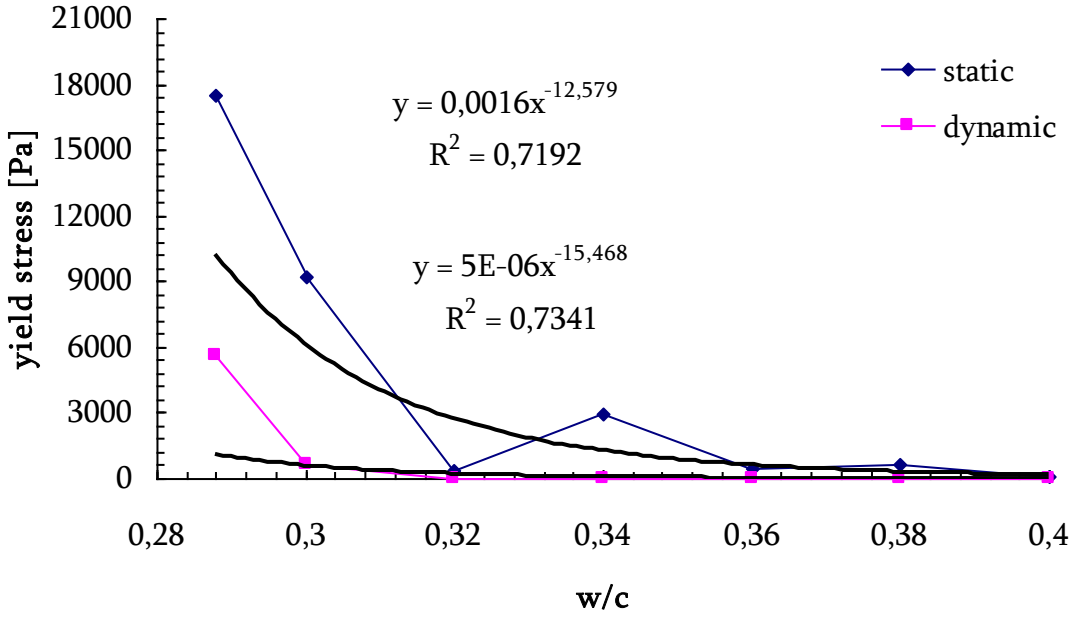

Fig. 123: Obtained dynamic and static yield stress from the measurement with parallel plate rheometer *concerning the cement Mokrá 52.5 N*

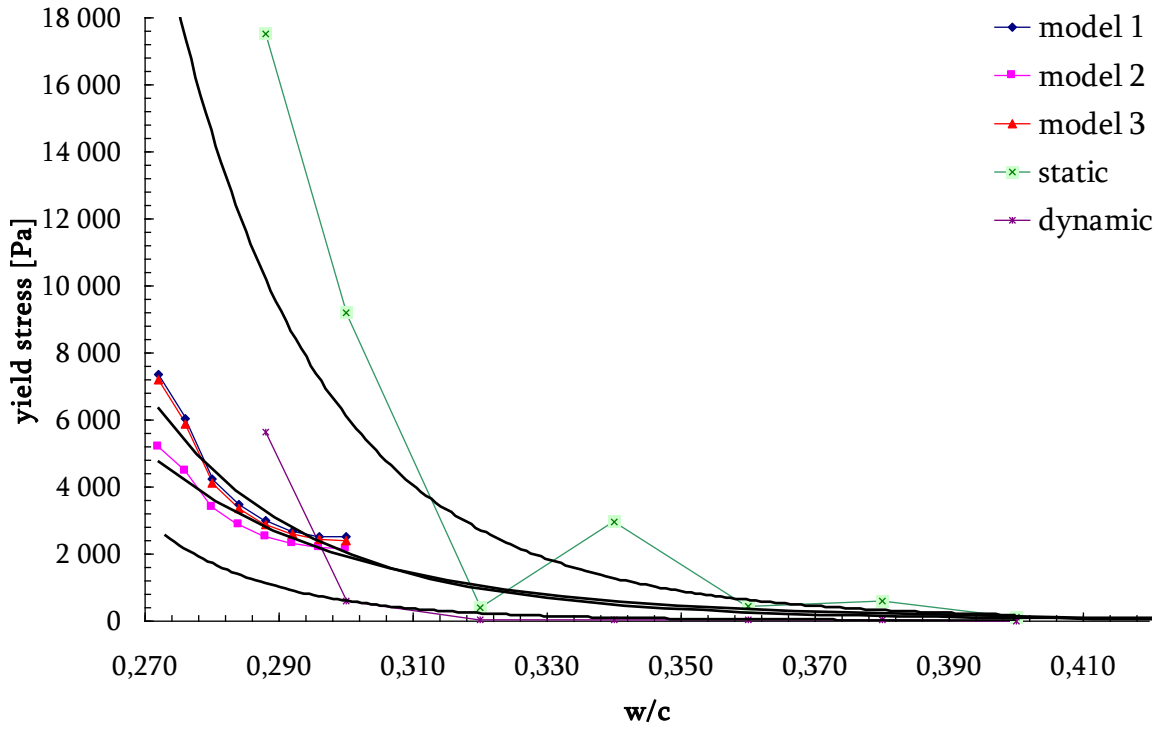

Fig. 124: Predicted and measured values of the yield stresses

If we compare the predicted results (yield stress obtained from the depth of penetration in Vicat test) with measured results the dependency on Fig. 124 is obtained. The predicted values lies in the middle between the static and dynamic yield stresses. This fact should come from the principle of testing with Vicat needle, where the conditions are between static and dynamic. We can not say, that the testing is static, because the needle fall down under the gravity as mentioned in theoretical part and is not absolutely dynamic as well, because the test involves very low velocities.

In case of the cement samples from the cement Ladce 42.5 N the obtained values of predicted yield stresses are in Table 57 and 58 and on Fig. 125 and 126.

Table 57: Predicted yield stresses from the first values obtained for the paste from the cement Ladce 42.5 N

w/c	h [mm]	τ_{01} [Pa]	τ_{02} [Pa]	τ_{03} [Pa]
0,232	3,7	26044	10798	25594
0,236	8,0	11937	7199	11702
0,240	12,3	7743	5399	7572
0,244	16,7	5730	4319	5589
0,248	24,7	3871	3154	3759
0,252	31,8	3000	2541	2919
0,256	39,0	2449	2127	2358

Table 58: Predicted yield stresses from the second values obtained for the paste from the cement Ladce 42.5 N

w/c	h [mm]	τ_{01} [Pa]	τ_{02} [Pa]	τ_{03} [Pa]
0,232	14,7	6511	4758	6358
0,236	19,7	4856	3794	4728
0,240	24,3	3924	3190	3811
0,244	28,8	3312	2766	3208
0,248	29,7	3219	2700	3117
0,252	32,5	2938	2496	2858
0,256	39,0	2449	2127	2358

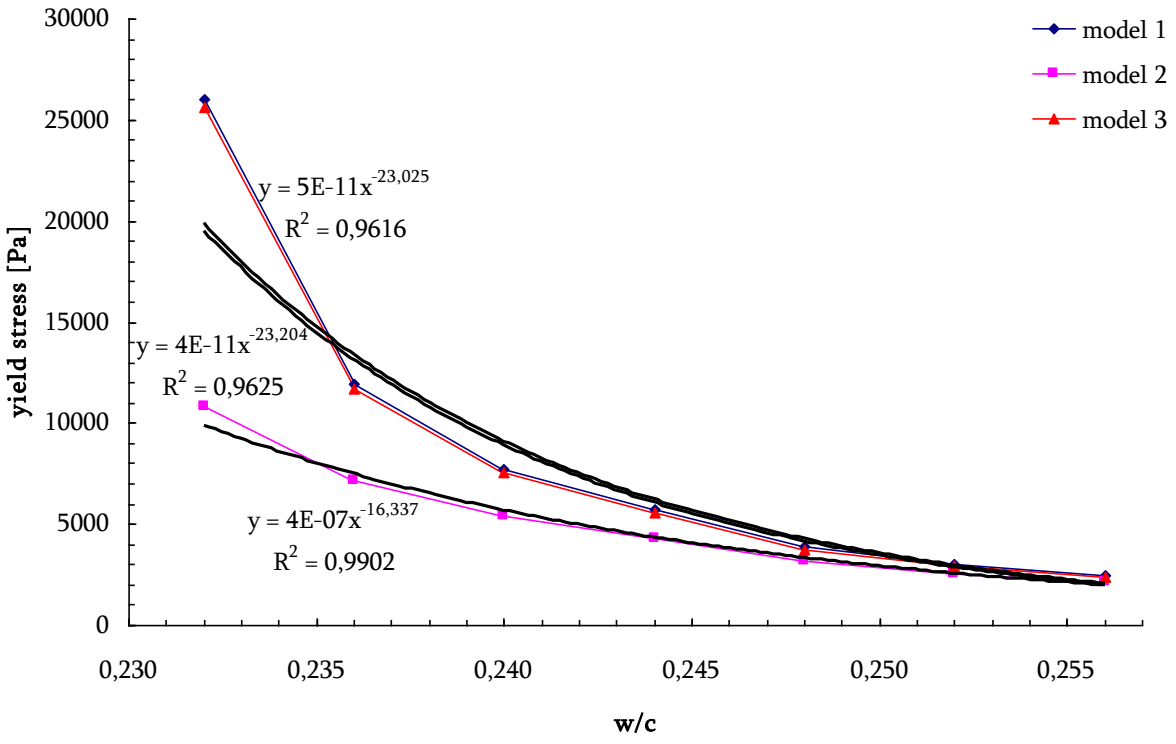

Fig. 125: Predicted yield stress according to the mentioned model, where the first values of measured depth of penetrationwere used; the samples were prepared from the cement Ladce 42.5 N

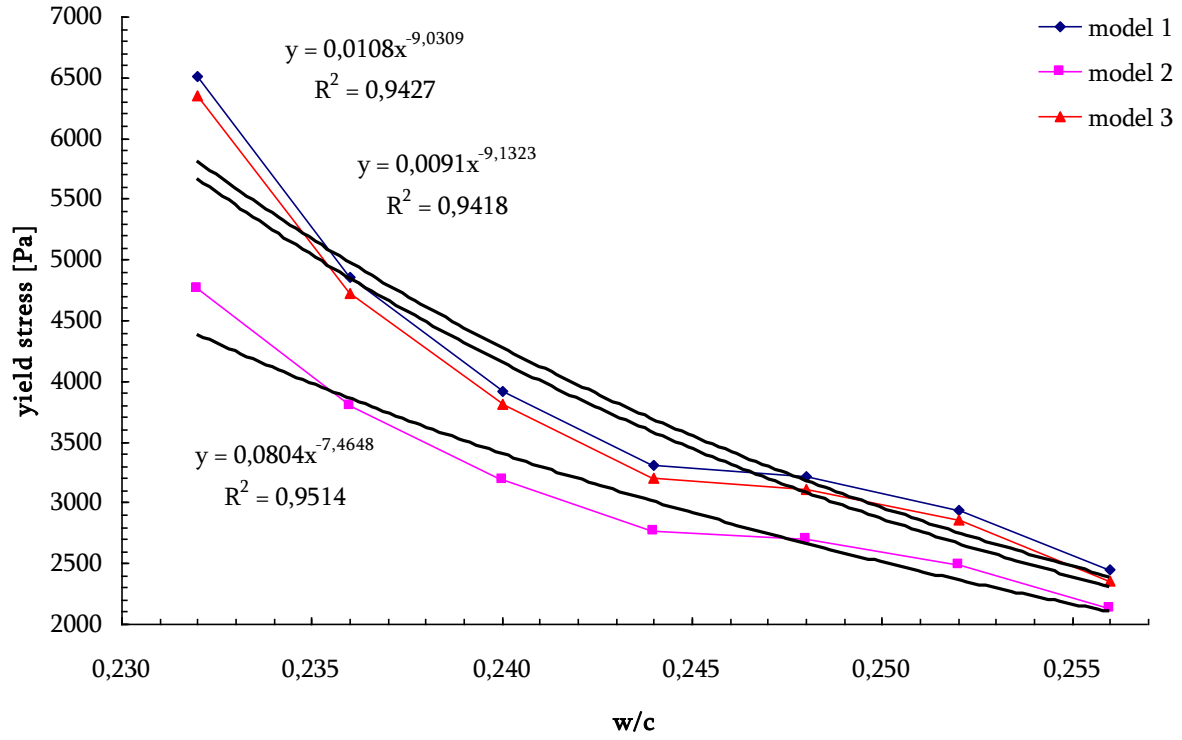

Fig. 126: Predicted yield stresses according to the mentioned models, where the second values of measured depth of penetration were used; the samples were prepared from the cement Ladce42.5 N

Same as in case of the samples from the cement Mokrá 52.5 N the differences between the predicted values from first and second values of depth of penetration are significant for sample with the lowest w/c.

For comparison reason the measured dependencies of the static and dynamic yield stress are shown in Fig. 127 with smoothing data with power function.

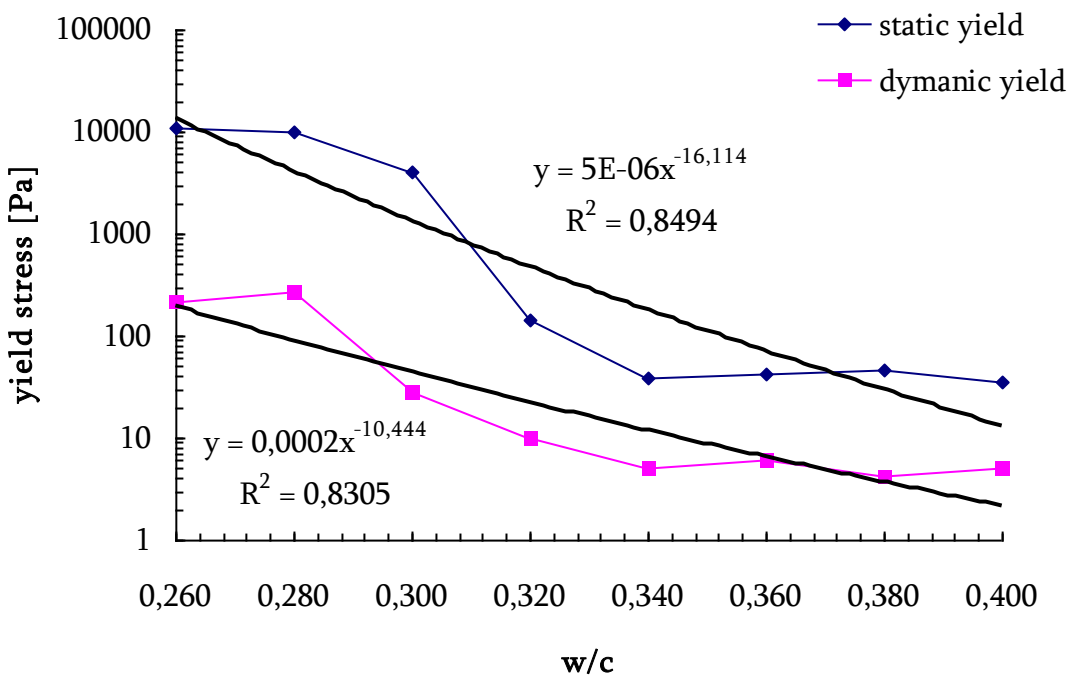

Fig. 127: Obtained dynamic and static yield stress from the measurement with parallel plate rheometer concerning the cement Ladce 42.5 N

The predicted data of yield stresses calculated according three models are shown in Fig. 128 together with the data obtained from parallel plate rheometer. Same as in previous case with the cement Mokrá 52.5 N the predicted data lie between the static and dynamic yield stresses.

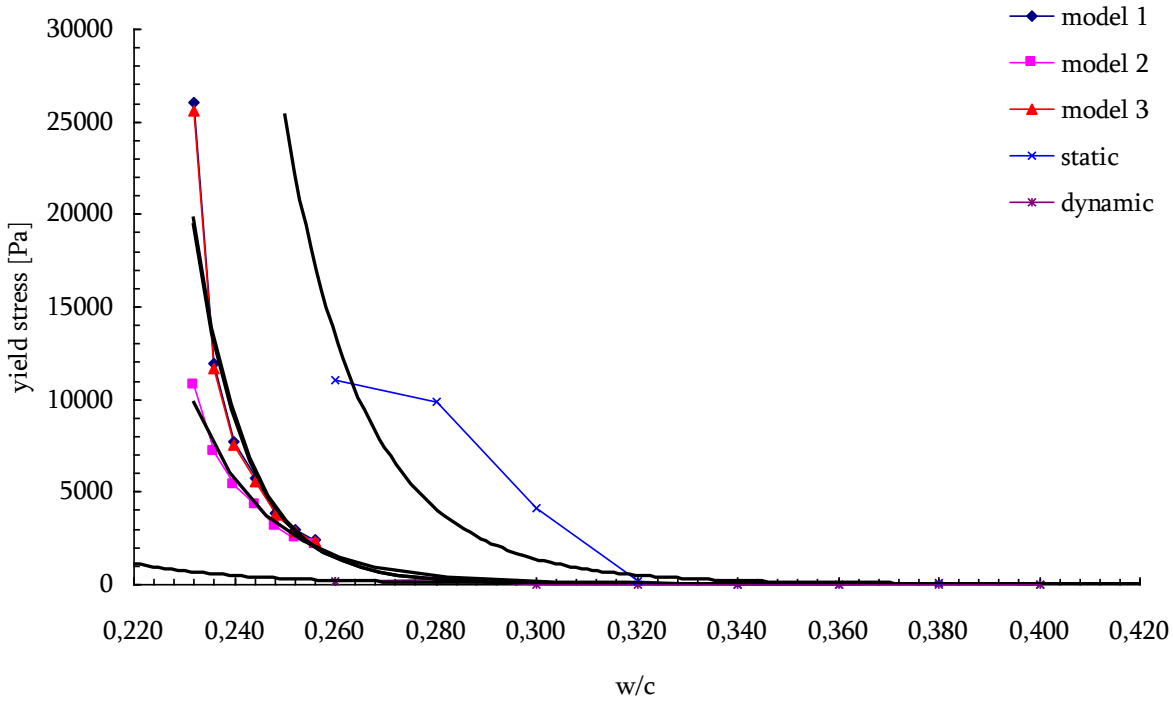

Fig. 128: Predicted and measured values of the yield stresses

It should be noted that in case of testing with parallel plate rheometer the first test was done at age 20 min compare to the 7 min of age when Vicat needle was dropped. So factor of time and structural build-up can not be neglected.

Other thing is, that mentioned models for the predicting the yield stress were obtained from depth of penetration of Vicat needle with the diameter 1 mm compare to the 10 mm in case of testing in this work.

7.4 Calorimetry

7.4.1 Measurement with isoperibolic calorimeter

The obtained curves from measurement with isoperibolic calorimeter are shown in Fig. 129 and Fig. 130 for cement paste prepared from the cement Mokrá 52.5 N and Ladce 42.5 N respectively. The maximal temperature and age of sample at this time are listed in Table 59. The absence of first peak is because of preparing of the samples outside of calorimeter.

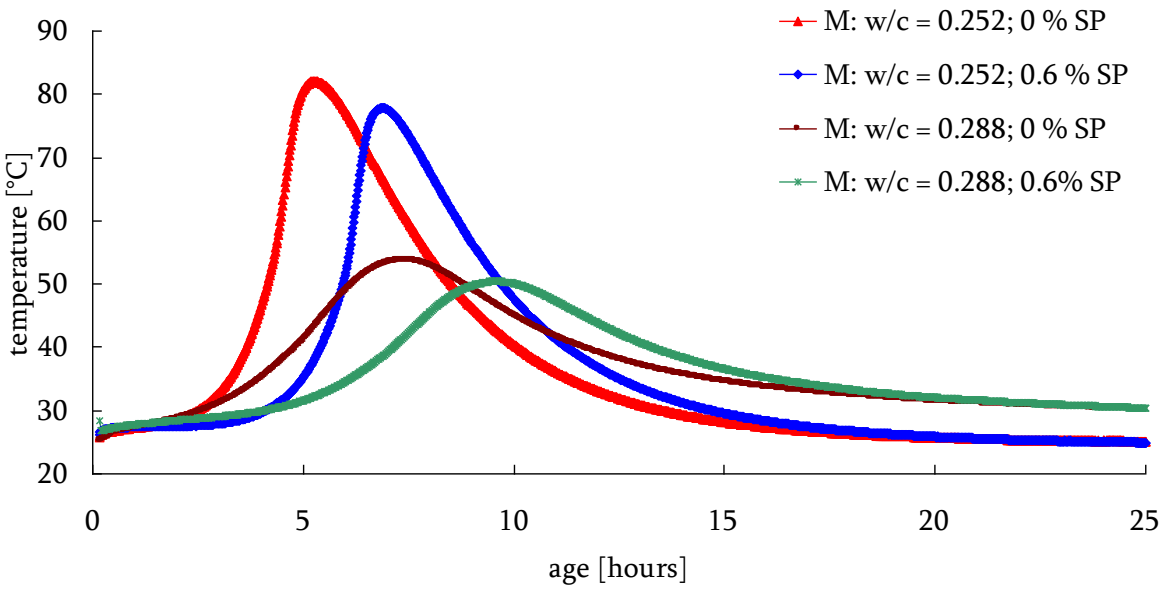

Fig. 129: C*alorimetric curves obtained for the cement pastes prepared from the cement Mokrá 52.5 N*

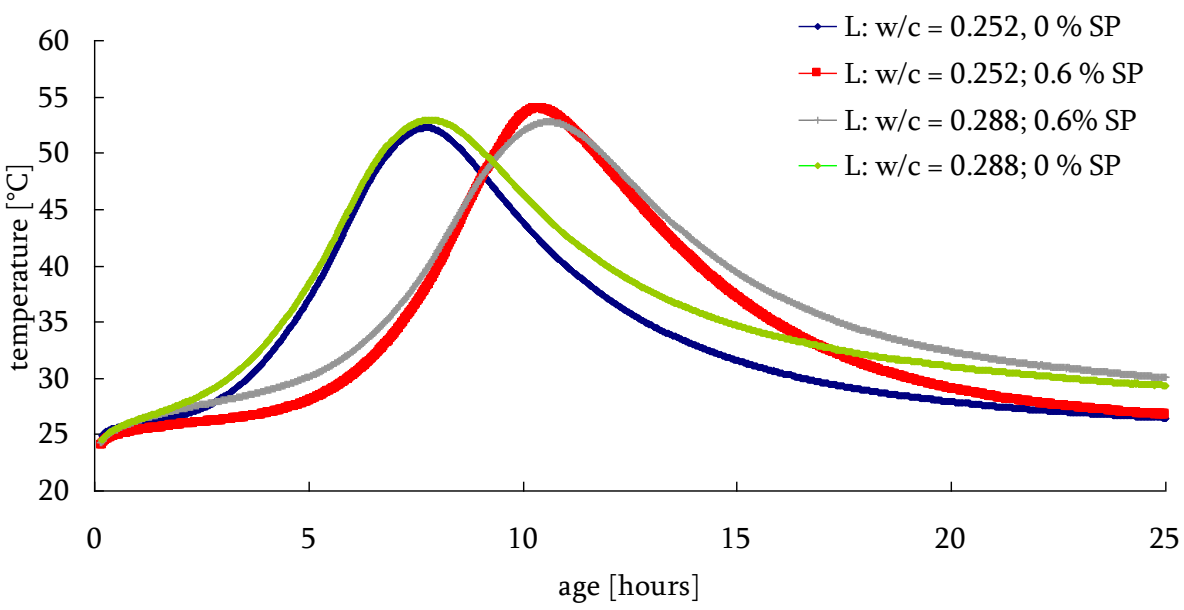

Fig. 130: Calorimetric curves obtained for the cement pastes prepared from the cement Ladce 42.5 N

Table 59: The obtained results from the measurement with isoperibolic calorimeter

Cement	w/c	% SP	Maximal temperature [°C]	Time of max. temperature [hour]
Ladce 42.5 N	0.252	0	52.3	7.7
		0.6	53.9	10.4
Mokrá 52.5 N		0	82.1	5.2
		0.6	77.8	6.9
Ladce 42.5 N	0.288	0	53.0	7.9
		0.6	52.8	10.5
Mokrá 52.5 N		0	53.8	7.5
		0.6	50.4	9.6

From obtained curves for the cement pastes from the cement Mokrá 52.5 N the effect of w/c and SP dosage is obvious. With the increasing water content (w/c increased from 0.252 to 0.288) the maximal temperature degreases from 82.1 °C to 53.8 °C and the time of reaching the maximal temperature growths from 5.2 hours to 7.5 hours. The effect of SP dosage shows expected influence, which consist in extension of the age of reaching the maximal temperature that means the extension of the dormant period. In case of the w/c = 0.252 the time of ending the stage 3 (final set) was 5.2 hours compare with 6.9 hours with was evaluated for the paste with SP dosage. Same effect was observed in case of w/c = 0.288, where SP dosage increased the time of maximal temperature from 7.5 to 9.6 hours.

In case of the samples from the cement Ladce 42.5 N there is observed very low influence of water content. The maximal temperature should be considered as the same in all cases and it was approximately 53 °C. The significant effect has the SP dosage, which again extended the time of reaching the maximal temperature from 7.7 to 10.4 hours and from 7.9 to 10.5 hours in case of samples with w/c 0.252 and 0.288 respectively.

7.4.2 Measurement with modular microcalorimeter

The calorimetric curves of different cement paste obtained with measuring with modular microcalorimeter are shown in Fig. 131-134. The time of the maximum of heat flow was evaluated as well as the heat release. The heat release was evaluated as the area under the measured curve during the one hour.

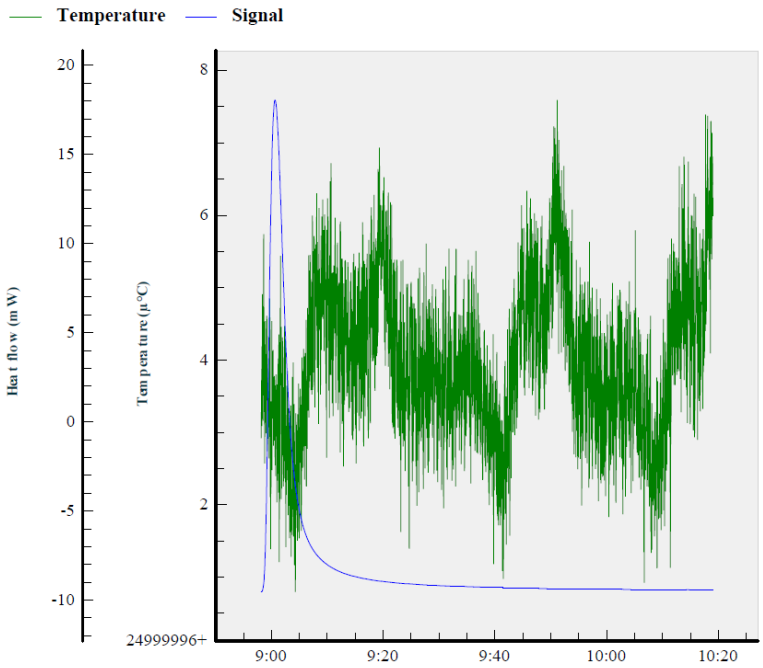

Fig. 131: *Calorimetric curve of the cement paste from the cement Mokrá 52.5 N* (w/c = 0.500, % SP = 0)

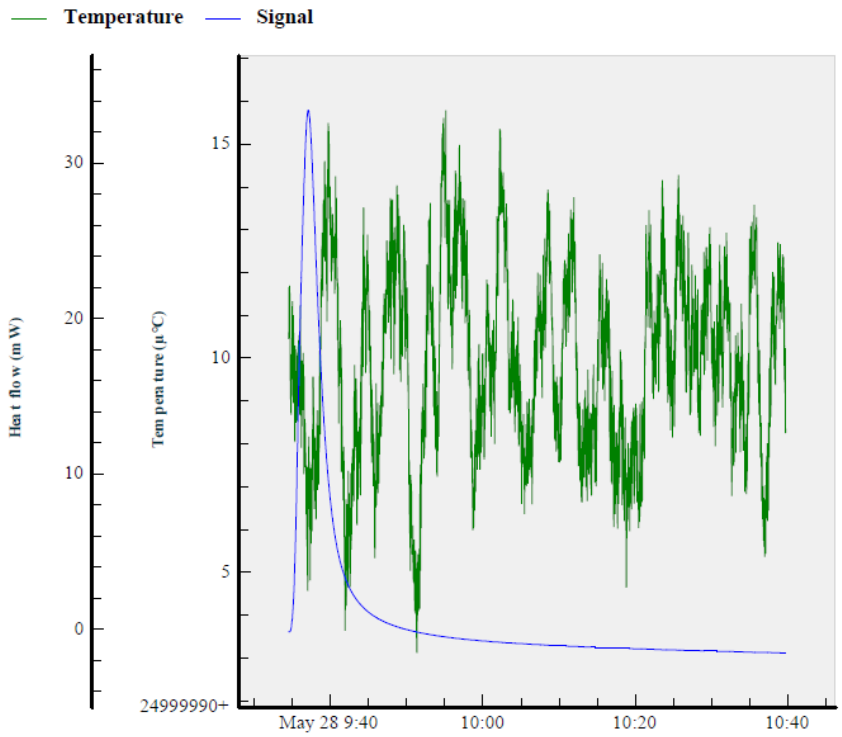

Fig. 132: *Calorimetric curve of the cement paste from the cement Mokrá 52.5 N* (w/c = 0.500, % SP = 0.6)

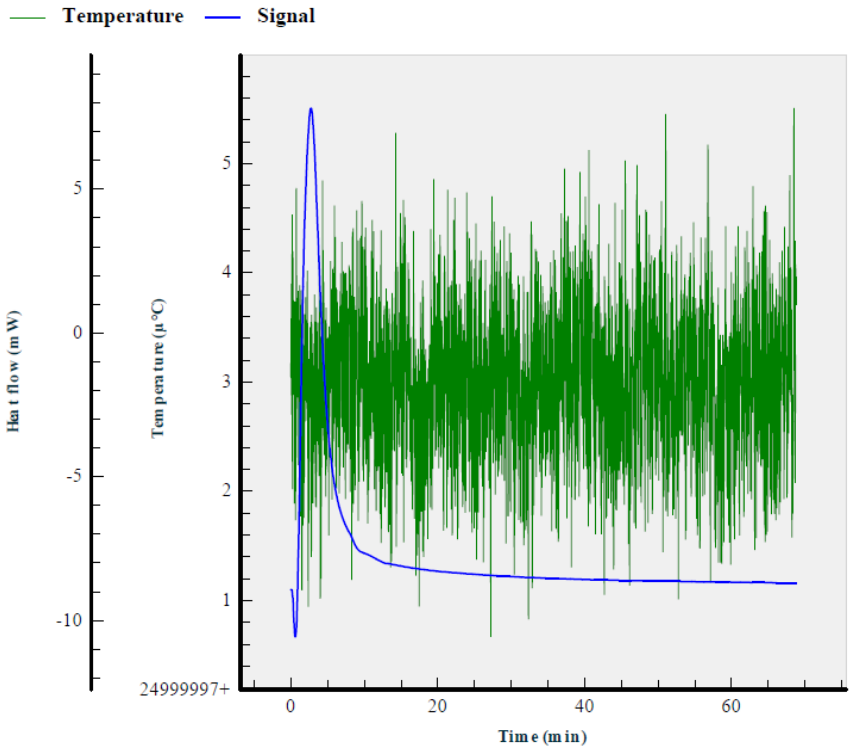

Fig. 133: Calorimetric curve of the cement paste from the cement Ladce 52.5 N (w/c = 0.500, % SP = 0)

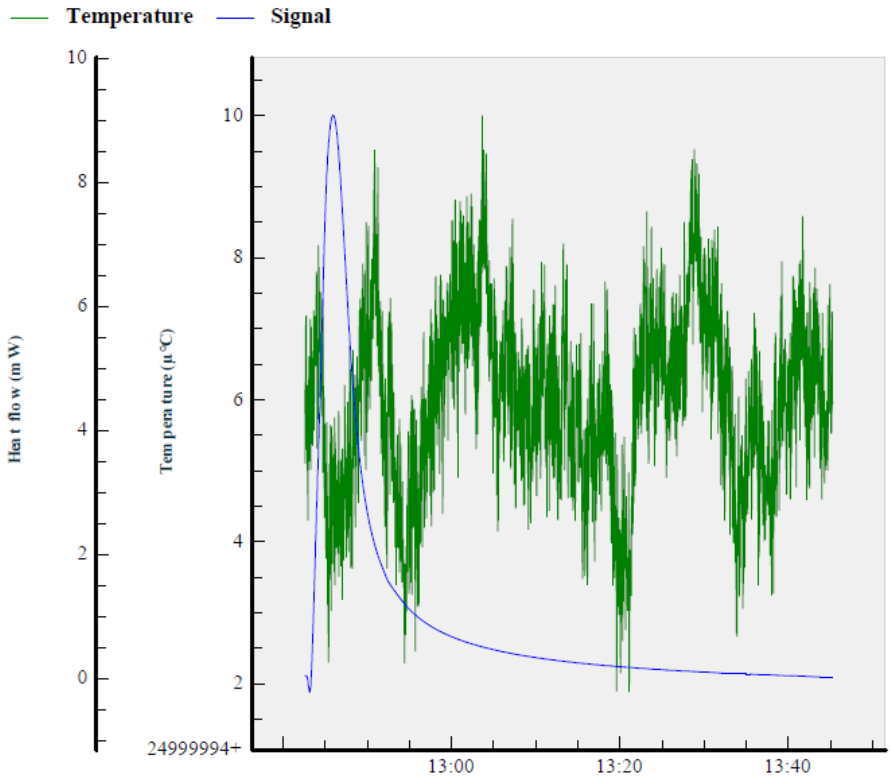

Fig. 134: Calorimetric curve of the cement paste from the cement Ladce 52.5 N with SP dosage (w/c = 0.500, % SP = 0)

Table 60: Obtained results from the measurements with modular microcalorimeter

cement	w/c	% SP	Time of maximum [min]	Released heat [J]
Ladce 42.5 N	0.50	0.0	2.7	4.0
		0.6	3.4	3.7
Mokrá 52.5 N		0.0	2.5	7.0
		0.6	2.6	7.1

The evaluated parameters are summarized in the Table 60. In case of the samples prepared from the cement Ladce 42.5 N, the released heat take the lower value approximately 4 J compare to the samples prepared from the cement Mokra 52.5 N, where the released heat was determined on 7 J. This difference corresponds with results obtained with isoperibolic calorimeter, where the pastes from the cement Mokrá always released more heat than the pastes from the cement Ladce 42.5 N. Effect of SP dosage should be observed only in case of the sample from the cement Ladce 42.5 N, where the maximal temperature was reached after 3.4 minutes of start of hydration in case of SP dosage and after 2.7 minutes in the sample without SP. In case of other samples, the times of reaching the maximal values were approximately same.

In summary, one can say, that effect of SP dosage on retardation of hydration is not as significant during preinduction period as during acceleratory period, which were studied with using the isoperibolic calorimeter.

7.5 XRD analyses of partly hydrated samples

7.5.1.1 C*ement Mokrá* 52.5 N

The XRD analyses of all partly hydrated samples of cement paste and the sample of cement which was used as a reference were carried out. There is shown X-ray diffractogram of reference sample on Fig. 135, where the peaks of present phases have been determined and are listed in the Table 61.

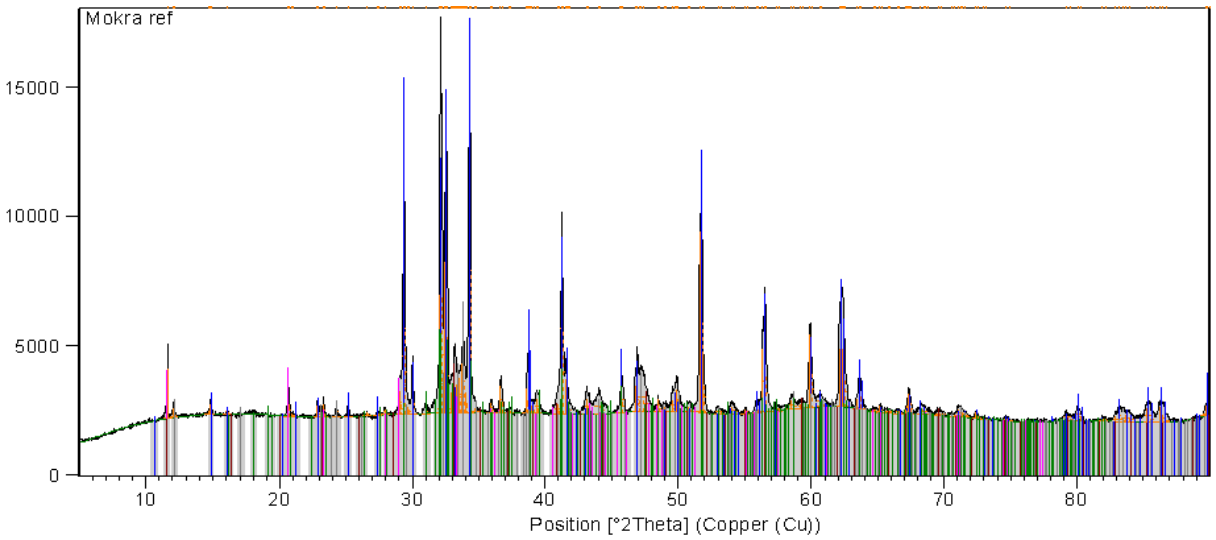

Fig. 135: X-ray diffractograme of cement powder *Mokrá 52.5 N* as a reference sample

Table 61: P*hase content of the cement Mokrá 52.5 N*

Phase	Formula (mineral)	Amount	Sign in diffractograme
Calcium oxide silicate	C_3S (hatrurite)	+++	Blue
Calcium Silicate	C_2S (larnite)	+++	Green
Calcium Iron Oxide	C_2F (brownmillerite)	+	Grey
Calcium Sulfate Hydrate	$CaSO_4 \cdot 2H_2O$ (gypsum)	+	Pink
Calcium Aluminum Oxide	C_3A	+	Brown

+++ high content; ++ medium content, + low content, - undetectable content

The amount of detected phase was determined via semiquantitative analysis, where the intensity of main diffractions was used for evaluating quantities. All important phases of the cement were detected via XRD analysis. The majority phase present tricalcium silicate and dicalcium silicate, which together make up 75 – 80 % of portland cement [12,58]. Other phases (calcium iron oxide, calcium sulfate hydrate, and calcium aluminum oxide) are represented in low amount. Comparing the X-ray diffractograms of all samples, the phase changes were observed with length of hydration. According to the XRD analysis, it has been demonstrated that the creating of ettringite starts immediately after the water is added to the cement. Comparing all measured diffractograms the important changes occur in first part, which is enlarged and shown in Fig. 136.

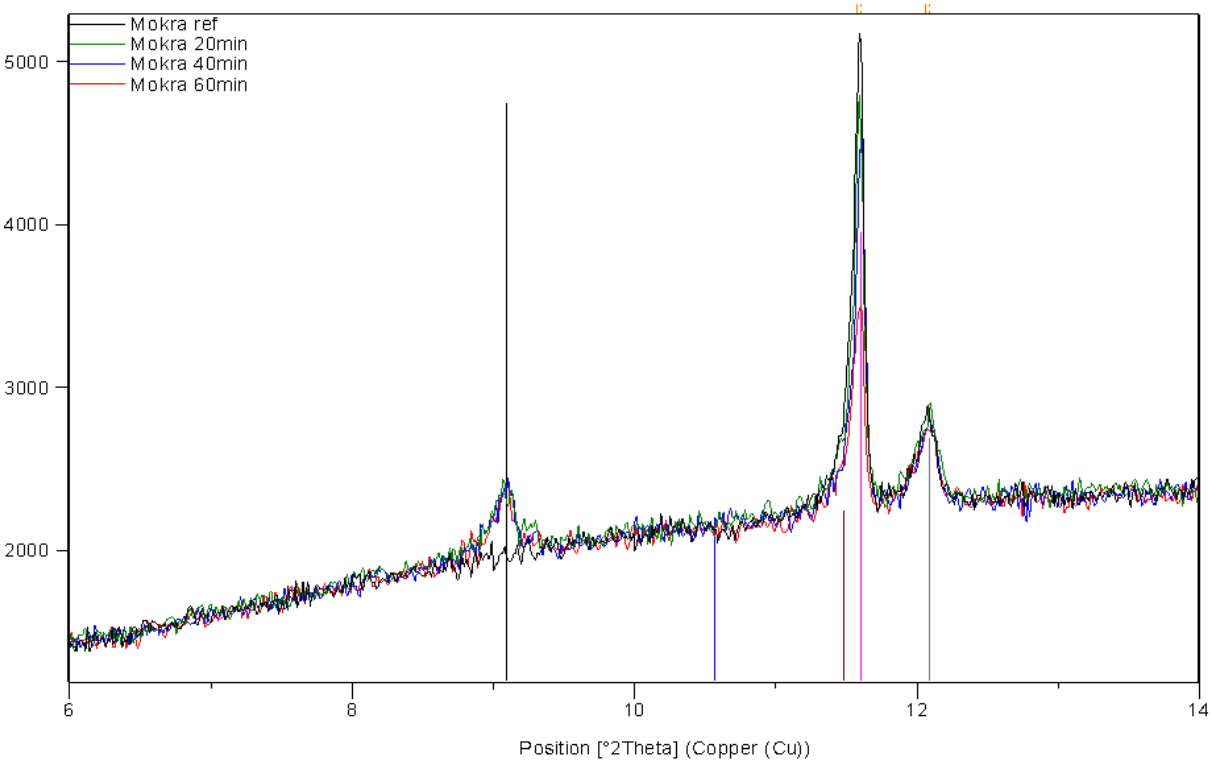

Fig. 136: First part of X-ray diffractograms where the creating of ettringite and decrease of gypsum is apparent

The first peak (9.1 °2θ, black pattern) belongs to ettringite. It is shown that this peak is detects in all cases of partly hydrated samples (green, blue and red lines) and no in case of the cement powder (black line). This correspond with theoretical knowledge, that C_3A phase reacts with gypsum in a few minutes to form ettringite (see chapter 3.6). Second peak (11.6 °2θ, pink pattern) correspond with diffraction of gypsum, which reacts with C_3A and therefore the decrease of amount of gypsum was monitored as a decrease of intensity in X-ray diffractogram. The third (12.1 °2θ, grey pattern) peak belongs to calcium iron oxide (brownmillerite), which stays unchanged.

7.5.1.2 Cement Ladce 42.5 N

Same as in case with the samples from the cement Mokrá 52.5 N the XRD analyses of all samples from the cement Ladce 42.5 N were done and the difractogram of reference sample is shown in following Fig. 137. The determined phases are listed in the Table 61.

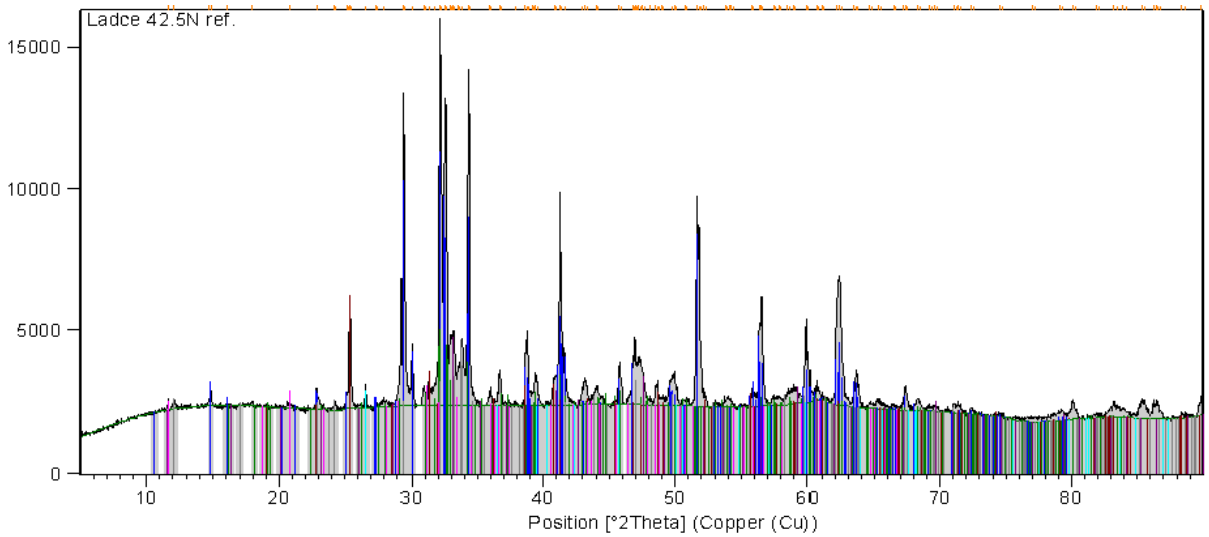

Fig. 137: X-ray diffractogram of cement powder Ladce 42.5 N as a reference sample

Table 62: Phase content of the cement Ladce 42.5 N

Phase	Formula (mineral)	Amount	Sign in diffractograme
Calcium Silicon Oxide	C_3S (hatrurite)	+++	Blue
Calcium Silicate	C_2S (larnite)	+++	Green
Calcium Iron Oxide	C_2F (brownmillerite)	++	Grey
Calcium Sulfate	$CaSO_4$ (anhydrite)	++	Brown
Calcium Sulfate Hydrate	$CaSO_4 \cdot 2H_2O$ (gypsum)	+	Pink
Calcium Aluminum Oxide	C_3A	+	Purple
Silicon Oxide	SiO_2 (quartz)	-	Cyan blue

+++ high content; ++ medium content, + low content, - undetectable content

According to the evaluated phase content in Table 62 the cement Ladce 42.5 N contains calcium sulfate (anhydrite) in addition compare with the cement Mokrá 52.5 N. The presence of this phase is given by cement production. One step in cement production consists in milling

of the cement with calcium sulfate hydrate. If the temperature runs over 110 °C, it occurs the dehydration of the gypsum and hemihydrate or anhydride forms, when the temperature will continue to grow. The content of silicon oxide was very low and should be introduce to the material as some contaminant.

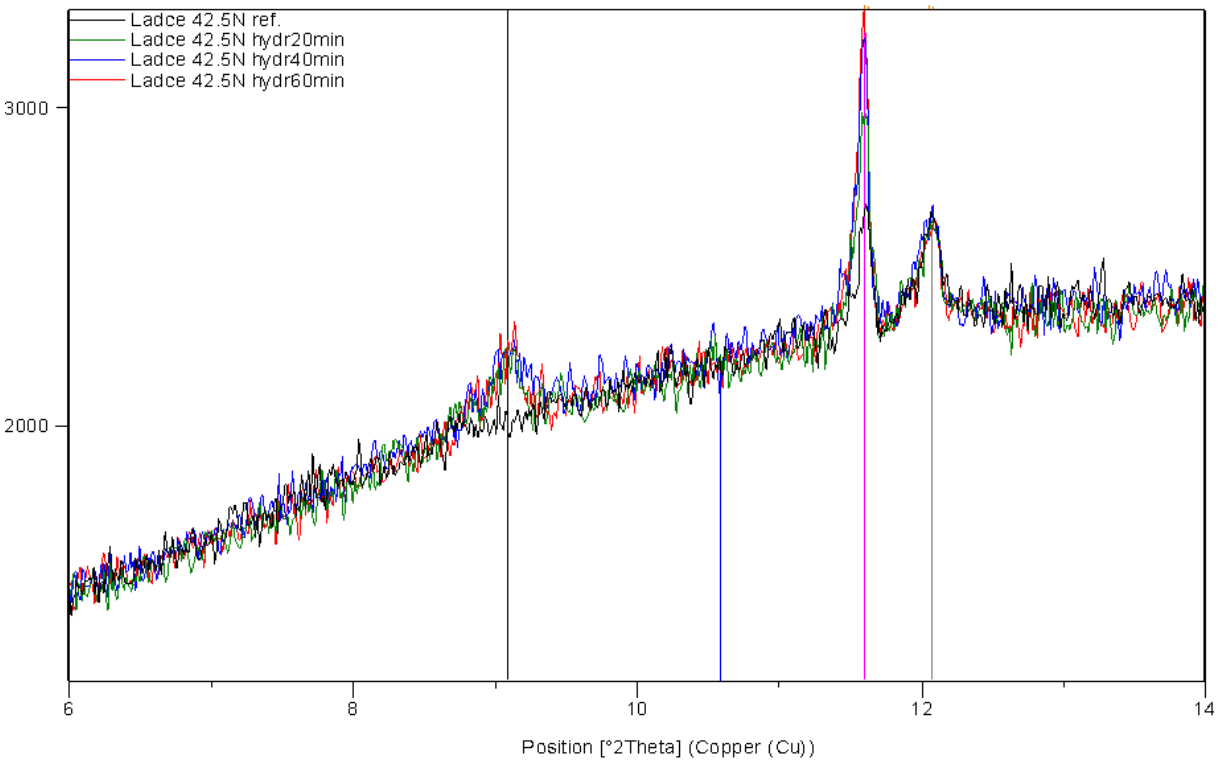

Fig. 138: First part of X-ray diffractograms where the creating of ettringite and increase of gypsum is apparent

Comparing all achieved diffractograms the similar changes in phase composition as in previous case can be observed (Fig. 138). The formation of ettringite is obvious on the first peak, which was detected in all partly hydrated samples. Second peak shows the increasing amount of the gypsum which is caused by hydration of anhydrite, which was detected in this cement. One can say that because of the presence of anhydrite the amount of gypsum is growing due to the hydration. The increasing amount of gypsum in the system should be caused by faster hydration of anhydrite then the reaction of gypsum with C_3A.

7.5.2 In-situ XRD analysis

The diffraction lines display in Fig. 139 reflect the changes in the phase composition of the cement paste during first 20 hours of hydration. The 3D scheme was created by adding measured diffractograms, whereas every 5 minutes was measured another one.

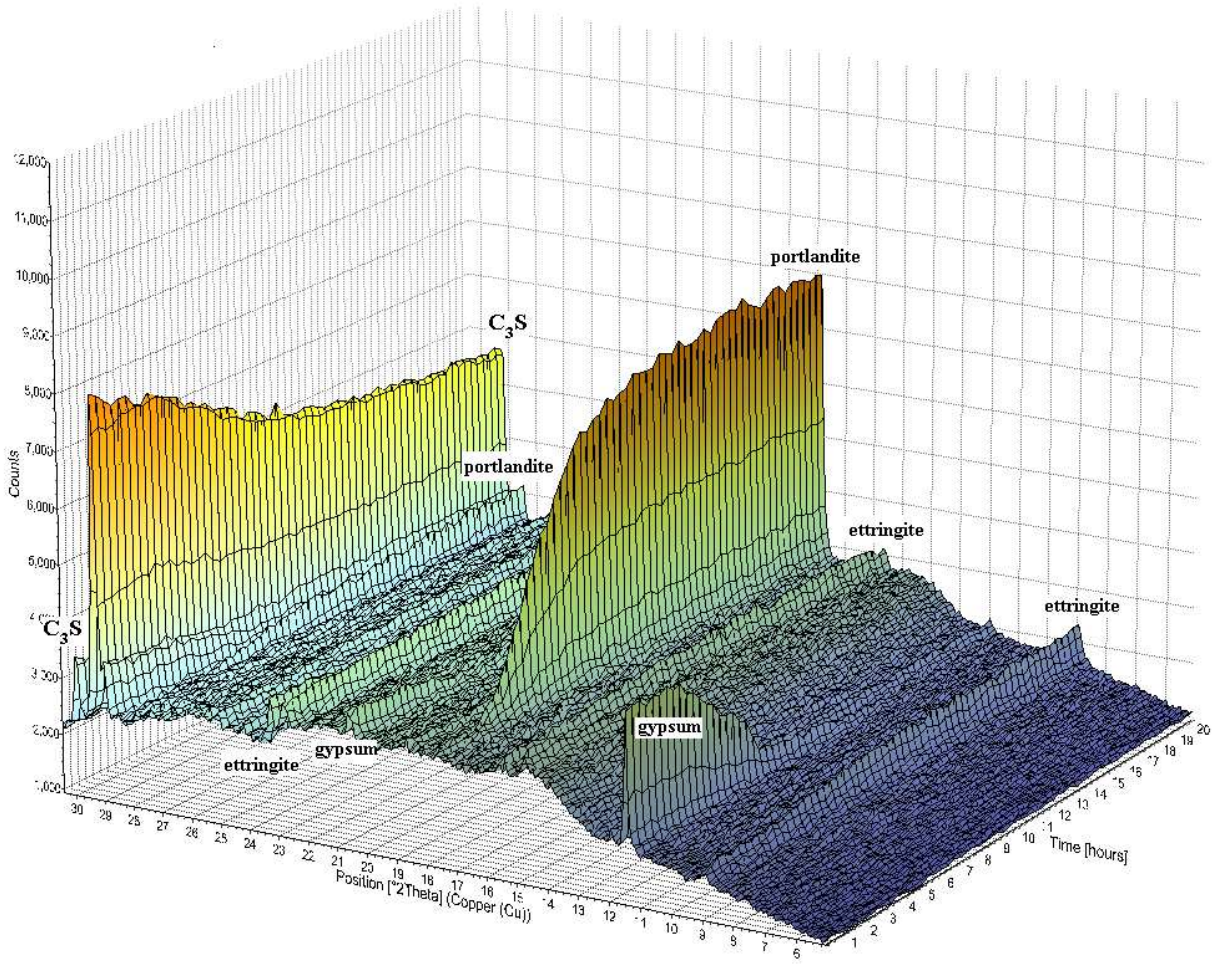

Fig. 139: 3D scheme of the cement paste from *the cement Mokrá 52.5 N*

The cement hydration starts directly after first contact cement with water. Within the first 30 minutes a part of C_3A and gypsum is dissolved rapidly resulting in a strong increase of ettringite content (eq. 27). The degrease of amount of gypsum can be seen as reducing of the peaks evaluated in position 11.6 °2θ and 20.7 °2θ. The decreasing amount of gypsum is connected with creating the ettringite (as mentioned before), which was detected in position 9 °2θ, 15.8 °2θ and 22.9 °2θ. The amount of gypsum slowly decreased (due the reaction with C_3A) and totally disappears at age around 9 hours. Last hours of this process is influenced by the rival reaction of C_3S. The amount of C_3S (in position 30 °2θ) decreases dramatically at the moment of creating portlandite as a new phase in the system (eq. 22). This starts at time approximately 2.5 hours after first contact cement with water.

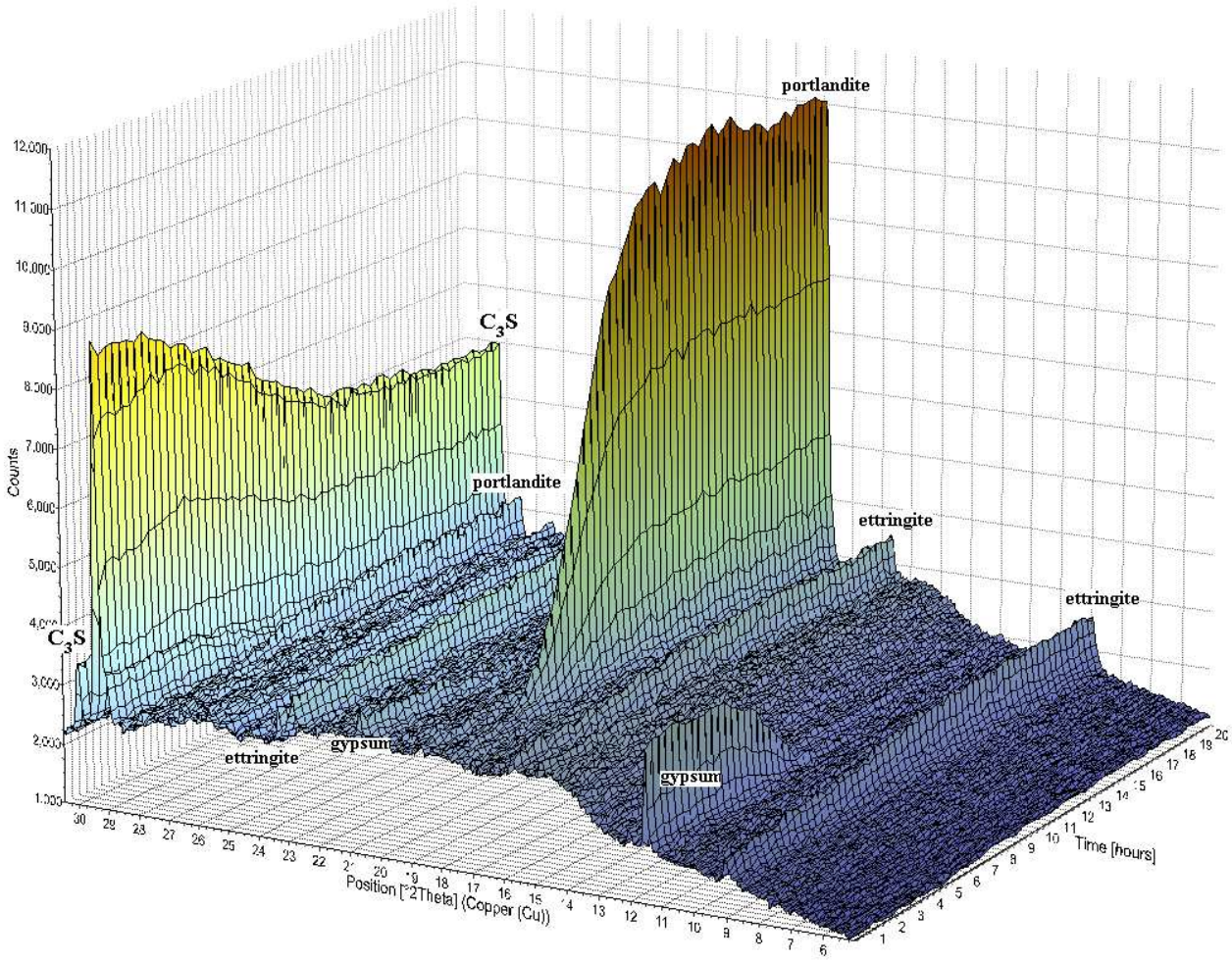

Fig. 140: *3D scheme of the cement paste from the cement Mokrá 52.5 N with SP dosage*

In case of sample with SP dosage the similar development of phases can be observed. The SP dosage influences the length of the dormant period (see chapter 7.4). The creation of portlandite is moved to age of sample 4 hours compare to the previous case, where this time was 2.5 hours. With this process is closely connected the faster consuming of gypsum (at age 7.5 hours), because the hydration of C_3S retarded.

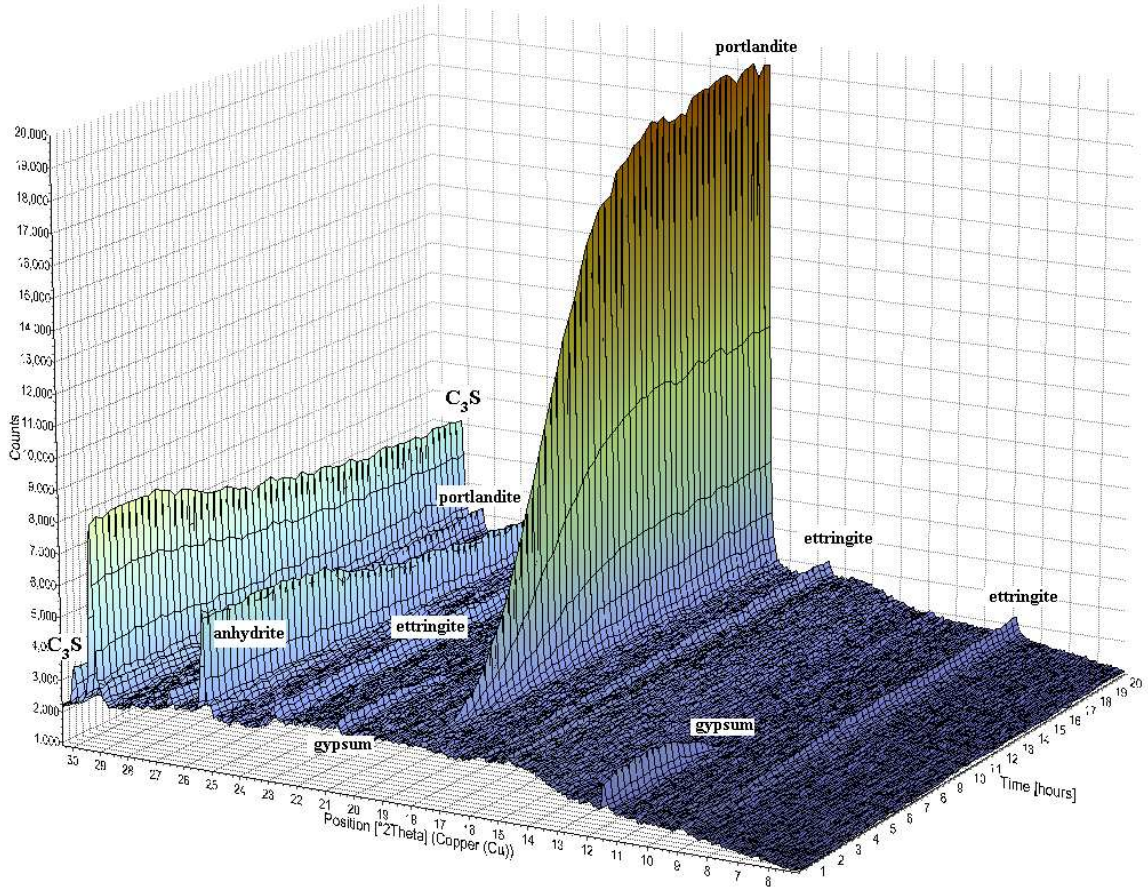

Fig. 141: 3D scheme of the cement paste from the cement Ladce 42.5 N

The measured diffractograms of the pastes from the cement Ladce 42.5 N (Fig. 141 and Fig. 142) show little bit different development because of the presence of anhydrite (evaluated in position 25.4 °2θ). Anhydrite reacts with water to form the gypsum and gypsum also responds to etringite. Gypsum is totally consumed at age 6 hours in case of the cement paste without SP and at age 6.7 hours in case of the cement paste with SP dosage. The creation of portlandite started at age 2.3 hours and this time is move to 3.3 hours in case of sample with SP dosage as shown in Fig. 142.

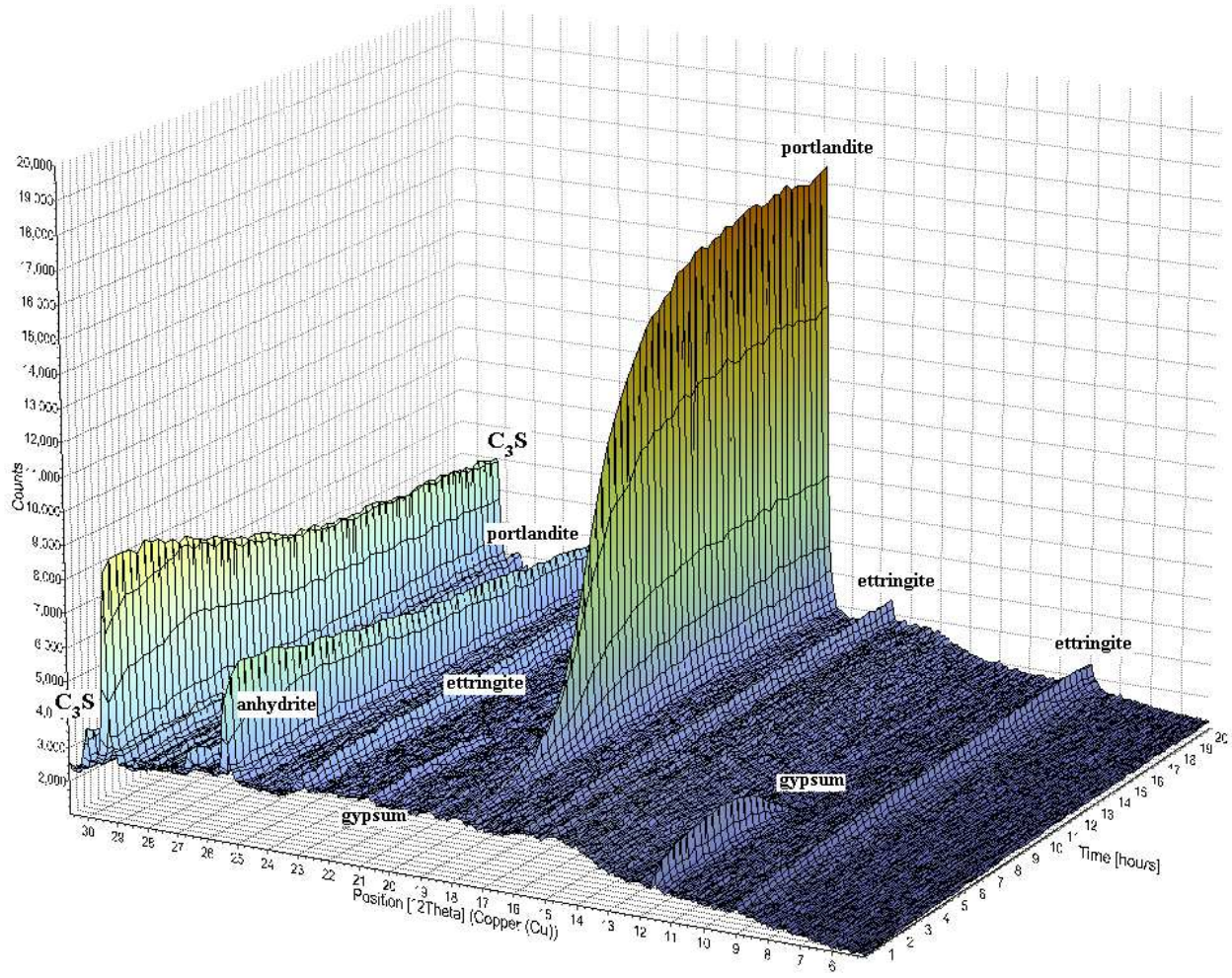

Fig. 142: 3D scheme of the cement paste from the cement Ladce 42.5 N with SP dosage

According to the obtained results from XRD analysis, one can say, that during rheological measurement (first hour after contact with water) there are not crucial changes in creating structure. The analyses of partly hydrated samples same as analyses in situ proved, that only the creation of ettringite start practically immediately. With this process is connected the decrease of C_3A and gypsum in the system.

7.6 SEM

SEM pictures of cement grains at different ages of hydration are displayed with the magnification 2 000 times in Fig. 143-152. There are the pictures taken in mode of detection of backscattered electrons on the left side and in mode of detection secondary electrons on the right side. In first series of SEM pictures the samples from the cement Mokrá 52.5 N are shown, then follow the results of EDX analysis with the information about elemental composition. The amount of detected elements is shown in the Table 63 and 64. As examples of obtained spectra and observed areas are reference samples of both type of cements (Mokrá 52.5 N and Ladce 42.5 N). The second series of SEM pictures is concerning the samples from the cement Ladce 42.5. In the end of this chapter is closed in the discussion of obtained results.

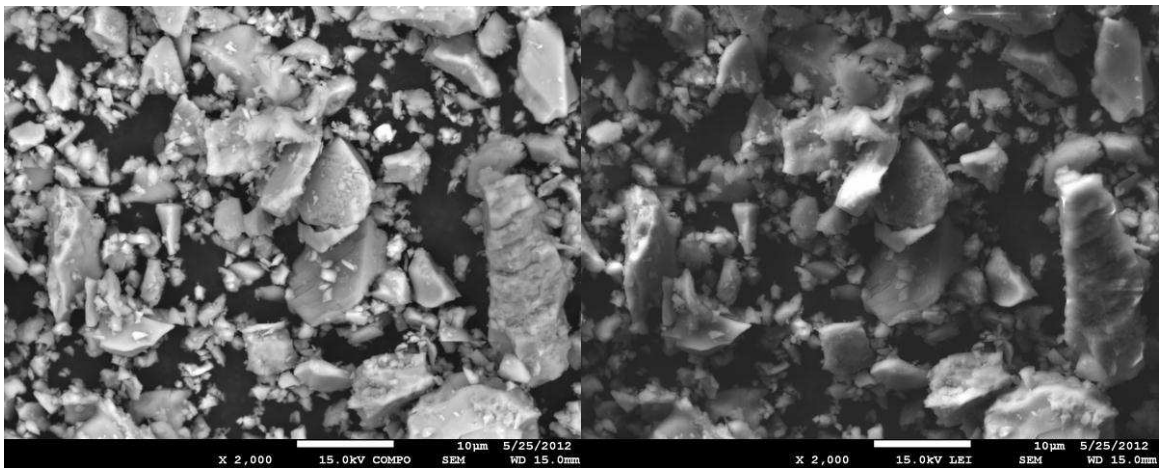

Fig. 143: SEM pictures of cement *Mokrá 52.5 N* – unhydrated particles

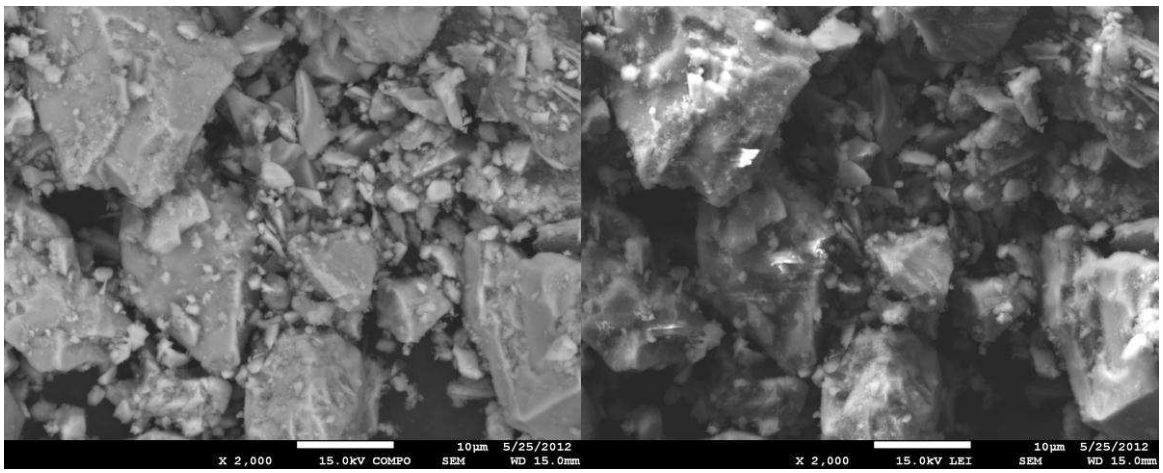

Fig. 144: SEM pictures of the cement *Mokrá 52.5 N* after 20 min of hydration

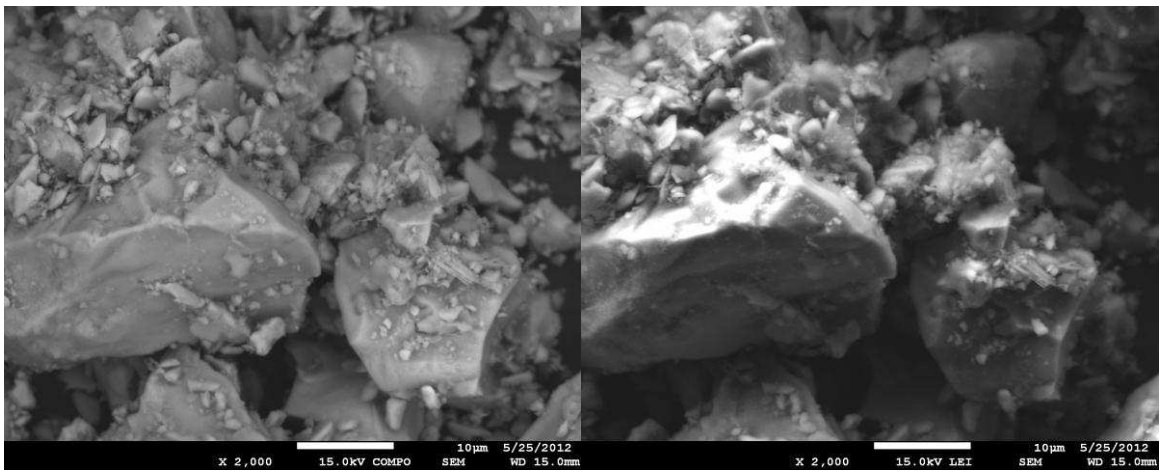

Fig. 145: SEM pictures of the cement *Mokrá 52.5 N* after 40 min of hydration

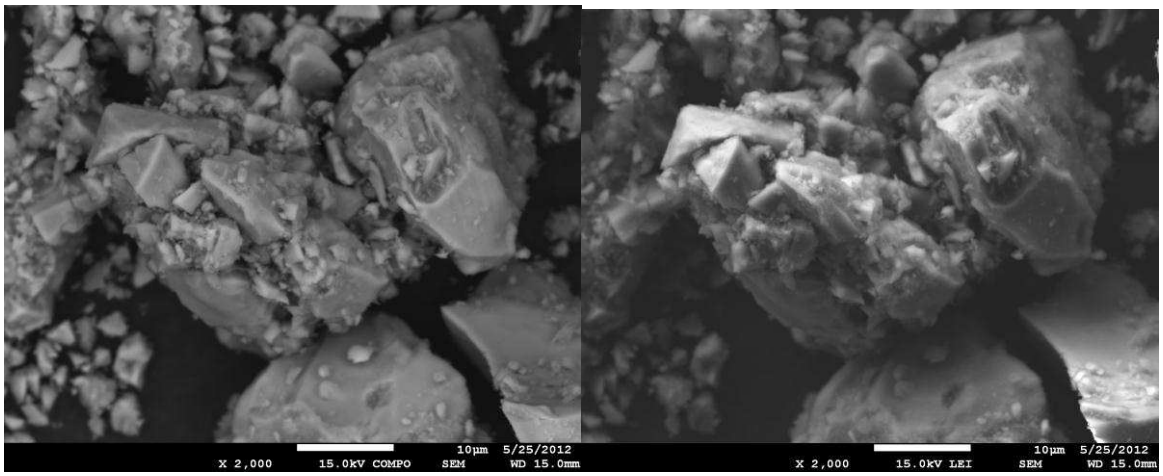

Fig. 146: SEM pictures of the cement *Mokrá 52.5 N* after 60 min of hydration

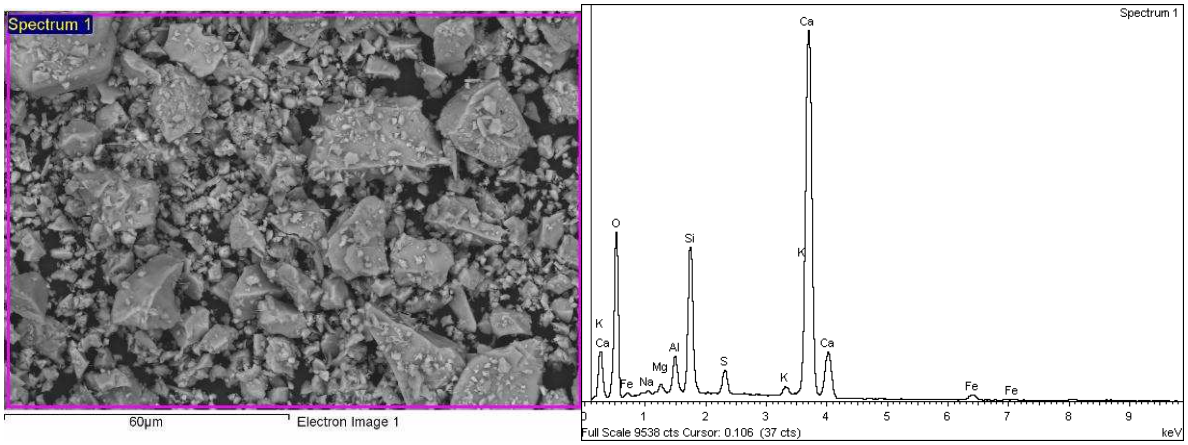

Fig. 147: SEM picture (the cement M*okrá 52.5 N)* of the area used for EDX analysis with obtained spectrum on right side

Table 63: The *amount of detected elements in the samples from the cement Mokrá 52.5 N*

	Atomic %			
Element	reference	20 min	40 min	60 min
O	66.5	66.3	68.4	67.0
Na	0.2	0.3	0.2	0.2
Mg	0.4	0.4	0.4	0.4
Al	1.4	1.3	1.5	1.4
Si	6.2	5.9	4.9	5.8
S	1.1	1.4	1.6	1.7
K	0.4	0.5	0.7	0.8
Ca	22.9	23.1	21.5	22.0
Fe	0.9	0.8	0.9	0.8

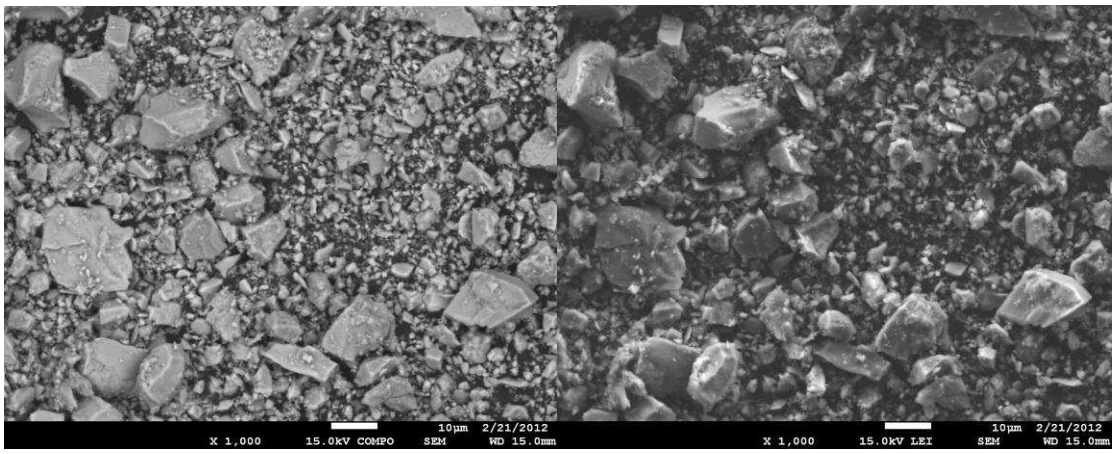

Fig. 148: SEM pictures of the cement Ladce 42.5 N – unhydrated particles

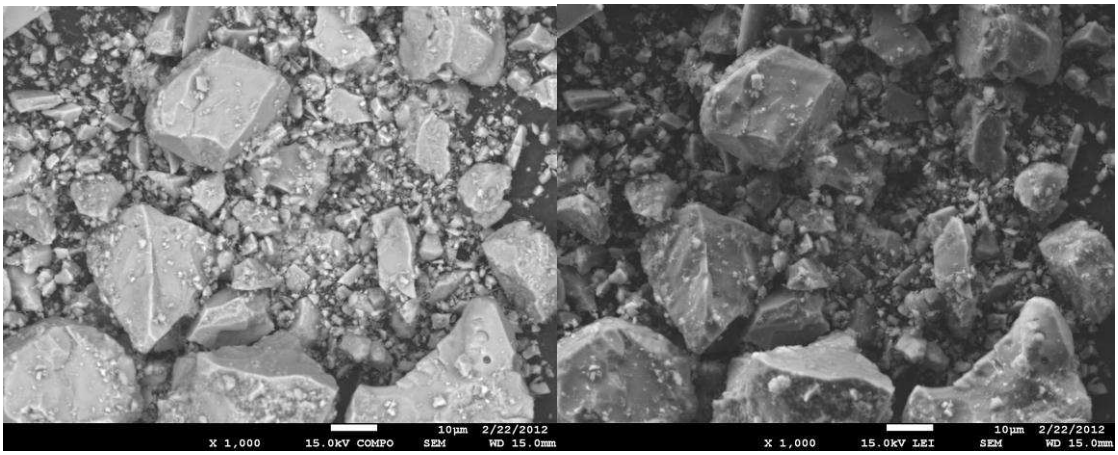

Fig. 149: SEM pictures of the cement Ladce 42.5 N after 20 min of hydration

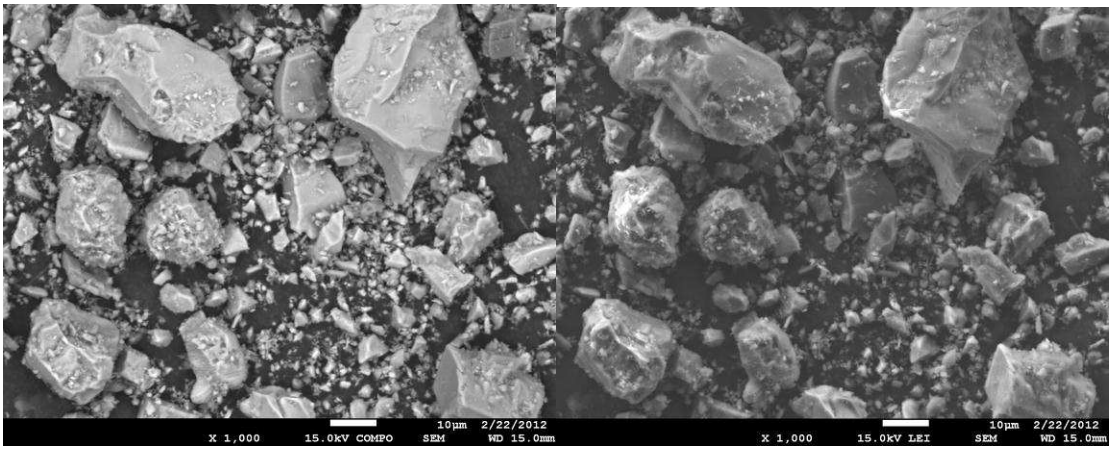

Fig. 150: SEM pictures of the cement Ladce 42.5 N after 40 min of hydration

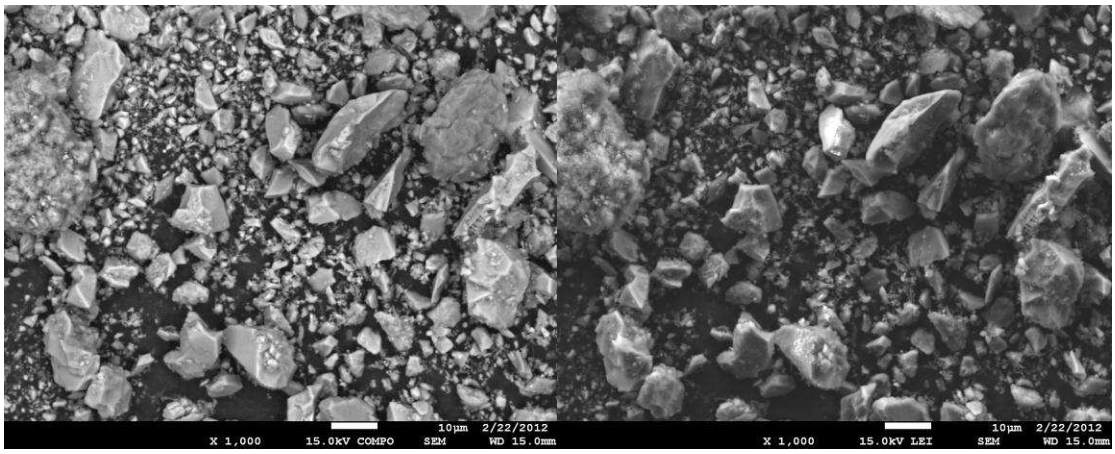

Fig. 151: SEM pictures of the cement Ladce 42.5 N after 60 min of hydration

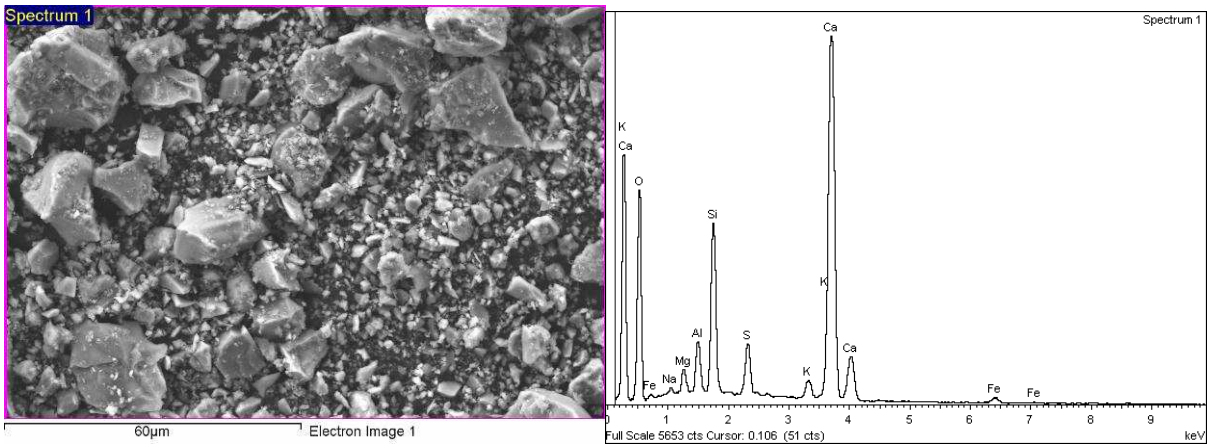

Fig. 152: SEM pixture (the cement Ladce 42.5 N) of the area used for EDX analysis with obtained spectrum on right side

Table 64: The amount of detected elements in the samples from the cement Ladce 42.5 N

	Atomic %			
Element	reference	20 min	40 min	60 min
O	67.6	66.7	67.8	68.6
Na	0.4	0.3	0.3	0.4
Mg	1.0	1.1	1.1	1.3
Al	1.8	1.7	1.8	2.3
Si	6.1	6.8	6.4	6.7
S	2.1	1.2	1.4	1.8
K	0.8	0.7	0.8	1.0
Ca	19.6	21.0	19.8	17.3
Fe	0.7	0.7	0.6	0.7

There are no significant changes on the SEM pictures during first 60 minutes of hydration, which correspond to the results obtained from XRD analysis. The SEM pictures of later stages of hydration (from 120 min up to 480 min) can be found for example in the work of Swedish researchers [91].

Via EDX analyses the expected results were found. During hydration the elemental composition is still same (the changes occur in chemical composition, when the new phases

create during hydration). If we compare the used cements, the cement Ladce 42.5 N has little bit lower content of Ca – the difference is approximately 3 atomic %.

If we compare the particle size, the reference sample contains smaller particles than the particles of partly hydrated cement powders. This fact is caused by preparation of samples as described in chapter 6.7.

7.7 Particle size distribution

The obtained distribution curves are shown on Fig. 153 and Fig. 154 for the cement Mokrá 52.5 N and Ladce 42.5 N respectively. In both cases, the measurement was performed three times, so three measured curves are displayed in following figures.

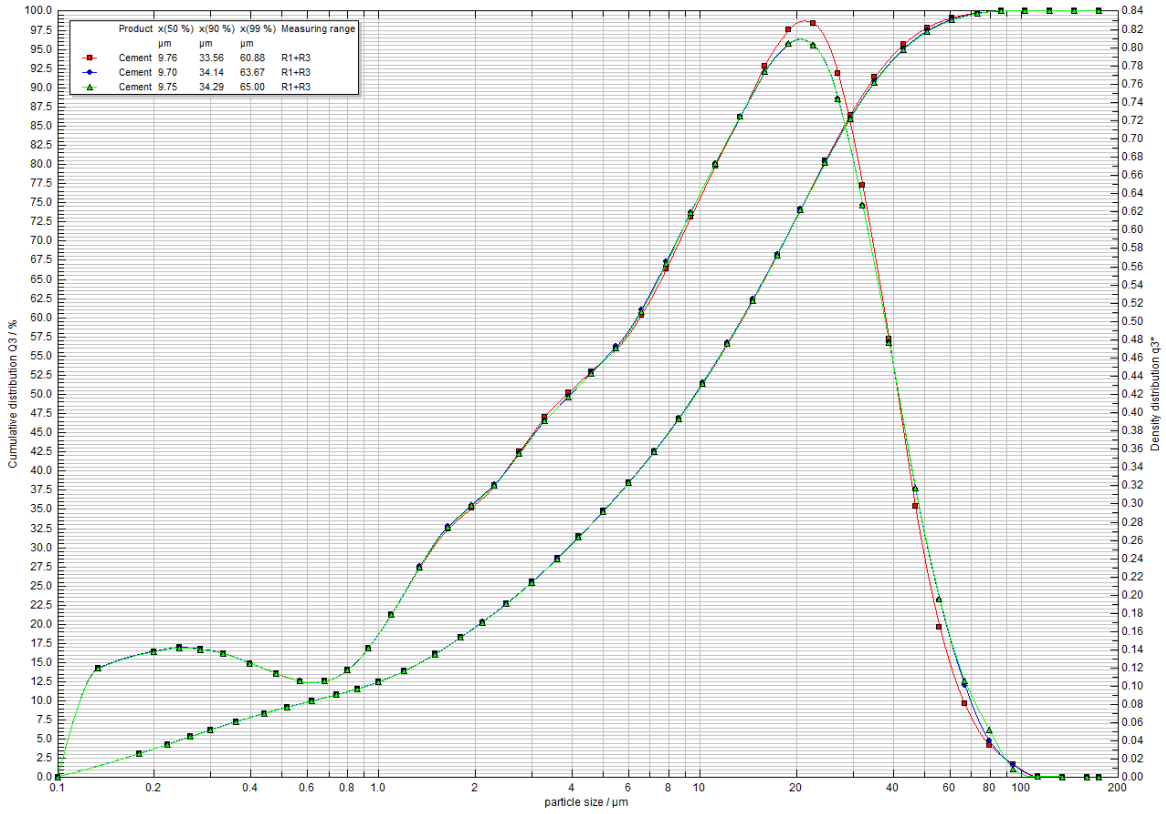

Fig. 153: Particle size distributions *of the cement Mokrá 52.5 N*

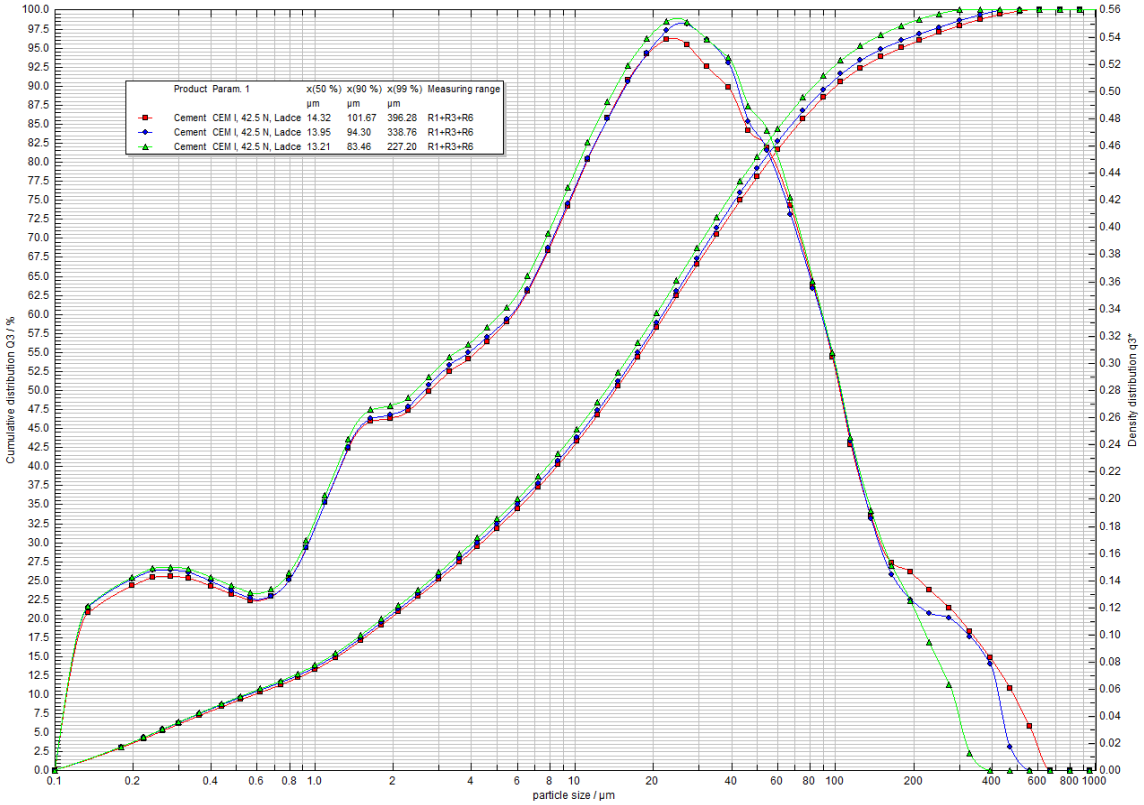

Fig. 154: Particle size distributions of the cement Ladce 42.5 N

Measured curves of the cement Mokrá 52.5 N shows that the most frequent size of particles is 22.51 µm. The median diameter was determined on 9.76 µm and 90 % particles are smaller than 34 µm. In case of the powder cement Ladce 42.5 N the most frequent size of particles is same as in previous case (22.51 µm). The median diameter was 14.32 µm and 90 % particles are smaller than 93 µm, which give higher sizes compare with the cement Mokrá 52.5 N.

8 SUMMARY AND FINAL REMARKS

Cement is a complex material and its hydration possibly provides additional complexity. Indeed, as yet no single method exist which completely determines all chemical reactions taking place in a cement structure from mixing and onward. Therefore several complementary techniques must be used.

In this work the cement based systems were studied. First part of this thesis, deals with theoretical knowledge about rheology and materials of interest. The experimental part is divided into two parts.

First part is concerning to the rheological properties of the self-compacting concretes (SCC) and their matrixes and was performed at Norwegian University of Science and Technology, Department of Structural Engineering in Trondheim. The idea was to investigate static yield stress via several tests. Prepared mixtures I and II were characterized by means of basic tests to obtain the density, slum-flow value and air content too. These properties were in very good agreement with the rheological parameters obtained from measurement with BML viscometer. The time development of the responses on the very slow deformation was performed with using the ConTec4 viscometer with applied rotation velocity 0.0015 rps. These types of tests gave huge amount of data, which were evaluated for obtaining static, dynamic, residual and mobilizes stresses. Two ways of evaluation were suggested: first one, where the torgue-time dependence was divided into several steps and second, where the every measured point was recalculated into value of stress. First way gave the valeus of stresses, which in case of the residual stresses showed slightly increasing tendency. In case of the static yield stresses the values were more affected by shaking with outer cylinder. The structuration rate, evaluated as the change of the static yield stress durig aging, range from 0.06 to 0.15 Pa/s and from 0.16 Pa/s to 0.09 Pa/s in case of mixture I and II respectively. This indicate a slow structural build-up of mixture. According to Roussel´s classification both mixtures belonged to thixotropic SCC. Second way of evaluation gave stress-time dependency and the G modulus was evaluted from the linear parts of curves. Same as in casse of the static yield stresses the G modulus was strongly affected by shaking and showed slightly increasing tendency during aging of mixture. The different kinds of peaks were observed during testing of mixtures, the gradual type and sharp type. Apparently the gradual type happened when the test start from an unconfined state immediately after pouring, whereas the steep rose and clear break were seen after start from rest in a more confined state. It seams, that time at rest in the container is the factor affecting the features of the detected peak.

An investigation on the time-dependant development of yield stress in two similar self-compacting mortars using slowly rotating ConTec4 viscometer and a newly developed plate test was made. The results from the ConTec4 viscometer revealed that both the static yield stress and structuration rate depend on the confinement conditions. A much higher static yield stress was obtained with a residual stress in the confined mortar in the viscometer gap compared to yield stress developing in unconfined state at start or after a release of the residual stress by a shaking movement of the viscometer. A more detailed analysis based on data filtration of negative rotation values showed structuration rate of similar magnitude and also allowed to evaluate the shear modulus G which also showed a very clear increase with time. The measurements with the plate test showed much lower absolute values of yield and lower structural build-up rate (the structuration rate took values 0.02 Pa/s and 0.01 Pa/s in case of mixture I and II respectively). Possibly the roughness of the sandpaper on the plate did

not reflect the same yield value as the rougher surface of the core of the viscometer, which has larger knifes and also the deformation conditions around the plate and the viscometer core varied.

Following the mortar studies a series of matrixes with same binder composition and filler content were investigated with using parallel plate rheometer. Proportioning of matrixes was varied so as to cover the composition of mixture II according to the particle-matrix model. For evaluating the rheological parameters the Bingham model was used. One can say that all rheological parameters are much more influenced by w/c than SP dosage. The static yield stress of the matrixes was very shear history dependant and varied only little over time for test I and was similar to the dynamic yield stress. The behaviour of martixes was studied under constant shear rate to obtain G modulus. G modulus is strongly influenced by magnitude of shear rate which is used for testing and lower shear rate gives higher values of G modulus. That is true for yield stress as well. Comparing the results concerning the matrixes and mortars, the plastic viscosity and yield stress of matrix was more than hundred times and ten times lower respectively. Much lower value of the structuration rate was found for matrix, only 0.005 $Pa \cdot s^{-1}$.

The inclined plane test, other test for finding static yield stress was carried out too. Some limitation factor for mixture was observed during testing, the testing sample should have proper rheological properties for this type of test, especially dynamic yield stress. That was the reason for testing mortar with higher SP dosage compare to the previous mixtures. It should be pointed out, that the plate test same as the inclined plane test were done for the first time in mentioned institution. Obtained values of structuration rate (0.13 Pa/s and 0.29 Pa/s for mortar with 1.0 % SP and 0.8 % SP respectively) confirmed the fact, that SP dosage influences the hydration and creating the new structures in the system. The influence of SP dosage on hydration was studied in second part of this thesis with using calorimetry and XRD analysis.

After studies of mortars and matrixes the static yield stress was measured on 3 different SCCs produced at a ready-mix plant. The rheological testing was a part of the study of the effect of stabilization on surface quality of concrete elements, which included casting of full scale wall elements. Three mixtures of SCC (filler stabilized, chemically stabilized and unstable) were subjected the rheological testing. The concrete was sieved to obtaining mortar with all particles smaller than sieve size 6.3 mm. The sieved mortars were characterized by Bingham parameters from flow curves using ConTec4 viscometer and static yield stress was determined as well.

Filler stabilized and chemically stabilized mixtures had similar plastic viscosity. Concerning static yield stress value, the filler stabilized mixture had higher yield stress. In the case of the unstable mixture, visible segregation was observed and therefore rheological properties of this mixture are less valid.

Testing of mortars gave surprising value of yield stresses and plastic viscosities, because these values were higher than in case of unstable and chemically stabilized concrete.

Static yield stresses of concrete determined by inclined plane test were always higher than dynamic yield stress and this measurement is more suitable for mortar than for concrete, because the determination of the angle of inclination is more difficult in case of concrete. The movement of coarse aggregate can occur first before the mixture starts to flow. So the inclined plane test is strongly dependent on the stability of the mixture. Thus visual observation when conducting the test rather than the yield stress value itself is possibly an

indication of stability. Another factor is the volume of the sample. In this test it was used only small sample volumes and sampling is tricky and difficult to make representative. So there is some limitation for samples which are suitable for using the plane test (stability, rheological properties….).

Static yield stresses of concretes were always higher than dynamic as it was expected and correspond to the increasing values of yield stresses evaluated from torque-time dependency in the ConTec4 viscometer.

According to the structuration rate all tested mortars were thixotropic mixtures. The structuration rate in all cases increased and the maximum values were found for unstable mixture, apparently because of unstability. The G modulus was highest in case of chemically stabilized mixture.

Yield stress was higher under confined conditions compared to under non-confined conditions. The rate of increase of static yield stress over time, however, is quite similar as observed from two series of tests made with almost a half year in between.

Second part of the experimental part is concerning the rheological properties of the cement pastes from two types of the cement (Mokrá 52.5 N and Ladce 42.5 N) with different w/c and SP dosage. The characterization of the rheological properties was performed with using the parallel plate rheometer, whereas several parameters were obtained. In all cases the effect of w/c and SP dosage played important role. Basically the increasing w/c and SP dosage led to decreasing the rheological parameters. The cement pastes were tested via Vicat test too to observe the depth of penetration with connection to the w/c. The three models from literature for prediction the yield stress were used. For applying one of them the densities of samples should be measured. The predicted values of yield stress were connected with the obtained values from rheological testing, where the static and dynamic yield stresses were evaluated. The predicted values lie between the static and dynamic yield stresses, which is in very good agreement with origin of Vicat test.

The heat evolution was studied with using isoperibolic calorimeter for observing first 25 hours of hydration of cement pastes. The first stage of hydration was studied with modular microcalorimeter. The results showed that effect of w/c led to decreasing maximal temperature (especially in case of the samples from the cement Mokrá 52.5 N) and SP dosage extended the dormant period.

The phase composition was studied with using in-situ XRD analysis for 20 hours of hydration. According to the obtained results, one can say, that during rheological maesurement there are not crucial changes in creating structure, only creation of ettringite start practically immediately after first contact cement with water. With this process is connected the decrease of tricalcium aluminate and gypsum in the system.

The partly hydrated samples of the cement were prepared for testing phase composition and microstructure. The XRD analysis gives basic information about phase content and confirmed the formation of ettringite, which starts immediately after the water is added to the cement. According to the SEM pictures there are no significant changes in the microstructure during 60 minutes of hydration.

The rheological behavior and properties of fresh cement based systems play important role in whole concrete industry and shouldn´t be marginalized. This thesis gives useful information about crucial properties and possibilities how to quantify or compare individual test results.

9 LIST OF SYMBOLS

A	shear area of the upper plate [m^2]
F	force [N]
v	velocity [m/s]
h	distance between the plates [m]
τ	shear stress [Pa]
$\dot{\gamma}$	shear rate [s^{-1}]
η	dynamic viscosity [Pa.s]
η_0	asymptotic values of viscosity at very low shear rates [Pa.s]
η_∞	asymptotic values of viscosity at very high shear rates [Pa.s]
K	constant parameter in Cross equation [sec]
M	dimensionless constant in Cross equation [-]
n	power-law index [-]
K_2	consistency [$Pa.s^n$]
τ_0	yield stress [Pa]
η_p	plastic viscosity [Pa.s]
X,Y,Z	constants in rheological models [-]
ϕ	volume fraction of solid [-]
η_s	viscosity of the suspension [Pa.s]
η_c	viscosity of the fluid phase [Pa.s]
ϕ_m	maximum possible volume fraction [-]
$[\eta]$	intrinsic viscosity [-]
C	CaO
S	SiO_2
A	Al_2O_3
F	Fe_2O_3
$\bar{S}$	SO_3
H	H_2O
N	Na_2O
C_3S	tricalcium silicate
C_2S	dicalcium silicate
C_3A	tricalcium aluminate
C_4AF	ferrite phase
SCC	self-compacting concrete
SF	slump flow
ρ	density [kg/m^3]
g	gravity [$m \cdot s^{-2}$]
V_c	conical volume [m^3]
D_f	final spread diameter [mm]
SP	superplasticizer
SMF	sulfonated melamine-formaldehyde condensates
SNF	sulfonated naphthalene-formaldehyde condensates
MLS	modified lignosulfonates

γ_c	critical strain [s^{-1}]
G	shear elastic modulus [Pa]
Q	amount of heat produced in a system during period of time [J]
T_{sample}	sample temperature [K]
T_s	surrounding temperature [K]
C_s	heat capacity [J/K]
K	heat exchange coefficient between the sample and the surroundings [$W \cdot m^{-2} \cdot K^{-1}$]
r	radius [m]
h	depth of penetration [m]
P	radius of cylinder [m]
r_0	radius of penetrator [m]
m	mass [kg]
F_g	gravity [N]
F_b	buoyancy [N]
R	needle radius [m]
XRD	X-ray powder diffraction
n_r	order of reflection [-]
λ	wavelength of x-rays [m]
d	characteristic spacing between the crystal planes [m]
θ	angle between the incident ray and the scattering plane [degree]
SEM	scanning electron microscope
T	torque [Nm]
N	rotational speed [rps]
τ_{dyn}	dynamic yield stress [Pa]
h_i	height of inner cylinder [m]
Ω	angular velocity of the outer cylinder [$rad.s^{-1}$]
R_i	radius of inner cylinder [m]
R_o	radius of outer cylinder [m]
γ	angle [degree]
α	angle [degree]
τ_{res}	residual stress [Pa]
τ_{mob}	mobilized stress [Pa]
τ_{fully}	fully mobilized stress [Pa]
S_p	immersed surface of the plate [m^2]
A_{thix}	structuration rate [$Pa \cdot s^{-1}$]
h_s	thickness of the spread in inclined plane test [m]
φ	angle of inclination of the inclined plane [degree]
R	rate of increasing of dynamic yield stress [Pa/s]
ω	angular velocity [$rad \cdot s^{-1}$]
N_a	average velocity [rps]
B	rate of increase the stress [Pa/s]
$\tau_{01\text{-}3}$	predicted yield stress according models [Pa]

10 BIBLIOGRAPHY

[1] BARNES H.A.: An Introduction to Rheology, Elsevier 1998, 199 s, ISBN 0-444-87469

[2] MALKIN A.I., ISAYEV A.I.: Rheology: Concepts, Methods and Aplications, ChemTec Publishing, 2006, 474 p, ISBN 9781895198331

[3] MEZGER T. G.: The Rheology Handbook: For Users of Rotational and Oscillatory Rheometers, Vincentz Network GmbH & Co KG, 2006, 299 p, ISBN 3878701748

[4] BERG J.C.: An introduction to interfaces & colloids: The bridge to nanoscience, Word Scientific Publishing, 2009, 785 s, ISBN 9814299820

[5] NEWMAN J., CHOO B.S.: Advanced Concrete Technology, Concrete properties, Elsevier Ltd. 2003, 349 s, ISBN 0 7506 5104 0

[6] JANALÍK J.: Viskozita tekutin a její měření, VŠB-TU Ostrava, 2010

[7] ESPING O.: Early age properties of self-compacting concrete – Effects of fine aggregate and limestone filler, Department of Civil and Environmental Engineering, Chalmers University of Technology, PhD thesis Sweden, 2007

[8] BARNES H.A.: Thixotropy – a rewiew, J. Non-Newtonian Fluid Mech. 70, 1997, 1-33

[9] WALLEVIK J.E.: Rheological properties of cement paste: Thixotropic behavior and structural breakdown, Cement and Concrete Research 39, 2009, 14-29

[10] VIKAN H. a kol.: Correlating cement characteristics with rheology of paste, Cement and Concrete Research 37, 2007, 1502-1511

[11] TURIAN R.M. et al: Characterization, settling and rheology of concentrated fine particulate mineral slurries , Powder Technology 93, 1997, 219-233

[12] RAMACHANDRAN V.S., BEAUDOIN J.J: Handbook of Analytical Techniques in Concrete Science and Technology, Principles, Techniques and Applications, Willian Andrew Publishing 2001, 1003 s, ISBN 0-8155-1437-9

[13] HEWLETT P. C: Lea´s Chemistry of Cement and Concrete, Butterworth-Heinemann Ltd; 4th Revised edition edition, 2003, 1092p, ISBN-10: 0750662565

[14] HLAVÁČ J.: Základy technologie silikátů, 2. uprav.vyd., Praha: SNTL, 1981. 516 p.

[15] TAYLOR H. F. W.: Cement chemisty, Academic Press, London 1990, 475 p, ISBN 0-12-683900

[16] OKAMURA H.: Self-compacting high-performance concrete, Concrete International. 1997 vol. 19, no. 7, p 50–54

[17] KHAYAT. K.: Workability, testing and performance of self-consolidating concrete, ACI materials journal, 1999, vol. 96, no. 3, p 346–353

[18] GAIMSTER R. and DIXON N.: Institute of Concrete Technology Yearbook 2002, 200

[19] OKAMURA H. and OUCHI M: Self-Compacting Concrete, Journal of Advanced Concrete Technology Vol. 1, No. 1, 2003, 5-15

[20] The Self-Compacting Concrete European Project Group: The European Guidelines for Self-Compacting Concrete- Specification, Production and Use; May 2005

[21] Grace introduces ADVA® 400 Admixture Series for Self Consolidating Concrete, available in http://www.aggregateresearch.com/article.aspx?ID=16077, changed 19. 6. 2012

[22] BOUVET A., GHORBEL E. and BENNACER R.: The mini-conical slump flow test: Analysis and numerical study, Cement and Concrete Research 40, 2010, 1517-1523

[23] ROUSSEL N., STEFANI C. and LEROY R.: From mini-cone test to Abrams cone test: measurement of cement-based materials yield stress using slump tests, Cement and Concrete Research 35, 2005, 817-822
[24] ROUSSEL N. and COUSSOT P.: Fifty-cent rheometer for yield stress measurements : from slump to spreading flow, Journal of Rheology, Vol. 49, N°3, 2005, 705-718
[25] RAMACHANDRAN V. S: Concrete Admixtures Handbook, 2nd Ed.: Properties, Science and Technology, Wiliam Andrew Publishing, 1996, 1183 s, ISBN 0815516541
[26] RAMACHANDRAN V. S. and BEAUDOIN J. J.: Handbook of Thermal Analysis of Construction Materials, Wiliam Andrew 2002, 680 p, ISBN 0815514875
[27] Social Media at BASF, The Chemical Company, available in http://newsroom.basf.com/kategorie/products-2/, changed June 2011
[28] LEVY S. M.: Construction Calculation Manual, Butterworth-Heinemann 2011, 700 p, ISBN 0123822440
[29] AÏTCIN P-C.: High-performance Concrete, E. and F. N. Spon 1998, 591 p, ISBN 0419192700
[30] WALLEVIK O.H. and WALLEVIK J.E.: Rheology as a tool in concrete science: The use of rheograpsh and workability boxes, Cement and Concrete Research 41, 2011, 1279-1288
[31] YAHIA A., KHAYAT K.H.: Analytical models for estimating yield stress of high-performance pseudoplastic grout, Cement and Concrete Research 31, 2001, 731 - 738
[32] VIKAN H., JUSTNES H.: Rheology of cementious paste with silica fume or limestone, Cement and Concrete Research 37, 2007, 1512-1517
[33] FERRARIS Ch.F., OBLA K.H. and Hill R.: The influence of mineral admixtures on the rheology of cement paste and concrete, Cement and Concrete Research 31, 2001, 245-255
[34] HANEHARA S. and YAMADA K.: Rheology and early age properties of cement systems, Cement and Concrete Research 21, 2008, 175-195
[35] LEEMANN A., WINNEFELD F.: The effect of viscosity modifying agents on mortar and concrete, Cement and Concrete Composites 29, 2007, 341-349
[36] FERRARIS F., BROWER L.E.: Comparison of Concrete Rheometers: International Tests at LCPC (Nantes, France) in October 2000 (NISTIR 6819), National Institute of Standard and Technology, Gaithersburg, USA, 2001
[37] CHIDIAC S.E. and MAHMOODZADEH F.: Plastic viscosity of fresh concrete – A critical review of predictions methods, Cement and Concrete Composites 31, 2009, 535-544
[38] TATTERSALL G.H.. BANFILL. P.F.G.: The rheology of fresh concrete, Pitman, 1983, ISBN 0273085581, 356p
[39] ROUSSEL N.: A theoretical frame to study stability of fresh concrete, RILEM Materials and Structutes, Vol. 39, 75-83, 2006
[40] FEYS D., Verhoeven R. and De Schutter G.: Fresh self compacting concrete, a shear thickening material, Cement and Concrete Research 38, 2008, 920-929
[41] GEIKER M. R. et al.: The effect of measuring procedure on the apparent rheological properties of self-compacting concrete, Cement and Concrete Research 32, 2002, 1791-1795

[42] FEYS D., VERHOEVEN R. AND DE SCHUTTER G.: Why is fresh self-compacting concrete shear thickening? Cement and Concrete Research 39, 2009, 510-523
[43] NEHDI M. and RAHMAN M.-A.: Estimating rheological properties of cement pastes using various rheological models for different test geometry, gap and surface friction, Cement and Concrete Research 34, 2004, 1993-2007
[44] COLLEPARDI M.: The rheological behaviour of cement pastes, Il Cemento 68, 1971, 99-106
[45] SHEINN A.M.M., HO D.W.S. and TAM C.T.: Rheological model for self-compacting concrete-paste rheology, in C.T. Tam (Ed.), Proceedings of the 27th Conference on Our World in Concrete and Structures, Singarope, CI-Premier, 28-29 August 2002, pp. 517-523
[46] GRESZCZYK S. and KUCHARSKA L.: The influence of Chemical Composition of Cement on the Rheological Properties, From the Proceedings of the International Conference organized by The British Society of Rheology; „Rheology of Fresh Cement and Concrete" Edited by P.F.G. Branfill, The British Society of Rheology, E.&F.F. Spon, London 1990
[47] BANFILL P.F.G.: A viscometric study of cement pastes containing superplasticizers with a note on experimental techniques, Mag. Concr. Res. 33, 1981, 37-47
[48] LEWIS J.A. a kol.: Polyelectrolyte effects on the reological properties of concentraced cement suspensions, J. Am. Ceram. Soc. 83, 2000, 1905-1913
[49] CHANDRA S. and BJÖRNSTRÖM J.: Influence of cement and superplasticizers type and dosage on the fluidity of cement mortars – Part I, Cement and Concrete Research 32, 2002, 1605-1611
[50] CHANDRA S. and BJÖRNSTRÖM J.: Influence of cement and superplasticizers type and dosage on the fluidity of cement mortars – Part II, Cement and Concrete Research 32, 2002, 1613-1619
[51] ROUSSEL N.: A thixotropy model for fresh fluid concretes: Theory, validation and applications. Cement and Concrete Research 36, 2006, 1797-1806
[52] FLATT R. J.: Towards a prediction of superplasticized concrete rheology, Materials and Structures 27, 2004, 289 - 300
[53] ROUSSEL et al.: Steady state flow of cement suspensions: A micromechanical state of the art, Cement and Concrete Research 40, 2010, 77-84
[54] ZUKOSKI C. F.: Particles and suspensions in chemical engineering: accomplishements and prospects, Chemical Engineering Science 50, 1995, 4073 - 4079
[55] ROUSSEL. N. et al: The origins of thixotropy of fresh cement pastes, Cement and Concrete Research 42, 2012, 148-157
[56] STEFFE J. F: Rheological methods in food process engineesing, Freeman Press, Secon edition, 1992, ISBN 9632036
[57] BILLBERG P.: Time-dependent Growth of Static and Dynamic Yield Stress of SCC, RILEM Materials and Structures Journal, 2006
[58] ŠAUMAN Z.: Maltoviny I, PC-DIR Brno, ISBN 8021405090, 198 p., 1993
[59] RAMACHANDRAN V. S. and Feldman R. F.: Significance of Low Water/Solid Ratio and Temperature on the Physico-Mechanical Characteristics of Hydrates of Tricalcium Aluminate, Journal of Applied Chemistry and Biotechnology, Vol. 23, 625–633, 1973

[60] ČERNÝ R. and ROVNANÍKOVÁ P.: Transport Process in Concrete, Taylor and Francis 2002, 547 p, ISBN 0415242649
[61] LAIDLER K.J: The World of Physical Chemistry, OUP Oxford, New Edition 1995, ISBN-10: 0198559194 488p
[62] ZIELENKIEWICZ W. and MARGAS E.: Theory of Calorimetry, Springer 2002, ISBN 1402007973, 188 p.
[63] STRENG W.H.: Characterization of Compounds oin solution: Theory and Practice, Springer 2001, ISBN 0306465957, 273p
[64] KRÁTKÝ, J.: The Use of Multi-Cell Isoperibolic Calorimeter for Assessing of the Properties of Cementitious Mixtures;:Brno VUT, 2001. 52 p Diploma thesis
[65] SCRIVENER K. and NONAT A.: Hydration of cementitious material, present and future, Cement and Concrete Research 41, 2011, 651-665
[66] VIKAN H.: Rheology and reactivity of cementitious binders with plasticirers, Department of Material Science and Engineering, Norwegian University of Science and Technology, PhD thesis, Norway, 2005
[67] Metody zkoušení cementu-část 3: Stanovení db tuhntí a objemové stálosti, norma ČSN EN 196-3, 2005
[68] COUSSOT P.: Rheometry of Pastes, suspensions and granular materials: Applications in industry, J.Wiley and Sons, 2005
[69] SLEIMAN H., PERROT A., AMZIANE S.: A new look at the measurement of cementitious paste setting by Vicat test, Cement and Concrete Research 40, 681-686, 2010
[70] LOOTENS D. et al: Yield stress during setting of cement pastes from penetration tests, Cement and Concrete Research 39, 401-408, 2009
[71] SANT G., FERRARIS F.CH. and WEISS J.: Rheological properties of cement pastes: A discussion of structure formation and mechanical property development, Cement and Concrete Research 38, 1286-1296, 2008
[72] STRUBLE L.J. and LEI W-G: Rheological changes associated with setting of cement paste, Advanced Cement Based Materials, Volume 2, Issue 6, 224-230, 1995
[73] TRTNIK et al.: Possibilities of using the ultrasonic wave transmission method to estimate initial setting time of cement paste, Cement and Concrete Research 38, 1336-1342, 2008
[74] MOUNANGA P. et al.: Autogenous deformations of cement pastes: Part I. Temperature effects at early age and micro-macro correlations, Cement and Concrete Research 36, 110-122, 2006
[75] BAROGHEL-BOUNY V. et al.: Autogenous deformations of cement pastes: Part II. W/C effects, micro-macro correlations, and threshold values, Cement and Concrete Research 36, 123-136, 2006
[76] JENKINS R. and SNYDER R. L.: Introduction to X-ray Powder Diffractometry, Wiley-Interscience, 1996, 432p, ISBN 0471513393
[77] Electron microscopy – ETH Zurich, modified 14 May, 2012 bz F.Krumeich, available in: http://www.microscopy.ethz.ch/bragg.htm
[78] GOLDSTEIN J. et al.: Scanning Electron Microscopy and X-Ray Microanalysis, 3rd edition, Springer, 2007, 689 p, ISBN 0306472929

[79] DIAMOND S.: The microstructure of cement paste and concrete – a visual primer, Cement and Concrete Composites 26, 2004, 919-933
[80] ConTec, A step forward in Concrete Technology, available in http://www.contec.is/index.htm, changed 26. 10. 2010
[81] WALLEVIK J.E: Rheology of particle suspensions – Fresh concrete. mortar and cement paste with various types of lignosulfonates, Department of Structural Engineering. Norwegian University of Science and Technology, PhD thesis, Norway, 2003
[82] PERROT A.. AMZIANE S.. OVARLEZ G.. ROUSSEL N.: SCC formwork pressure: Influence of steel rebars, Cement and Concrete Research 39, 2009, 524-528
[83] AMZIANE S.. PERROT A.. LECOMPTE T.: A novel settling and structural build-up measurement method, Measurement Science and Technology 19, 2008, 105702
[84] TCHAMBA J.C.. AMZIANE S.. OVARLEZ G.. ROUSSEL N.: Lateral stress exert by fresh cement paste on formwork: Laboratory experiments, Cement and Concrete Research 38, 2008, 459-466
[85] BILLBERG P.: Form Pressure Generated by Self-Compacting Concrete – Influence of Thixotropy and Structural Behaviour at Rest; Doctoral Thesis in Concrete Structures. Stockholm, Sweden 2006
[86] SMEPLASS S.. MØRTSELL E.: The applicability of the particle matrix model to self compacting concrete (SCC), Nordic Concrete Research no. 26-6, 2001, 13p
[87] KHAYAT K.H. OMRAN A.F. and PAVATE T.V.: Inclined Plane Test to Evaluate Structural Build up at Rest of Self-Consolidating Concrete, ACI Materials Journal, V. 107. No 5, 2010
[88] DE WEERDT K.. EIDE M.B. and SMEPLAS S.: The effect of stabilization with either filler or chemical stabilizer on the surface quality of concrete elements, SINTEF report, 2011
[89] WILLIAMS D. A., SAAK A. W. and JENNINGS H. M.: The ingluence of mixing on the rheology of fresh cement paste, Cement and concrete Research 29, 1999, 1491 – 1496
[90] BETIOLI A. M. et al: Effect of HMEC on the consolidation of cement pastes: Isothermal calorimetry versus oscillatory rheomotry, Cement and concrete Research 39, 2009, 440-445
[91] YLMEN R. et al.: Earlz hzdration and setting of Portland cement monitored bz IR, SEM and Vicat techniques, Cement and Concrete Research 39, 2009, 433-439

11 Appendix: Material Data sheets

Portland cement of type CEM II/A-V 42.5 R

PRØVNINGSRAPPORT

Oppdragsgiver: KOK
Prøven merket: STD FA sement fra Rescon Mapei

Prøve kode: AZ15-11 Ref. 71-11

KJEMISK ANALYSE EN 196-2

Glødetap		2.04	%
Fri kalk		1.26	%
Flyveaske		18.20	%
Svovel trioksyd	(SO_3)	3.41	%
Silika	(SiO_2)	25.57	%
Aluminiumoksyd	(Al_2O_3)	8.40	%
Jernoksyd	(Fe_2O_3)	4.06	%
Kalsiumoksyd	(CaO)	52.32	%
Magnesiumoksyd	(MgO)	2.45	%
Fosfor pentoksyd	(P_2O_5)	0.27	%
Kaliumoksyd	(K_2O)	1.11	%
Natriumoksyd	(Na_2O)	0.56	%
Alkali		1.29	%

FYSIKALSK PRØVNING EN 196

FINHET

Partikkelanalyse	+90my	0.1	%
" "	+64my	1	%
" "	-24my	77.6	%
" "	-30 my	85.1	%
Spesifikk overflate; Blaine		503	m^2/kg

NORMAL KONSISTENS

Vannbehov - %

VOLUMBESTANDIGHET

Le Chatelier - mm

BINDETIDER

Størkning begynt - min.

TRYKKFASTHET

1 døgn	-	MPa
2 døgn	-	MPa
7 døgn	-	MPa
28 døgn	-	MPa

Norcem A.S Brevik, Sement- og betonglaboratoriet, 4. july 2011

ae.

Laboratoriesjef

Sand

Natural “low-filler” sand 0/8 mm from Årdal quarry (NorStone AS)
Particle density: 2650 kg/m^3
Saturated-surface-dry water absorption: 0.3 %
Please see following figure for particle size distribution of the aggregate.

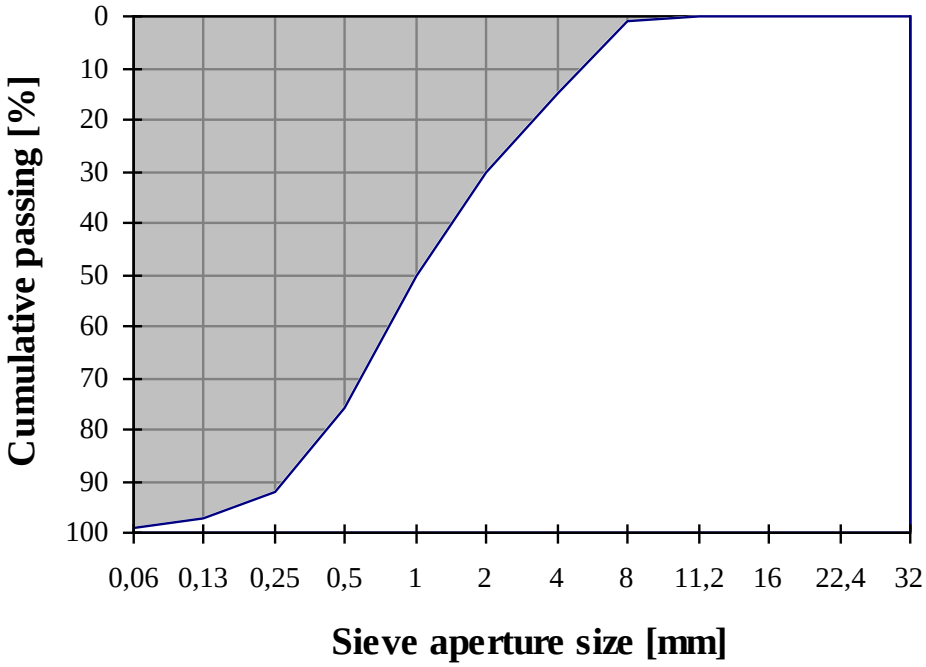

Fig. A1: particle size distribution of send

Tau

NorStone Tau
Density: 2780 kg/m^3
Saturated-surface-dry water absorption: 0.3%
rock type: quartz diorite
All particles are lower than 0.13 mm.

Superplasticizer Dynamon SR-N from Rescon Mapei AS

Dynamon SP-130 is a high performance superplasticizing admixture based on modified acrylic polymers. Please see following figure for technical specifications.

TECHNICAL SPECIFICATIONS

Form:	Liquid
Colour:	Yellowish brown
Viscosity (Brookfield Viscometer DV-1, LV1, 100rpm at 20±2°C):	Low viscosity;<30 cP
Dry solids content, %:	19.5 ± 1.0
Density, g/cm³:	1.05 ± 0.02
pH-value:	6.5 ± 1
Chloride content,%:	< 0.01
Alkali content (equiv. Na_2O) %:	< 2.0

CHARACRERISTICS OF CONCRETE CONTAINING DYNAMON SR-N

As water reducing admixture

Quantity of cement kg/m³ (CEM I- 42.5R):	350	350
Admixture dosage (% by weight of cement)	0	1,1
Mass ratio (w/c ratio):	0.5	0.41
Compressive strength (N/mm²):		
1 day	26	37
7 days	43	56
28 days	52	66

CHARACTERISTICS OF CONCRETE CONTAINING DYNAMON SR-N

As superplasticising admixture

Quanity of cement, kg/m³ (CEM I-42.5R):	350	350
Admixture dosage (in % of cement weight):	0	1.1
Mass ratio (w/c ratio):	0.49	0.49
Air content:	2.4	1.9
Workability, mm:		
- slump, 5 min	40	200
- slump, 30 min	30	200
- slump, 60 min	20	210
- slump, 90 min	20	180
- slump flow, 5 min	200	430
- slump flow, 30 min	200	340
- slump flow, 60 min	200	330
- slump flow, 90 min	200	320

Portland cement of type CEM I 52.5 N, Mokrá

ČESKOMORAVSKÝ CEMENT
HEIDELBERGCEMENT Group

Českomoravský cement, a.s.
nástupnická společnost
závod Mokrá

Statistické hodnocení kvality cementu
dle ČSN EN 197–1

Období od: **1.2.2011** do: **28.2.2011** Cement: **CEM I 52,5 N**						
	jedn.	**průměr**	max.	min.	STD	četnost
Fyzikální vlastnosti						
Měrný povrch	m^2/kg	**425**	451	403	16.74	8
Normální konzistence	%	**29.1**	29.8	28.4	0.42	8
Počátek tuhnutí	minuty	**201**	210	180	8.45	8
Konec tuhnutí	minuty	**263**	280	235	15.60	8
Objemová stálost	mm	**1.2**	1.5	1.0	0.25	8
Mechanické vlastnosti						
Pevnost v tlaku – 2 dny	MPa	**36.7**	37.9	33.7	1.41	8
Pevnost v tlaku – 28 dní	MPa	**63.8**	65.2	61.9	0.94	8
Pevnost v ohybu – 2 dny	MPa	**6.8**	7.2	6.4	0.28	8
Pevnost v ohybu – 28 dní	MPa	**9.1**	9.5	8.7	0.29	8
Chemické vlastnosti						
Ztráta žíháním	%	**2.85**	3.16	2.63	0.19	4
Nerozpustný podíl	%	**0.47**	0.65	0.29	0.18	4
Obsah síranů (jako SO_3)	%	**2.94**	3.06	2.72	0.11	10
Obsah Cl	%	**0.059**	0.069	0.046	0.007	10
Obsah K_2O	%	**0.83**	0.86	0.82	0.01	10
Obsah Na_2O	%	**0.18**	0.21	0.16	0.01	10
Na_2O ekv.	%	**0.73**	0.76	0.70	0.02	10

Výrobek CEM I 52,5 N vyhovuje EN 197–1: 2001.

Dne: 10.4.2011

② **Českomoravský cement, a.s., nástupnická společnost**
Mokrá-Horákov, Mokrá 359, PSČ 664 04
závod Mokrá

Ing. Jiří Lerch
vedoucí útvaru řízení jakosti

Portland cement of type CEM I 42.5 N, Ladce

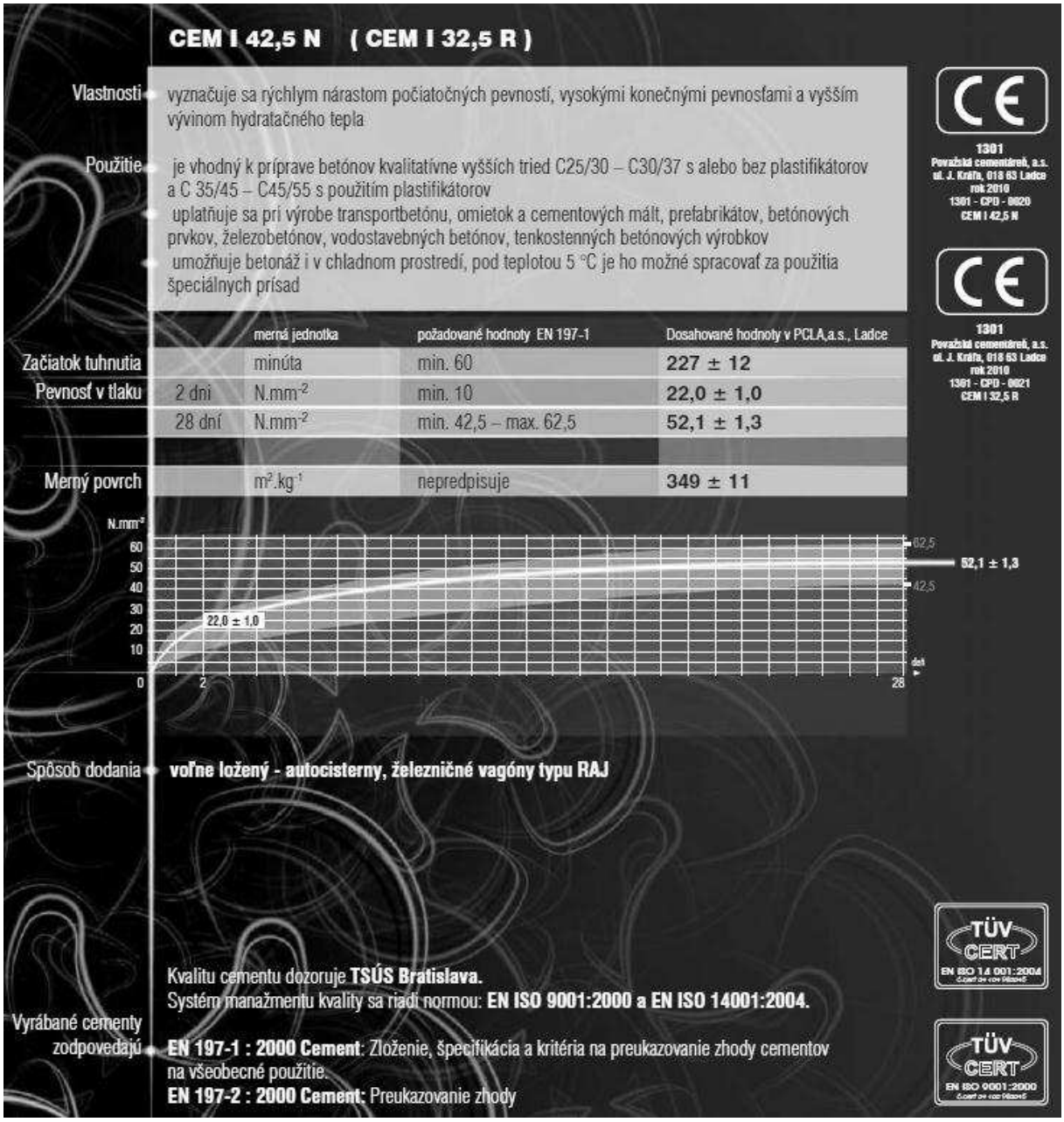

Superplasticizer Glenium ACE 40 from BASF

Glenium ACE 40 is a second generation of high performance superplasticizing admixture based on the polycarboxylate ether polymers. Please see following figure for technical specifications.

BASF
The Chemical Company

Technický list č.: 630

GLENIUM ACE 40

Základní komponenta systému Zero Energy System. Nová generace superplastifikační přísady polykarboxylátetheru. Přísada je optimalizována pro výrobu prefa – dílců. Přísada odpovídá normě EN 934-2.

Popis

- **GLENIUM ACE 40** je inovovaný superplastifikátor druhé generace polymerů polykarboxyetherů.
- Zvláště vyvinutý pro beton s vysokou teplotou.
- Molekulární uspořádání **GLENIA ACE 40** urychluje hydrataci cementu.
- Rychlá adsorpce molekul na cementové částice, kombinovaná s účinným disperzním efektem, odkrývá zvětšený povrch cementovch částic pro reakci s vodou.
- Výsledkem tohoto efektu je rychlý vývoj hydratačního tepla, rychlý vývoj hydratačních produktů a následně vyšší počáteční pevnost.

Použití

- **GLENIUM ACE 40** je vhodný pro výrobu prefa výrobků s využitím betonu s vysokou konzistencí, bez segregace, s nízkým vodním součinitelem a s vysokými počátečními a konečnými pevnostmi.
- **GLENIUM ACE 40** může být použit v kombinaci s přísadou Viscoguard 916 pro samozhutňovací betony.
- **GLENIUM ACE 40** je doporučeno používat při teplotách nad 15°C.

Technické údaje

vzhled	hnědá tekutina
obj. hmotnost (při 20 °C)	1,06 g/ml
obsah chloridů max.	0,1 % hm.

Dávkování

- Účinné dávkování obecně je mezi 0,6–1,0 % cementu.
- Konkrétní dávkování je závislé na množství faktorů, např. požadované zpracovatelnosti, druhu cementu, technologii výroby atd.
- Před použitím je nutné provést průkazní zkoušku dle ČSN EN 206-1.

Zpracování

- **GLENIUM ACE 40** je tekutá látka, která se přidává v průběhu míchání.
- V betonárně se doporučuje přidat přísadu společně s poslední třetinou záměsové vody popř. dodatečně do hotové betonové směsi.
- Nejlepších výsledků je dosahováno pokud přísadu přidáme do míchačky jako poslední, po všech složkách a nejméně po 80% záměsové vody.
- Nutné dodržet dobu pro zamíchání do směsi podle konkrétních podmínek, ale minimálně 1 min.

Balení

- Kanystr 20 kg
- Sud 200 kg
- Kontejner 1000 kg
- Cisterna

Skladování

- **GLENIUM ACE 40** musí být skladován při teplotě vyšší než 5°C.
- V případě přemrznutí výrobek přemístit do prostředí s teplotou kolem 30 °C a promíchat.
- Při obvyklém skladování (uzavřená nádoba, 20 °C) je výrobek neomezeně použitelný 12 měsíců.

Bezpečnostní předpisy

- Při skladování a manipulaci je třeba dbát ustanovení vyhlášky č. 6/1977 Sb. pro látky uvedené v § 1 bod j) – jiné rozpustné volně skladovatelné látky.
- V případě potřísnění kůže důkladně omýt vodou a mýdlem. Při zasažení očí vyplachovat několik minut pod proudem vody a vyhledat lékaře.
- Při požití nevyvolávat zvracení a vyhledat lékaře.
- Při práci používat pracovní oděv, při přečerpávání ochranné brýle.
- Nevylévat do kanalizace.
- Další podrobné údaje jsou uvedeny v Bezpečnostním listě, který zasíláme na vyžádání.

Technická podpora

Příslušný spolupracovník firmy BASF Stavební hmoty Česká republika s.r.o. je Vám s dalšími informacemi a technickou podporou rád k dispozici.

WOERMANN